

# Proceedings

## 13<sup>th</sup> Working Meeting on European VLBI for Geodesy and Astrometry

Viechtach/Wetzell, February 12-13, 1999

Edited by  
W. Schlüter and H. Hase

Bundesamt für Kartographie und Geodäsie  
Fundamentalstation Wetzell



# Proceedings of the 13<sup>th</sup> Working Meeting on European VLBI for Geodesy and Astrometry

Viechtach/Wetzell, February 12-13, 1999

## Preface

The 13<sup>th</sup> Working Meeting on European VLBI for Geodesy and Astrometry took place near the Fundamental Station of Wetzell in the town of Viechtach in the Bavarian Forest, Germany, on February 12-13, 1999. These proceedings contain contributions about many aspects of Very Long Baseline Interferometry (VLBI) from experts in this field working as operators at radiotelescope sites, developers, data analysts, researchers and scientists in various parts of the world.

The proceedings are structured in the following manner:

- **International VLBI Service**

The results of the initial meeting of the directing board of the International VLBI Service (IVS) had been presented at the workshop. We expect that IVS will play an important role for the geodetic and astrometric VLBI activities in the future.

- **Reports from Stations**

This chapter illustrates the various activities at the observatories at Wetzell, TIGO, Effelsberg, Medicina, Noto, Matera, Madrid, Yebes, Onsala, Ny Alesund, Kashima, Tsukuba, stations involved in the Key Stone Project and the current status of the Bonn correlator. Special concern is given to the observations of the reference point of the radiotelescopes and its tie to a local survey network. Monitoring of local motions of the reference point of the radiotelescopes is believed to help to eliminate systematic errors and to improve accuracy.

- **Analysis and Modelling**

Various analysis strategies, results of analysis of VLBI observations and their interpretation are presented. Several contributions touch topics of general relativity, methods of constructing reference systems, signal propagation in the atmosphere, variations of Earth orientation, ocean loading effects, crustal dynamics. Comparisons of VLBI with GPS techniques have also been used to evaluate the consistency of techniques. Methods for investigation of source structure of radio objects which are observed in geodetic observation programmes are considered in some articles.

- **New Developments and Ideas**

A technique which is not continuously improved will become obsolete very easily. Therefore the next steps in VLBI developments concern the compatibility of different data formats, new recording systems, electronic VLBI in near real-time and in general more automatization of the processing of VLBI-data. Project of new generation of water-vapour radiometer is considered. In the future the determination of Earth rotation parameters by laser gyroscopes may be feasible as well as as the determination of the orbits of transmitters of satellites by the means of VLBI phase-referencing techniques as completion to existing orbit determinations based on satellite techniques.

## Citation Instruction

These proceedings are published in a printed and in an electronic version by the Bundesamt für Kartographie und Geodäsie, Wettzell, in 1999. The copyrights for the articles in these proceedings are by the authors. Any material used from the printed or the electronic version of the proceedings must be cited in the following manner:

*Name of author: Title of contribution*, In: Proceedings of the 13th Working Meeting on European VLBI for Geodesy and Astrometry, held at Viechtach, February 12-13, 1999, edited by W. Schlüter and H. Hase, Bundesamt für Kartographie und Geodäsie, Wettzell, 1999

Any article of the proceedings can be printed for personal use only.

## Electronic Version

The full text electronic version of these proceedings is available on the WWW under the address

<http://fw1.wettzell.ifag.de/euro13>

The electronic version is identical to the printed version from March 18, 1999.

## Acknowledgement

The editors acknowledge the common efforts of the authors to keep the deadlines and are thankful for the support of Leonid Petrov, Geodetic Institute of University of Bonn, in the quick preparation of the proceedings.

## Table of Contents

<b>Preface</b>	<b>1</b>
<b>Table of Contents</b>	<b>3</b>
<b>International VLBI Service</b>	
1 <i>N. Vandenberg: IVS is Established</i> . . . . .	6
<b>Reports from Stations</b>	
2 <i>R. Kilger: Status Report of 20m - Radiotelescope - Wettzell</i> . . . . .	11
3 <i>R. Zernecke: Seasonal Variations in Height demonstrated at the Radiotelescope Reference Point</i> . . . . .	15
4 <i>H. Hase, L. Petrov: The First Campaign of Observations with the VLBI-Module of TIGO</i> . . . . .	19
5 <i>A. Nothnagel: Local Survey at the Effelsberg Radio Telescope 1997 - Preliminary Results</i> . . . . .	25
6 <i>W. Alef, R.W. Porcas: Observatory Report from Effelsberg</i> . . . . .	32
7 <i>A. Orfei, G. Tuccari, F. Mantovai: Medicina and Noto Stations Report</i> . . . . .	33
8 <i>G. Colucci, F. Vespe, D. Del Rosso, L. Garramone: Matera VLBI Station: status report</i> . . . . .	38
9 <i>D. Behrend, A. Rius: Geodetic Control of the Madrid DSS65 VLBI Antenna</i>	42
10 <i>A. Rius, A. Alberdi, D. Behrend, C. Garcia-Miro, J.A. Perea: Radioastronomy at the NASA Madrid Deep Space Communications Complex (MDSCC) - Status Report</i> . . . . .	51
11 <i>F. Colomer, P. de Vicente, M. Rioja: Observatorio Astronomico Nacional - Yebes - Status Report</i> . . . . .	59
12 <i>G. Elgered, R. Haas: Geodetic Very-Long-Baseline Interferometry at the Onsala Space Observatory 1997 - 1998</i> . . . . .	60
13 <i>H.-P. Plag: Measurement of vertical crustal motion in Europe by VLBI: Station report for Ny-Alesund; Norwegian Mapping Authority</i> . . . . .	65
14 <i>A. Mueskens, W. Alef: Bonn Correlator Report</i> . . . . .	78
15 <i>T. Kondo, N. Kurihara, Y. Koyama, J. Nakajima, R. Ichikawa, E. Kawai, M. Sekido, T. Yoshino, J. Amagai, T. Sebata, M. Furuya, Y. Takahashi, H. Kiuchi, A. Kaneko: Recent VLBI activities at the Communications Research Laboratory, Japan</i> . . . . .	80
16 <i>S. Ogi: Status Report of Geographical Survey Institute</i> . . . . .	89
<b>Analysis and Modelling</b>	
17 <i>M. Sorgente, L. Petrov: Overview of performance of European VLBI Geodetic Network in the Europe campaigns in 1998</i> . . . . .	95
18 <i>R. Lanotte, C. Ferraro, A. Nardi, C. Sciarretta, F. Vespe: The CGS VLBI EUR98 Geodetic Solution and Comparison with the CGS GPS results</i> . . . . .	101

19	<i>R. Haas, A. Nothnagel: A two-step approach to analyze European geodetic Very Long Baseline Interferometry (VLBI) data</i> . . . . .	108
20	<i>K. Boerger: A geocentric relativistic VLBI-Model</i> . . . . .	115
21	<i>K. Boerger: Comparison of European network solutions</i> . . . . .	121
22	<i>L. Petrov: Absolute methods for determination of reference system from VLBI observations.</i> . . . . .	138
23	<i>L. Petrov: Steps towards phase delay VLBI</i> . . . . .	144
24	<i>M. Rioja, P. Tomasi: Integrating GPS zenith path-delay measurements into the analysis of geodetic VLBI observations from the European network</i> . . . . .	152
25	<i>L. Gradinarsky: Comparison of atmospheric parameters estimated from VLBI, GPS and microwave radiometer data</i> . . . . .	161
26	<i>D. S. MacMillan, W. E. Himwich, N. R. Vandenberg, C. C. Thomas, J. M. Bosworth, B. Chao, T. A. Clark, C. Ma: CORE: Continuous, High-Accuracy Earth Orientation Measurements</i> . . . . .	166
27	<i>H. Schuh, O. Titov: Short-period variations of the Earth rotation parameters as seen by VLBI</i> . . . . .	172
28	<i>R. Haas, H.-G. Scherneck: The effect of ocean tide loading on the determination of earth rotation parameters</i> . . . . .	178
29	<i>O. Titov: Tectonic motion of European VLBI sites</i> . . . . .	186
30	<i>K. Kaniuth: Crustal deformations in the Central Mediterranean derived from the WHAT A CAT GPS project</i> . . . . .	192
31	<i>E. Gueguen, P. Tomasi: Geodynamic interpretation of the Central Mediterranean combining geological and VLBI data.</i> . . . . .	198
32	<i>V. Tornatore, F. Sacerdote, M. Crespi: Comparison of deformations resulting from GPS and VLBI data: problems and preliminary results</i> . . . . .	206
33	<i>P. Charlot, A. L. Fey: A Classification of ICRF Sources Based on Observed Structure for Ultra-precise VLBI Astrometry and Geodesy</i> . . . . .	217
34	<i>C. Ma, M. Eubanks: Extension and Maintenance of the ICRF</i> . . . . .	224
35	<i>V. Tornatore, C. Stanghellini, Silke Britzen: Status report of the project 'EVN observations of radio sources used for geodetic EUROPE experiments'</i> . . . . .	226
36	<i>M. Rioja, R. Porcas, S. Garrington, A. Alberdi, D. Saikia: Relative astrometry and phase-reference mapping in the 1636+473 system using MERLIN and Global VLBI</i> . . . . .	233
37	<i>W. Alef, A. Benz, J. Conway, M. Pestalozzi, T. Beasley: Phase-reference mapping of nearby stars: status report</i> . . . . .	241

## New Development and Ideas

38	<i>A. Whitney: Advanced Technology Development in VLBI</i> . . . . .	249
39	<i>W. Cannon: The Canadian S2-VLBI-System</i> . . . . .	260
40	<i>B. Stoew, C. Rieck: Dual Channel Water Vapour Radiometer Development</i> . . . . .	261
41	<i>W. Schwegmann, H. Schuh: On the Automation of the MarkIII Data Analysis System</i> . . . . .	265
42	<i>H. Hase: Phase Centre Determinations at GPS-Satellites with VLBI</i> . . . . .	273

43 *U. Schreiber, M. Schneider, G. E. Stedman, W. Schlueter: Characteristics of a Ring  
Laser for Geodesy* . . . . . 278

# IVS Is Established

N. R. Vandenberg  
IVS Coordinating Center Director

## 1. Summary

IVS is the *International VLBI Service for Geodesy and Astrometry*. IVS groups geodesy and astrometry together because they use the same observations and the same analysis gives both types of results.

IVS is established under the International Association of Geodesy's (IAG) Commission VIII – the International Coordination of Space Techniques for Geodesy and Geodynamics, or CSTG, chaired by Gerhard Beutler of the University of Berne, Switzerland.

IVS is the third of this type of service to be established. The first was the IGS (International GPS Service) which has been highly successful as a service for GPS. The second service was the ILRS (International Laser Ranging Service) which started in late 1998.

## 2. Chronology

This section presents a brief history of the events leading up to the formation of IVS.

In May 1997 the CSTG Chairman initiated discussions about a VLBI service that would operate in a manner similar to the IGS. By September the CSTG VLBI Subcommittee, chaired by Thomas Clark of NASA Goddard Space Flight Center, published a draft Terms of Reference. At the end of the year Dr. Clark resigned as chairman of the VLBI Subcommittee and James Campbell of the Geodetic Institute of the University of Bonn was appointed as chairman.

Community response to the draft Terms of Reference was strong, and an electronic workshop was convened to re-write the Terms. The workshop members met only via e-mail during February and March 1998. Different members of the workshop with varying areas of expertise re-wrote sections of the Terms and all the members reviewed them. It was at this point that the name IVS was determined, following a lively debate among the workshop members about the mandate for the organization.

In April 1998 the new Terms of Reference were presented to the CSTG Executive Committee for approval at a meeting held in Nice, France. See section 3 for a summary of the Terms. At this time the VLBI Subcommittee formed a Steering Committee to do the work of establishing the IVS.

The Steering Committee released the Call for Participation in IVS on 1 June 1998, and proposals were received through the end of September. At its meeting in October in Munich, Germany, the Steering Committee evaluated the proposals and decided to accept all of them. See section 4 for a summary of the results.

In mid-November 1998 the Steering Committee released the Call for Nominations for representative positions on the Directing Board. Also released was the Call for Proposals for the positions of Network, Analysis, and Technology Coordinators. Following the close of nominations the general elections were held via e-mail ballots.

The Steering Committee held its final meeting in January 1999 at Goddard Space Flight

Center to form the initial IVS Directing Board. The Board members were selected based on the proposals for Coordinators, the elections, and nominations for At Large positions. See section 5 for the list of the members of the initial Directing Board.

### 3. Summary of IVS Terms of Reference

This section provides a summary of the bylaws, or Terms of Reference, by which IVS as an organization is governed. The full text of the Terms of Reference may be found at <http://ivscc.gsfc.nasa.gov/org/tor.html>.

The objectives of IVS are stated first in the Terms of Reference. They are 1) to provide a service to support geodetic, geophysical, and astrometric research and operational activities; 2) to promote research and development for VLBI; and 3) to interact with users of VLBI products. The service aspect of IVS is meant to serve both outside users and the geodetic and astrometric community itself. Both the contributors and users of data will be served.

IVS provides data and products for the scientific community. Some of the products are a terrestrial reference frame (TRF), the international celestial reference frame (ICRF), and Earth orientation parameters (EOP). All IVS data and products are archived and are publically available. IVS products contribute to research in many areas, including areas such as the solid Earth, tides, studies of the vertical, and VLBI technique improvement.

The goals of IVS are realized through seven types of components:

- ▶ Network Stations are high performance VLBI stations that acquire data.
- ▶ Operation Centers coordinate the activities of a network of Network Stations.
- ▶ Correlators process data, provide feedback to stations, and provide processed data to analysts.
- ▶ Analysis Centers analyze data and produce results and products.
- ▶ Data Centers distribute products to users, and provide storage and archive functions.
- ▶ Technology Development Centers develop new VLBI technology.
- ▶ The Coordinating Center coordinates the daily and long-term activities of IVS.

In addition to the above types of components, IVS has the following:

- ▶ The Directing Board determines policies, standards, and goals. The Board is composed of elected and *ex officio* members.
- ▶ Associate Members are individuals participating in the work of any of the IVS components.
- ▶ Corresponding Members are individuals who want to be informed of IVS activities.
- ▶ The Network Coordinator is responsible for station data quality and performance standards.
- ▶ The Analysis Coordinator is responsible for VLBI product development and delivery.
- ▶ The Technology Coordinator is responsible for VLBI technique advancement and system compatibility.

### 4. IVS Components

At the initiation of IVS there were 73 components, representing 29 organizations in 15 countries. The distribution of types of components is as follows:

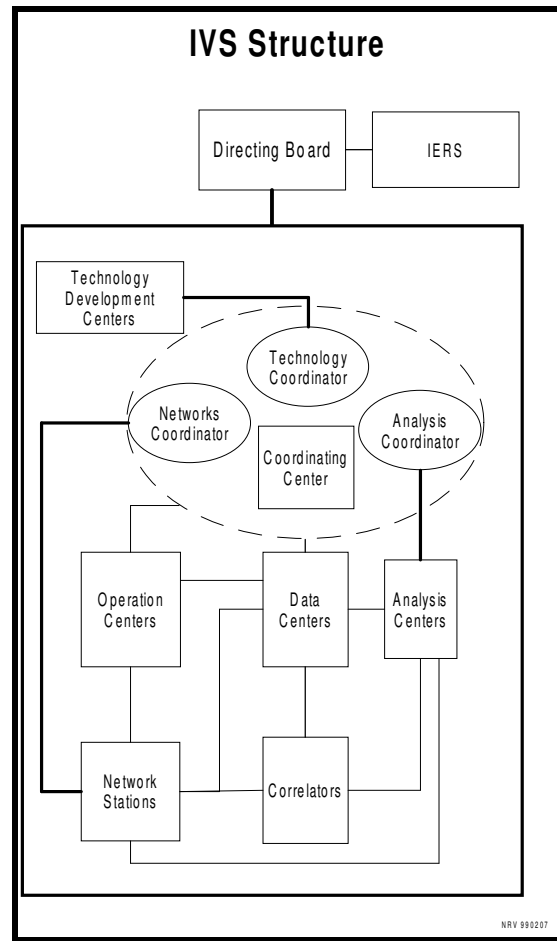
- 30 Network Stations
- 3 Operation Centers
- 7 Correlators
- 6 Data Centers
- 17 Analysis Centers
- 9 Technology Development Centers
- 1 Coordinating Center

There are 229 Associate Members.

By country, the 73 IVS components are distributed as follows:

Brazil	1
Canada	3
China	3
France	2
Germany	8
Italy	7
Japan	14
Netherlands	2
Norway	3
Russia	5
South Africa	1
Spain	2
Sweden	3
Ukraine	2
USA	17

There are noticeably no IVS components from Australia. This is an issue that the IVS Board is working on.



The structure and interactions of IVS are shown in the figure above. The link to the IERS (International Earth Rotation Service) indicates that the IVS is now the VLBI Coordinating Center for IERS. The Directing Board provides overall guidance. The Coordinating Center and the three Coordinators work closely together. Each Coordinator has a special relationship with the components they work with. All of the components interact with each other on a daily basis.

### 5. Directing Board

The initial IVS Directing Board is listed in the table below. There are *ex officio* positions for persons representing the International Association of Geodesy (IAG), the International Astronomical Union (IAU), and the International Earth Rotation Service (IERS). The IVS Coordinating Center Director is also an *ex officio* position. The three Coordinators are each Board members. There are five Representative positions and two At Large positions.

The Chairman of IVS is one of the Board members, chosen by the Board themselves. All Board members will eventually serve staggered 4-year terms. Some of the initial terms had to be 2 years to achieve this.

IVS Directing Board				
Name	Affiliation	Country	Position	Term
Gerhard Beutler	Univ. of Berne	Switzerland	IAG Representative	<i>ex officio</i>
Wayne Cannon	Space Geodetic Laboratory	Canada	At Large Member	2
Nicole Capitaine	Paris Observatory	France	IAU Representative	<i>ex officio</i>
Marshall Eubanks	U.S. Naval Observatory	USA	Correlators and Operation Centers Representative	4
Ed Himwich	NVI, Inc./Goddard Space Flight Center	USA	Network Coordinator	4
Tetsuro Kondo	Communications Research Laboratory	Japan	Technology Development Centers Representative	2
Chopo Ma	Goddard Space Flight Center	USA	IERS Representative	<i>ex officio</i>
Shigeru Matsuzaka	Geographical Survey Institute	Japan	Networks Representative	4
Axel Nothnagel	University of Bonn	Germany	Analysis and Data Centers Representative	2
Wolfgang Schlueter	Bundesamt fuer Kartographie und Geodaesie	Germany	Networks Representative, Chairman	4
Paolo Tomasi	CNR Bologna	Italy	At Large Member	4
Nancy Vandenberg	NVI, Inc./Goddard Space Flight Center	USA	Coordinating Center Director	<i>ex officio</i>
Alan Whitney	Haystack Observatory	USA	Technology Coordinator	4
tbd			Analysis Coordinator	2

## 6. First Board Meeting

This section summarizes the highlights of the first Directing Board Meeting.

As its first act the IVS Directing Board elected Wolfgang Schlueter as Chairman. The Board feels that Dr. Schlueter's links to the other techniques and his experience managing a fundamental station will be very valuable to the initial growth and collaborations of the new IVS.

The Board named NEOS (National Earth Orientation Service, a joint effort of the U.S. Naval Observatory and NASA's Goddard Space Flight Center for VLBI) as the acting Analysis Coordinator. NEOS will develop an initial plan for IVS product presentation and write a new solicitation for the Analysis Coordinator activities.

Each of the Coordinators and the Coordinating Center presented their initial plans for activities. The plans are:

- ▶ The Technology Coordinator will focus on the proposed standard VLBI interface, and visibility of technology at meetings.
- ▶ The Network Coordinator will develop written station performance standards and

- ▶ establish a regular program of station visits.
- ▶ The Analysis Coordinator will make existing VLBI products easily available through IVS.
- ▶ The Coordinating Center has set up the initial version of the IVS web site and will announce the IVS e-mail service. The IVS web site may be found at <http://ivscc.gsfc.nasa.gov>. The site aims to be the center of communications and information for all IVS components and members.

The Board discussed the appropriate method for interaction with astronomy organizations such as JIVE, NRAO, and ATNF. Because we use many of the same facilities as the astronomers and share the same reference frames we need to have a formal relationship with these groups.

The Coordinating Center will announce a contest for the IVS logo. First prize will be free t-shirts with the logo on them for all of the Associate Members at the winner's institution. The Board will select the winning entry.

Presented at the 13<sup>th</sup> Working Meeting for European VLBI Geodesy and Astrometry  
February 12, 1999

Nancy R. Vandenberg  
NVI, Inc./GSFC Code 920.1  
Greenbelt, MD 20771  
[nrv@gemini.gsfc.nasa.gov](mailto:nrv@gemini.gsfc.nasa.gov)  
phone 301-286-9019  
fax 301-286-0213

# Status Report of 20m-Radiotelescope-Wetzell

R. Kilger\*

## Abstract

This report presents the activities of the 20m-radiotelescope in Wetzell since our last meeting in Hoenefoss/Norway in 1996. Our telescope is fully dedicated to geodetic application and participates only occasionally in astrometric or astronomical observations, if telescope-time allows it. The report has a section dealing with the observations Wetzell has participated and a section describing hard- or software changes.

## 1 Observations

A fully geodetic focussed VLBI-telescope has no big changes in its observing program over the years. Table 1 shows our VLBI-activities since the beginning of regular observations in 1983.

In spite of this two major changes will happen in our geodetic observations in the next future. Starting at July 1st, 1999, 20m-RT-Wetzell shall participate in Wednesday-CORE-session every week; there is still a strong question mark behind it, since Wetzell does not have its Mark-IV formatter (ordered from and paid to GSFC in 1995); assuming this problem can be solved, participation in Wednesday-CORE-session has the consequence for Wetzell (and the users), that we run observations every week through the following years:

- from Tue, 18:00 until Wed, 18:00 NEOS-A,
- from Wed, 18:30 until Thu, 18:30 CORE-3.

Additionally it is planned, that 20m-RT-Wetzell will increase the amount of observations with Japanese telescopes after having a K-IV DAT and the ability to run it with the Field System. Up to now we participated with a K-IV unit on loan from CRL in VLBI-time transfer observations and 24h-sessions to improve the connection of RT-Wetzell with the Japanese telescope family. Thereby we operated the K-IV-DAT with an old HP computer and the antenna including IF-distributor and VC's with the Field System PC.

Regarding the already mentioned daily Intensives with Greenbank and the ability of running K-IV sessions at Wetzell there are plans to combine 2 INTENSIVE-sessions:

- INTENSIVE: between RT-Greenbank and RT-Wetzell, Mk IIIA > Mk IV, recorded on magn.tape, with correlation at USNO, as done since 1984,
- INTENSIVE: RT-JAPAN and RT-Wetzell, K-IV, recorded on cassette, with correlation at TOKYO, (the telescope in Japan still has to be determined; RT-Tsukuba or 26m-RT-Kashima).

Attempting to realize two INTENSIVES Gb-Wz and Wz-Japan following aspects could be considered:

---

\*Forschungseinrichtung Satellitengeodäsie der Technischen Universität München, Fundamentalstation Wetzell, Email: kilger@wetzell.ifag.de

1. Both INTENSIVES should run as simultaneously as possible, to have a
  - better comparison of the two INTENSIVE series,
  - smaller interrupt of parallel observed 24h sessions (a smaller hole in Europe, IRIS-S).
2. That means INTENSIVE Wz-Japan should precede INTENSIVE Gb-Wz. (This helps avoiding regular observations during inhuman observing times . If we cannot avoid it totally, is our technique safe enough to try an unattended observation?)
3. Can sources with high declination (or all sources visible from all three places) be observed with Mark-III/IV on tape and simultaneously with KIV on cassette? (thereby reducing observing time and leading to a better comparison of the two techniques?)
4. Can we add a third INTENSIVE between Gb and Japan to close a ring of daily ) UT1-UTC measurements? (Greenbank would need a K-IV DAT.)
5. In the future: Can we run INTENSIVE in real time transferring the observed data via fiber link to the (or better one) correlator?

Anyhow Wettzell follows a project REAL TIME VLBI ([1], [2]) having in mind the Japanese KEYSTONE project, where 4 VLBI-telescopes are connected with the correlator by 2,5 Gbps ATM communication link. The Japanese have successfully performed fringes during observation. This technique seems to be a desirable alternative for projects, as daily INTENSIVE, to determine UT1 – UTC in the fastest way.

## 2 Hard- and Software Changes

Regarding hard- and software changes I should mention, that we replaced

- antenna pointing computer by VERTEX-ACU, (With this change the antenna pointing software has been adapted. Also we experienced a lot of ACU-computer failures after the upgrade. Meanwhile with the aid of our crew (Mr. Kronschnabl) we reached an even tolerable level of failures.)
- CAMAC interface unit by serial interface, (between FS-PC and antenna pointing computer; with this change the communication software between FS-PC and the pointing computer (ACU) had to be programmed new. This task has been solved by Mr. Zeitlhöfler excellently.)
- Az+El-encoders ROC-Dual 63.6 by Az+El-encoders RCN 723.5 DSK, resolution 20 bit resolution 23 bit
- analog rotation speed control by digital rotation speed control of the motors.

Regarding Field System we have implemented version 9.3.25 with Debian Kernel 2.0.34 into 2 new PC's; Ed Himwich kindly assisted Wettzell in these days to adapt the K-IV DAT (Wettzell has presently on loan) to the Field System. Then Wettzell can run K-IV VLBI-sessions or Mk-III/IV sessions with the same FS-software and schedules made by DRUDG from SKD-files. Our Mark-III/IV DAT will be upgraded to Mark-IV at the end of February 99 by Haystack to be compatible with the requirements of a participation in CORE-3 in July 99.

Tab. 1: Summary of VLBI-Sessions observed at the 20m-Radiotelescope Wettzell 1983-1998

Observations	1983	1984	1985	1986	1987	1988	1989	1990	1991	1992	1993	1994	1995	1996	1997	1998	$\Sigma(1998)$
IRIS-A, NEOS-A+B	3	67	72	72	72	73	73	73	59	48	60	62	52	53	52	45	936
Intensive $\Delta(UT1)$	-	73	211	276	281	282	287	287	292	236	281	225	287	200	277	247	3742
IRIS-S	-	-	-	4	5	3	3	12	12	12	12	12	12	12	12	10	121
EUROPE	-	-	-	-	-	5	2	4	3	5	4	6	6	6	6	5	52
NASA-Geodesy	-	2	12	12	12	5	1	-	21	22	15	23	15	33	5	6	184
NASA-Astrometry	-	-	-	-	2	2	-	-	-	-	-	-	2	-	8	3	17
USNO	-	-	-	-	-	-	-	-	1	11	6	14	4	4	-	-	40
Uni, MPIfR	-	-	-	-	-	-	-	3	5	-	2	2	3	5	2	4	26
Mobile Campaigns	-	-	-	-	-	-	10	-	4	21	4	4	-	-	-	-	43
1...8 h Measurements	-	16	13	25	27	1	19	23	22	1	1	2	6	10	1	-	167
Other 24 h Mk2	-	-	1 -	- -	1 -	7 3	18 3	3 4	9 1	13 -	- -	2 -	- -	2 -	-	-	56 11
Wettzell staff [h]	344	2640	3688	3908	4032	3976	3408	3976	3842	2921	2703	3468	2957	3140	2701	2203	49.907
Students [h]	-	-	-	192	224	56	1140	56	443	1690	1365	808	390	504	214	175	7.457
Total Obs. [h]	344	2640	3688	4100	4256	4032	4548	4232	4285	4611	4068	4276	3347	3644	2915	2378	57.564

## References

- [1] Hayo Hase, Wolfgang Schlüter, Reiner Dassing, Richard Kilger: Proposal: Real Time for VLBI-Intensive-Series, in: Real-Time VLBI Forum, Proceedings of A Discussion on Emerging Opportunities Using Data Network Technologies For Very Long Baseline Interferometry, held at MIT Haystack Observatory, Westford, Massachusetts, U.S.A., May 3, 1998
- [2] W. Schlüter, J. Campbell, H. Schuh: Neuantrag eines Forschungsvorhabens zur Breitbandübertragung von VLBI-Daten

# Seasonal Variations in Height demonstrated at the Radiotelescope Reference Point

R. Zernecke

March 8, 1999

## Abstract

Due to thermal expansion the height of a radiotelescope shows daily and seasonal variations. Since February 26, 1997 the height variations of the reference point are continuously monitored. The maximum of variation is up to 1 mm during a day and more than 3 mm a year, which is regarding the precision of VLBI not negligible.

The air temperature difference between summer and winter are in the domain of  $+30^{\circ}\text{C}$  in summer and  $-20^{\circ}\text{C}$  in winter. Due to the thermal expansion of steel and concrete the height of the telescope shows the temperature influence. With an expansion factor of approximately  $11.0 * 10^{-6} \frac{\text{m}}{\text{C}}$  for steel and concrete and  $1.5 * 10^{-6} \frac{\text{m}}{\text{C}}$  for invar one can expect more then 3 mm height variation of the reference point (12 m above the ground) over the year. This is regarding the precision of VLBI not negligible.

Therefore the height variations of the radiotelescope in Wettzell are continuously monitored. Figure 1 shows the set up of the invar measuring system. The reference point is the intersection between vertical and horizontal rotation axes. The invar wire (length 11.05 m, diameter 1.65 mm) is fixed below the reference point. There is a visibility from the reference point down to the ground through a steel pipe, which was useful for the purpose of surveying and was also suitable to hang up an invar wire. Because of the rotation of the reference point during observations, the ends of the invar wire are fixed with revolving swivels to prevent the wire from twisting, as they are used at a distometer. A weight of 1 kg at the lower end of the invar wire is fixed in this way that it can move up and down, but not rotate (figure 2). An anchor is fixed at the lower end of this weight and sticks into a inductive detector measuring the height variations precisely.

Figure 4 and 6 show the results of 2 measuring periods. The gap between these periods is due to an installation of a new servo and drive system inside the radiotelescope. The temperature ( $T$ ) is measured in the middle of the central pipe in a small air chamber inside the steel construction. This temperature has the highest correlation with the measured height variations ( $L$ ), compared to other temperatures measured at other places. The height variations are not corrected by the expansion of the invar wire due to temperature. This correction ( $C$ ), which should be subtracted from ( $L$ ), is shown separately.

Figure 4 and 6 show the results of a simple computation which was done to elucidate the grade of correlation between temperature and height variations. Starting with the values of figure 4 and 5, the average value of each day ( $T'$  and  $L'$ ) is taken. In this case the time lag of about 2 hours up to 4 hours between the two curves does not play a role. The difference curve ( $D$ ) is derived from

$$D[\text{mm}] = L'[\text{mm}] - 0.126\left[\frac{\text{mm}}{\text{C}}\right] * T'[\text{C}]$$

The factor 0.126 is chosen in this way that the difference curve is as flat as possible. The value of this factor is slightly higher than expected. At October 26, 1997 the anchor was carefully readjusted and for this moment a jump in the difference curve ( $D$ ) becomes visible. Little peaks occur persistently at each 24-hour-observation, maybe due to movements of the telescope during the observations and the waste heat of the motors. These temperature rise have little or no effect on the height.

# Radiotelescope Wettzell

Distribution of the 5 electronic sensors

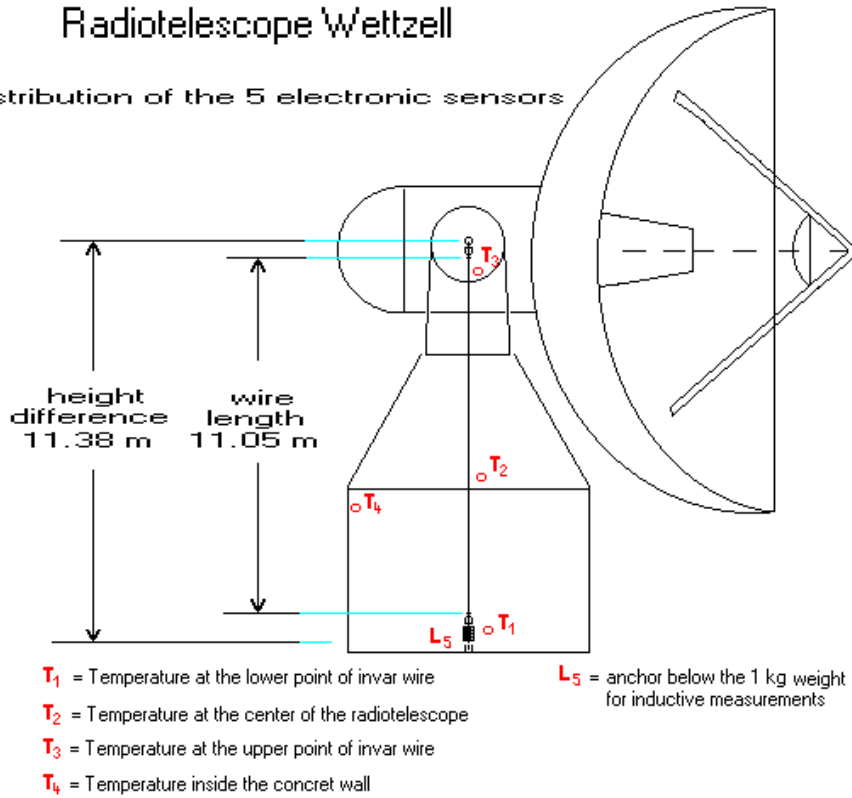


Fig. 1: Principle of Measurements.

# Radiotelescope Wettzell

Invar measurement system

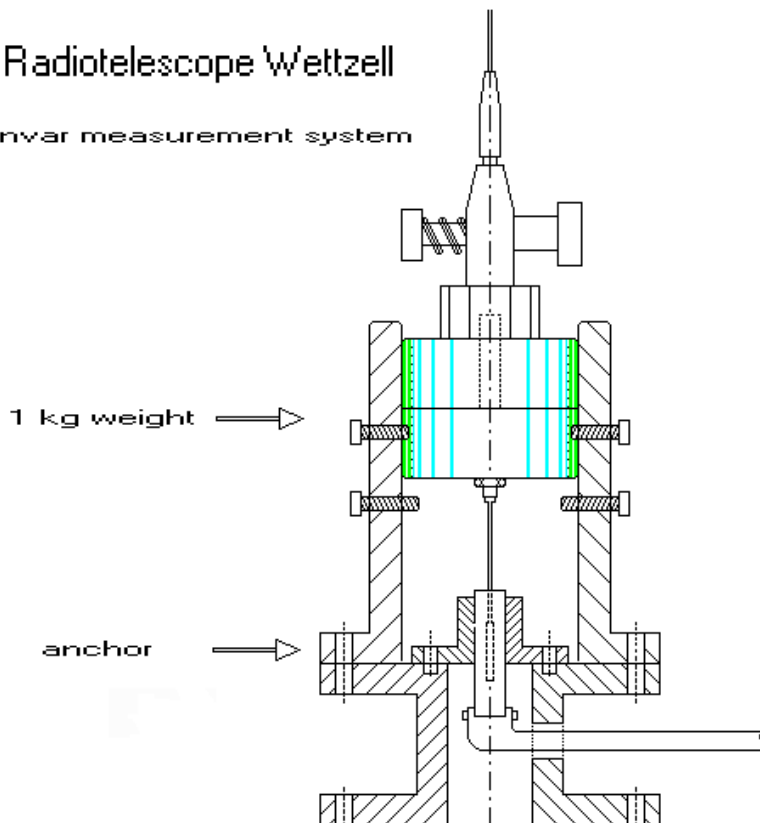


Fig. 2: Inductive Detector and the Principle.

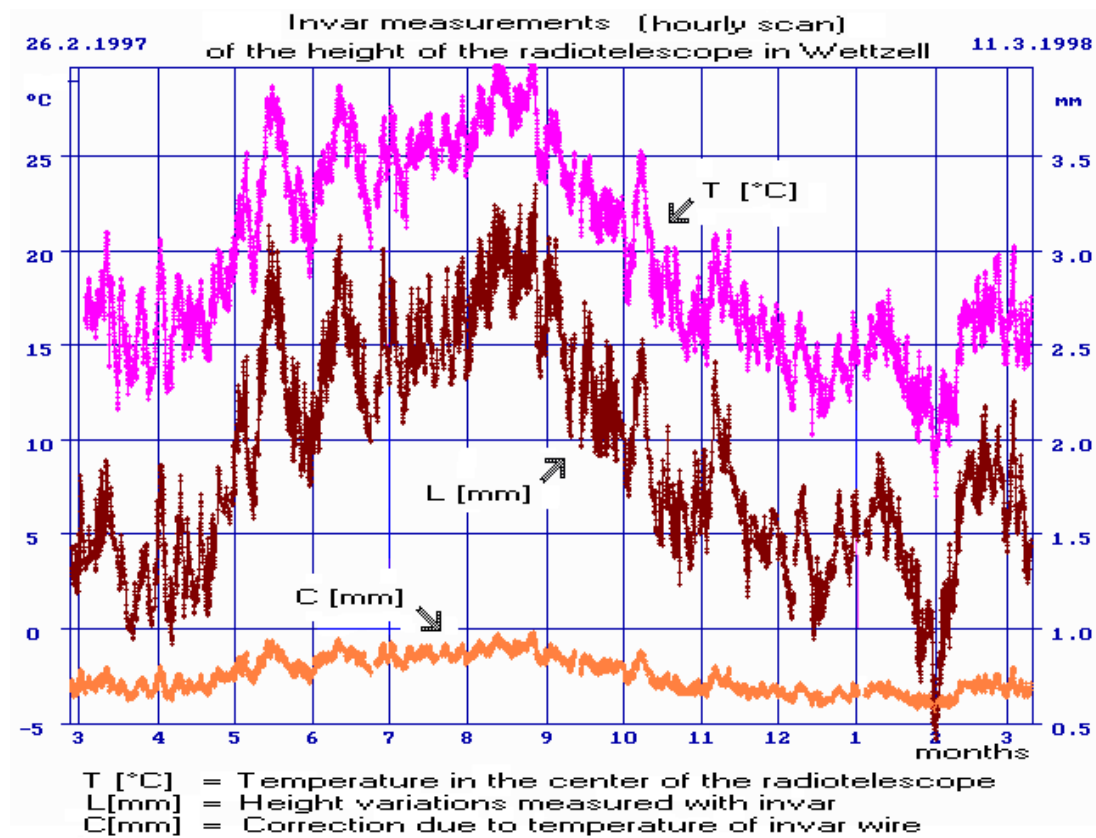


Fig. 3: Measurements of the First Period.

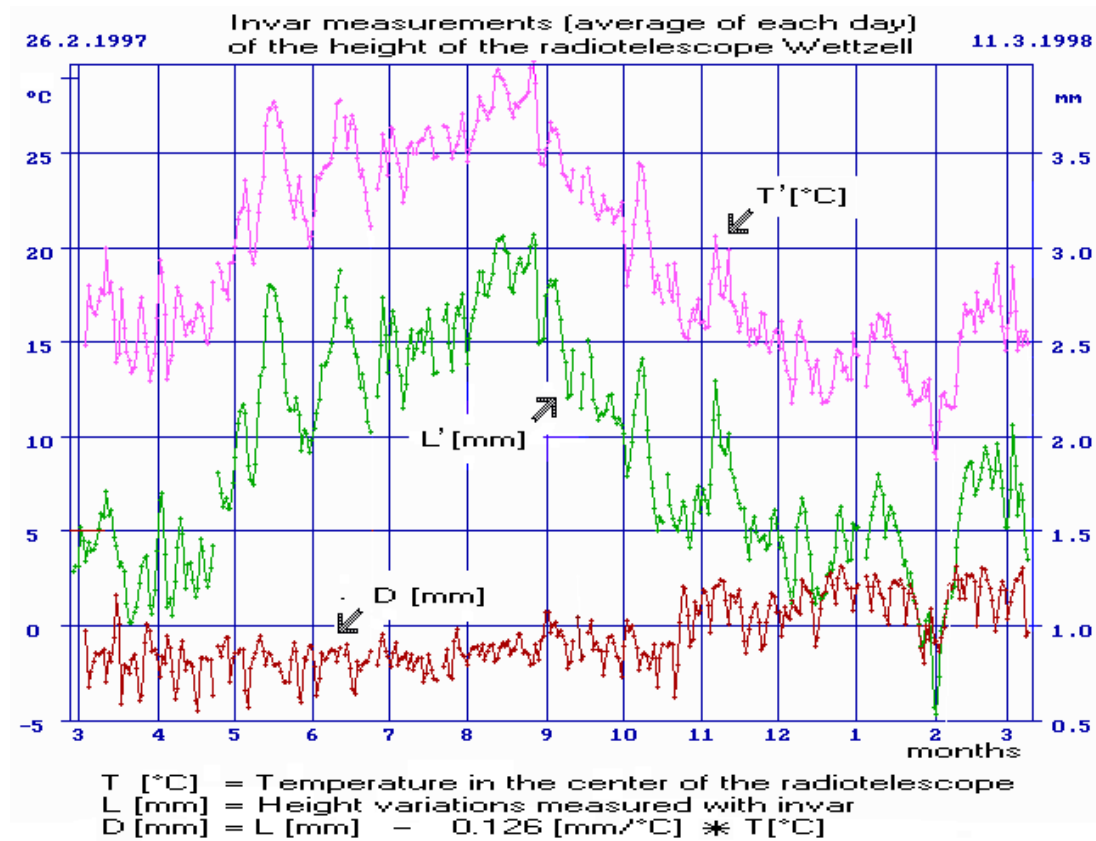


Fig. 4: Correlation between Temperature and Height of the First Measuring Period.

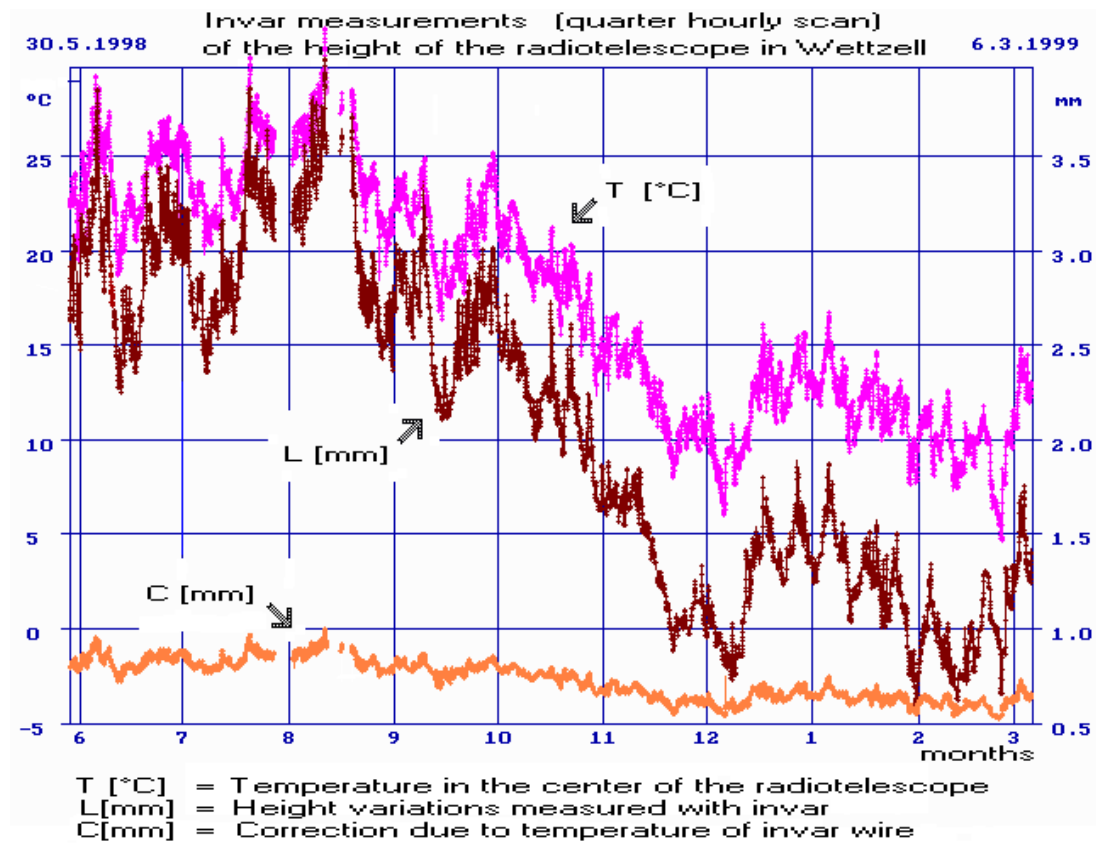


Fig. 5: Measurements of the Second Period.

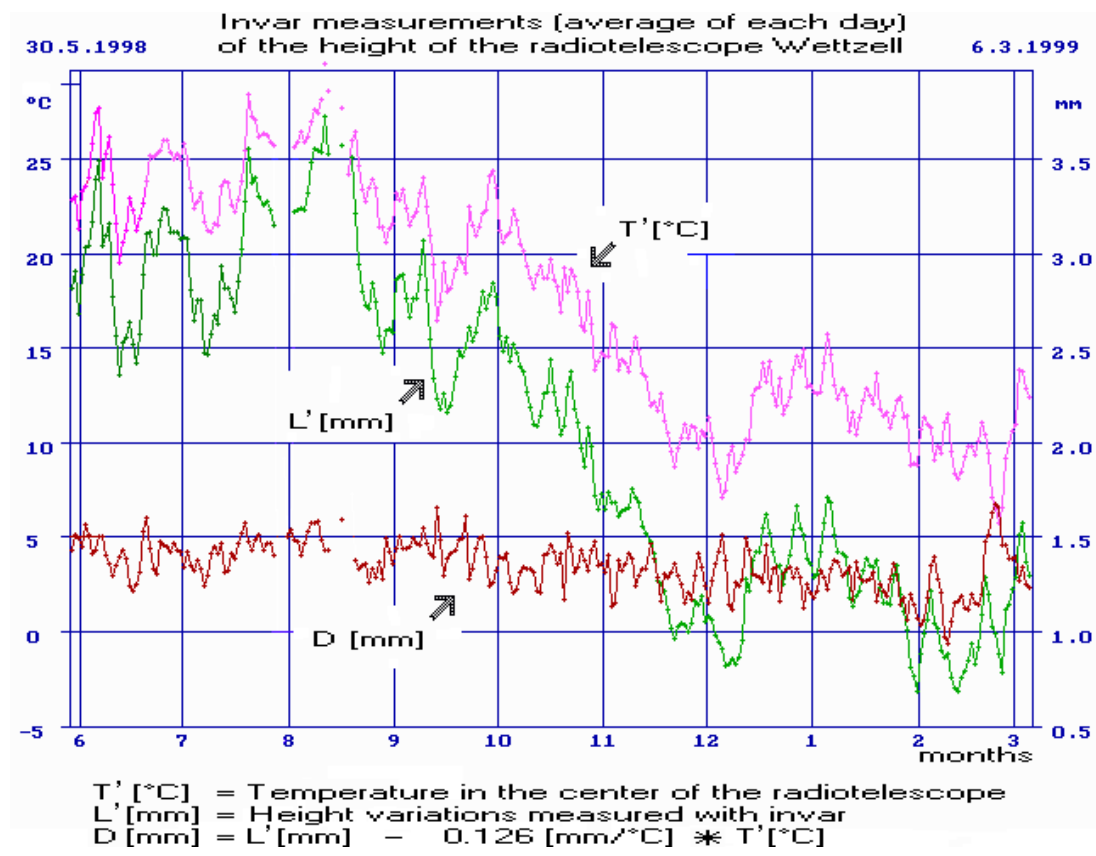


Fig. 6: Correlation between Temperature and Height of the Second Measuring Period.

# The First Campaign of Observations with the VLBI-Module of TIGO

HAYO HASE\*, LEONID PETROV†

## Abstract

The new 6m radiotelescope TIGO located in 60 meter distance from the 20 meter WETTZELL antenna participated in several VLBI experiments since November 1997. The purpose of this observations was to evaluate performance of the antenna and to acquire experience in short baseline phase-delay VLBI. The results of these first experiments are presented. VLBI measurements of length of the short baseline TIGOWTZL–WETTZELL show submillimeter repeatability and agree with results of local survey within its formal uncertainty.

## 1 Design of the TIGO-Radiotelescope

The Transportable Integrated Geodetic Observatory (TIGO) is designed as a fundamental station. Fundamental stations are the backbone for the realization of the terrestrial reference system since they are equipped with all relevant geodetic instruments. Therefore TIGO includes currently a VLBI-module, a SLR-module, GPS-receivers, super conducting gravity meter, seismometer, meteorological sensors including a water vapour radiometer.

The ideal terrestrial reference system would be based on a globally uniform distribution of observing sites. A poor representation of Earth by observing stations within the terrestrial reference frame will result in systematic errors. The reality shows wide areas without fundamental stations, especially in the southern hemisphere. Within the international efforts to improve the distribution of observing sites supporting the terrestrial reference frame, the Bundesamt für Kartographie und Geodäsie has developed and built the transportable fundamental station TIGO. The *transportability* of TIGO enables to setup a fundamental station at the *most beneficial* site for the realization of a terrestrial reference system [2].

The largest component of TIGO is the radiotelescope for VLBI which had to be designed to fit in a 12m-container. This requirement is a strong restriction for the design and the construction of the radiotelescope for geodetic VLBI. It requests

- high slewing velocity,
- reflector as large and as stiff as possible with high surface accuracy,
- high antenna efficiency,
- truly intersecting axes for the definition of the geometrical reference point as invariant point regarding source tracking,
- accessibility of the geometrical reference point for control surveys for verification of site stability.

In order to fit these criteria the concept of an offset-antenna with a receiver in the primary focus had been chosen. The asymmetrical construction allowed to tilt the receiver from the vertex axis of the primary mirror by 35.8°. The full dish is illuminated and the reflected signal is completely used. The optical scheme of the antenna is shown in figure 1.

---

\*Bundesamt für Kartographie und Geodäsie Fundamentalstation Wettzell, e-mail: hase@wettzell.ifag.de

†Geodätisches Institut der Universität Bonn e-mail: petrov@kuestner.geod.uni-bonn.de (on leave from Pulkovo Observatory)

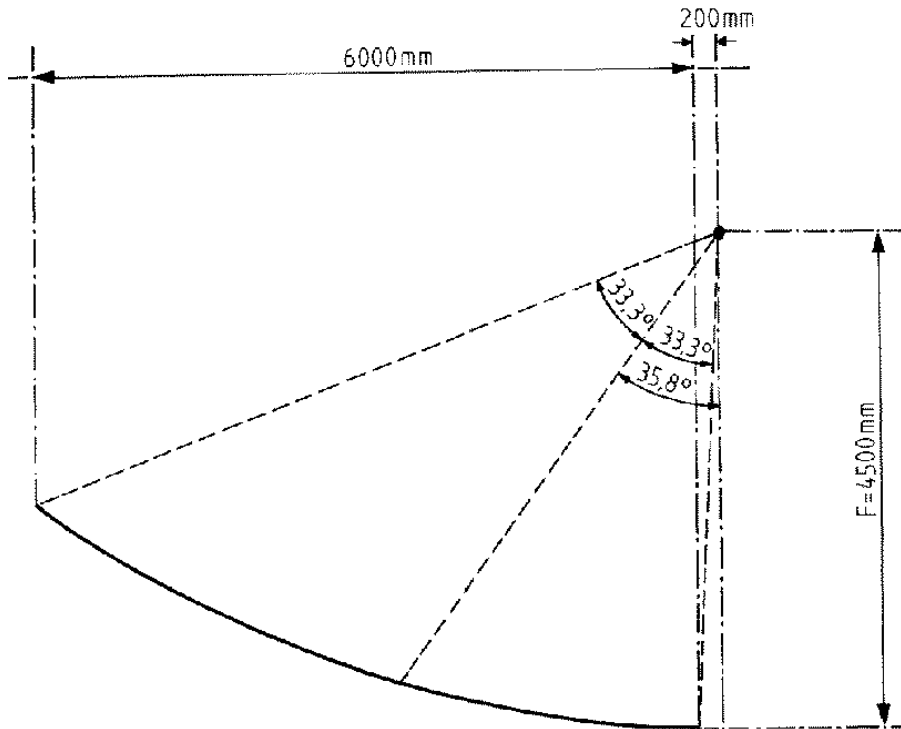


Fig. 1: Optical scheme of the antenna

At the primary focus of the offset reflector a NASA standard S/X dualband cryogenic receiver is installed. Its first amplifier stages consist of HEMTs operated at about 22K resp. 60K. It is possible to observe right hand circulated polarization in the frequency spectra of 2.216... 2.350 GHz and of 8.108... 9.036 GHz. The TIGO VLBI-module is equipped with a VLBA4 terminal, which supports the Mk4 and the Mk3a standard. Recording is done on one-inch-video-thintapes with a VLBA4 tape recorder.

## 2 First Observations

The first fringe test was carried out on November 11, 1997.

TIGO has participated in a number of EUROPE, NEOS-A and some Wettzell-tie experiments. Table 1 shows successful experiments.

Tab. 1: Successful experiments with TIGO.

N	Date	Experiment
1	02-FEB-98	Europe-41
2	19-MAY-98	NEOS-A-264
3	22-JUN-98	Europe-43
4	20-JUL-98	Wettzell-tie-1
5	17-AUG-98	Europe-44
6	14-DEC-98	Europe-46

### 3 System Performance

The conducted experiments allowed to investigate the reached system performance in detail. The dependence of system temperature at X- and S-band is shown in fig. 2).

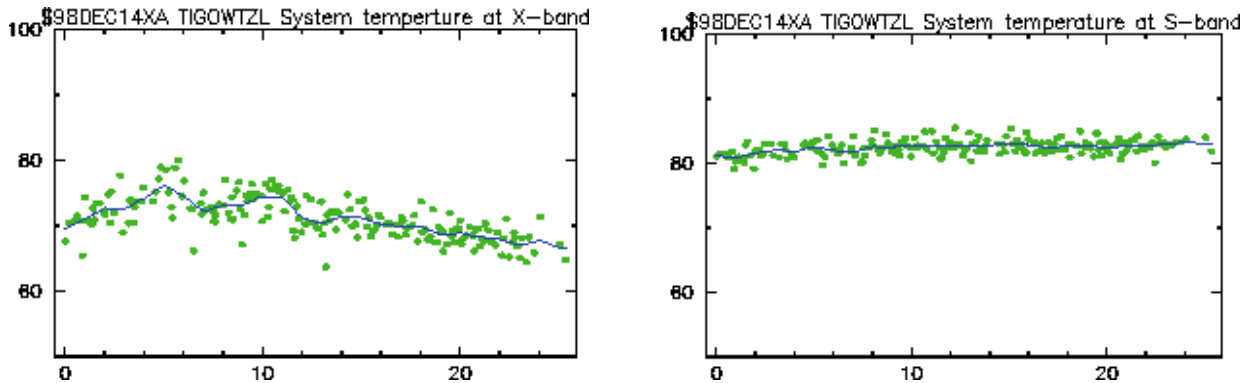


Fig. 2: System temperature in X- and S-band versus time in hours during EUROPE-46.

A number of air masses was computed on the basis of elevation angle using Chao wet mapping function [1]. It was found that the system temperature has a weak dependency on a number air mass except slight increasing in observations near zenith (fig. 3). This indicates a little spillover of ground noise due to the small dish diameter.

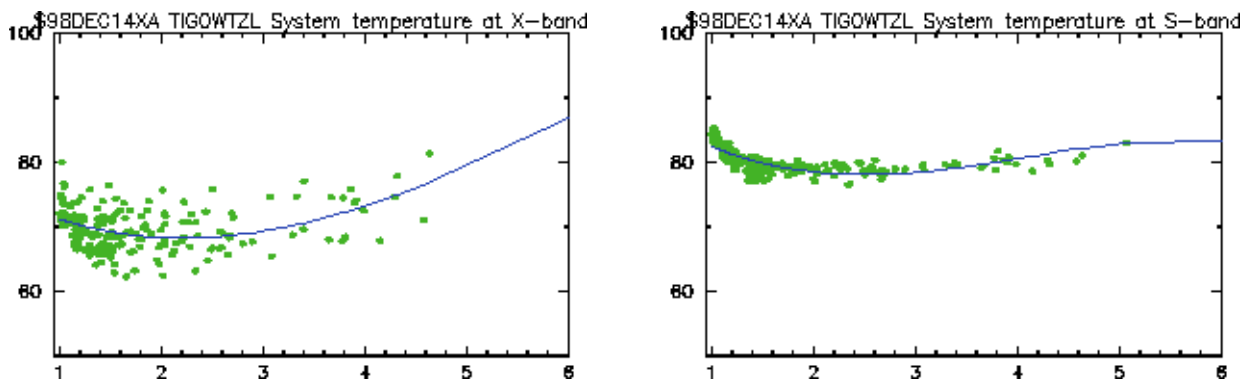


Fig. 3: System temperature in X- and S-band versus number of air masses.

TIGO and Wettzell used their own H-masers in all experiments. Therefore the clock performance could be studied. The analysis of clock performance didn't reveal any problems. Plots of the TIGO clock behaviour relative to Wettzell during the experiment 98JUL20XK as a function of time obtained from the baseline TIGOWTZL-WETTZELL (after subtraction of a linear trend) are shown in figure 4 (phase delay solution left and group delay solution right). We see only smooth variations within  $[-100, +100]$  psec interval which indicate both a good quality of hydrogen frequency standards and the lack of strong instrumental errors of clock-like nature. There is no substantial deviation between the clock function derived from phase and group delay measurements.

Under the best sky conditions (clear night) the system equivalent flux density (SEFD) is about 7000 Jy at X-band and 13000 Jy at S-band. Aperture efficiency is 70% at X-band. The S-band performance is not as good as in X-band.

One of the reasons might be that the S-band polarizer is realized by outcouplers from the feed and a coaxial combining networking. It therefore requires a piece of cable to guide the S-band signals into the dewar. This is different for the X-band which is guided through waveguides and via a waveguide polarizer directly into the dewar. Therefore the signal flow between the feed and the dewar with its first, cryogenic amplifier is different for both bands. Dual frequency feedhorns require always a compromise in their optimization. Since the wavelengths in X-band are shorter and therefore more

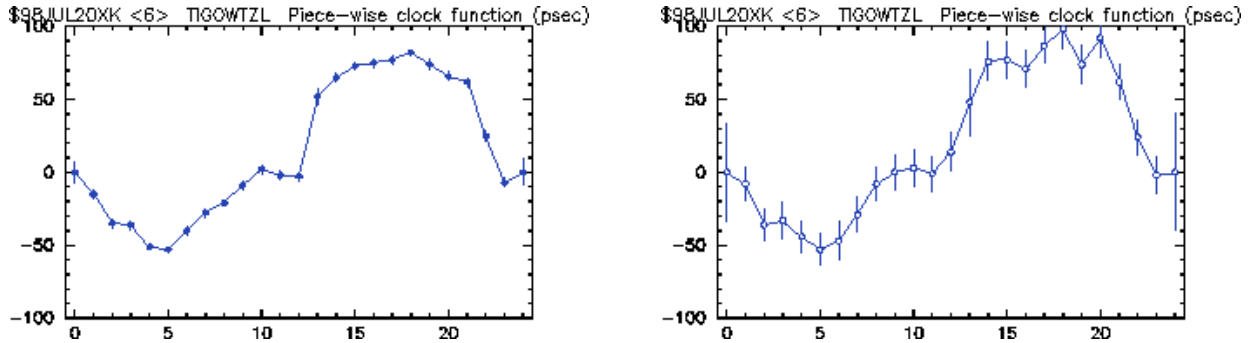


Fig. 4: Clock behavior of TIGOWTZL relative to WETTZELL in phase delay and group delay solution after removal of linear trend. Argument is time in hours.

accurate, the TIGO feedhorn was optimized for X-band reception. However the losses in the short piece of cable before the amplifier are critical for the performance in S-band and can still be optimized.

Another possible cause for the high SEFD in S-band might be spillover in S-band, which has been experienced and is a known problem with primary focus antennas. In addition a parasite leakage of left hand circulated polarization is possible. These suggestions are still under investigation.

TIGO participated in too few campaigns to gather sufficient statistics for the investigation of its repeatability on long baselines. We can compare formal uncertainties of TIGO position adjustments with uncertainties of station position adjustments of the 20-meter antenna WETTZELL. A special analysis of the experiment EUROPE43 has been made. The data set was slightly reduced: only those scans where both TIGOWTZL and WETTZELL provided observations of good quality were left, other scans where one of the stations didn't observe or yielded observations of bad quality were not used in this analysis. Two solutions were produced: all observations of WETTZELL had been excluded in the first run and all observations of TIGOWTZL had been excluded in the second run. Formal uncertainties of the stations position obtained in these solutions are presented in the table 2.

Tab. 2: Comparison of station coordinates from two analyses of EUROPE-43 with either TIGOWTZL or WETTZELL as a network station. The network configuration is almost exactly the same.

Comp	TIGOWTZL	WETTZELL
U-comp	16.0 mm	10.7 mm
E-comp	3.8 mm	2.4 mm
N-comp	5.0 mm	3.6 mm

We modeled the situation what would occur if the 6-meters TIGO radiotelescope would replace the 20-meter WETTZELL antenna in that experiment. The geometry of the network is almost identical, the number of measurements is the same, the only factors which affect the results are differences in stations performance. The answer is: the formal uncertainties of the station position would increase by 50%.

Phase delay and group delay solutions were obtained using only observations at the short baseline TIGOWTZL–WETTZELL (see fig 5). Phase delay ambiguities can be easily resolved for a short baseline. Residual plots of the baseline length are presented in figure 6.

The values of the baseline length agree very well with the results of measurements of the baseline derived from local surveys. Up to now only two independent local surveys have been carried out. In 1996 one survey of the control network of existing Wettzell station was carried out by H. Lang with high precise theodolites, ranging instrument Mekometer 5000 and GPS receivers [3]. At that time the TIGO reference markers for the TIGO network had not been installed. In 1997 another local survey of the TIGO network and its reference markers which can be seen as an appendix to the Wettzell control network had been conducted by C. Jocham with a tachymeter Sokkia Net2B and leveling instrument Zeiss DiNi10 [4]. Both independent campaigns have been transformed using identical points of both networks and resulting in the baseline length derived from the local survey given in table 3. A new

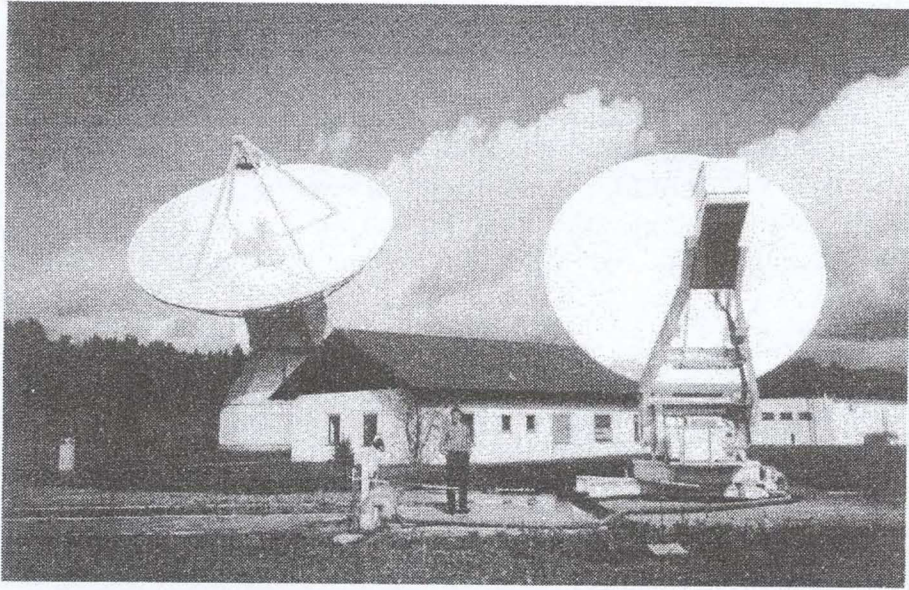


Fig. 5: 20-meter antenna WETTZELL (left) and 6-meter antenna TIGO(right)

local survey of the new extended Wettzell control network with the direct measurement of the baseline WETTZELL-TIGOWTZL is planned in 1999.

Tab. 3: Baseline WETTZELL-TIGOWTZL determined with different methods (in mm).

Data	Average	$\sigma$	repeatability
X-band group delay	59124.8	2.5	1.6
X-band phase delay	59124.8	0.3	0.4
local survey	59125.9	0.7	—

The formal errors of the baseline length determination from phase delay VLBI are about 0.3mm and the repeatability of the adjustments over 5 experiments provides the estimates of the formal errors. They indicate due to the lack of systematics of instrumental nature the possibility to achieve an accuracy in the determination of station position at submillimeter level. This accuracy approaches the mechanical limit of 0.2 mm which is the amount of space in each of the bearings in order to allow the antenna to move.

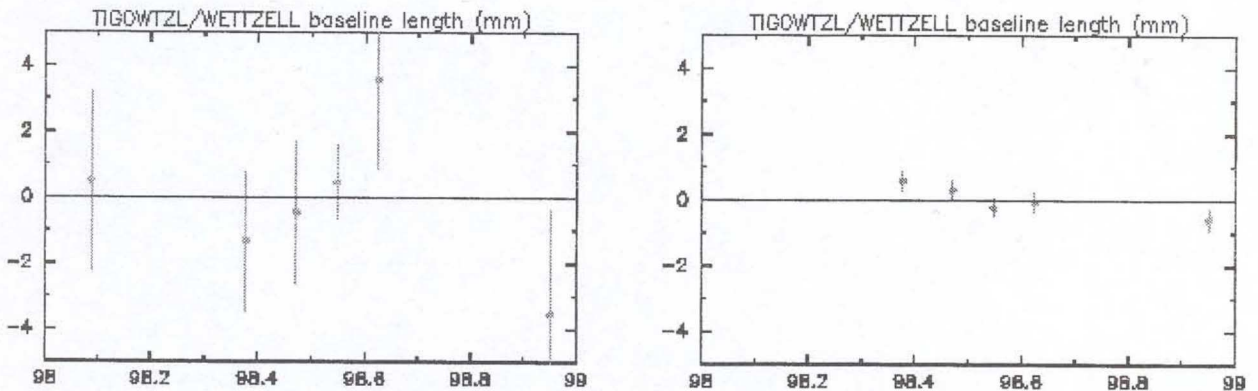


Fig. 6: Baseline length evolution after removal the average value obtained from group delay solutions (left) and from phase delay solutions (right). Argument is time in years.

## 4 Conclusions

The participation of 6-meter TIGO antenna in real VLBI experiments is considered as successful. Formal uncertainties of vertical position are in the range 10–20mm and formal uncertainties of determination of horizontal position are in the range 2–4mm. Accuracy of determination of the short baseline TIGOWTZL–WETTZELL shows the lack of systematic effects exceeding 1mm level. The VLBI-Module is ready for its operational use. The major remaining problem is the sensitivity at S-band which is lower than expected. Ways of increasing the sensitivity at S-band are being investigated.

## Acknowledgement

The authors would like to thank the radiotelescope group at Wettzell, the VLBI group at the Geodetic Institute of the University of Bonn, the VLBI teams at Goddard Space Flight Center NASA and MIT Haystack Observatory for their support.

## References

- [1] Chao, C.C.: A model for tropospheric calibration from daily surface and radiosonde balloon measurements. Technical Memo, 391-350, Jet Propulsion Laboratory, 1972
- [2] Hase, H.: TIGO and its Future Application for the ITRF, Proceedings of the GEMSTONE Meeting, Tokio-Koganei, January 25-28, 1999, (*in preparation*)
- [3] Jocham, C.: Einmessung und Koordinierung eines Radio- und eines Laserteleskopes auf der Fundamentalstation Wettzell, Fachhochschule München, unpublished diploma thesis, 1998 (*in German*)
- [4] Lang, H.: Das 3D-Überwachungsnetz der Fundamentalstation Wettzell als Kombination von GPS- und terrestrischen Messungen. Allgemeine Vermessungsnachrichten, S. 203-213, Karlsruhe, 1996 (*in German*)

# Local Survey at the Effelsberg Radio Telescope 1997 - Preliminary Results

Axel Nothnagel, Christiane Wirtz, Martin Sauerbier, Martin Sobanski

Geodetic Institute of the University of Bonn, Nussallee 17, D-53115 Bonn

E-mail: nothnagel@uni-bonn.de

## Abstract

In summer 1996 a major repair of the Effelsberg 100 m radio telescope's ground track had to be carried out due to cracks in the tracks surface. This led to a significant permanent displacement of the VLBI reference point. A local survey was, therefore, organized to measure the position of the reference point with respect to three permanent ground markers which had also been used in earlier measurements of this type. Since the reference point is not accessible physically an excentric target mark close to the reference point had to be used which complicated the work extraordinarily. For the analysis of the measurements a model is developed which a) describes the movements of the excentric target mark when the telescope is moved in azimuth and elevation and b) which corrects for thermal expansion effects. In order to compare the 1997 survey with another one carried out in 1992 a re-computation of the earlier measurement is done on the basis of the model mentioned above. The comparison of the two surveys yields a significant increase in height of the Effelsberg telescope of  $+25.4 \pm 3$  mm from 1992 to 1997.



*Fig. 1: Location of target mark at telescope in the middle of the cross-bar*

## 1 Introduction

After 24 years of operation the Effelsberg 100 m radio telescope of the Max-Planck-Institute for Radio Astronomy suffered severe damage of the ground track on which the antenna rotates. Cracks in the metal distorted the horizontal plane and satisfactory pointing accuracy which is necessary at higher observing frequencies could not be maintained any more. The telescope was jacked up temporarily and

the track was replaced completely. In addition, the wheels were milled into a conical shape with the tip of the conus being fictitiously located at the azimuth rotation axis. Through these modifications the telescope could not be placed in the same position as before the repairs when it was lowered onto the track again.

In geodetic VLBI all parameters estimated in the data adjustments are referred to the so-called VLBI reference point. In the case of an azimuth-elevation mount as the Effelsberg telescope is constructed the reference point is either the point where both axis intersect or, if they do not intersect, it is the point of the azimuth axis where the distance to the elevation axis is minimal (e.g. MA 1978; NOTHNAGEL et al. 1995). This point is invariant to any antenna movements necessary for the observations. Since any man-made changes in the 3-dimensional position of the reference point causes discontinuities in the time series measured with geodetic VLBI the displacements have to be determined to permit a correction of the time series.



*Fig. 2: Location of target mark within cross-bar. The little sphere is mounted at the end of the rod in the middle of the circular plate.*

## 2 Measurement setup

The VLBI reference point of the Effelsberg 100 m telescope, as of almost all other telescopes, is, unfortunately, not physically accessible and has to be represented indirectly. Here, the reference point lies within the main support beam which serves as the physical elevation axis (Fig. 1). In 1978 an excentric marker was, therefore, brought in place by mounting a target mark to this beam relatively near the VLBI reference point (MIEBACH AND WERTGEN 1980). The target consists of a little sphere of 15 mm in diameter (Fig. 2). In order to check the behaviour of the main beam the target was fixed to a rod which was mounted vertically in the beam and which has an additional target mark close to the geometrical elevation axis (Fig. 3). The rod was placed as centric as possible in the middle of the cross-bar supporting the vertex of the parabola. The middle of this intersection should mark the azimuth axis if the telescope points towards zenith.

However, measurements at the time of the implementation of the marker yielded an offset of the elevation axis in front of the azimuth axis of 10.3 mm. The mounting point of the rod holding the marker was determined to be 9.5 mm in front of the azimuth axis (Fig. 3). In the vertical the little sphere was mounted 1186.5 mm below the elevation axis.

The little sphere was used as the sole representation of the reference point. When the telescope is driven to different azimuth and elevation positions the little sphere describes a body with the VLBI reference point as the center. Therefore, the coordinates of the little sphere in different positions of the telescope had to be determined in a first step.

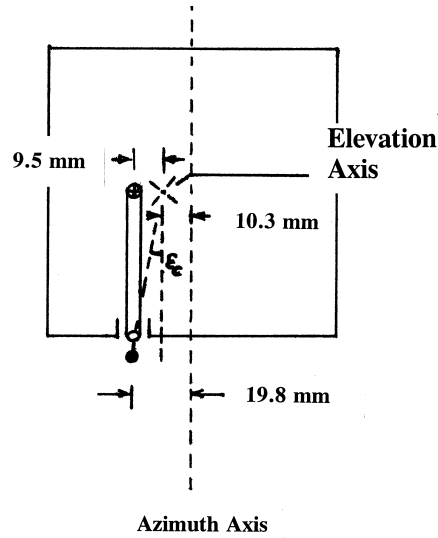


Fig. 3: Location of target mark at the end of the vertical rod at the bottom of the main support beam as seen from elevation bearing.

On the basis of earlier measurements three ground markers served as the ground network which was checked by precise angle and distance measurements before and after the locations of the target mark were measured. For the determination of the coordinates of the target mark the three ground points were occupied with electronic theodolites (2 Wild TC 1600, 1 Geodimeter 520 S). In order to compute the horizontal coordinates of the sphere by the surveying method of "Cut by Angles" in each position the sphere had to be aimed at by at least two theodolites simultaneously. The vertical positions were determined by measuring zenith distances.

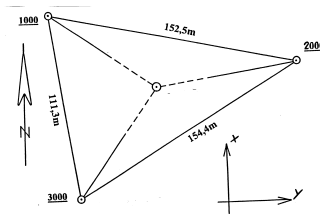


Fig. 4: Layout of ground network.

From an error propagation point of view it would have been preferable to determine coordinates of the sphere with a homogeneous distribution of azimuth and elevation angles. However, the beams of the parabola support structure and the extended dimensions of the elevators at the elevation bearing towers inhibited an unobstructed view onto the sphere in all orientations of the telescope. During a five hour period the little sphere was aimed at in 52 different positions simultaneously by pairs of theodolites. Only for three positions at elevation angles above  $85^\circ$  elevation the sphere was visible by all three theodolites and the respective redundant readings could be taken.

### 3 Data reduction

The initial reduction of measurements and the computations of the set of coordinates of the sphere yields a cloud of raw point coordinates. In order to end up with the coordinates of the VLBI reference point there has to be a two step approach. In a first step the raw points have to be corrected for thermal expansion of the telescope and for gravitational deformation of the main support beam. In a

second step the movements of the sphere when the antenna turns in azimuth and elevation has to be modelled in order to estimate the VLBI reference point which is, as mentioned already, invariant against any movements of the telescope.

### 3.1 Temperature corrections

The thermal expansion of a telescope depends on the temperature of the metal rather than on the ambient temperature which needs some time to creep into the metal structure. The metal temperature was available from several sensors mounted at different locations of the telescope structure and an average was computed for further use. During the course of the measurements which started at 8h00 in the morning the temperature rose steadily from 8° to 13° C at 1h00 p.m.. Due to the height of the support beams of 50 m a temperature correction of

$$dh[mm] = -0.625 \cdot (T - T_0)[^\circ C] \quad (1)$$

had to be applied leading to a 3 mm height difference between the beginning and the end of the measurements.

### 3.2 Bending corrections

The main reflector surface of the Effelsberg radio telescope is constructed as a paraboloid which, if tilted, will always appear as a paraboloid but with slightly different parameters and a different focal point owing to homologous deformation. Most of the weight of the reflector, therefore, presses upon the center of the main horizontal support beam. Although manufactured as rigid as possible the middle of the beam encounters a vertical bending of 19 mm with respect to a straight line when the antenna points at zenith (MIEBACH AND WERNTGEN 1980). At the same time the beam is not bent horizontally or, in other words, it lies in a vertical plane (Fig. 5a).

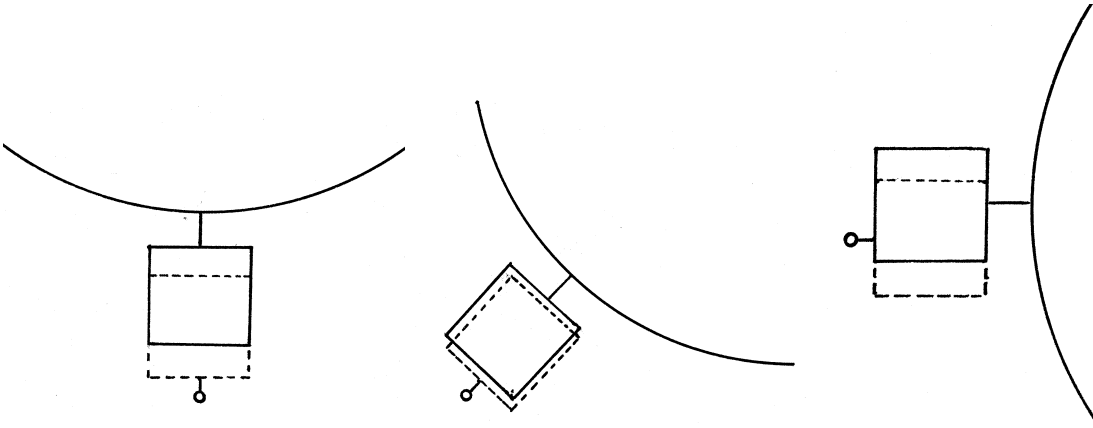


Fig. 5: Displacement of reference point due to gravitational bending as seen from one of the elevation bearings. The dashed profile represents the middle of the beam where the target is mounted.

When the antenna points at a lower elevation the main beam relaxes towards the radio source but, at the same time, bends towards the ground in the direction perpendicular to the main axis (Fig. 5b). In the extreme case of an observation at zero degrees elevation there is maximum bending towards the ground and zero bending in the direction where the antenna points at (Fig. 5c). Earlier measurements of a reference marker in the middle of the hollow beam produced a non-linear relationship between the position of the marker and the elevation (Fig. 6) (MIEBACH AND WERNTGEN 1980). With a semi-analytical function the corrections in the vertical and in the direction of the tilted telescope were computed and applied as corrections to the respective local coordinates of the target points.

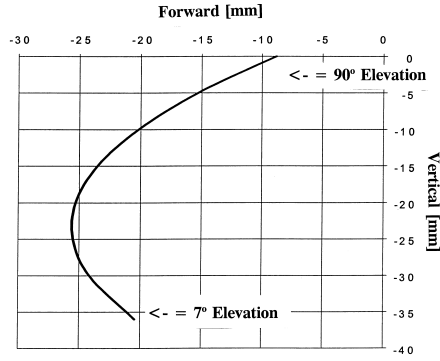


Fig. 6: Movement of a point in the middle of the main beam depending on the elevation angle of the telescope. Forward in this context means towards the tilting direction. The zero point for the vertical is chosen for the geometry when the telescope aims at zenith.

### 3.3 Envelope model

After correcting the raw coordinates the target sphere is supposed to describe an envelope which consists of two components. When the telescope points at zenith and rotates about the azimuth axis the target mark describes a circle due to the excentricity of the marker. A second component is added when the telescope turns about the elevation axis rotating the target mark upwards on a segment of a circle (Fig. 7).

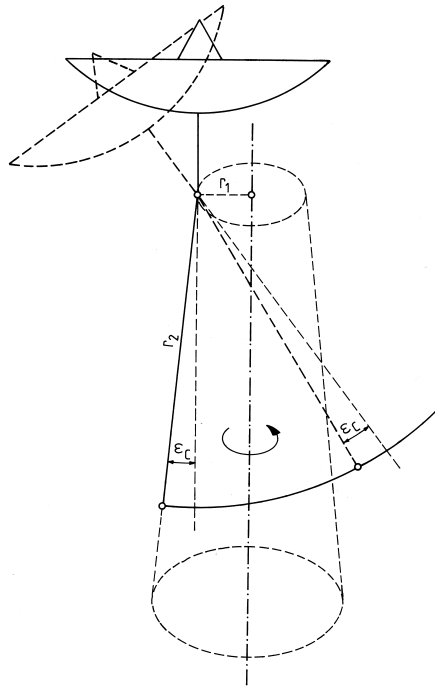


Fig. 7: Geometry of the target mark relative to elevation bearing. When the telescope points at zenith and it is turned about the azimuth axis the  $r_2$  vector with the target mark at the end describes a conus. Tilting the telescope about the elevation axis moves the target mark on a circle about the elevation axis with the radius  $r_2$ .

The movements of the target mark can be described by simple functions of three dimensional coordinates  $X_i, Y_i, Z_i$  depending on azimuth  $\kappa$ , elevation angle  $\epsilon$ , the center point  $X_M, Y_M, Z_M$ , the excentricity  $r_1$  and the length of the rod  $r_2$ . Due to the fact that the little sphere is not mounted directly vertically

underneath the elevation axis an additional constant elevation angle  $\epsilon_c = 0.46^\circ$  has to be added.

$$X_i = X_M + r_1 \cdot \cos\kappa - r_2 \cdot \cos(\epsilon + \epsilon_c) \cos\kappa \quad (2)$$

$$Y_i = Y_M + r_1 \cdot \sin\kappa - r_2 \cdot \cos(\epsilon + \epsilon_c) \sin\kappa \quad (3)$$

$$Z_i = Z_M - r_2 \cdot \sin(\epsilon + \epsilon_c) \quad (4)$$

Unfortunately, this function was available only shortly before the presentation of this paper. Therefore, a coarse approximation had to be used for the preliminary computations. In a least squares adjustment the coordinate triplets corrected in 3.1 and 3.2 served as observations with the above observation equations for the coordinates of the center point and the distance  $r_2$  as unknown parameters. The least squares fit yielded the coordinates for the reference point in table (1).

Tab. 1: Preliminary coordinates of VLBI reference point in the Gauß-Krüger coordinate system from 1997 measurements

$X_M$	5 599 160,434 m	$\pm 0.7$ mm
$Y_M$	2 562 702,079 m	$\pm 0.7$ mm
$Z_M$	368,978 m	$\pm 1.0$ mm
$r_2$	1.1601 m	$\pm 0.9$ mm

It should be mentioned here that the vertical component is referred to a metal temperature of  $0^\circ$  C.

### 3.4 Recomputation of 1992 measurements

In order to determine the displacement of the VLBI reference point two sets of measurements, one before and one after the replacement of the ground track, have to be performed. In 1992 the surveying authority of the state of North Rhine-Westfalia had carried out a similar set of measurements which could be used as a zero-epoch basis. For a rigorous determination of the displacement these measurements were re-computed on the basis of the corrections and models described above.

Tab. 2: Preliminary coordinates of VLBI reference point in the Gauß-Krüger coordinate system from 1992 measurements

$X_M$	5 599 160,429 m	$\pm 1.2$ mm
$Y_M$	2 562 702,078 m	$\pm 1.2$ mm
$Z_M$	368,954 m	$\pm 2.5$ mm
$r_2$	1.1623 m	$\pm 1.4$ mm

Again the vertical component is referred to  $0^\circ$  C. However, the temperature correction could only be applied through an approximation since only one temperature reading was taken during the measurements. Thus, there is no way of correcting for any changes in temperature during the course of the measurements.

## 4 Results

Table 3 contains the differences in the local topocentric coordinates between the epochs of 1992 and 1997. Due to the fact that the model of the movement of the target mark with respect to the VLBI reference point as described in formulas (2) - (4) was applied only in a coarse approximation the results have to be considered preliminary and the formal errors were, therefore, inflated by a factor of 3.

Tab. 3: Preliminary coordinate differences between the 1997 and 1992 measurements in the sense 1997 - 1992

$\Delta North$	0,001 m	$\pm 5$ mm
$\Delta East$	0,005 m	$\pm 5$ mm
$\Delta Vertical$	0.0254 m	$\pm 8$ mm

Considering that the movements of the target within the main elevation axis support beam as described by figure 6 were determined already 20 years ago the results contain some further uncertainties. In order to check the response of the elevation beam to tilting in elevation the measurements within the beam as carried out by MIEBACH AND WERNTGEN (1980) should be repeated. In addition, the determination of the VLBI reference point within the adjustment of individual positions of the target mark has to be repeated with the correct model as described in formulas (2) to (4). Furthermore, this type of measurement has to be repeated in closer intervals in order to monitor the stability of the Effelsberg telescope with respect to the surroundings.

## 5 References

- Ma C. (1978): *Very Long Baseline Interferometry Applied to Polar Motion, Relativity and Geodesy* NASA Technical Memorandum 79582, Goddard Space Flight Center, Greenbelt Maryland
- Miebach P., H.-J. Werntgen (1980): UNTERSUCHUNGEN ZUR STABILITÄT DES ACHSENSCHNITTPUNKTES AM EFFELBERGER RADIOTELESKOP Diploma Thesis, Geodetic Institute of the University of Bonn
- Nothnagel A., M. Pilhatsch, R. Haas (1995): *Investigations of Thermal Height Changes of Geodetic VLBI Telescopes* Proceedings of the Tenth Working Meeting on European VLBI for Geodesy and Astrometry, Matera, Italy; 121 - 133

## Observatory Report from Effelsberg

W. Alef, R. Porcas (MPIfR, Bonn)

February, 1999

1. The new 8.4 GHz receiver has not yet been installed on the telescope but it is now planned to support the "R&D" wide frequency range at X-band.
2. A vacuum switch has been installed on the MK4 terminal to permit both thick and thin tape operation.
3. The tape drive electronics of the MK4 recorder is being upgraded to VLBA style, to permit its use as a second recorder with the VLBA terminal, and to increase its reliability. This is planned for March 1999.
4. An additional 4 BBCs have been ordered for the VLBA terminal, to bring the total to 8, making better compatibility for joint observations with the VLBA. An upgrade of the VLBA formatter is also planned, to permit dual-recorder ("double burst mode") operation together with the VLBA.
5. Replacement of the outer antenna panels with perforated aluminium panels has now been completed.
6. The "friend of VLBI" in Effelsberg (Reinhard Schulze) will retire in the middle of this year. It is planned to appoint a new person to support VLBI observing.

# Medicina and Noto Stations Report

Alessandro Orfei, Gino Tuccari, Franco Mantovani

*Istituto di Radioastronomia, Bologna, Italy*

## Abstract

In this contribution we report on the progresses made after the 12th Working Meeting held in Hønefoss, Norway, at the two Radioastronomy Stations of Medicina and Noto run by the Istituto di Radioastronomia di Bologna del Consiglio Nazionale delle Ricerche.

## Introduction

In the last couple of years, the main goal at both the Medicina and the Noto Stations was to get the telescope agile in changing the observing frequency. Achieving this goal will greatly increase the observational efficiency of the telescopes. Moreover it will make the operation of changing the receivers more safe and it makes this task independent to the weather conditions.

The first part of the project has been completed at both telescopes and the new subreflector is fully in operation at both stations. The increased flexibility in changing frequency, together with the facility of recording both thick and thin tapes implemented at all the European VLBI Network (EVN) stations, has immediately produced an increase in the number of geodetic VLBI observations to which mainly the Medicina Station will take part in 1999.

On the other hand, the increased observational efficiency asks for more time to be spent as telescope operators to the technicians during the observations. In order to get a reasonable compromise between the time spent checking and upgrading hardware and software, and the time spent as operator by this personnel, we have implemented the remote control for both the observations and the equipment, working at the same time for a greater reliability of the telescope as a whole. The goal is to safely run absentee observations.

## Medicina Station Report

In the following we list the main upgrading in both hardware and software done at the Medicina Station:

### Tape Recording

- a) The thin tape capability has been installed at the station with good results.

b) A problem due to the sliding of thin tapes has been solved adopting a new capstan with deeper grooves.

c) The write-head has been replaced at the end of 1998, since it worned out. The new one is of the old Metrum type. The read-head is also on its way to die. The new ordered head, made by Spin Physics, will have two triple cap heads to be mounted.

## Computer Control

a) A new version of the remote control programme for the SX receiver has been implemented. It allows a monitoring of the receiver status (criogenic temperature, vacuum pressure and so on) in real time.

b) To serve different type of observational projects, the computers facilities have been reorganized. Three computers are now available:

- a computer runs the Field System. It can be used to prepare schedules and procedures. The Fiels System version implemented is 9.3. This machine is connected to the server of the computer centre in Bologna.

- a computer with the Windows NT operating system, serves equipments like the polarimetre and the antenna levelmeters. Moreover, it acquires the GPS-Formatter clock offsets data, it keeps under control the receivers and it drives the movements of the secondary mirror.

- a computer with either Linux or Windows95 operating systems, is used as a general purpose machine and for data acquisition during spectroscopic observations making use of the autocorrelator, etc.

## Upgrading of the telescope

There are two projects for upgrading the telescope. The first is the completion of the frequency agility project. The second aims to a better efficiency at higher frequencies.

a) In order to complete the frequency agility project for the Medicina dish we are planning to place in the secondary focus room a series of receivers which covers the frequencies between 4.3 GHz and 48 GHz. The electromagnetic design of the eight feeds system is ready and the parameters to design the mechanical support for the receivers are now available. The design of the electronics part of the eight receivers is also at a good stage. The priority is to build the 6 cm and the 5 cm receivers first, to fulfil the EVN requirements about the observing bands which should be available at any station.

b) A project is going on for the implementation on the telescope of an active surface to compensate the loss in efficiency due to gravity deformation of the primary mirror of the parabolic antenna. After a series of tests with the prototype of a mechanical actuator, calculations have been made to figure out the parameters for an 'actuators network' which will keep under control the full surface of the dish. In the meantime we are looking for a proper electronics to be used and for an engineering phase of the linear actuator. Furthermore, the cost of more accurate panels for the dish and of the actuators itself have been assessed. A system of this kind, together with new panels of enhanced precision surface, will rise very much the antenna efficiency at frequencies up to 43GHz.

## Equipment for Single Dish Observations

- a) Polarimetric observations facilities has been implemented. Besides astronomic uses, it is now possible to measure the amount of crosstalk polarization between Left and Right Circular Polarization locally.
- b) A project is in progress to design a dichroic mirror to observe at two different frequencies (7 GHz and 22 GHz) at the same time.
- c) By exploiting a new system for very high resolution spectrum analyzer (Serendip IV), which is working in parallel with the observations, a window on a real time database of the narrow band interferences situation at Medicina should be open. In the next months the machine will be enhanced to cover about 15 MHz of instantaneous bandwidth. The software to accumulate files, processing and displaying the results is almost ready and preliminary outputs are already available.
- d) The software of the 'time and frequency high resolution spectrometer' it has been completed. A single dish observation with up to 20 MHz instantaneous bandwidth and up to 132000 channels can now be automatically performed. Single shot as well as more complicated observing schedule are possible. A real time displaying of the accumulating spectra is available.

## Geodetic Observations

The geodetic experiments run by the Medicina Station in **1998** are listed in Table 1. Three experiments 'Mars Pathfinder VLBI', designed for the determination of the Martian

**Tab. 1 - List of Geodetic VLBI observations in 1998**

EXPERIMENT	DATE	TIME	STATIONS
CORE-B207	26-JAN	18:30	Ft-Gc-Kk-Ka-Ny-Sm-Mc
EUROPE-7	02-FEB	12:00	Ny-On-Wz-Sm-Ma-Mc-Nt-Yb
VLBA7	09-FEB	14:00	VLBA- Kk-On-Gc-Mc-Gn-Gg-Wf-Ny
VLBA8	15-APR	20:00	VLBA- Kk-On-Gc-Mc-Gn-Gg-Wf-Ny
EUROPE-42	20-APR	12:00	Ny-On-Wz-Sm-Ma-Mc-Nt-Yb
CORE-B208	22-APR	18:30	Ft-Gc-Kk-Ka-Ny-Sm-Mc
CORE-B209	17-JUN	18:30	Ft-Gc-Kk-Ka-Ny-Sm-Mc
EUROPE-43	22-JUN	12:00	Ny-On-Wz-Sm-Ma-Mc-Nt-Yb
VLBA9	24-JUN	20:00	VLBA- Kk-On-Gc-Mc-Gn-Gg-Wf-Ny
CORE-B210	15-JUL	18:30	Ft-Gc-Kk-Ka-Ny-Sm-Mc
VLBA10	10-AUG	14:00	VLBA- Kk-On-Gc-Mc-Gn-Gg-Wf-Ny
EUROPE-44	17-AUG	12:00	Ny-On-Wz-Sm-Ma-Mc-Nt-Yb
VLBA11	01-OCT	14:00	VLBA- Kk-On-Gc-Mc-Gn-Gg-Wf-Ny
CORE-B211	07-OCT	18:30	Ft-Gc-Kk-Ka-Ny-Sm-Mc
EUROPE-45	12-OCT	12:00	Ny-On-Wz-Sm-Ma-Mc-Nt-Yb
EUROPE-46	14-DEC	12:00	Ny-On-Wz-Sm-Ma-Mc-Nt-Yb-Eb
CORE-B212	16-DEC	18:30	Ft-Gc-Kk-Ka-Ny-Sm-Mc
VLBA12	21-DEC	16:00	VLBA- Kk-On-Gc-Mc-Gn-Gg-Wf-Ny

Precession Constants, of the relativistic precession of the perihelion of Mars to a few parts per thousands, of the Martian Length of Day to about 1 millisecond, were run on the following dates:

- 07 Jul MARS-15 (04:00 - 16:00 UT)
- 14 Aug MARS-16 (03:00 - 15:00 UT)
- 04 Sep MARS-17 (03:00 - 16:00 UT)

Since the Station has fulfilled the requirements to be a 'CORE' (Continuous Observations of the Rotation of the Earth) Station (namely: a) flexible and automatic frequency change; b) MKIV terminal; c) TAC for station timing system; d) daily GPS acquisition), it will take part to the 'CORE' projects. Moreover, during the present year **1999**, the Station will continue to observe the EUROPE and VLBA experiments. The 38 scheduled projects are listed in Table 2. The list contains 20 experiments more than in 1998, which represents an increase of more than 100% in observing time allowed for geodetic VLBI.

**Tab. 2 - List of Geodetic VLBI observations in 1999**

DATE	EXPERIMENT	DATE	EXPERIMENT
12-JAN	CORE-A053	29-JUN	CORE-A065
13-JAN	CORE-B401	13-JUL	CORE-A066
26-JAN	CORE-A054	15-JUL	CORE-B404
01-FEB	EUROPE-47	27-JUL	CORE-A067
09-FEB	CORE-A055	02-AUG	VLBA17
08-MAR	VLBA13	10-AUG	CORE-A068
09-MAR	CORE-A057	12-AUG	CORE-B405
23-MAR	CORE-A058	16-AUG	EUROPE-50
24-MAR	CORE-B402	24-AUG	CORE-A069
06-APR	CORE-A059	07-SEP	CORE-A070
15-APR	VLBA14	05-OCT	CORE-A072
20-APR	CORE-A060	11-OCT	EUROPE-51
26-APR	EUROPE-48	19-OCT	CORE-A073
04-MAY	CORE-A061	02-NOV	CORE-A074
05-MAY	CORE-B403	13-DEC	EUROPE-52
10-MAY	VLBA15	14-DEC	CORE-A077
18-MAY	CORE-A062	16-DEC	CORE-B406
21-JUN	VLBA16	20-DEC	VLBA18
28-JUN	EUROPE-49	28-DEC	CORE-A078

## **NOTO Station Report**

In the following, the main upgrading done in the recent past at the Noto Station are described.

### **The new subreflector**

During 1998 summer the new automatic subreflector positioning system has been mounted and successfully tested. The system similarly to Medicina, allows now to switch between the secondary mirror and the primary focus receiver in few minutes. The new equipment avoids the possibility to loose geo-experiments due to bad weather conditions.

### **A 12 GHz receiver for holography**

A new 12 GHz receiver has been added in the primary focus box, able to work phase-locked with H-maser. It is mainly oriented to holography of the main dish. Indeed the efficiency at 22 GHz is only a little bit increased with respect to the past, due to the use of a new subreflector mirror (rms 0.12 mm), and then the determination of the surface errors is mandatory.

### **A new primary focus receiver system**

The new primary focus receiver system is under construction and is expected to be operative in middle 1999. It includes 2.5, 3.6, 13, 18, 21, 49, 92 cm bands in dual polarization. It represents the second phase of the frequency agility program in Noto. The third phase will get the 0.7, 1.3, 6 cm bands operative in the secondary focus switching in few seconds through subreflector movement. In particular the new X will cover 8.1-8.9 GHz (wide band), and both SX bands will be cryogenically cooled.

### **New software**

New software procedures has been created in order to automatically set the system with the requested observing band.

### **The MKIV formatter**

The MKIV formatter is fully integrated in the VLBA environment and both formatters, VLBA and MKIV, are available.

### **Geodetic Observations**

In 1998 the Noto Station took part to 12 Geodetic VLBI experiments, namely 5 CORE-B, 5 EUROPE, 1 NEOS and BF43A.

In 1999 6 CORE-B, 6 EUROPE and 1 CRF experiments involving the Noto Station have been scheduled.

It is worth to mention that the Noto telescope is deeply involved in the VSOP (plus ground based telescopes which make use of the Canadian S2 recording terminal) survey, of compact extragalactic radiosources.

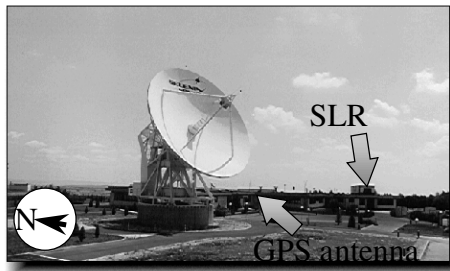
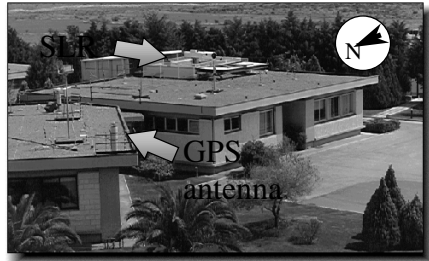
# Matera VLBI Station Status Report

F. Vespe<sup>(1)</sup>,  
G.Colucci<sup>(2)</sup>, D.Del Rosso<sup>(2)</sup>, L.Garramone<sup>(2)</sup>

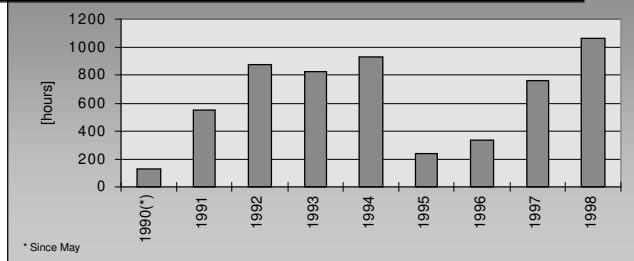


## The System

- The Matera VLBI system is operated, on behalf of Italian Space Agency (**ASI**), by ~~Nuova~~ Telespazio at **Centro di Geodesia Spaziale (CGS)** of Matera.
- The **CGS** came into operation on 1983 in the framework of an agreement with the Basilicata Regional Government and **ASI**.
- A fixed SLR system and a network of permanent GPS receivers (including one at Matera site) are also operated at **CGS**.
- The Matera VLBI system includes
  - X/S bands receiver
  - 20 meter diameter cassegrain antenna;
  - MARK-III D.A.T. and VLBA Recorder;



1998	Core-A			Europe		Intensive			Iris			Neos-A			Astron.			TOT.			
	#	Tot. [hh]	Lost [hh]	#	Tot. [hh]	Lost [hh]	#	Tot. [hh]	Lost [hh]	#	Tot. [hh]	Lost [hh]	#	Tot. [hh]	Lost [hh]	#	Tot. [hh]	Lost [hh]	#	Tot. [hh]	Lost [hh]
January	2	48	1.3																2	48	1.3
February	1	24		1	24				1	21									2	48	0.0
March	2	48					14	29	1.3	1	21		2	48					19	146	1.3
April	2	48		1	21		21	42	0.4	1	21		2	48	1.1				27	180	1.5
May	2	48				16	31			1	21		1	24					20	124	0.0
June	3	72		1	24														4	96	0.0
July	2	48	0.5																2	48	0.5
August	2	48		1	24														3	72	0.0
September	2	48	0.4													1	9		3	57	0.4
October	2	48	2.2	1	24	0.2	4	9							1	9		8	90	2.3	
November	2	48																	2	48	0.0
December	3	72		1	26														4	98	0.0
Tot.	25	600	4.3	6	143	0.2	55	111	1.7	3	63	0.0	5	120	1.1	2	18	0	96	1054	7.3



## Performed Upgrade

- In December 1996, in order to upgrade the system to the NASA Wide Band Standard, a new receiver (by ATSC) front end was installed.
  - Input frequencies:
    - S-band 2210 MHz to 2450 MHz
    - X-band 8180 MHz to 8980 MHz
- In January 1999 Linux FS 9.3.23 PC has been installed; the Antenna Control SW has been ported on the new platform by Telespazio. The new system is now ready to go.

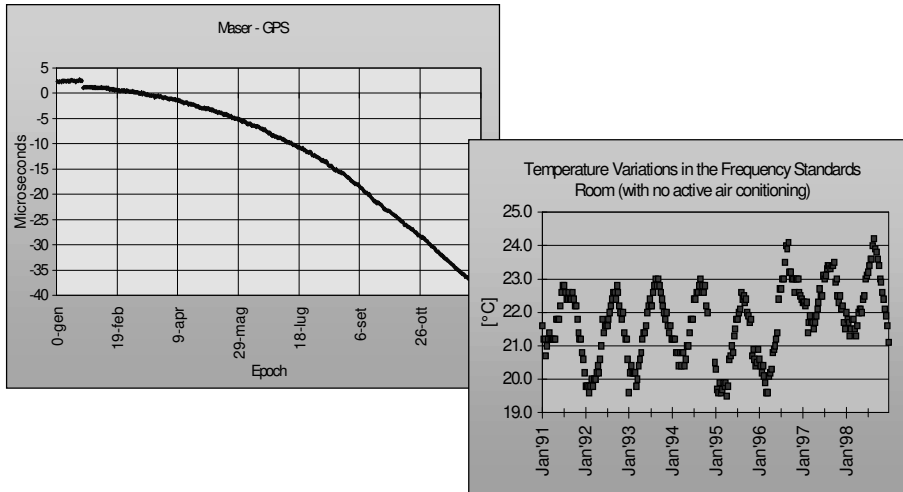
## Planned Upgrade

- In April 1999 Mark-IV upgrade (DAT and Recorder) will be performed by MIT Haystack.

## Most Significant System Failures

- January Cryogenic System Rotary Vane Vacuum Pump failure.
- February Cryogenic System failure.
- Marc P.C. Field System Hard Disk failure.
- May MAT board failure in V/C s/n 294.
- June RS 232-422 board failure due to thunderstorm.
- July VLBI recorder failure. Replaced relay on dual reel servo amplifier board.
- September Replaced cable from Antenna Unit to Ground Unit of Calibrator Delay with spares one.
- October Cryogenic System failure.
- October Elevation motor brake failure.
- December Local Oscillator failure on VC s/n 298. (Reported by Jim Martin of Washington correlator). Replaced by VC spare part.
- January '99 Headstack/inchworm failure. Repaired by Haystack.

## H-Maser



## On-line resource and contact points

**GeodAF** <http://geodaf.mt.asi.it>

**F. Vespe (ASI)**  
[vespe@asi.it](mailto:vespe@asi.it)

ASI CGS Geodesy Activities Manager

**D. Del Rosso (Tpz)**  
[domenico\\_delrosso@telespazio.it](mailto:domenico_delrosso@telespazio.it)

Telespazio Geodesy Activities Manager

**L. Garramone (Tpz)**  
[garramone@asi.it](mailto:garramone@asi.it)

Station Engineer

**G. Colucci (Tpz)**  
[vlbi@asi.it](mailto:vlbi@asi.it)

VLBI contact

# Geodetic Control of the Madrid DSS65 VLBI Antenna

Dirk Behrend and Antonio Rius

Institut d'Estudis Espacials de Catalunya (IEEC),  
Edif. Nexus-204, Gran Capità 2-4, 08034 Barcelona, Spain

## 1 Introduction

The NASA Madrid Deep Space Communications Complex (MDSCC), Spain, DSS65 VLBI antenna participates in the European geodetic VLBI network for determining horizontal as well as vertical crustal motion in Europe. In order to prevent local (site) movements from diluting the VLBI-derived plate motions the stability of the antenna over time must be secured. This is usually done by monitoring the stability of the reference point of the antenna which can be defined as the intersection point of the azimuth and elevation axes of the antenna.

In this report we investigate the stability of the DSS65 antenna using geodetic surveillance data taken by the Instituto Geográfico Nacional (IGN), Spain, at different epochs. Furthermore, we discuss the possibility of using levelling data of the azimuth runner level in order to determine the location of the reference point by means of an upward continuation model and to infer stability evidence from this.

## 2 Antenna Stability by a Multiple Intersection Technique

The standard procedure to monitor the stability of an antenna site is to look into geodetic surveillance data. To this end a local geodetic network has been set up at the MDSCC site consisting of 13 stations and having an inter-station separation of some 100 m. The stations are realized through massive concrete pillars and are tied to the higher order regional net. For the determination of the reference point of the DSS65 antenna a subnet of 6 stations was selected (see figure 1). The selection criteria were mainly good visibility of and short distance to the antenna. For the actual observations Wild T2 theodolites were mounted on the pillars of these stations. An additional station (MIRADOR) was chosen in order to have a well-defined reference for direction measurements. Figure 1 gives an overview of the local subnet including the DSS65 antenna. In the further evaluation it is assumed that the coordinates of the reference stations were stable over the past decade, i.e. that they did not show significant changes ( $> 0.5$  mm).

Following the same observation scheme the IGN performed 4 measurement campaigns (December 1988, March 1997, June 1997, and April 1998):

- The VLBI antenna was equipped with two markers (yellow and red) at the two extreme ends of the elevation axis. They have a diameter of about 3 cm and a height of approx. 2 cm.

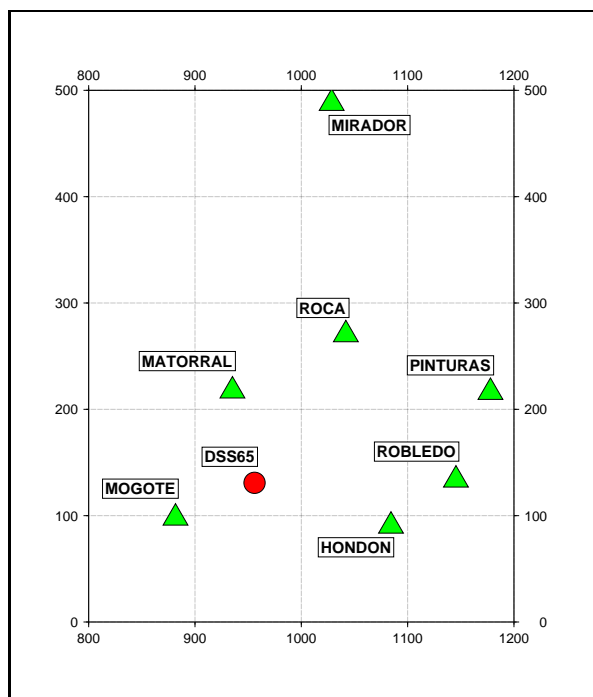


**Fig. 1:** Local geodetic subnet (6+1 stations) utilized in the geodetic measurements of the DSS65 VLBI antenna. Adding a constant of 393 000 m to the abscissae and 4 476 000 m to the ordinates results in UTM30 coordinates.

- The VLBI antenna was brought into the zenithal position and steered to the azimuth of  $0^\circ$ .
- From the local geodetic network direction and zenith angle measurements were taken to the markers.
- After a complete observation set the antenna was rotated about its azimuth axis and every  $30^\circ$  further sets were taken.

The two campaigns in 1997 are due to a repair work of the azimuth runner level (replacement of tracks and wheels) in April/May 1997 for which the upper part of the antenna was lifted up. This could have affected the location of the reference point creating a discontinuity in the VLBI data. With the help of the two campaigns such a discontinuity can be bridged.

Using all four data sets it is possible to determine 3D-coordinates of the reference point as well as changes thereof over time. The evaluation shall be broken down into the determination of the horizontal position and of the height. The former is used to check the horizontal stability, whereas the latter is taken to control the vertical stability.

## 2.1 Horizontal Stability

The determination of the horizontal coordinates is equivalent to finding the location of the azimuth axis. As the antenna was rotated about its azimuth axis in the observation procedure the two markers describe two concentric circles with the azimuth axis as the centre location.

### 2.1.1 Computational Procedure

The computation of the horizontal coordinates (UTM30) for the reference point shall be split as follows:

1. computation of the horizontal coordinates of the markers for the different positions of the VLBI antenna;
2. fitting of two concentric circles to these locations.

These two adjustment problems will be discussed in more detail in the following.

#### (a) UTM30 coordinates of the two markers

The available observables for computing UTM30 coordinates of the two markers in the different antenna positions are the direction observations taken from the 6 stations of the local subnet whose UTM30 coordinates are considered to be known and errorless. The computation of the unknown coordinates is equivalent to a multiple intersection method which can be solved in a least squares adjustment (Gauss-Markov model). The observation equation reads:

$$r_{i,N} = \arctan \left( \frac{x_N - x_i}{y_N - y_i} \right) + o_i .$$

In this equation the index  $i$  represents an arbitrary known station, whereas  $N$  stands for an unknown point. The unknown parameters are the coordinates of  $N(x, y)$  (i.e. of a marker position) and the orientation unknown  $o_i$  of the direction observations on the known station.  $r_{i,N}$  is the direction observation itself.

After linearization of the observation equation  $\underline{L} = \boldsymbol{\psi}(\underline{X})$  with a Taylor expansion and introduction of approximate values for the parameters  $\underline{X}_0$  a solution to the adjustment problem is found by

$$\hat{\underline{X}} = \underline{X}_0 + (\underline{\mathbf{A}}^T \cdot \underline{\mathbf{P}} \cdot \underline{\mathbf{A}})^{-1} \underline{\mathbf{A}}^T \cdot \underline{\mathbf{P}} \cdot \underline{\boldsymbol{\ell}} ,$$

where the design matrix and the reduced observation vector are

$$\underline{\mathbf{A}} = \left( \frac{\partial \boldsymbol{\psi}(\underline{X})}{\partial \underline{X}} \right)_0 ,$$

$$\underline{\boldsymbol{\ell}} = \underline{L} - \boldsymbol{\psi}(\underline{X}_0) .$$

The weight matrix is defined as the inverse of the co-factor matrix of the observations which, according to the stochastic model, is the covariance matrix of the observations divided by the variance of the unit weight (a priori):

$$\underline{\mathbf{P}} = \underline{\mathbf{Q}}_{\boldsymbol{\ell}\boldsymbol{\ell}}^{-1} = \left( \frac{1}{\sigma_0^2} \underline{\boldsymbol{\Sigma}}_{\boldsymbol{\ell}\boldsymbol{\ell}} \right)^{-1} .$$

In the problem at hand there are 48 (= 2 markers · 2 coordinates · 12 points) coordinate parameters (if all marker positions are to be determined) and 6 orientation parameters to be solved for. Hence, an adjustment problem is given if at least 55 direction measurements are taken. As the observations are considered to be uncorrelated and of the same accuracy, the weight matrix becomes the identity matrix:  $\underline{\mathbf{P}} = \underline{\mathbf{I}}$ .

## (b) Fitting of two concentric circles

The UTM30 coordinates of the marker positions (red and yellow) are used as input for the following least squares fitting of two concentric circles. In this case the unknowns are the UTM30 coordinates of the centre  $(x_c, y_c)$  of the two circles as well as the two radii  $R_a$ . The functional model can be formulated as follows:

$$\psi(\underline{\mathbf{L}}, \underline{\mathbf{X}}) = (x_{i_a} - x_c)^2 + (y_{i_a} - y_c)^2 - R_a^2 = 0 ,$$

where the subscript  $a$  represents the red and the yellow marker, resp. A Taylor expansion (limited to first order terms) yields the linearized functional model

$$\frac{\mathbf{B}}{r,n} \cdot \frac{\mathbf{v}}{n,1} + \frac{\mathbf{A}}{r,n} \cdot \frac{\hat{\mathbf{x}}}{u,1} + \frac{\mathbf{w}}{r,1} = \frac{\mathbf{0}}{r,1}$$

with the design matrices

$$\frac{\mathbf{A}}{r,u} = \frac{\partial \psi(\underline{\mathbf{L}}, \underline{\mathbf{X}})}{\partial \underline{\mathbf{X}}} ,$$

$$\frac{\mathbf{B}}{r,n} = \frac{\partial \psi(\underline{\mathbf{L}}, \underline{\mathbf{X}})}{\partial \underline{\mathbf{L}}} ,$$

and the misclosure vector

$$\frac{\mathbf{w}}{r,1} = \psi(\underline{\mathbf{L}}, \underline{\mathbf{X}}_0)$$

where  $n$  denotes the number of observations,  $r$  the number of conditions, and  $u$  the number of unknowns.

The stochastic model shall be

$$\underline{\Sigma}_{\ell\ell} = \sigma_0^2 \underline{\mathbf{Q}}_{\ell\ell}$$

where the covariance matrix  $\underline{\Sigma}_{\ell\ell}$  of the observations equals the covariance matrix of the marker positions determined in the previous adjustment.

A solution of the adjustment problem at hand is obtained by introducing the condition that the sum of the weighted residuals shall be a minimum. This condition plus the linearized functional model lead to a Lagrangian extreme value problem which, in turn, leads to the formation of the normal equations:

$$\begin{bmatrix} \frac{\mathbf{B}}{r,n} \cdot \frac{\mathbf{Q}_{\ell\ell}}{n,n} \cdot \frac{\mathbf{B}^T}{n,r} & \frac{\mathbf{A}}{r,u} \\ \frac{\mathbf{A}^T}{u,r} & \frac{\mathbf{0}}{u,u} \end{bmatrix} \begin{bmatrix} \frac{\mathbf{k}}{r,1} \\ \frac{\mathbf{0}}{u,1} \end{bmatrix} + \begin{bmatrix} \frac{\mathbf{w}}{r,1} \\ \frac{\mathbf{0}}{u,1} \end{bmatrix} = \frac{\mathbf{0}}{r+u,1} .$$

The normal equations are solved by inverting the normal matrix:

$$\begin{bmatrix} \frac{\mathbf{Q}_{11}}{r,r} & \frac{\mathbf{Q}_{12}}{r,u} \\ \frac{\mathbf{Q}_{21}}{u,r} & \frac{\mathbf{Q}_{22}}{u,u} \end{bmatrix} = \begin{bmatrix} \frac{\mathbf{B}}{r,n} \cdot \frac{\mathbf{Q}_{\ell\ell}}{n,n} \cdot \frac{\mathbf{B}^T}{n,r} & \frac{\mathbf{A}}{r,u} \\ \frac{\mathbf{A}^T}{u,r} & \frac{\mathbf{0}}{u,u} \end{bmatrix}^{-1} .$$

The adjusted parameters (position of circle centre, radii) are given by

$$\hat{\underline{\mathbf{X}}} = \underline{\mathbf{X}}_0 - \underline{\mathbf{Q}}_{21} \cdot \underline{\mathbf{w}} .$$

Their accuracy can be taken from the covariance matrix of the parameters

$$\underline{\Sigma}_{\mathbf{x}\mathbf{x}} = s_0^2 \underline{\mathbf{Q}}_{\mathbf{x}\mathbf{x}} = -s_0^2 \underline{\mathbf{Q}}_{22}$$

with the empirical variance of the unit weight

$$s_0^2 = \frac{(\underline{Q}_{11} \underline{w})^T (\underline{w} + \underline{A} \hat{\underline{x}})}{r - u}$$

and  $f = r - u$  the degrees of freedom. Here the empirical value  $s_0^2$  is favoured before the theoretical one ( $\sigma_0^2$ ), as  $s_0^2$  reflects the actual conditions prevailing during the time of observation. The theoretical value may be used in simulation studies.

### 2.1.2 Numerical Results

Using this evaluation procedure all four campaigns have been analysed. After several tests the a priori standard deviation of the direction observations was chosen to  $s_r = \pm 1.2$  mgon. The adjustment of the horizontal net resulted in coordinates for the single marker positions with standard deviations of  $\pm 1 \dots 8$  mm. These points were fitted to two concentric circles resulting in UTM30 coordinates for the reference point at the different epochs (cf. table 1).

**Tab. 1:** Horizontal position (UTM30 coordinates) of the DSS65 reference point determined at different epochs.

Campaign	Northing [m]	Easting [m]	s.d. (N) [mm]	s.d. (E) [mm]
December 88	4 476 130.9987	393 955.9346	$\pm 1.2$	$\pm 1.2$
March 97	131.0053	955.9328	$\pm 2.5$	$\pm 2.6$
June 97	130.9983	955.9343	$\pm 2.8$	$\pm 2.9$
April 98	130.9984	955.9338	$\pm 1.3$	$\pm 1.3$

The standard deviations ( $1\sigma$ ) of the UTM30 coordinates of the reference point are in the range of  $\pm 1 \dots 3$  mm. Accordingly, the DSS65 antenna can be considered stable (i.e. showing no significant change) over the time span of 10 years at least in the east component. In the north component there was a change of 7 mm which only showed up in March 97. The physical meaning and/or the exclusion of errors (e.g. human error, modelling error) are still under investigation.

## 2.2 Vertical Stability

The determination of the height of the reference point (orthometric heights referring to the tide gauge at Alicante) follows a relatively simple procedure. As there were no distance measurements taken the necessary distance information is to be taken from the horizontal adjustment resp. the computed horizontal coordinates (cf. section 2.1).

### 2.2.1 Computational Procedure

The height transfer from the pillars to the single marker positions had to be done by trigonometric levelling. Thus, the control of the vertical stability was also split into two steps:

1. trigonometric height determination (distance taken from horizontal adjustment) for the different marker positions;
2. computation of weighted means  $\overline{H}$  for the two markers and a simple mean thereof:

$$\overline{H} = \frac{g_1 H_1 + \dots + g_n H_n}{g_1 + \dots + g_n}$$

$$s_{\overline{H}}^2 = \frac{s^2}{g_1 + \dots + g_n}$$

The weights  $g_i$  are the quotients of an arbitrary unit variance  $s^2$  and the variance of the single height determinations:

$$g_i = \frac{s^2}{s_i^2}$$

Here the largest variance of the single determinations is taken as the unit variance.

The two weighted means (red and yellow) are averaged (simple mean) to give a height which corresponds more or less to the height of the reference point. There probably exists a small difference to the true value as the two markers might not be exactly mounted in prolongation of the elevation axis. Hence, the obtained height of the reference point is biased by an unknown value. Since most of the users are solely interested in height changes and not in the height itself, these heights are still of value. Also the weighted means for the red and yellow marker can be utilized for monitoring height changes.

## 2.2.2 Numerical Results

Following the procedure outlined in section 2.2.1 first heights of the single marker positions have been determined. The height values vary during a full completion of a circle between 6 mm (December 88) and 16 mm (March 97). The standard deviations are in the range of  $\pm 2 \dots 6$  mm. Then weighted means for the two markers separately and a simple average thereof was computed (cf. table 2).

**Tab. 2:** Weighted means for the heights of the two markers and simple average thereof for all campaigns.

Campaign	Height of Marker		s.d.	s.d.	Simple Mean
	red [m]	yellow [m]	(r) [mm]	(y) [mm]	
December 88	781.2537	781.2612	$\pm 0.9$	$\pm 0.6$	781.257
March 97	781.2682	781.2784	$\pm 1.6$	$\pm 1.1$	781.273
June 97	781.2766	781.2844	$\pm 1.8$	$\pm 1.1$	781.281
April 98	781.2726	781.2837	$\pm 1.8$	$\pm 1.1$	781.278

The standard deviations of the weighted means are in the range of  $\pm 1 \dots 2$  mm. Hence, there are two significant height changes in the past decade: an uplift of about 17 mm in the time from 1988 to 1997 and a further rise of 6 mm from March 97 to June 97. The latter can be attributed to the runner level repair performed in between the campaigns. In the time from June 97 to April 98 the antenna eventually stabilized, i.e. only an insignificant change of  $-0.7$  mm has been found.

### 3 Antenna Stability using Runner Level Data

In section 2 the antenna stability was checked with the help of four geodetic measurement campaigns. Unfortunately, there is a large time span between the first and the second epoch of almost 9 years. Hence, the utilization of other data sets for the stability control should be considered and investigated in order to be able to fill this time gap.

As part of the station monitoring program the azimuth runner level is spirit levelled (accuracy of  $\pm 0.2$  mm) relative to the real azimuth of  $200^\circ$ . The measurements are done on a monthly basis and have been taken for the first time in 1991. For the intended investigation the levelling results from March 97 have been chosen, because then the data showed the largest height variation in the runner level of up to 17 mm (cf. figure 2) and, furthermore, an IGN campaign is available for the same period.

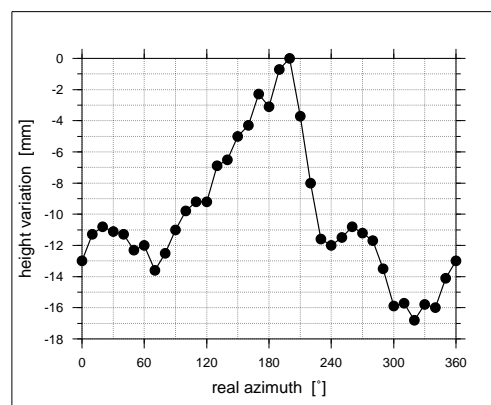


**Fig. 2:** Height variations of the azimuth runner level w.r.t. the real azimuth of  $200^\circ$  (March 97).

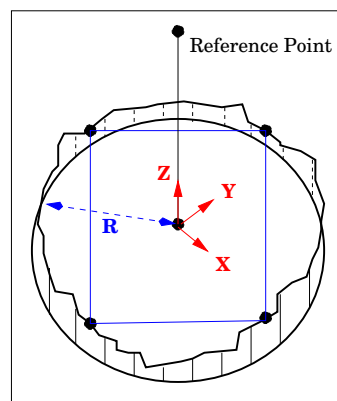


**Fig. 3:** Simple rigid body model used in the upward continuation process.

The upper part of the antenna moves on 4 wheels on the azimuth runner level. In a least squares sense these wheels define a plane which alters its parameters according to the location of the wheels on the runner level (figure 3). Assuming that the whole antenna follows the tilting of this plane (simple rigid body model), 3D-displacements of the reference point can be determined, i.e. height variations of the runner level are modelled into variations of the reference point.

The upward continued height variations induce displacements of the “reference point” with variations of 4...6 mm where the “mountain” in the runner level shows up as 4 peaks (figure 4). The error estimates have at least the same size as the signal. Hence, it appears that the simple tilted rigid body model is insufficient for upward continuing the runner level variations. This is supported by the fact that the model displacements do not correlate with the results from the IGN data, i.e. the computed Pearson correlation coefficients are close to zero. Hopefully, a refinement of the upward continuation model will cure this deficiency.

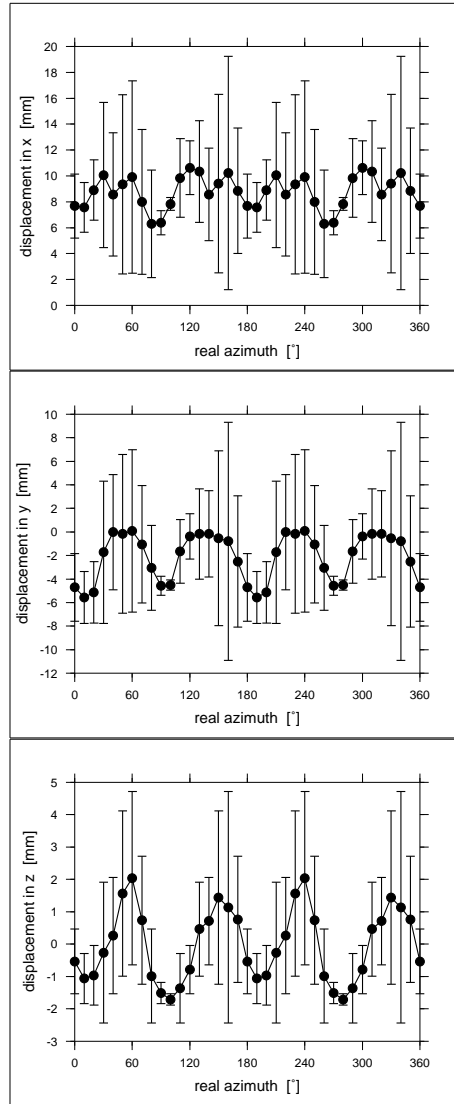


**Fig. 4:** Displacements (including error bars) of the reference point caused by variations in the azimuth runner level (simple tilted rigid body model).

## 4 Conclusions

In this study geodetic surveillance data have been analysed to control the stability of the DSS65 VLBI antenna. A least squares evaluation procedure yielded 3D-coordinates of the antenna reference point with an accuracy of a few mm. Thus, the antenna can be considered stable in position (showing no significant change) over the past decade. This excludes a

significant 7 mm change in the north component in March 97. The height, on the other hand, has undergone two significant height changes: an uplift of 17 mm from December 88 to March 97 and an uplift of 6 mm from March 97 to June 97. The latter can be attributed to the azimuth runner level repair in April/May 97. In the time from June 97 to April 98 the antenna eventually stabilized. A new observation campaign is planned for this spring/summer.

In order to fill a time gap of about 9 years in the geodetic surveillance data a simple model for propagating height variations of the azimuth runner level to the reference point has been developed. This model proved the general possibility of an upward continuation, but also revealed its limitations.

**Acknowledgements.** This research work was supported by the European Union under the TMR network grant FMRX-CT960071 “Measurement of Vertical Crustal Motion in Europe by VLBI”. We are grateful to the geodetic division of the Instituto Geográfico Nacional (Antonio Barbadillo) for providing the original data of the field campaigns. Furthermore, the provision of the levelling data of the azimuth runner level by the MDSCC (Jose Urech) is gratefully acknowledged.

# Radioastronomy at the NASA Madrid Deep Space Communications Complex (MDSCC)

## — Status Report —

A. Rius<sup>1,2</sup>, A. Alberdi<sup>2,3</sup>, D. Behrend<sup>1</sup>, C. García-Miró<sup>2</sup>, J.A. Perea<sup>4</sup>

Corresponding author: A. Rius (rius@ieec.fcr.es)

## 1 Introduction

The purpose of this report is to summarize the radioastronomical activities which have been performed during the second half of the year 1997 and the year 1998, using the facilities provided by the **NASA Madrid Deep Space Communications Complex (MDSCC)**. The projects performed at the MDSCC required the unique resources available at the **Deep Space Network (DSN)** such as large antennas, precise and accurate clocks, low noise receivers, wide bandwidth recorders, and high sensitivity as well as its geographical location (in the case of interferometric observations).

We note that the reported activities have been performed in the specific environment of a **NASA spacecraft tracking station**. The positive action of many individuals at JPL and at the MDSCC/INTA have been necessary for the successful accomplishment of this work. We hope that our activities have also contributed to improve the primary activities of the DSN: **tracking spacecrafts**.

More details on the radioastronomical activities can be obtained from the different authors, and in Technical Reports included in the Web-pages of the DSN radio observatory and of the MDSCC at the following URL addresses:

<http://dsnra.jpl.nasa.gov> ,  
<http://www.ieec.fcr.es/gps/intro.html> ,  
<http://www.laeff.esa.es/~alberdi/mdsc.html> .

## 2 The Radio Astronomy Program in the DSN

### 2.1 Segmentation

The radio astronomy program in the DSN may be divided into the following segments:

- **Applied Radio Astronomy:** Direct support of the DSN.
- **Support of the NASA:** Office of Space Sciences and Applications (OSSA).

---

<sup>1</sup>IEEC/CSIC, Barcelona, Spain

<sup>2</sup>LAEFF, INTA, Spain

<sup>3</sup>IAA/CSIC, Granada, Spain

<sup>4</sup>MDSCC, Madrid, Spain

- **Host Country Observations:** These include both single-dish and interferometric observations.
- **Radio Astronomical Observations which require the unique capabilities of the DSN:** An agreement has been signed with the EVN (European VLBI Network) permitting the participation of the NASA dishes in a few projects, requiring very high sensitivity, in each EVN observing session. The proposals must be submitted to the Program Committees of the VLBA (Very Long Baseline Array) and of the EVN (European VLBI Network).
- **Co-observations with VSOP at 18 cm:** The co-observations were taken twice a week. Due to (i) satellite eclipse problems and (ii) malfunctioning of the satellite some planned observations could not be performed.

## 2.2 Instrumentation

Detailed accounts of the available instrumentation can be found in the 'Radio Astronomy and the Deep Space Network' reports generated yearly by the JPL Telecommunications and Data Acquisition Science Office, M/S 303-401, Pasadena, California 91109. Here we give a short outline.

### 2.2.1 VLBI Antennas

The following radio antennas are available for VLBI work:

- DSS63 (70 m)
- DSS65 (34 m)

### 2.2.2 Information on the DSS63

BAND	L	S	X	K
Freq. Range (GHz)	1.60-1.70	2.2-2.3	8.4-8.5	18-26*
Antenna Beamwidth (arcmin)	10.8	6.5	1.8	0.75
Apert. Efficiency(%)	60	72	65	50
Sensitivity (K/Jy)	0.84	1.0	0.9	0.7
Feed Polarization	LCP	RCP-LCP	RCP-LCP	RCP-LCP
Low noise Amplifier	FET	Maser	Maser	HEMT
Tsys (K)	35	16	21	70

\* Expected to be operational in May 1999

### 2.2.3 Information on the DSS65

BAND	S	X	X
Freq. Range (GHz)	2.2-2.3	8.4-8.5	8.2-8.6
Antenna Beamwidth (arcmin)	16.2	4.2	4.2
Apert. Efficiency(%)	57	72	72
Sensitivity (K/Jy)	0.19	0.24	0.24
Feed Polarization	RCP-LCP	RCP-LCP	RCP-LCP
Low noise Amplifier	FET	Maser	HEMT
Tsys (K)	40	21	38

### 2.2.4 Recording Terminals

- 1 Mark IV A DAT (with two WCB recorders). It is controlled by the standard Linux-based field system.
- The Video Converters have 2, 4, 8 and 16 Mhz filters, with the capability to use them in the USB or LSB or both at the same time. 4 of the Video Converters have 125 KHz and 500 KHz filters available.

### 2.2.5 The Local Oscillators

- X Band: 8100 MHz
- S Band: 2000 MHz
- K Band: Tunable (from 18 to 26 GHz)
- L Band: 1380 MHz

### 2.2.6 Time and Frequency

- 2 Redundant Hydrogen MASERS.

### 2.2.7 Other Equipment

- SNR-8 ROGUE GPS Receiver.
- Pressure, humidity and temperature sensors integrated in the system.
- Water Vapour Radiometer.

### 3 News about the MDSCC

- On March 23, 1998 a *Memorandum of Understanding (MOU)* was signed between the European VLBI Network (EVN) and the NASA/JPL Telecommunications and Mission Operations Directorate (TMOD) for the use of NASA Deep Space Network. The purpose of this MOU is to establish a working relationship between NASA/JPL and the EVN:
  - The DSN Radio Observatory facilities will have “*associate member*” status within the EVN consortium.
  - The EVN will have access to schedule DSN antennas in support of EVN VLBI experiments to provide additional baselines with high sensitivity.

- The MKIV recording system is fully operational in Madrid. The MKIV terminal of the MDSCC can utilize both **thin** and **thick tapes**.

The MkIV terminal is completely integrated in the station network via **new interface systems** [Radio Astronomy Controller (RAC) and Equipment Activity Controller (EAC)] with other peripherals (e.g. antennae, front ends, phase-cal systems, communications, etc.).

- The L-band operations at DSS63 are fully automated; the K-band operations will also be fully automated. X-band and S-band operations are not automated.
- The L-band FET LNAs were upgraded to HEMT at all complexes.
- In Canberra an S-2 VLBI system is already operational. Two S-2 recorders and S-2 DAS were purchased in order to equip also the Madrid and Goldstone 70 m telescopes. The first S-2 recorder will be installed in Madrid in Spring 1999.
- The DSN is developing a software correlator: the correlator will be completed by spring 1999. Later, the copies of this correlator will be installed at each complex in order to provide real time monitoring of the VLBI performance.

### 4 Experiments Performed at the MDSCC During the Year 1998

- **Euro4165:** DOY 33 – DSS65 – S/X Band
- **c9811 - EVN:** DOY 52 – DSS63 – L Band
- **GM033 - global VLBI:** DOY 53 – DSS63 – L Band
- **cb10765 - CORE-B:** DOY 70 – DSS65 – S/X Band
- **GM33-15:** DOY 95 – DSS63 – S/X Band
- **cb30965 - CORE-B:** DOY 126 – DSS65 – S/X Band
- **GB27B - global VLBI:** DOY 154 – DSS63 – S/X Band – Dual Polzn
- **ER006 - EVN:** DOY 155 – DSS63 – L Band
- **GM33-15:** DOY 157 – DSS63 – S/X Band

- **GG036 - global VLBI:** DOY 158 – DSS63 – L Band
- **Euro4398:** DOY 173 – DSS65 – S/X Band
- **BM87 - VLBA:** DOY 185-186 – DSS63 – X Band
- **BR053B - global VLBI:** DOY 193 – DSS63 – X Band – Dual Polzn
- **CORE-B 310:** DOY 210-211 – DSS65 – S/X Band
- **BR053C - global VLBI:** DOY 219-220 – DSS63 – X Band – Dual Polzn
- **Euro4498:** DOY 229-230 – DSS65 – S/X Band
- **BR053D - global VLBI:** DOY 259-260 – DSS63 – X Band – Dual Polzn
- **Euro4598:** DOY 285-286 – DSS65 – S/X Band
- **GP018 - global VLBI:** DOY 331 – DSS63 – L Band
- **GM035C - global VLBI:** DOY 334 – DSS63 – L Band
- **GB033B - global VLBI:** DOY 340-341 – DSS63 – X Band – Dual Polzn
- **Euro4698:** DOY 348-349 – DSS65 – S/X Band
- **CORE-B 312:** DOY 362-363 – DSS65 – S/X Band
- **Multiple non-VLBI radioastronomical observing sessions.**
- **Multiple VSOP co-observing sessions (2 per week).**

## 5 Observational Problems

Last year, different circumstances have affected the VLBI system and prevented the fringes to be found. In particular, fringes were not found between DOY 139 and DOY 160. There were several reasons:

- Station Power Failure on DOY 146.
- FTS hydrogen maser swaps on DOY's 153-160.
- Failure in the MkIV associated TCT (Time Code Translator) Unit: The TCT unit supplying 1 pps and code data to the PCFS computer was adding an extra time of +7.783  $\mu$ sec to the individual experiment reported station time delay between GPS and station standard.

Besides that, some other experiments have **failed** due to operational problems.

## 6 Scientific Objectives and Results

The scientific objectives included the following items:

- **Study of the angular expansion of SN1993J.** A sequence of images from VLBI (DSS63 and DSS14 were essential part of the array due to their very high sensitivity) shows that the young radio supernova SN1993J has expanded with circular symmetry for nearly 5 years. Its expansion has suffered a slight deceleration and has proceeded in general accord with models of shock excited emission. To date SN1993J is the radio supernova whose evolution has been monitored in greatest detail and the one which holds

best promise for a comprehensive theoretical-observational analysis. Dual frequency monitoring of the evolution of its structure at present stages, where hydrodynamical instabilities may develop, is essential for providing data needed for modelling and theoretical analysis. The precise determination of the deceleration allows to parametrize the density profiles of the supernova ejecta and circumstellar medium (CSM) in standard supernova explosion models.

- **Study of the young radio remnant of SN1979C.** SN1979C in M100 has been one of the strongest radio supernovae, but the distance to M100 and the emission decline typical of RSN conspired to prevent a study of the structure of the radio emission by VLBI. Now the radio emission is increasing again due to the onset of a young remnant phase. The size of the remnant can be large enough to be studied by a sensitive VLBI array at 13cm and 18cm (including DSS63 and DSS14). The structure of this radio remnant might be anything from a simple shell to a very complicated structure generated by the interaction of the shock with the material deposited by a presupernova mass loss.
- **Study of the parsec-scale relativistic jets** associated with quasars and Active Galactic nuclei. DSS63 has taken part in dual polarization VLBI experiments at X-band .
- **VLBI differential astrometry.** High precision VLBI differential astrometry observations have permitted to i) study the stability of the cores of the compact radio sources and ii) determine absolute motions of the VLBI components with precisions better than a tenth of a milliarcsecond.
- **Single-dish monitoring** of variable radiostars and galactic plane variable radio sources. The 70 meter antenna (DSS63) has been used to monitor the flux density of variable radiostars (as X-ray binaries, flare stars). Several campaigns were performed coordinated with X-ray, millimetre and sub-millimetre observations at other observatories.
- **VLBI astrometry**, using the phase-referencing technique, provides submilliarcsecond-precision positions **of weakly-emitting radio stars**. Combining multi-epoch VLBI astrometric observations and Hipparcos satellite data, a low-mass companion ( $0.08 - 0.11 M_{\odot}$ , on the boundary between a brown dwarf and a very low-mass star) was detected orbiting the radio star AB Doradus, a member of the Pleiades Moving Cluster. This result is the first detection of a low mass stellar companion using the VLBI technique, a technique which will become an important tool in future searches for planets and brown dwarfs orbiting other stars. In fact, a whole sample of radio stars (spectral types F, G, K, M) is under study with the extremely sensitive baseline DSS63 - DSS14 at S/X bands.
- **VSOP observations at 1.6 GHz.** During the last year, DSS63 has been regularly co-observing with VSOP compact radio sources at 18cm. These observations have not been included in the previous list.

- **Applications of VLBI to Geodynamics.** The antenna DSS65 has participated in geodetic VLBI campaigns, in particular in the *Europe* and in the *CORE* experiments. The DSS65 antenna has again been surveyed in this period to determine possible displacements of the VLBI reference point. The results of different surveillance campaigns have been analyzed and intercompared.
- **Applications of GPS to Ionospheric Studies:** During the report period the GPS data from the MDSCC has been processed to study the ionosphere. The main results have been obtained with the application of occultation techniques.
- **Applications of GPS to Meteorology:** Data obtained at the MDSCC and in a local network of GPS receivers, have been used to study the spatial and temporal distribution of the atmospheric delays for meteorological applications. With the beginning of this year, we have started to produce “near real time estimates” of the total zenith delay at Madrid and Wettzell using the data stored hourly at the BKG (formerly IfAG) and CDDIS servers.

## 7 Recent Publications Containing Data From DSS63-DSS65

### 7.1 Refereed Journals

1. Alberdi, A. 1998, “Interferometría: en busca de la alta resolución en astronomía”, *Universo*, 35, 20-29
2. Alberdi, A., Krichbaum, T.P., Graham, D.A., Greve, A., Grewing, M., Marcaide, J.M., Witzel, A., Booth, R.S., Baath, L.B., Colomer, F., Doeleman, S., Marscher, A.P., Rogers, A.E.E., Schalinski, C.J., and Standke, K. 1997, “The high frequency radio structure of 4C 39.25”, *Astronomy & Astrophysics*, 327, 513-521
3. Elósegui, P., Rius, A., Davis, J.L., Ruffini, G., Keilm, S., Bürki, B. 1998, “An Experiment for Estimation of the Spatial and Temporal Variations of Water Vapor Using GPS and WVR Data”, *Physics and Chemistry of the Earth*, Vol. 23, No. 1, pp. 125-130
4. Gómez, J.L., Marscher, A.P., Alberdi, A., Martí, J.M., Ibáñez, J.M. 1998, “Sub-parsec polarimetry radio observations of 3C 120: A close-up look at superluminal motion”, *Astrophysical Journal*, 499, 221-226
5. Marcaide, J.M., Alberdi, A., Lara, L., Pérez-Torres, M.A., Diamond, P.J., Preston, R.A. 1998, “A decade of unchanged 1.3cm VLBI structure of SgrA\*”, *Astronomy & Astrophysics*, in press
6. Rius, A., Ruffini, G., Cucurull, L. 1997, “Improving the Vertical Resolution of Ionospheric Tomography with GPS Occultations”, *Geophysical Research Letters*, Vol. 24, No. 18, p. 2291

7. Rius, A., Ruffini, G., Romeo, A. 1998, "Analysis of Ionospheric Electron Density Distribution from GPS/MET Occultations", *IEEE Transactions on Geoscience and Remote Sensing*, Vol. 36, No. 2
8. Ruffini, G., Flores, A., Rius, A. 1998, "GPS Tomography of the Ionospheric Electron Content with a Correlation Functional", *IEEE Transactions on Geoscience and Remote Sensing*, Vol. 36, No. 1
9. Ruffini, G., Cardellach, E., Flores, A., Cucurull, L., Rius, A. 1998, "Ionospheric Calibration of Radar Altimeters Using GPS Tomography", *Geophysical Research Letters*, Vol. 25, No. 20
10. Ruffini, G., Cucurull, L., Flores, A., Rius, A. 1998, "A PIM-aided Kalman Filter for GPS Tomography of Ionospheric Electron Content", *Physics and Chemistry of the Earth*, in press

## 7.2 Conference Proceedings

1. Alberdi, A., Gómez, J.L., Marcaide, J.M., Pérez-Torres, M.A., Marscher, A.P. 1998, "The parsec-scale radio jet of 4C39.25: witnessing the interaction between a superluminal and stationary component", in "BLLac Phenomenon", ed. L.O. Takalo, ASP Conference Series, 1998, in press
2. Alberdi, A., Gómez, J.L., Marcaide, J.M., Pérez-Torres, M.A., Marscher, A.P. 1998, "4C39.25: Multi-epoch polarization observations at 15, 22 and 43 GHz", in "EVN/JIVE Symposium No. 4", ed. M. Garrett & L. Gurvits, *New Astronomy Reviews*, 1999, in press
3. Alberdi, A., Lara, L., Gómez, J.L., Marcaide, J.M., Pérez-Torres, M.A., Kembell, A., Leppänen, K., Marscher, A.P., Patnaik, A., Porcas, R. 1998, "Magnetic Field Configuration in 4C39.25", in "Radio Emission from Galactic and Extragalactic Compact Sources", ed. G. Taylor, J. Wrobel and J.A. Zensus, ASP Conference Series Vol. 144, 1998, pp. 115-116
4. Alberdi, A., Lara, L., Marcaide, J.M., Leppanen, K., Patnaik, A., Porcas, R. 1997, "Dual high frequency polarization images of the quasar 3C395", in "Blazars, Black Holes and Jets", ed. M. Kidger and J.A. de Diego, Kluwer Academic Publishers (Dordrecht, The Netherlands), in press
5. Behrend, D., Rius, A. 1998, "Reference Point Stability of the DSS65 VLBI Antenna", *EOS Transactions*, AGU 1998 Fall Meeting, Vol. 79, No. 45, Supplement, p. F208
6. Marcaide, J.M., Alberdi, A., Ros, E., Diamond, P., Shapiro, I.I., Guirado, J.C., Jones, D.L., Mantovani, F., Pérez-Torres, M.A., Preston, R., Schilizzi, R.T., Sramek, R.A., Trigilio, C., Van Dyk, S.D., Weiler, K.W., Whitney, A.R. 1998, "Deceleration in the Expansion of SN 1993J", in "Radio Emission from Galactic and Extragalactic Compact Sources", ed. G. Taylor, J. Wrobel and J.A. Zensus, ASP Conference Series Vol. 144, 1998, pp. 353-354

## Observatorio Astronómico Nacional – Yebes

### *Status report*

#### 13<sup>th</sup> Working Meeting on European VLBI for Geodesy and Astrometry

Viechtach, February 12<sup>th</sup> 1999

- OAN–Yebes has successfully become a network station in the International VLBI Service for Geodesy and Astrometry (IVS). Associate IVS members are Jesús Gómez–González (OAN director), Paco Colomer, Pablo de-Vicente, and Maria Rioja.
- The new MK IV system arrived in January and is now being installed. We will resume our participation in the EVN and geodetic campaigns, stopped since the failure of our VLBA formatter more than a year ago.
- A new PC has been installed to control the MK IV terminal. The system now runs the Field System version 9.3.25 on Debian 2.0rb1 (kernel 2.0.34) Linux.
- OAN has purchased 45 thin tapes, 30 of which have already been sent to the EVN pool for astronomical VLBI observations.
- The construction of a 22 GHz receiver continues, and is expected to be installed at the 14 meter telescope by the end of 1999.
- The design study of a new 40 meter radiotelescope by MAN GHH GmbH to be placed at Yebes has been completed. Works on the telescope foundation and pedestal will start before the summer of 1999.

Table 1: Available receivers at the Yebes 13.7–m radiotelescope

Band	Tunable range (GHz)	Bandwidth (MHz)	SEFD <sup>a</sup> (Jy)	Pol	Rec <sup>b</sup>
Q	41.0 – 49.0	400	4160	LCP	CS
S	2.21 – 2.35	140	3800	RCP	HEMT
X	8.13 – 8.63	500	3300	RCP	HEMT

<sup>a</sup> All numbers include radome effects.

<sup>b</sup> Receiver: CS = Schottky diode. HEMT = High Electron Mobility Transistor amplifier. All cooled to 20 K.

Francisco Colomer, Pablo de Vicente, and Maria Rioja.  
vlbi@oan.es

# Geodetic Very-Long-Baseline Interferometry at the Onsala Space Observatory 1997–1998

Gunnar Elgered and Rüdiger Haas

Onsala Space Observatory, Department of Radio and Space Science, Chalmers University of Technology, SE-439 92 Onsala, Sweden

**Abstract.** We summarize the performed geodesy VLBI activities at the Onsala Space Observatory for the period 1997–1998. This presentation concentrates on the observations and the technical issues, whereas data analysis and studies of error sources are reported in other contributions to this meeting. A total of 35 experiments were planned for the two year period. Two of these were never carried out due to a failing inch-worm motor in the tape recorder. The development of a new S/X-band feed system resulting in an improved efficiency and dual polarizations is ongoing. An update of the results from the measurement system for continuous monitoring of the height of the concrete foundation of the 20 m telescope is reported.

## 1 VLBI Observations

The Onsala 20 m antenna participates regularly in the experiments of the European network. Six experiments were planned and carried out during 1997. Of the six experiments planned for 1998, five were carried out. Other experiments with Onsala participation have been in the CORE-B network (five in both 1997 and 1998); and RDV experiments including the US Very-Long-Baseline Array (VLBA) (six each year). In November 1997 a TIGO test experiment was carried out between Effelsberg, Onsala, and TIGO (at the Wettzell site). All the experiments are listed in Table 1.

## 2 Technical Developments During 1997–1998

The development of a new S- and X-band is ongoing. It consists of two feed reflectors used for both the S- and the X-band. A description of the feed was reported at the previous meeting [Elgered and Haas, 1997]. Two dual-band corrugated horns have been manufactured. The rescaled version was measured and showed a good antenna diagram for both bands. The coaxial waveguide transformer (COWAT) is the component which makes it possible to have access to the X-band ports (RCP and LCP) that are inside the coaxial S-band waveguide, before transforming the S-band coaxial waveguide into the S-band septum polarizer in circular waveguide. The prototype COWAT was found to have the centre frequency slightly off the desired value and it is now being redesigned. Earlier simulations show that a reduction in length of some parts of the COWAT will lower the centre frequency. The amount of reduction has not yet been decided. For X-band a polarizer has been built and measurements show that it works though more measurements are needed before it can be decided if it fully meets the specifications. The S-band polarizer will be a scaled version of the X-band polarizer and has not yet been manufactured.

The Mark-IV data acquisition terminal has been equipped with new power supplies and the formatter is connected to an uninterruptable power supply (UPS). The input connector for the intermediate frequency (IF) band has been connected to a microwave switch in order to reduce the changeover time between the different receivers used in the VLBI observations.

In addition to our long term VLBI activities and the operation of the Onsala GPS station in the “International GPS Service for Geodynamics (IGS)” we are since October 19, 1998 participating in the International GLONASS experiment (IGEX). These observations are made with the same antenna using an Ashtech Z18 receiver. It is a combined two frequency receiver with 18 channels for both GPS and GLONASS satellites. This means that 18 satellites can be tracked at the two frequencies simultaneously.

Table 1: Geodetic VLBI experiments at Onsala Space Observatory 1997–1998

Experiment	Date	Remark
EUROPE–35	1997 January 13	
RDV–1	1997 January 29	
CORE–B101	1997 February 3	
EUROPE–36	1997 March 17	
RDV–2	1997 March 31	Two tapes lost in shipment
CORE–B102	1997 April 16	
RDV–3	1997 May 19	
EUROPE–37	1997 June 16	
CORE–B103	1997 June 25	Cancelled centrally
CORE–B104	1997 July 23	
RDV–4	1997 July 24	
CORE–B105	1997 August 20	
EUROPE–38	1997 August 25	
RDV–5	1997 September 8	
CORE–B106	1997 October 29	
EUROPE–39	1997 October 30	
TIGO TEST	1997 November 12	3 hours long
EUROPE–40	1997 December 8	
RDV–6	1997 December 17	Unstable fringes, unexplained
EUROPE–41	1998 February 2	
RDV–7	1998 February 9	
CORE–B107	1998 March 11	
CORE–B108	1998 April 8	
RDV–8	1998 April 15	
EUROPE–42	1998 April 20	
CORE–B109	1998 May 20	
EUROPE–43	1998 June 22	50% data loss, tracks overwritten
RDV–9	1998 June 24	
CORE–B110	1998 July 1	
RDV–10	1998 August 10	
EUROPE–44	1998 August 17	50% data loss, tracks overwritten
CORE–B111	1998 August 26	antenna pointing problems
RDV–11	1998 October 1	
EUROPE–45	1998 October 12	
CORE–B112	1998 November 4	
EUROPE–46	1998 December 14	inch-worm motor failure
RDV–12	1998 December 21	inch-worm motor failure

### 3 Measurements of the Stability of the Antenna Tower

A data acquisition system for monitoring of the temperature and the vertical motion of the concrete tower of the 20-m antenna was described at the Onsala meeting [Elgered, 1996] and results were reported in Hønefoss [Elgered and Haas, 1997]. Figure 1 shows the data acquired from October 1, 1996 to December 31, 1998. The estimates of the height variations in Figure 1 are corrected for the expansion of the invar rod estimated by measuring the temperature of the rod (at the mid point) and using the theoretical temperature coefficient of invar,  $1.5 \cdot 10^{-6} (\text{° C})^{-1}$ . Using all the data we find that the time lag between the air temperature and the mean concrete temperature is typically 6–8 hours which is consistent with earlier results [Carlsson, 1996]. Furthermore it is interesting to note that the time lag obtained from a cross-correlation analysis of the time series in Figure 1, of the observed height variation and the mean concrete temperature, is less than one hour.

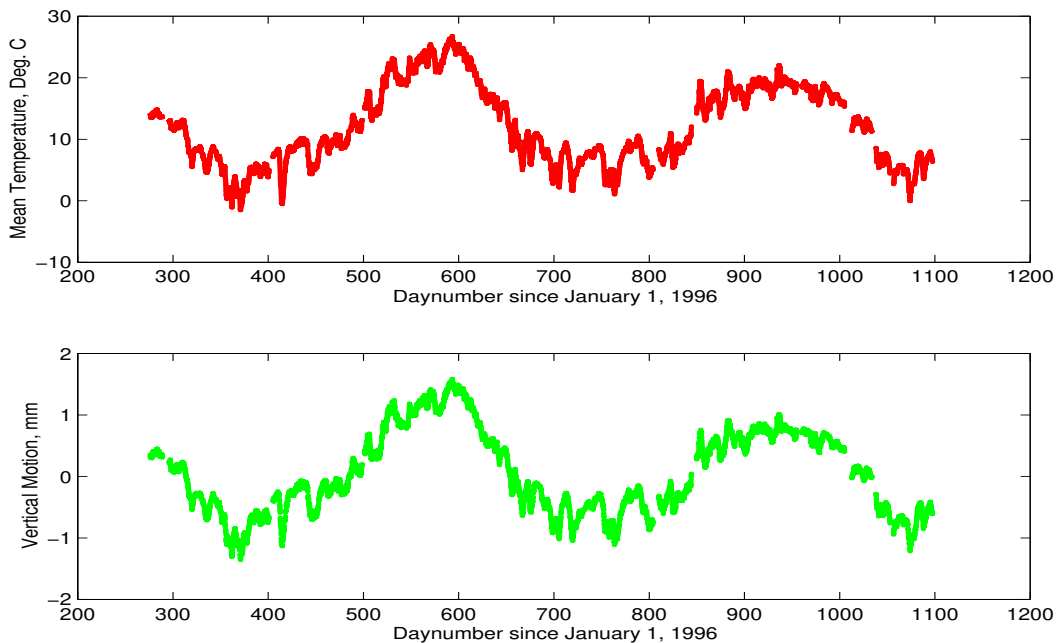


Figure 1: Approximately two years of data from measurements of the temperature and the vertical motion of the concrete tower of the 20 m antenna. The upper plot shows the mean concrete temperature and the lower plot shows the vertical motion. The mean temperature is the arithmetic mean of all readings from the 16 temperature sensors.

A least squares fit of the data in Figure 2 gives a height change of  $0.11 \text{ mm}(\text{° C})^{-1}$ . This is slightly less than the expected value for an 11 m high concrete tower, which is  $0.13 \text{ mm}(\text{° C})^{-1}$ . This is consistent with previous results and indicates that the temperature sensors are not located correctly in order to yield a representative mean for the effective temperature of the concrete. For example, Figure 3 shows that there is not a linear relation between the temperature in the top of the foundation and the mean temperature.

The agreement between the vertical motion and a linear model with the measured temperatures as input data is sufficient given the present repeatability in the estimated vertical coordinate. The rms residual about the estimated straight line in Figure 2 is only 0.05 mm.

Finally, it is interesting to note in Figure 1 that the height of the concrete foundation is an excellent parameter for measuring the quality of the summer weather in the Onsala area. (The summer of 1998 was significantly colder and more lousy compared to the summer of 1997.)

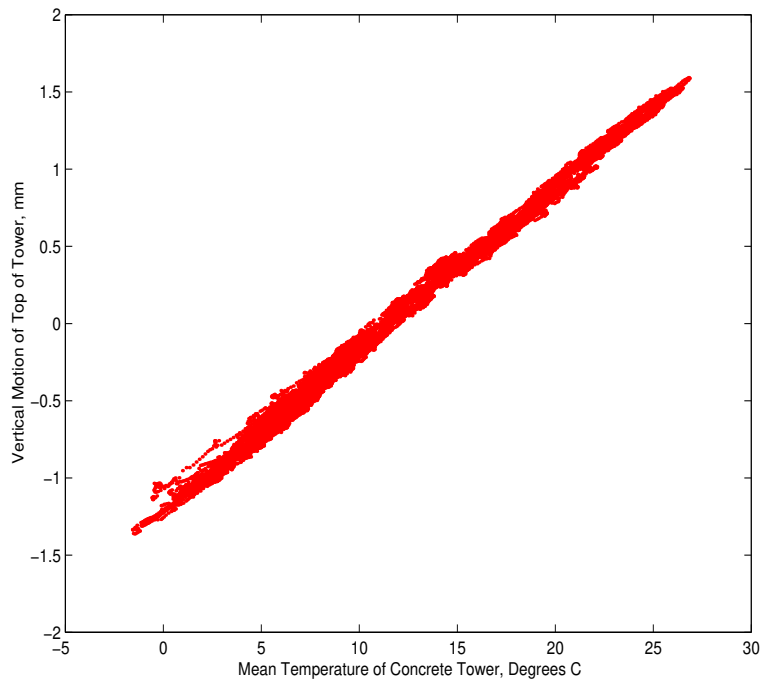


Figure 2: The same data as in Figure 1. The strong correlation between the motion and the inferred mean temperature is obvious.

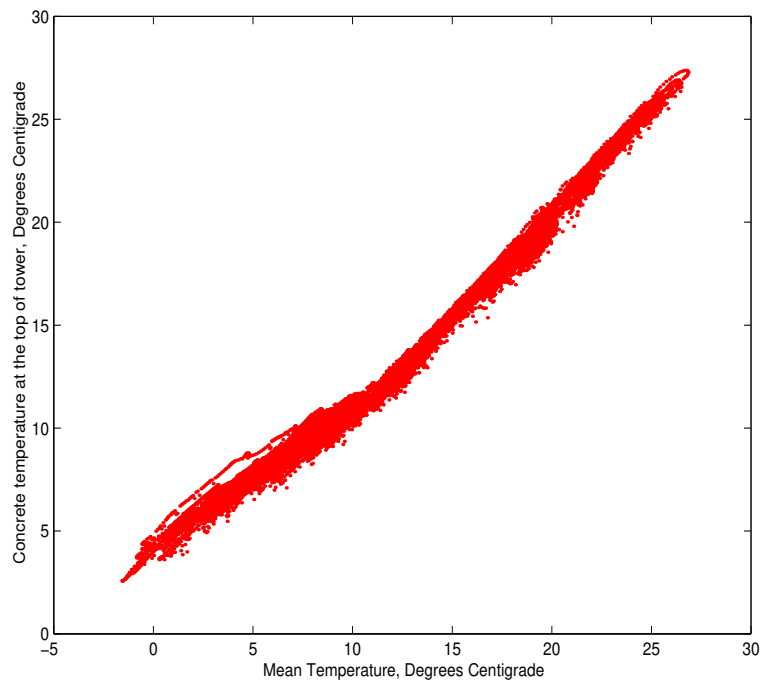


Figure 3: The temperature measured in the concrete at the top of the foundation shows the effect of heating the azimuth encoder of the antenna. The heating is normally switched on when the temperature is below 12°C.

## 4 Work Related to the VLBI Observations and the Future

Contributions to this working meeting dealing with the data analysis are:

- VLBI data analysis resulting in estimates of crustal motion in Europe [*Haas and Nothnagel, 1999, this meeting*]
- The influence of the ocean tide loading on the estimated earth rotation parameters [*Haas and Scherneck, 1999, this meeting*]
- The atmospheric influence on atmospheric model parameters such as linear horizontal gradients in the refractivity has been studied using data from VLBI, GPS, and microwave radiometry [*Gradinarsky et al., 1999, this meeting*].
- A second microwave radiometer is being developed [*Stoew and Rieck, 1999, this meeting*]. The main application will be comparison measurements at the Onsala site as well as collocations at other sites. A major difference compared to the existing Onsala radiometer is that the half power antenna beam widths are approximately  $2^\circ$  instead of  $6^\circ$ .

VLBI will continue to be an important component in our regional studies of crustal motions in Fennoscandia [*Scherneck et al., 1998*]. In terms of the observation schedule we will begin with a more frequent participation in the CORE network.

## References

- Carlsson, T.R., Site Dependent Error Sources in Geodetic Very-Long-Baseline Interferometry, *Tech. Rep. 224L*, School of Electrical and Computer Engineering, Chalmers Univ. Tech., 1996.
- Elgered, G., Geodetic very-long-baseline interferometry at the Onsala Space Observatory 1995–1996, *Proc. of the 11th Working Meeting on European VLBI for Geodesy and Astrometry, Research Report 177*, Ed. G. Elgered, Onsala Space Observatory, Chalmers University of Technology, 55–61, 1996.
- Elgered, G., and R. Haas, Geodetic Very-Long-Baseline Interferometry at the Onsala Space Observatory 1996–1997, *Proc. of the 12th Working Meeting on European VLBI for Geodesy and Astrometry*, Statens Kartverk, Hønefoss, Norway, pp. 49–53, 1997.
- Gradinarsky, L.P., R. Haas, J.M. Johansson and G. Elgered, Comparison of atmospheric parameters estimated from VLBI, GPS and microwave radiometer data, *Proc. of the 13th Working Meeting on European VLBI for Geodesy and Astrometry*, (this volume), 1999.
- Haas, R., and A. Nothnagel, A two-step approach to analyze European geodetic Very Long Baseline Interferometry (VLBI) data, *Proc. of the 13th Working Meeting on European VLBI for Geodesy and Astrometry*, (this volume), 1999.
- Haas, R., and H.-G. Scherneck, The effect of ocean tide loading on the determination of earth rotation parameters, *Proc. of the 13th Working Meeting on European VLBI for Geodesy and Astrometry*, (this volume), 1999.
- Scherneck, H.-G., J.M. Johansson, J.X. Mitrovica, and J.L. Davis, The BIFROST project: GPS Determined 3-D displacement rates in Fennoscandia from 800 days of continuous observations in the SWEPOS network, *Tectonophysics*, **294**, pp. 305–321, 1998.
- Stoew, B., and C. Rieck, Dual channel water vapour radiometer development, *Proc. of the 13th Working Meeting on European VLBI for Geodesy and Astrometry*, (this volume), 1999.

# Measurement of vertical crustal motion in Europe by VLBI

## Station report for Ny-Ålesund

### Norwegian Mapping Authority

Hans-Peter Plag, Norwegian Mapping Authority, Kartverksveien, N-3500 Hønefoss, Norway,  
phone: +47-32118100, fax: +47-32118101, Email: plag@gdiv.statkart.no

#### Abstract

The Norwegian Mapping Authority (NMA) participates in the project "Measurement of vertical crustal motion in Europe by VLBI" with the space-geodetic observatory at Ny-Ålesund. This observatory is a multi-parameter monitoring site contributing to global geodetic networks. Due to its remote location in the Arctic, the station constitutes a unique cornerstone for these networks. The environmental parameters recorded at the station include sea level, surface deformations and gravity. Meteorological observations including daily radio-sondes are available for the nearby research station of the Alfred-Wegener-Institute.

In the project, NMA contributes to several of the tasks defined in the project workplan. For each task, the status is reported. Up to now, progress has been close to the workplan with some additional contributions reported here.

The comparison of horizontal station velocities to those predicted by the NUVEL-1A model for the Eurasian plate shows a good agreement. Comparison between GPS and VLBI results for station velocities results in significant disagreement for vertical velocities, the reason of which remains to be clarified.

## 1 Introduction

Within the EU-Project *Measurement of vertical crustal motion in Europe by VLBI*, the Norwegian Mapping Authority participates with the geodetic observatory in Ny-Ålesund. The observatory is a multi-parameter environmental monitoring site located at 78.9 °N and 11.9 °W on the West coast of Spitsbergen, the main island of Svalbard. At this research and monitoring facility, surface displacements of the Earth's crust are monitored with mm precision utilising the most advanced space-geodetic techniques. The geodetic activities at Ny-Ålesund are

strongly interwoven with international programs and organisations, which provide the background for monitoring the state of the Earth system and for studies of the system's dynamics and climate. Thus, the Very Long Baseline Interferometry (VLBI) station is contributing to the global VLBI network and all observations are coordinated with international programs such as the one for Continuous Observations of the Rotation of the Earth (CORE). The Global Positioning System (GPS) receivers deliver data to the International GPS Service (IGS), which maintains a network of more than 150 stations globally distributed, though with large spatial gaps in the Arctic. Both networks contribute to the definition and maintenance of the International Terrestrial Reference Frame (ITRF) and the monitoring of the Earth Orientation Parameters (EOP) as available from the International Earth Rotation Service (IERS). The Global Sea Level Observing System (GLOSS) includes the tide gauge operated at Ny-Ålesund. GLOSS strongly recommends the collocation of tide gauges with permanent GPS receivers and gravity measurements, conditions which are both met at the station. The geographical distribution of the sites in all these nets is characterised by a low number of Arctic stations, thus emphasising the importance of Ny-Ålesund for the networks.

According to the workplan of the EU-Project, NMA is supposed to participate in the following tasks within the project:

- The post-processing consisting of the fringe analysis and the geodetic least squares adjustment of baselines, site positions and site velocity vectors.
- Securing the operation of the VLBI facilities for the scheduled Geo-VLBI-experiments including maintenance and test of equipment.
- Survey of antenna stability by local geodetic techniques.
- The processing of GPS data collected at the VLBI sites.

Below, we will report the status concerning each of these tasks. Moreover, at NMA work has been carried out,

which is contributing to the following tasks, though NMA according to the workplan originally was not obliged to contribute to these:

- comparison of VLBI and GPS results through data analysis of the continuously operating GPS stations in Europe;
- separation of vertical crustal motions related to different geophysical phenomena;
- connection of tide-gauges, monitoring of sea level changes, subsidence of North Sea lowlands.

For these additional tasks, the status is described below as well. For the last task, it should be mentioned that the connection of tide-gauges and monitoring of sea-level changes is restricted to Svalbard and does not include the North Sea area.

Sections 7 and 8 are slightly more elaborated. In Section 7, the scientific background for determining the vertical crustal motion due to ice-load changes is briefly reviewed, as this defines the requirements for observations. Moreover, the available station velocities are compared to model predictions for tectonic motions. In Section 8, the tide gauge records for Ny-Ålesund and Barentsburg are used to emphasise the value of the geodetically determined vertical crustal motion for the interpretation.

## 2 Post-processing and Analysis

An initial analysis of the available experiments including Ny-Ålesund was carried out with the OCCAM software by B. R. Pettersen in 1997 in co-operation with O. Titov (see Titov and Pettersen, 1997). Additional processing and determination of co-ordinates for Ny-Ålesund were carried out with OCCAM under an external contract by E. Repstad (see Repstad, 1997). The contract covered the following parts, which were delivered satisfactorily in 1997:

1. Installation of the program OCCAM 3.4 on a PC.
2. Establishment of a database in NGS-format of correlated data for VLBI observations where Ny-Ålesund took part.
3. Diverse calculations with OCCAM 3.4 on the basis of the established database.
4. Presentation of program documentation, user's handbook and results of calculations in a report.

Since autumn 1997, no processing or analysis was done at NMA. Despite considerable efforts, it was not possible to fill a new permanent position dedicated to VLBI analyses. In several rounds attempting to fill the position, no qualified person could be appointed. Currently, another round is in progress and it is hoped to fill the position soon.

Steps have been taken recently to install the CALC/SOLVE software at NMA. If the open position can be filled, then NMA will be able to contribute

to the processing and analysis of the VLBI data. In this case, initial focus will be on the European experiments.

As mentioned above, preliminary results of the analysis were described in a paper published in the proceedings of the VLBI workshop held in Hønefoss in 1997 (Titov and Pettersen, 1997). It is interesting to note here that these authors find a discrepancy between the EW-velocity determined from the VLBI observations and the NUVEL1-A prediction. This result is not confirmed by a recent analysis of Ma (1998, personal communication), where a much better agreement between the horizontal components for the VLBI site in Ny-Ålesund and the NUVEL1-A predictions is found. These velocities are also in reasonable agreement with the horizontal velocities determined from the GPS record of the IGS site in Ny-Ålesund. However, the vertical velocities of VLBI and GPS differ significantly from each other (see Section 7 for numbers and a more detailed discussion). In 1999, one focus of the analysis work will be on the reconciliation of these discrepancies between the different analyses as well as the different techniques. Motivated by the significant seasonal signal found particularly in the GPS-heights, emphasis will be on the tropospheric effects on GPS and VLBI co-ordinates.

## 3 Participation in experiments and maintenance of the VLBI antenna

In Table 1 all experiments for the period Oct. 96 to Dec. 98 are compiled. The table demonstrates that Ny-Ålesund managed to participate in all but one of the scheduled experiments.

At Ny-Ålesund VLBI is operated by the observatory staff of currently one station manager and two engineers. The VLBI activities are dominated by taking part in international VLBI-experiments (VLBI Europe, pre-CORE, NEOS, and VLBA) as well as the testing of equipment and the maintenance of the station. For example, in 1997, 41 experiments with a total of 35 observing days were successfully carried out, while six of the scheduled days were lost due to overhaul of the receiver, broken capstan motor and problems resulting from an upgrade of the tape station. In 1998, the level of activity increased slightly compared to 1997.

To maintain the ever improving technical level required for international co-operation and participation in future experiments, several major actions have been necessary, namely (1) to change the dewar and carry out an overhaul of the receiver (March 1997), (2) to change the Field System computer and upgrade it from FS 8 to FS 9.3.16 (July 1997), (3) to upgrade the tape station and MARK III to MARK IV with thin tape (September 1997), (4) to mount an extra timer for TAC - Formatter measurement during experiments (October 1997), and (5) to carry out a thorough maintenance of the Maser (March 1997).

The remote location of the observatory requires special

Table 1: Participation of Ny-Ålesund in the EUROP experiments.

Year	Exper.	Date	Comment
1996	Europ5	3 Nov.	Small problems with two video converters within the first hour Field system computer stopped once. No other specific problems
	Europ6	5 Dec.	
1997	Europ1	17 Mar. 16 Jun. 25 Aug. 30 Oct. 8 Dec.	participation of NMA not scheduled Not participated due to repair of receiver
	Europ2		
	Europ3		
	Europ4		
	Europ5		
	Europ6		
1998	Europ41	02.02.	loss of one pointing due software failure in field system (on-off procedure) a few problems due to short power dip; high SEFD values for S-band
	Europ42	20.04.	
	Europ43	22.06.	
	Europ44	17.06.	
	Europ45	20.10.	
	Europ46	14.12.	

considerations concerning possible break-downs, thus, for example, a spare FS computer was acquired for the site. Yielding to the climate conditions, heating cables were isolated and mounted on the gearboxes to the antenna. Moreover, the antenna was painted in 1997 in order to reducing effects due to solar warming and thus to increase the over-all receiving characteristics.

Considerable activity has focused on determining the stability of the observatory with respect to the surrounding area and to control the stability of the antenna. The status of this work is reported in Section 4.

Other activities at the observatory relevant to the EU Project include the connection of the tide gauge to the observatory, the observation of Earth tides (relative gravity), absolute gravity measurements and the operation of the IGS receivers.

At the IGS site, the old monument was sitting in permafrost and some instabilities were suspected. Therefore, a new monument firmly attached to the bedrock was constructed (in June 1997), and an additional GPS receiver was installed at the new location. IGS requests to operate the two receivers in parallel for a total period of one years. Today, the two receivers continue to observe in parallel. Both receivers provide high-quality data. Analysis results show a clear seasonal signal in the height component, which is most likely due to tropospheric effects.

Relative gravity is continuously monitored at a location in the vicinity of the observatory and the analysis of the time series indicates high-quality results.

Absolute gravity measurements were carried out (by BKG, Germany) at the observatory in early July 1998 on a solid monument attached to the bedrock. Since the small laboratory planned to be built above the monument could not be finished in time, a temporary cabin was erected to shelter the instrument. A preliminary analysis of the observations shows an extremely low noise level at the site. It is now planned to finish the laboratory in 1999 and to install (in international co-operation) a superconducting

gravimeter at this monument.

The tie between the near-by tide gauge and the geodetic observatory has been re-measured. The measurements indicated that there is no significant movement of the tide gauge with respect to the land.

## 4 Surveying the antenna

The local control network in Ny-Ålesund consists of 8 reinforced concrete pillars with Wild brass screws for horizontal reference and a brass levelling bolt for vertical reference (Grimstveit and Rekkedal, 1998). The pillars are drilled into bedrock and they are insulated and protected against sunlight. Moreover, the ground around the pillars is insulated to avoid melting during summer. Additionally, brass bolts have been located in the fundaments of the different antennas. While most of the local control network was established in the period 1991 to 1995, the bolts in the fundament of the VLBI antenna were attached in 1998.

Major campaigns were carried out in 1992 (levelling), 1995 (directions and zenith angles), 1997 (levelling, some directions and zenith angles). The main goals of the measurements were to check the axes of the VLBI antenna and to tie the different techniques together. However, the severe weather conditions did not allow to fix the orientation of the VLBI with the available instruments. Therefore, the antenna could not be tied to the other techniques, and changes in the position of the VLBI antenna could not be determined.

In 1999, a new attempt to measure the antenna will be made based on more advanced instruments allowing a much faster measuring. Moreover, the bolts in the fundament of the antenna have been measured in 1998 and will be re-measured in 1999.

The analyses of geodetic measurements of the local control network around the VLBI antenna and the GPS sites

indicate some deformations in the control network, which may be due to movements of the pillars in the permafrost.

To assess the regional stability, a regional control network has been established in July 1998 around Ny-Ålesund with eight new geodetic markers drilled into what was considered to be stable bedrock. The network has an extension of about 50 km in east-west and 30 km in north-south direction and crosses several major geological faults. Apparently, these faults are not active today. In a first-epoch campaign carried out in September 1998, seven of these points could be measured simultaneously with GPS for five full days. In addition, simultaneous GPS measurements were carried out on a mountain close to the observatory (Zeppelinfjellet), and these observations are currently being used together with the data from the regional network for tropospheric and ionospheric studies.

It is planned to re-measure the control network in August/September 1999 with GPS. This campaign will not only include all regional but also all local points.

The large east-west extension of the control network, which is almost perpendicular to the ice sheet east of Ny-Ålesund may allow to use the observations to determine the surface deformations due to changes in the ice load. The application of the GPS and VLBI measurements for this task is part of a co-operation with GFZ Potsdam (Germany).

## 5 Processing the GPS data

The processing of the data from the continuously recording GPS (CGPS) sites operated by NMA is carried out routinely. Using the precise point-positioning technique (Zumberge *et al.*, 1997), daily co-ordinates are estimated for all CGPS sites as soon as the precise orbits and clocks become available from IGS/JPL. For most of the sites, data have been processed in this way since January 1997.

For Ny-Ålesund, this routine analysis includes the observations of two GPS receivers. One of them delivers data to IGS since 1991. This long record has been analysed by M. Heflin (JPL), and the resulting time series is used below for comparison with the VLBI series.

## 6 Comparison of VLBI and GPS data

In Figures 1 - 2, we compare the time series of GPS and VLBI for the three components. The VLBI series were produced in a global analysis (Ma, personal communication) of all available data up to the beginning of 1998. The GPS series was taken from Heflin (1998) in May 1998. In the two horizontal components, the linear trends for VLBI and GPS are in good agreement with each other. This is also demonstrated by the numbers given in Table 2A for

these two analyses. This agreement lead to correlation coefficients of the order of 0.8. However, if the linear trends are removed from the two time series, then there is virtually no correlation between the VLBI and GPS co-ordinate variations. Partly, this may be due to differences in the analyses and the models used to account for atmospheric effects. But it may also indicate that at time scale of days, the two techniques may be affected by noise sources in a different way. For geophysical applications such as studies of atmospheric loading, it is crucial to understand the reason for the un-correlated variations in the co-ordinates as determined by VLBI and GPS.

In the height component, apparently significant discrepancies are found in Ny-Ålesund (see also Table 2). It is important to mention that the time series given by Heflin (1998) are continuously up-dated and the velocities given may change with time. Thus, in May 1998, the vertical rate for Ny-Ålesund was as large as 5.54 mm/yr while in February 1999 it has decreased to 4.20 mm/yr. The uncertainties estimated for the global analysis are formal errors which are rather optimistic. Thus, a large part of the discrepancy may still be due to underestimated uncertainties. Moreover, the VLBI time series at Ny-Ålesund is still short (in the Ma analysis, slightly more than three years were used) and the trend is likely to change with increasing length.

A similar comparison of the two analyses for Wettzell and Onsala (Table 2B and 2C, respectively) results in an agreement in horizontal velocities on the 1-2 mm/yr level, while in Wettzell disagreement in height is at the same level as in Ny-Ålesund, i.e. at 3 mm/yr.

Comparing the results of Titov and Pettersen (1997), which are based on the EUROPE experiments, only, to the global analysis, good agreement is found in the north-south rate while the east-west rate resulting from the Europe analysis is too small by a factor of two. Titov and Pettersen (1997) consider the geometry of the network as a possible explanation for this result.

In height, no significant difference is found between the two analyses. However, analyses of the VLBI data carried out in other studies result in vertical rates differing significantly from those of Ma (1998). For example, Tomasi and Rioja (1998) report a vertical rate of  $6.4 \pm 1.0$  mm/yr for Ny-Ålesund. However, their value is associated with an unrealistic result for the horizontal motion.

Comparing NMA's results of the analysis of the Ny-Ålesund GPS data to those provide by Heflin (1998) results in correlation coefficients of the order of 0.7 to 0.8 for the residual time series (i.e. when linear trends are removed). This indicates that small differences in the analysis strategies and models used have a large effect on the day-to-day variations. Again, for geophysical applications, these differences need to be understood in detail.

The comparison of different techniques and analyses so far started, emphasises the need for further studies. At the moment, it is not possible to resolve the discrepancies between the different VLBI analyses as well as

```

correlation coefficient:  -0.07125 < 0.14942 < 0.35616
excess: x: 0.20069E+00 y: 0.26151E-01
curtesy: x: -0.33799E+00 y: 0.20908E+00
y = ( 0.68129E+01 +- 0.36188E-01) + ( 0.10401E+00 +- 0.74450E+00) * x
x = ( 0.16503E+01 +- 0.69185E+00) + ( 0.21467E+00 +- 0.74450E+00) * y

```

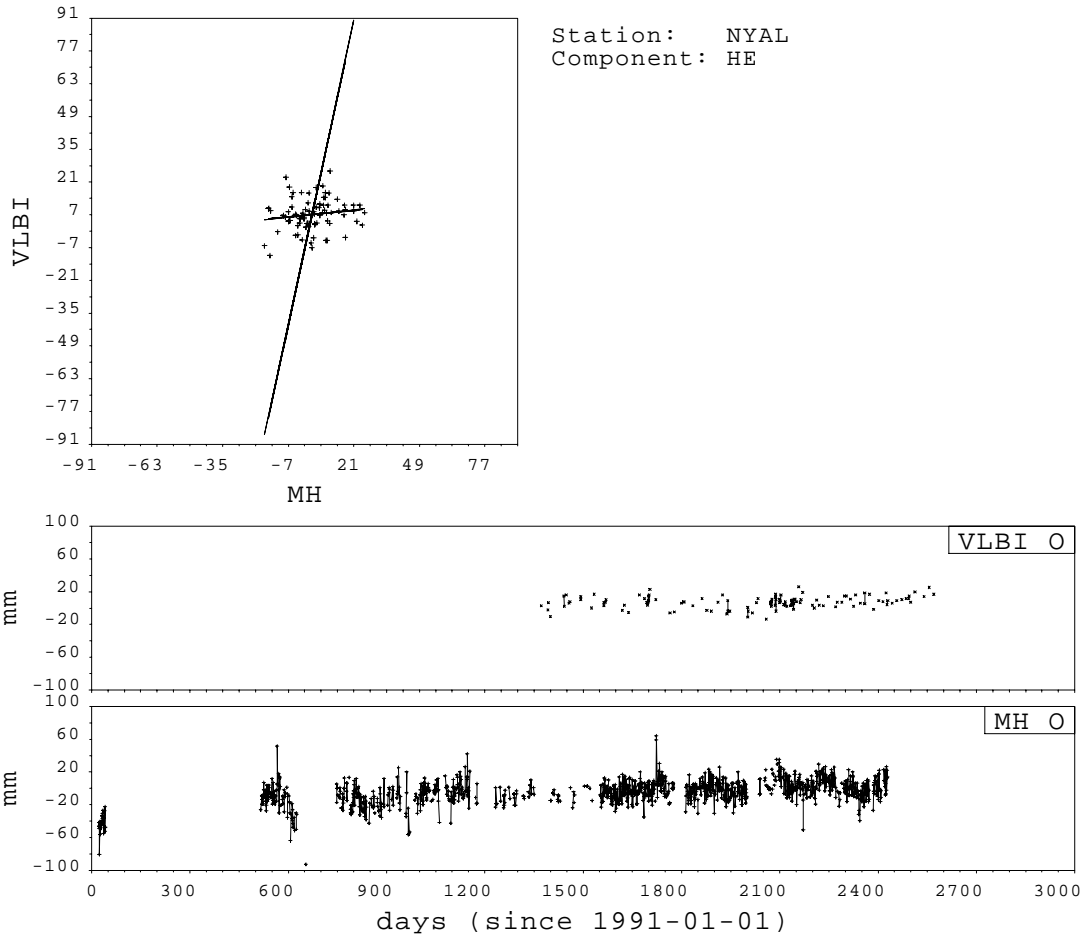


Figure 1: Variations of VLBI and GPS heights at Ny-Ålesund

Lower diagram: GPS taken from Heflin (1998); middle: VLBI taken from Ma (1998, private communication); upper: regression of GPS and VLBI.

```

correlation coefficient:  0.78068 < 0.85353 < 0.90350
excess:  x: -0.36450E+00 y: -0.72346E+00
curtesy: x: -0.85226E+00 y:  0.76094E-02
y = ( 0.66420E+02 +- 0.81512E-02) + ( 0.87767E+00 +- 0.68681E-01) * x
x = (-0.52694E+02 +- 0.80387E-01) + ( 0.83006E+00 +- 0.68681E-01) * y

```

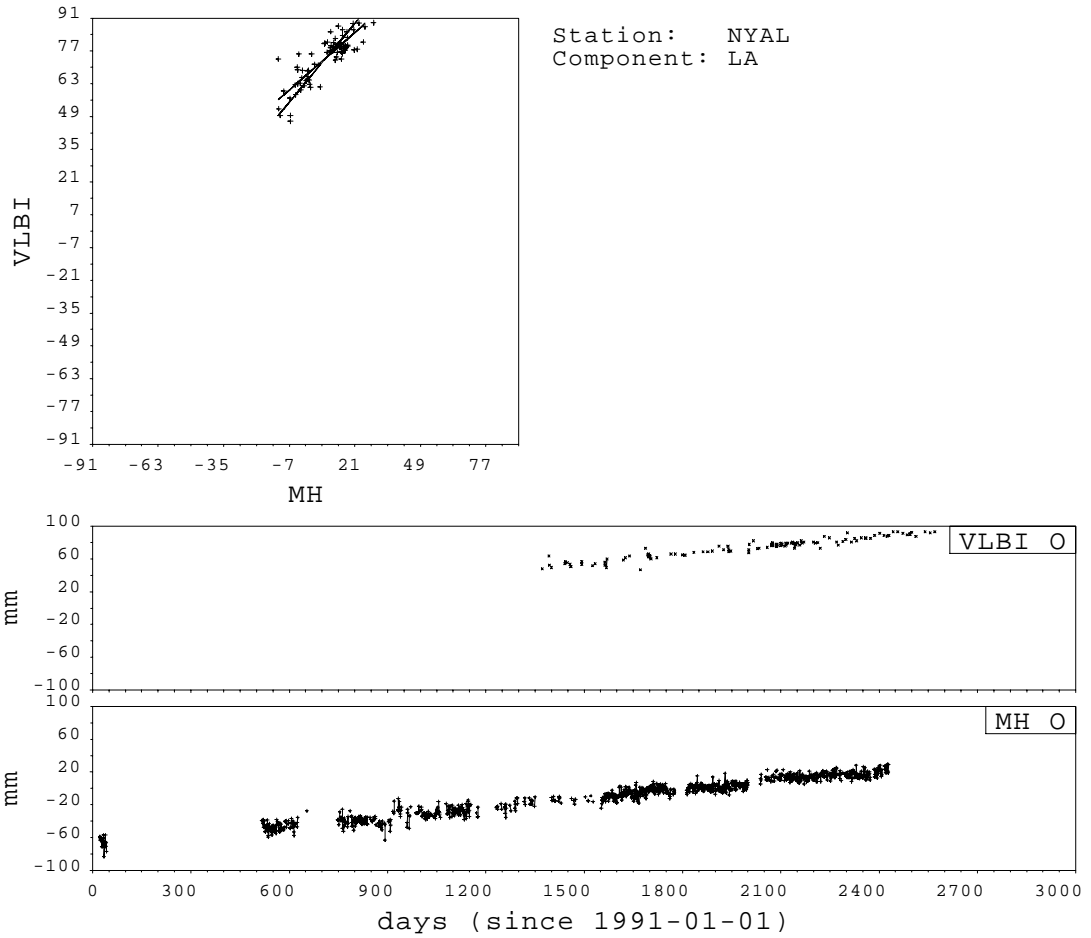


Figure 2: Variations of VLBI and GPS latitudes at Ny-Ålesund

Lower diagram: GPS taken from Heflin (1998); middle: VLBI taken from Ma (1998, private communication); upper: regression of GPS and VLBI.

```

correlation coefficient: 0.70503 < 0.80019 < 0.86705
excess: x: -0.10160E+00 y: -0.31839E+00
curtesy: x: -0.42117E+00 y: -0.64860E+00
y = ( 0.59509E+02 +- 0.71396E-02) + ( 0.93156E+00 +- 0.84325E-01) * x
x = (-0.38958E+02 +- 0.96032E-01) + ( 0.68735E+00 +- 0.84325E-01) * y

```

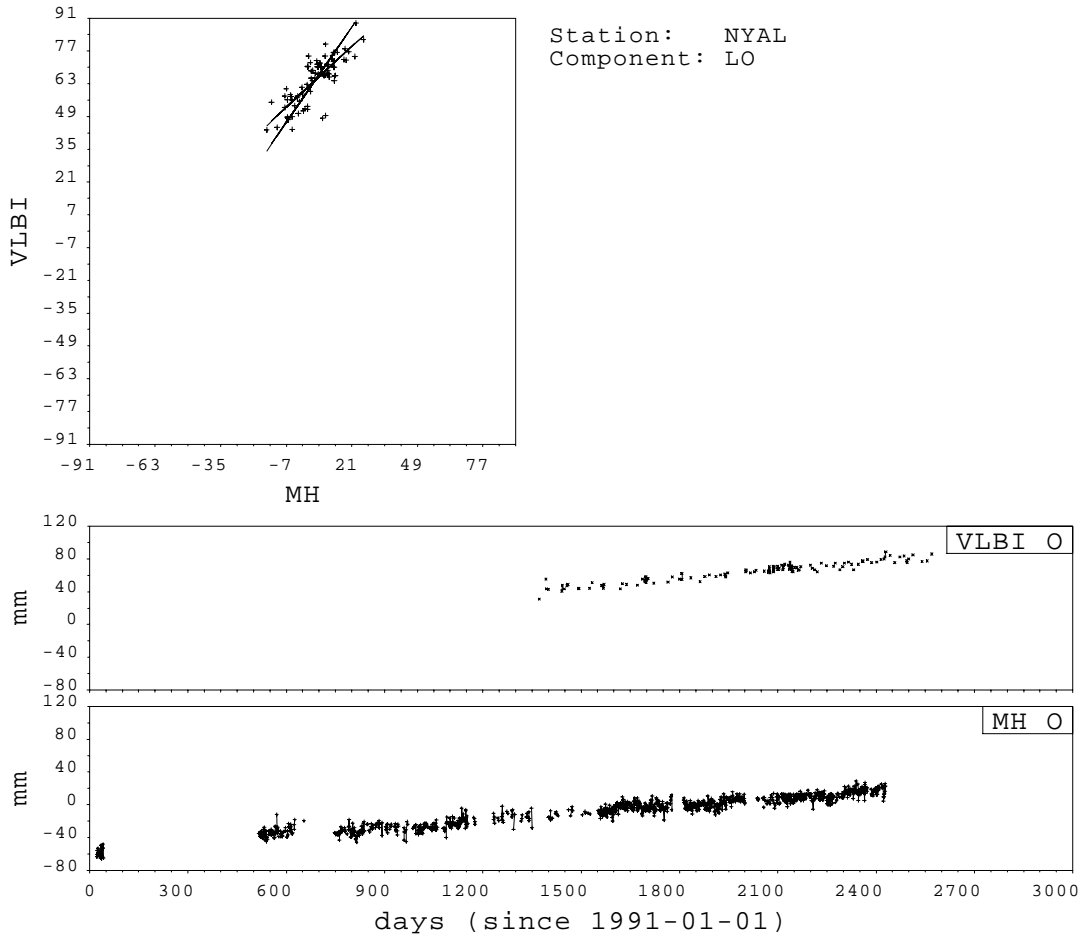


Figure 3: Variations of VLBI and GPS longitudes at Ny-Ålesund  
Lower diagram: GPS taken from Heflin (1998); middle: VLBI taken from Ma (1998, private communication); upper: regression of GPS and VLBI.

Table 2: Crustal motion at Ny-Ålesund.

Velocities are in mm/yr. NUVEL1-A (NUV.) are from Ma (1998, personal communication). VLBI rates are from Titov and Pettersen (1997) (VLBI T&P) and Ma (1998, personal communication; VLBI MA). GPS results are from Heflin (1998) in the version of 8 February 1999.

A) At Ny-Ålesund

Component	NUV.	VLBI T&P	VLBI MA	GPS
Radial	0.00	$0.4 \pm 3.6$	$1.16 \pm .54$	$4.20 \pm 0.28$
Latitude	13.60	$13.9 \pm 1.3$	$13.50 \pm .17$	$14.63 \pm 0.07$
Longitude	12.95	$6.0 \pm 2.4$	$11.75 \pm .17$	$10.64 \pm 0.08$

B) Wettzell

Component	NUV.	VLBI MA	GPS
Radial	0.00	$-0.82 \pm .16$	$-3.75 \pm 0.33$
Latitude	13.46	$13.58 \pm .12$	$14.48 \pm 0.09$
Longitude	20.34	$20.35 \pm .02$	$21.14 \pm 0.13$

C) Onsala

Component	NUV.	VLBI MA	GPS
Radial	0.00	$3.40 \pm .20$	$1.53 \pm 0.16$
Latitude	13.61	$12.84 \pm .05$	$13.74 \pm 0.05$
Longitude	18.65	$17.63 \pm .06$	$16.61 \pm 0.07$

between GPS and VLBI. The discrepancy between the global VLBI results and the GPS results in Ny-Ålesund may be due to a problem of the reference frame and the realisation of the no-net-rotation and no-net-translation criteria in the VLBI analysis. If we assume, for a moment, that the global VLBI analysis and the GPS result provide correct vertical rates for Ny-Ålesund in nearly the same reference frame, then the differential motion between GPS and VLBI antenna could be due to a sinking of the VLBI antenna or a slow uplift of the GPS monument in the permafrost. These possibilities and the wide range of vertical rates obtained emphasises the need for a control of the local ties between the various techniques with a high temporal resolution.

Unfortunately, the available classical techniques for obtaining these ties require considerable human resources (see also Section 4). Based on these techniques, a high temporal resolution will be difficult if not impossible to achieve. The development for techniques that would allow a more or less continuous tie between different antennas would be most welcome.

## 7 Identifying the cause of crustal motion

### 7.1 Surface-load induced deformations

Climatologically, Svalbard is located within the northernmost part of the area with strong seasonal changes in sea-ice (see, e.g., Barry, 1989). This area is likely to be affected by climate change at an early state. The main ice drift in the Arctic Ocean is characterised by the Transpolar Drift, which carries ice from the Beaufort Sea and the eastern Arctic Ocean westward towards the Fram Strait

west of Svalbard, through which most of the ice exits into the North Atlantic (see Gordienko and Laktionov, 1969). Moreover, the main current due to the Arctic Ocean Interbasin exchange passes along the Fram Strait, too (see, e.g., Fig.1-1 in Schmitz, 1996).

A large part of Svalbard is covered by ice and it can be expected that the ice mass responses sensitively to changes in the climate around Svalbard. In fact, changes in the ice mass on Spitsbergen can already be deduced from observations (see, e.g. Amelien *et al.*, 1998). However, our current knowledge of changes in the cryosphere is uncertain in several aspects. Consequently, recent estimates of the contribution of glaciers and ice sheets to sea level changes vary by a factor  $>2$  (see Warrick *et al.*, 1996, for a recent summary). Geodetic measurements of changes in the ice surface are either sparse (levelling) or still controversial (satellite altimetry). Mass balance models based on observations are hampered by large uncertainties in the contributing factors and often poorly constrained by observations (Warrick *et al.*, 1996). Therefore, additional constraints are most helpful in understanding the response of ice sheets and glaciers to climate variability and, eventually, climate change.

Changing ice loads induce significant visco-elastic deformations of the Earth's crust and mantle as is documented by a wealth of observations related to the post-glacial rebound induced by the last ice age. The present-day deformations are the results of a convolution of the Green's function (i.e., the impulse response of the Earth to surface loading) with the complete time history of the combined ice and water load. Therefore, these deformations are also affected by recent changes in both the present-day ice sheets and the ocean waters. The effect of the present-day forcing potentially is large enough to use the induced deformations to constrain, for example, concurrent changes in the volume of the Antarctic and Green-

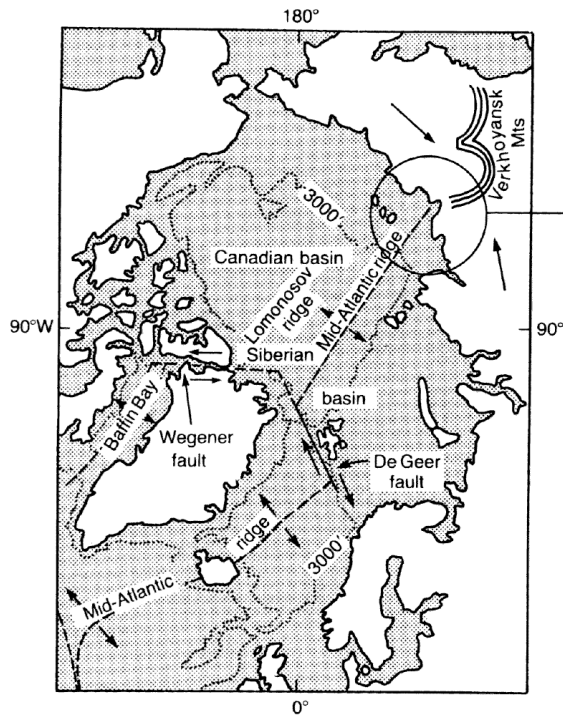


Figure 4: Tectonics of the Arctic Ocean. From (Kearey and Vine, 1990).

land ice sheets (e.g. Conrad and Hager, 1995; James and Ivins, 1995; Wahr and Han, 1997). However, the post-glacial signal in these deformations is of the same order as the deformations induced by present-day ice changes. Any interpretation therefore requires the separation of the two effects. According to the results of extensive numerical experiments carried out by Wahr *et al.* (1995), the ratio between gravity and height changes  $\dot{g}/\dot{u}$  associated with purely viscous deformations due to past mass movements (i.e. ice and water load) is approximately equal to  $-0.15 \mu\text{gal}/\text{mm}$ . This constant ratio provides the basis for the required separation. Presently, the only observations to test this empirical relation are found in Scandinavia. A comparison of observed gravity and height changes in the land-uplift area in Scandinavia indicates a ratio of  $\dot{g}/\dot{u} = -0.24 \mu\text{gal}/\text{mm}$  (Ekman and Mäkinen, 1990). However, the  $\approx -0.09 \mu\text{gal}/\text{mm}$  in excess of the theoretically expected value may represent the elastic response to present-day mass changes, which partly are to be explained by the deloading of the Baltic Sea as a consequence of the land uplift. In summary, we can expect that high-precision space-geodetic observations of present-day deformations in the vicinity of ice sheets together with gravity measurements, in principle, provide valuable constraints on changes in the ice cover. However, the combination of vertical rates with gravity changes is mandatory for a meaningful interpretation.

## 7.2 Tectonic movements

Tectonically, Svalbard is located on the north-eastern side of a long north-northwest striking transform fault (the De Geer fault, Fig. 4), which connects two parts of the mid-Atlantic ridge, namely the north-east striking ridge segment in the Norwegian Sea (north of Iceland) to the more north-northeast striking segment in the Siberian basin (Kearey and Vine, 1990). The active mid-Atlantic ridge passing through Iceland terminates SW of Svalbard at the De Geer Fault. This dextral ridge-ridge transform connects to the northernmost part of the mid-Atlantic ridge, which in turn transforms into the Verkhoyansk Mountains of Siberia by means of rotation about a fulcrum in the Siberian Islands. However, there are rather large uncertainties in the actual structure of the ridge segment southwest of Svalbard. For example, in Johnson *et al.* (1979), the large DeGeer transform fault is replaced by a north striking spreading centre. Again another sketch can be found, for example, in Birkenmajer (1981). Nevertheless, the distance of the ridge-related tectonically active region to Svalbard is small (of the order of 100 km) and the activity might well have some regional to local effects at the Kings Bay and Ny Ålesund. At large scales, the motion across the ridge segment in the Siberian basin and particularly its change along the ridge leads to a rotation in the Arctic affecting the position of Svalbard in a global reference frame.

Detailed knowledge of the present-day motion of the tectonic plates is fundamental for the validation of geophysical and geological models related to plate tectonics. The plate motion also constitutes a crucial contribution to the motion of any point on the Earth's surface. As the plate move, any fixed co-ordinates for observing sites become inconsistent. Relative motion between observing sites in the global geodetic networks are of the order of 5 cm/yr or larger. Therefore, accounting properly for the motion is a principle task in the definition and realisation of any terrestrial reference frame. The 1996 IERS conventions (McCarthy, 1996) recommend that the NNR-NUVEL1A model (DeMets *et al.*, 1994) is used to represent the velocities due to plate motion. The residual velocity vectors at all geodetic sites can then be used to validate and/or improve this model.

In Table 2, we compare the horizontal and vertical motion determined in different VLBI and GPS analyses. It should be mentioned that the uncertainties given for the global VLBI analysis are too optimistic (Ma, 1998, personal communication). Taking into account this comment, then the horizontal velocities determined in the global VLBI analysis and for the long GPS time series agree well with each other and with the model predictions.

In summary, the results indicate that this part of Svalbard, despite its nearness to the Mid-Atlantic ridge, is already on the stable part of the European plate. This is further supported by the small base line changes between Ny-Ålesund and Wettzell (see, e.g. Tomasi and Rioja, 1998).

## 8 Monitoring sea-level changes

Sea level changes due to mass exchange between cryosphere and ocean are not globally uniform (Farre and Clark, 1976). Due to the combined effect of the visco-elastic response of the Earth to ice unloading and the change in the gravitational potential, relative sea level will fall close to a melting ice sheet while at intermediate distances there will be nearly no changes. A rise in sea level will only be observed in the far-field. Thus, melting/accreting Antarctic ice will have a sea-level signature distinctively different from melting/accreting Greenland ice. Tide gauges should record the "footprint" in relative sea level due to present-day changes in the large ice sheets. Tide gauges in the near-field are particularly important for this detection. Therefore, the tide gauge data observed at Ny-Ålesund combined with space-geodetically observed crustal motion at the location is an important contribution to the monitoring of the current pattern in relative sea level changes particularly in the Arctic ocean.

In Figure 5 the monthly mean values for the tide gauge records at Ny-Ålesund and Barentsburg are shown. The data are taken from the global database of the *Permanent Service for Mean Sea Level* (PSMSL), which contains more than 1700 quality-controlled records (Spencer and Woodworth, 1993). At both locations, the monthly means are dominated by a seasonal signal with an amplitude of  $\approx 150$  mm and a maximum sea level in November. Non-seasonal variations are generally of the order of  $\pm 150$  mm with a few exceptional sea levels exceeding  $\pm 200$  mm. Also shown is the monthly difference between the two time series. The distance between Ny-Ålesund and Barentsburg is roughly 100 km and long-period sea level changes should be rather similar at both sites. In fact, for most of the months the difference is of the order of  $\pm 50$  mm, while only a few months show differences of more than  $\pm 200$  mm. Particularly for 1980, large differences occur indicating data errors in one of the two records. After 1993, the differences contain a strong linear trend, which is due to an apparent decrease of the relative sea level at Barentsburg. This may be related to a poor maintenance of the local tide gauge benchmark or a problem with the tide gauge itself. However, the overall trend in Barentsburg is not significantly affected by this possibly erroneous part of the record.

To determine the trend in RSL, a model consisting of a seasonal cycle and a linear trend is fitted to the two time series in a least squares fit. The seasonal cycle is represented by an annual and a semi-annual harmonic constituent. The trends resulting from the fits are compiled in Table 3 together with other relevant parameters of the two time series.

A change in sea level measured relative to a benchmark on land is the difference between geocentric sea surface changes and geocentric vertical motion of the tide gauge benchmark (ideally this is identical to the vertical motion

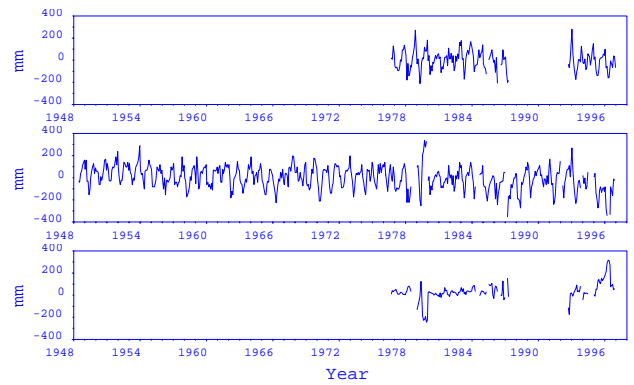


Figure 5: Tide gauge records at Ny-Ålesund and Barentsburg.

Upper diagram: Ny-Ålesund; middle: Barentsburg; lower: Ny-Ålesund - Barentsburg. The time series are monthly mean sea levels in mm.

of the crust). For linear trends, we therefore can write

$$r = t + v \quad (1)$$

where  $r$  is the geocentric sea level trend (positive for rise),  $t$  the RSL trend (positive for rise), and  $v$  the geocentric vertical crustal motion (positive for uplift). The determination of the geocentric sea-level changes thus requires knowledge of the vertical crustal motion  $v$ . At Ny-Ålesund, the tide gauge is regularly connected to the space-geodetic benchmarks by precise levelling. As reported in Section 4, the measurements so far do not indicate a relative movement of the tide gauge with respect to land. VLBI and GPS provide information on the three-dimensional movement of the crust. Unfortunately, the results from the two main techniques monitoring crustal movements in Ny-Ålesund do not agree for the height component (see Table 2 and Section 7). Possible explanations for the discrepancies may be in problems of connecting VLBI and GPS in a unique way to the solid Earth or local effects at the VLBI and/or GPS antenna in Ny-Ålesund. A more detailed investigation is required before reliable estimates of  $v$  can be deduced. Nevertheless, after eliminating known contributions by using available models we can extract useful information from the RSL trends.

Currently, a major contribution to RSL changes is coming from the on-going post-glacial rebound induced by the disintegration of the large ice sheets at the end of the last ice age. To decontaminate RSL trends from the post-glacial signal (pgs), Peltier and Tushingham (1989) used a geophysical model to compute the pgs in RSL,  $p$ , and computed a decontaminated geocentric sea level

$$\hat{r} = t - p. \quad (2)$$

In another approach, Zerbini *et al.* (1996) used

$$v_o = -(t - p - r'); \quad (3)$$

assuming  $r' = 1.8$  mm/yr to determine crustal vertical motion in the Mediterranean and found small (of the order of  $\pm 1$  mm/yr) and spatially consistent values for the

Table 3: Trends in sea level at Ny-Ålesund and Barentsburg.

N is the number of monthly values in the record.  $t$  is the linear term and  $\delta t$  the standard error resulting from the fit of a trend plus annual and semi-annual constituent to the time series.  $\hat{r}$  is computed from eq. 2, while  $v_o$  results from eq. 3 assuming  $r = 1.8$  mm/yr. The indices 1 and 2 refer to the two models for the pgs (see text). All rates in mm/yr.

Station	Long.	Lat.	Begin	End	N	$t$	$\delta t$	$p_1$	$p_2$	$\hat{r}_1$	$\hat{r}_2$	$v_{o1}$	$v_{o2}$
Ny-Ålesund	11°56'E	78°56'N	1976	1996	175	-1.373	0.8	-0.9	-1.3	-0.5	-0.1	2.3	1.9
Barentsburg	14°15'E	78°04'N	1948	1996	560	-2.253	0.3	-2.0	-2.6	-0.3	0.3	2.1	1.5

crustal motion. In Table 3,  $\hat{r}$  and  $v_o$  are given for the two stations using two different post-glacial rebound models provided by Mitrovica (1996, personal communication). Model 1 has an elastic lithosphere of 120 km, and upper and lower mantle viscosities of  $1 \times 10^{21}$  Pas and  $2 \times 10^{21}$  Pas, respectively. Model 2 is identical to Model 1 except for a lower mantle viscosity of  $4.75 \times 10^{21}$  Pas. The ice model used is ICE-3G (Tushingham and Peltier, 1991).

For both post-glacial rebound models, the values for  $\hat{r}$  are close to zero indicating that any vertical crustal motion others than post-glacial rebound is nearly compensating any geocentric sea level change. Assuming tentatively a geocentric sea level rise of 1.8 mm/yr (Douglas, 1997), non-post-glacial vertical crustal uplift rates of the order of 2 mm/yr can be deduced. However, since both steric and non-steric sea-level changes are likely to display a large spatial variability, this assumption is not very helpful.

The determination of vertical crustal motion with an accuracy of better than 1 mm/yr would allow to separate the crustal motion and geocentric sea-level changes. Using, for example, the GPS-determined rate of  $v = 4.20$  mm/yr, we get a geocentric sea-level rate  $r$  of +2.93 mm/yr at Ny-Ålesund. It would be interesting to compare this trend to sea-level rates determined from satellite altimetry.

For further interpretation, it will be helpful to separate the pgs in RSL according to  $p = p_s - p_v$  with  $p_s$  the geocentric pgs in sea level and  $p_v$  the geocentric pgs in vertical crustal motion. Thus we get

$$r' = t - (p_s - p_v) + v_o \quad (4)$$

with  $v = v_o + p_v$  and  $v_o$  the vertical crustal motion others than the pgs. The uncertainty of the pgs predicted by geophysical models is for the Svalbard area at least of the order of 1 mm/yr. Nevertheless, using model predictions of the pgs would help to explain a part of the 3 mm/yr geocentric sea-level rate quoted above.

## 9 Additional comments

The Earth tide observations have resulted in a long and high-quality time series, which has been used to determine preliminary Earth tide parameters for Ny-Ålesund. Particularly in the semi-diurnal band, a large ocean loading signal is found. Preliminary computations of ocean loading carried out by Scherneck (1998, personal communication) and Baker (1998, personal communication)

reveal considerable discrepancies between the observations and the model predictions as well as between different ocean tidal models. Using the observed parameters in the processing of the absolute gravity measurements, small residual tidal signals were left in the absolute measurements indicating that the tidal parameters were not adequate. The distance between the Earth tide observatory and the absolute point is about 1.8 km. Due to the large ocean loading signal and the short distance to the coast, a large spatial gradient in the Earth tide parameters can be expected. Moreover, significant temporal variations have been detected in the Earth tide parameters, and these may be due to seasonal changes in the semi-diurnal ocean tides or to unaccounted variations in the calibration factor of the gravimeter.

To get precise Earth tide parameters for the geodetic observatory to be used in the VLBI analysis, it will be important to carry out tidal measurements at the observatory with a superconducting gravimeter.

## 10 Conclusions

The VLBI station at the geodetic observatory of NMA in Ny-Ålesund has participated in the European VLBI experiments nearly as scheduled. A proper maintenance of the antenna and the equipment has been provided. Due to a lack of human resources, analysis work has been delayed. However, it is expected that new analysis work can be started in 1999. The discrepancies between GPS and VLBI determined vertical rates will be one of the problems to focus on. In this context, the contribution of unmodelled tropospheric effects to station co-ordinates will be investigated.

Summarising the results of the interpretations reported above, we can state that the geodetic multi-parameter observations collected at Ny-Ålesund are of high potential value for global change studies and the value of the data set is expected to increase greatly as the observation period is extended into the future. Nevertheless, results relevant to the EU project can be expected from a continuation of the exploitation of the available data. In particular, more advanced analyses of the space-geodetic observations will allow to reduce the uncertainty of the geocentric vertical crustal motion and thus provide a better estimate of the geocentric sea-level trend.

## Acknowledgements

Among others, the following persons from NMA contribute(d) to the project or other parts of the work reported here: Helge Geir Digre (station staff), Leif Grimstveit (local surveys and analyses), Gunn Marit Hernes (station manager until 1997), David Holland (station staff), Oddgeir Kristianson (GPS analyses), Svein Rekkedal (drift of permanent stations), Knut Røthing (Earth tide analysis), John Sundsby (tide gauge levelling), Leif Morten Tangen (station manager).

The author would like to thank Jerry X. Mitrovica, who provided the models for the post-glacial rebound signal in RSL, and Chopo Ma, who made available the results of a global analysis of the VLBI data.

## References

- Amelien, J., Rolstad, C., and Isaksson, E. (1998). Monitoring glaciers in svalbard. In *Proceedings for the 27-th Int. Symp. on Remote Sensing of Environment: Information for Sustainability, June 8-12, 1998, Tromsø, Norway*, pages 38–43. Norwegian Space Centre.
- Barry, R. G. (1989). The present climate of the arctic ocean and possible past and future states. In Y. Herman, editor, *The Arctic Sea - Climatology, Oceanography, Geology and Biology*, pages 1–46. New York.
- Birkenmajer, K. (1981). The geology of Svalbard, the western parts of the Barents Sea, and the continental margin of Scandinavia. In A. E. M. Nairn, M. J. Churkin, and F. G. Stehli, editors, *The Arctic Ocean*, volume 5 of *The Ocean Basins and Margins*, pages 265–329. Plenum Press, New York and London.
- Conrad, C. P. and Hager, B. H. (1995). The elastic response of the Earth to interannual variations in Antarctic precipitation. *Geophys. Res. Lett.*, **22**, 3183–3186.
- DeMets, C., Gordon, R. G., Argus, D. F., and Stein, S. (1994). Effect of recent revisions to the geomagnetic reversal time scale on estimates of current plate motions. *Geophys. Res. Lett.*, **21**, 2191–2194.
- Douglas, B. C. (1997). Global sea level rise: a redetermination. *Surveys Geophys.*, **18**, 279–292.
- Ekman, M. and Mäkinen, J. (1990). Land uplift and gravity change in Fennoscandia 1966 - 1989. In *11th General Meeting, Copenhagen 1990*. Nordic Geodetic Commission.
- Farrell, W. E. and Clark, J. A. (1976). On postglacial sea level. *Geophys. J. R. Astron. Soc.*, **46**, 647–667.
- Gordienko, P. A. and Laktionov, A. E. (1969). Circulation and physics of the Arctic Basin waters. *Annals of the International Geophysical Year*, **46**, 94–112.
- Grimstveit, L. and Rekkedal, S. (1998). Geodetic control of permanent sites in tromsø and ny-ålesund. In H.-P. Plag, editor, *Book of Extended Abstracts for the Ninth General Assembly of the Working group of European Geoscientists for the Establishment of Networks for Earth-science Research. Second Edition*, pages 25–28. Norwegian Mapping Authority.
- Heflin, M. B. (1998). GPS time series. <http://sideshow.jpl.nasa.gov/mbh/series.html>.
- James, T. S. and Ivins, E. R. (1995). Present-day Antarctic ice mass changes and crustal motion. *Geophys. Res. Lett.*, **22**, 973–976.
- Johnson, G. L., Taylor, P. T., Vogt, P. R., and Sweeney, J. F. (1979). Arctic basin morphology. *Polarforschung*, **48**, 20–30.
- Kearey, P. and Vine, F. J. (1990). *Global Tectonics*. Geoscience Texts. Blackwell Scientific Publications, Oxford. 302 pp.
- McCarthy, D. D. e. (1996). IERS Conventions 1996. Iers technical note 21, IERS, Observatoire de Paris, Paris. 95 pages.
- Peltier, W. R. and Tushingham, A. M. (1989). Global sea level rise and the Greenhouse effect: Might they be connected? *Science*, **244**, 806–810.
- Repstad, E. (1997). Very long baseline interferometry: Beregning av eksperimententer fra perioden mellom 4. oktober 1994 og 22 april 1997. Unpublished report, Norwegian Mapping Authority.
- Schmitz, W. J. j. (1996). On the World Ocean Circulation: Volume I: Some Global Features/North Atlantic Circulation. Technical report, Woods Hole Oceanographic Institution, Technical Report, WHOI-96-03.
- Spencer, N. E. and Woodworth, P. L. (1993). Data holdings of the Permanent Service for Mean Sea Level. Technical report, Permanent Service for Mean Sea Level, Bidston, UK. 81pp.
- Titov, O. and Pettersen, B. R. (1997). Analysis of tectonic motion for the ny-ålesund VLBI station. In B. R. Pettersen, editor, *Proceed. 12th Working Meeting on European VLBI for Geodesy and Astrometry*, pages 86–93. Statens Kartverk, Hønefoss.
- Tomasi, P. and Rioja, M. (1998). South-western Europe movements with VLBI. In H.-P. Plag, editor, *Book of Extended Abstracts for the Ninth General Assembly of the Working group of European Geoscientists for the Establishment of Networks for Earth-science Research*, pages 64–65. Norwegian Mapping Authority.
- Tushingham, A. M. and Peltier, W. R. (1991). Ice-3G: a new global model of late pleistocene deglaciation based upon geophysical predictions of post-glacial relative sea level change. *J. Geophys. Res.*, **96**, 4497–4523.

- Wahr, J. M. and Han, D. (1997). Predictions of crustal deformation caused by changing polar ice on a viscoelastic Earth. *Surveys Geophys.*, **18**, 303–312.
- Wahr, J. M., Dazhong, H., and Trupin, A. (1995). Prediction of vertical uplift caused by changing polar ice volumes on visco-elastic earth. *Geophys. Res. Lett.*, **22**, 977–980.
- Warrick, R. A., Provost, C. I., Meier, M. F., Oerlemans, J., and Woodworth, P. L. (1996). Changes in sea level. In J. T. Houghton, L. G. Meira Filho, B. A. Callander, N. Harris, A. Kattenberg, and K. Maskell, editors, *Climate Change 1995–The science of climate change*, pages 359–405. Cambridge University Press, Cambridge, UK.
- Zerbini, S., Plag, H.-P., Baker, T., Becker, M., Billiris, H., Bürki, B., Kahle, H.-G., Marson, I., Pezzoli, L., Richter, B., Romangoli, C., Sztobryn, M., Tomasi, P., Tsimplis, M., Veis, G., and Verrone, G. (1996). Sea level in the Mediterranean: a first step towards separation of crustal movements and absolute sea-level variations. *Global and Planetary Change*, **14**, 1–48.
- Zumberge, J. F., Heflin, M. B., Jefferson, D. C., and Watkins, M. M. (1997). Precise point positioning for the efficient and robust analysis of GPS data from large networks. *J. Geophys. Res.*, **102**, 5005–50017.

# Bonn Correlator Report

A. Müskens

*Geodätisches Institut der Universität Bonn (GIUB), Nussallee 17, D-53115 Bonn, Germany*

W. Alef

*Max-Planck-Institut für Radioastronomie (MPIfR), Auf dem Hügel 69, D-53121 Bonn, Germany*

**Abstract.** The correlator at the Max-Planck Institute for Radioastronomy, Bonn has played an important role in European VLBI since the mid-seventies, catering to the needs of astronomers and geodesists. The operation in Bonn has been additionally supported by the Geodetic Institute of the University of Bonn (GIUB) and later by the Institute for Applied Geodesy in Frankfurt (IFAG: now BKG). This report will give a short description of the status and future activities at the Bonn VLBI Correlator.

## Playback Recorders

8 of the 9 Metrum/Honeywell playback drives have already been upgraded with Mk4/VLBA style control electronics and thin tape capability; the 9th drive will be finished in February. Due to problems (oscillations) in 3 of the 5 drives with MPIfR modified playback electronics, and in order to prepare for the MK4 correlator (32 tracks) we have started to change these 3 drives to the VLBA/MK4 "standard" read electronics. We expect to have 9 operational playback drives available by the end of February. The Penny&Giles prototype playback recorder has been removed from the correlator.



Figure 1. Playback Recorders (all and one single rec. front)

## Throughput

Due to the above mentioned problems and the preparations for the MK4 processor the priorities at the correlator were changed. The highest priority is now preparing the tape drives for the MK4 correlator, the delivery of which is expected in summer or autumn of this year. The number of tape drives that can at present be used for correlation has gone down to 5 or 6. As a consequence of that the throughput went down from 90 to about 60 delays in the delivery of replacement heads. We expect to reach about 90 throughput again in March using both the MK3A and the old MK3 correlators. The present backlog for astronomical projects is about 3

months, while there is no backlog for the correlation of geodetic observations. History usage of the passed year 1998 was 36/64 percentage (geodesy/astronomy) for the CPU processor time.

## Operations

The playback quality of thin tape recordings has improved in the last year. It is now comparable to that of thick tape recordings. Log access via the ftp areas at CDDIS (geodesy) and Bologna (astronomy) is routine. Logs are stored on these 2 computers promptly, with few exceptions. NRAO's tape tracking program TRACK is used by all stations now, again with the exception of places where access to the Internet is difficult or impossible. In general tapes arrive at the correlator within 2 weeks after the observation.

## EVN Support

EVN in absentia correlation is now supported by Bob Campbell from Dwingeloo. Correlation of EVN projects has been made easier and more reliable by using GPS measured clock and clock rate offsets for the correlation; fringe search is nearly never needed any more for preparing the correlation of EVN observations. The reliability was increased as clock rates and jumps are monitored and compensated.



Figure 2. Mk3A and Mk3 processor

## Mark IV Correlator

Haystack's schedule for the installation of the MK4 correlator in Bonn is as follows:

- Jan/Feb Physical configuration of the MK4 correlator is finalised
- Jun/Jul Final testing of the BKG correlation hardware at Haystack  
Observatory and acceptance from BKG and MPI
- Jul ship all hardware to Bonn (processor, station units, control computer)
- Aug Arrival and installation of correlator by Haystack crew;  
training of Bonn personnel

**Bonn:** The upgrade of the 9 tape drives to full MK4 compatibility will have been finished by the end of February. The old MK3 correlator will be removed by the end of May to make space for the MK4 correlator and the station units. In August start correlating with both the MK3A and the MK4 correlator: each with 4 to 5 tape units. After September phase out correlation on the MK3A correlator with end open. Note: the MK3 correlator can still correlate on 1.1.2000.

## Recent VLBI activities at the Communications Research Laboratory, Japan

Tetsuro Kondo<sup>1</sup>, Noriyuki Kurihara, Yasuhiro Koyama, Junichi Nakajima,  
Ryuichi Ichikawa, Eiji Kawai, and Mamoru Sekido

*Kashima Space Research Center  
Communications Research Laboratory  
893-1 Hirai, Kashima, Ibaraki 314-0012, Japan*

Taizoh Yoshino, Jun Amagai, Kouichi Sebata, Masato Furuya,  
Yukio Takahashi, Hitoshi Kiuchi, and Akihiro Kaneko

*Communications Research Laboratory  
4-2-1 Nukui-kita, Koganei, Tokyo 184-8795, Japan*

### Abstract

Communications Research Laboratory (CRL) has led the development of VLBI technique in Japan and is keeping high activities in both observations and technical developments. CRL has promoted Key Stone Project (KSP) dedicated to monitoring the crustal deformation around the Tokyo metropolitan area using the space geodetic technique such as VLBI and SLR. In the KSP, real-time VLBI technique was developed and it has been applied to form a large big radio telescope connected by a high speed communications link. As for the next generation VLBI terminal, the Giga-bit VLBI system consisting of a high speed sampler (1Gsps/4ch/2bit) and a high speed digital data recorder (1024 Mbps) has also been developed. The first fringes using this system were successfully observed. Besides these developments, optical-linked RF interferometer has been investigated to measure phase delay precisely. The performance of GPS frequency reference receiver was tested to evaluate the possibility of its adoption as a frequency standard in VLBI observations in order to deploy VLBI-like techniques widely.

## 1. Introduction

A VLBI group in the Communications Research Laboratory (CRL) has a long history more than 20 years. In this report, we introduce our recent activities related to VLBI. CRL has developed a compact VLBI network named KSP consisting of four stations in and around the Tokyo metropolitan area, which is dedicated to monitoring the crustal deformation there. In 1995, the KSP started regular observations. Observations and analyses are fully automated in the KSP. Real-time VLBI technique was also developed on the KSP network. Now routine observations spanning 24 hours are carrying out every other day using the real-time VLBI technique. This real-time VLBI technique is now expanded to connect a 64-m antenna at USUDA and a 34-m antenna at Kashima besides KSP stations to increase sensitivity to detect very weak radio sources. Test observation was successfully carried out in December 1998. In parallel with the KSP operation, the

---

<sup>1</sup>E-mail: kondo@crl.go.jp

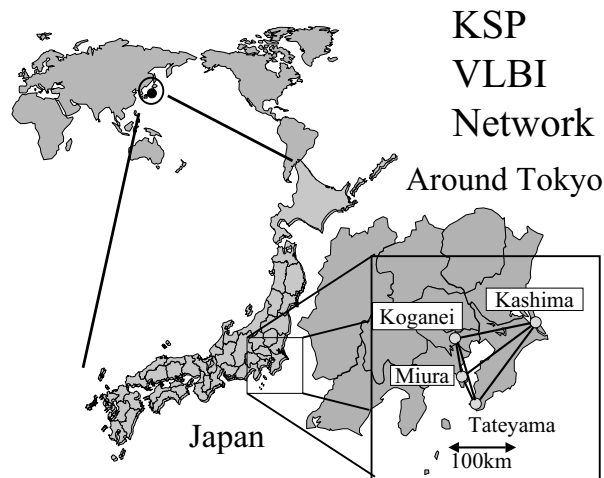


Figure 1. Location of the Keystone Project VLBI network.

Giga-bit VLBI system consisting of a high speed sampler (1Gsps/4ch/2bit) and a high speed digital data recorder (1024 Mbps) has been developed to increase the sensitivity of observations. The test observation using this system was made in July 1998, and the first fringes were successfully obtained. In addition to these developments, different approach to increase the accuracy of measurements has been investigated. It is optical-linked RF interferometer aiming to measure phase delay precisely. In the meantime, a GPS time and frequency reference receiver has shown remarkable progress in performance in recent years. It can supply stable signals at low cost. In order to deploy VLBI-like techniques widely, the performance of GPS frequency reference receiver was tested to evaluate the possibility of its adoption as a frequency standard in VLBI observations.

## 2. Key Stone Project

In 1993, CRL started the establishment of the VLBI network dedicated to monitoring the crustal deformation around the Tokyo metropolitan area in Japan. This VLBI network consists of four stations (Fig.1), and was named “Key Stone Project” (KSP) network after the Japanese traditional saying that relates to earthquake prevention [Koyama *et al.*, 1998]. In September, 1996 the KSP entered a full operation phase consisting of daily observations spanning 5 to 6 hours using a conventional tape recording method system. Along with these daily observations, we established a real-time VLBI in cooperation with the Nippon Telephone and Telegraph Co [Kiuchi *et al.*, 1999]. Real-time VLBI means a correlation processing in real time using high-rate transmission links (maximum network speed is 2.4 Gbps) between the four KSP stations (Fig.2). This real-time processing has been used in routine operations since June 4, 1997. Since then the length of a session, which is a series of scans of quasars, has become free from a restriction arising from the correlation processing in the case of a tape-recording-based VLBI. We began routine 24-hour observations every two days on September 30, 1997.

Thus we have been making continuous improvement both in system hardware and in the observation method to improve measurement accuracy. Now repeatability reaches about a 2-mm level in baseline length in our VLBI network [Kondo *et al.*, 1998].

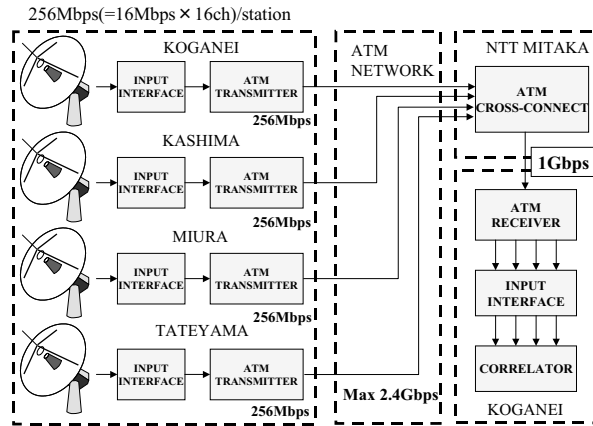


Figure 2. Block diagram of the KSP real-time VLBI system.

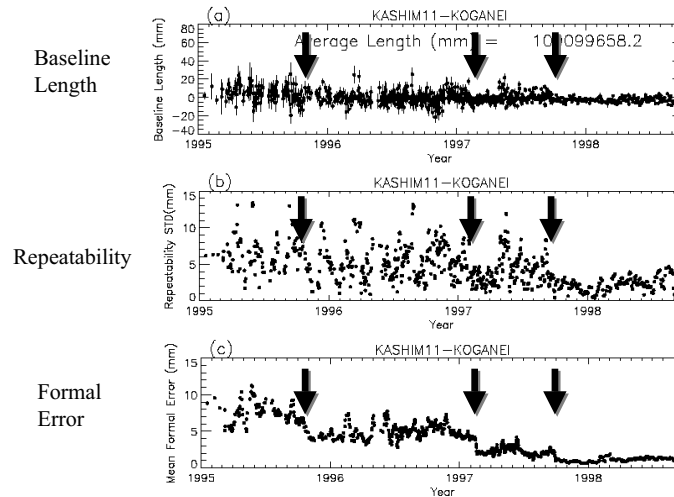
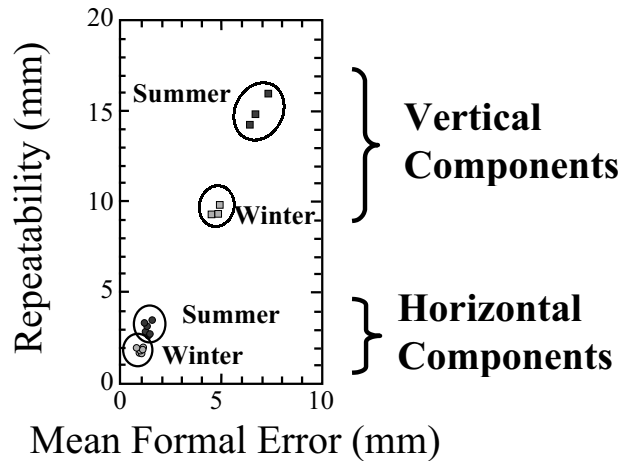


Figure 3. Evolution of baseline length between Kashima and Koganei (a), repeatabilities (b), and mean formal errors (c) of five continuous samples of baseline length.



**Figure 4.** Scatter plots of repeatabilities and formal errors for horizontal station positions and vertical station positions, for the two sub-periods.

Figure 3 shows the evolution of measured baseline lengths for the Kashima-Koganei baseline, and the standard deviations and mean formal errors of the five continuous samples of the baseline length data for the period from January, 1995 to September, 1998. The formal error obtained from each baseline analysis almost corresponds to the standard deviation of O-C residuals after parameter fitting in a session. We can see stepwise structures in the plot of mean formal errors, in particular at three epochs (at the end of October, 1995, at the middle of February, 1997, and at the end of September, 1997). This demonstrates a drastic improvement in system. The first two correspond to improvements in the system hardware (such as an increase in temperature stability in a receiver room) while the last one corresponds to the extension of the session time. As a seasonal effect can be seen in Figure 3, we divided a year into two sub-periods representing winter and summer seasons (i.e, October, 1997 to March, 1998 and April, 1998 to September, 1998) and made statistical calculations for the two sub-periods. In Figure 4, averaged repeatabilities and mean formal errors of station positions are plotted for these two sub-periods. The simple average of repeatabilities (formal errors) of station positions for all stations for east-west, north-south, and vertical components for the winter season are 1.9 mm (0.9 mm), 1.8 mm (1.0 mm), 9.5 mm (4.7 mm), those for the summer season are 3.0 mm (1.3 mm), 3.0 mm (1.4 mm), and 15.0 mm (6.8 mm), and those for full year are 2.5 mm (1.1 mm), 2.4 mm (1.2 mm), and 12.3 mm (5.9 mm), respectively.

Both repeatability and mean formal error become worse in the summer season by factors about 1.6 and 1.4 compared with those in the winter season. Moreover the repeatability is worse than the mean formal error by about a factor of two.

The real-time VLBI technique realized on the KSP-VLBI network has been expanded to connect a 64-m antenna at USUDA and a 34-m antenna at Kashima to form a “large virtual radio telescope” to increase sensitivity to detect very weak radio sources [*Takahashi et al.,1998*]. Test observation was successfully carried out in December 1998.

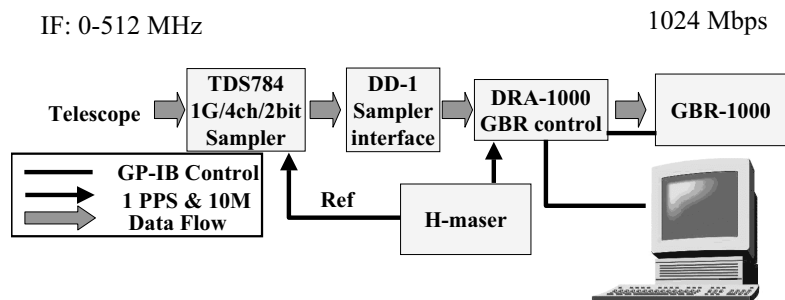


**Figure 5.** Schematic diagram of the Giga-bit VLBI system for observations.

### 3. Giga-bit VLBI System

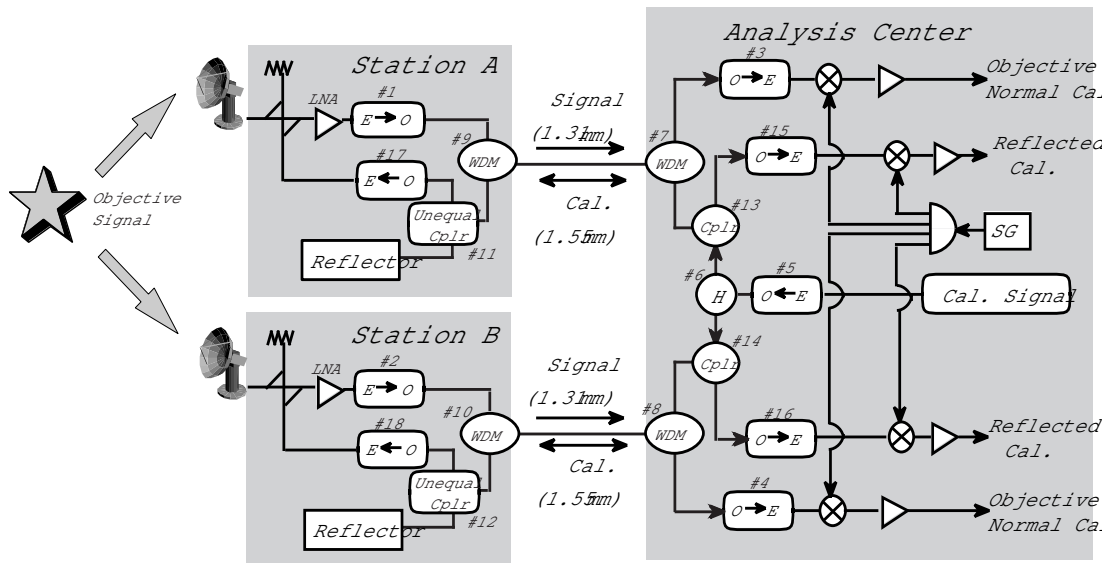
We started the development of the Giga-bit VLBI system in 1995 to improve sensitivity of the VLBI system. Test observations were carried out on the Kashima-Koganei baseline of KSP VLBI network on July 10, 1998. And the first fringes were successfully detected [*Koyama et al.*, 1998].

Figure 5 shows the block diagram of the giga-bit VLBI system. Baseband IF signals are sampled by TDS784 (Tektro) sampler with a speed of 1 Gbps (=1024 Mbps). TDS784 can digitize four analog data channels at 1 Gbps with 2 bits per sample. A DD-1 sampler interface selects one channel data and transfer the 1 Gbps 1 bit per sample data to a high speed digital data recorder TOSHIBA GBR-1000. The original GBR-1000 recorder has a recording speed at 958 Mbps. The internal clock rate was hence increased by 7 % to achieve the recording speed of 1 Gbps.

Data were processed by GICO (Giga-bit CORrelator) which consists of UWBC (Ultra Wide Band Correlator) originally developed for the Nobeyama Millimeter array of the National Astronomical Observatory. The processor is an XF type correlator with the 256 lags of cross-correlation function capable to process at 2048 Mbps.

### 4. Optical-linked RF Interferometer

The concept of optical-linked RF interferometer is a connected-element interferometer. RF signals received by antenna are directly converted into optical signals and then transmitted through a fiber optic link instead of use of metal lines like a coaxial cable. In a connected-element interferometer, common local oscillator signals are used for the frequency conversion of RF signals from each antenna. Thus no clock parameter estimation is necessary in a baseline analysis unlike an general VLBI analysis for geodetic



**Figure 6.** System configuration of the optical-linked RF interferometer.

purpose. Even though higher stability against the temperature change is expected for optical fiber link than metal lines, delay change occurred in the transmission line should be compensated for the application of precise geodetic observation.

Figure 6 shows the configuration of the optical-linked RF interferometer that can compensate the fiber delay with high accuracy [Amagai *et al.*, 1998]. Signals received by antenna at each site are amplified by a low-noise amplifier (LNA) and converted to optical signals on the carrier at a wavelength of 1310 nm by a laser diode. The optical signals are then transmitted through optical fiber to the analysis center. There optical signals are converted to electronic signals and they are further converted into video signals using common local signals. Then video signals are cross-correlated. In this system, delay changes occurring in the optical fibers are compensated by using phase calibration signals injected in front of LNA. This is the same method used in the geodetic VLBI. Further delay changes caused by refractive index difference are compensated by using calibration signals optically reflected from each site.

Maximum fiber length capable to use in this system was estimated from signal-to-noise ratio analysis at fiber optic links. It was estimated to be about 40 km when the combination of Ortel 3541A laser diode and Ortel 4515A photo detector is used.

## 5. GPS Receiver for Use of VLBI Frequency Standard

The performance of GPS time-and-frequency reference receivers has advanced to the point where they are now widely used to supply a highly stable signals ( $1 \times 10^{-12}$ /day) at a low cost. Although their stability is less than that of the hydrogen-maser frequency standard (H-maser clock) ( $\sim 1 \times 10^{-14}$ /day) conventionally used for VLBI, their lower cost is attractive when we consider the wide deployment of VLBI and VLBI-like techniques. We evaluated the performance of a GPS receiver by measuring its phase stability to determine whether it is suitable for supplying a standard frequency for VLBI observations.

We conducted test VLBI observations on May 13, 1998 on the Kashima-Koganei baseline (about 109 km in length) to confirm the performance of a GPS time-and-frequency reference receiver. The configuration of the test observation is shown in Fig. 7. At the

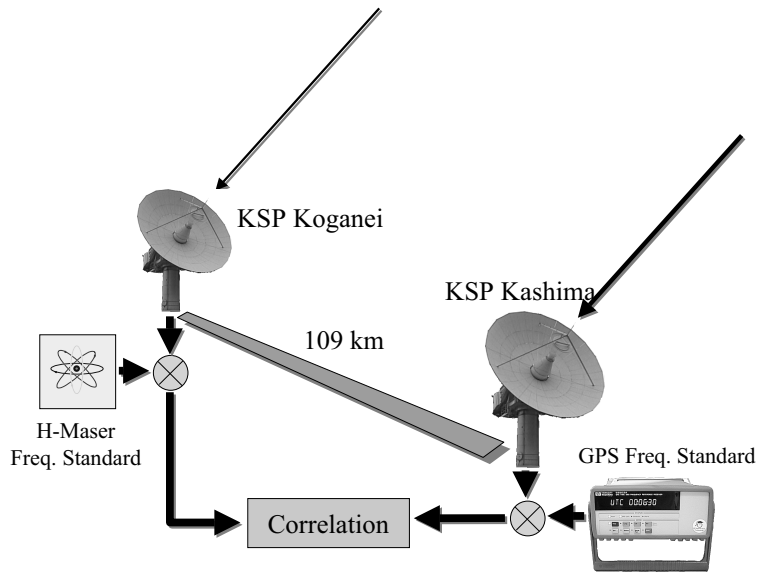


**Figure 7.** Configuration of test VLBI observation using GPS frequency standard.

Kashima station, the system-reference frequencies were supplied by a GPS reference receiver (HP 58503A) instead of an H-maser clock, while an H-maser clock was used at the Koganei station. Both “real-time” VLBI and “tape-based” VLBI were carried out. Cross-correlation processing was carried out in real time at the Koganei station using data transmitted through an asynchronous transfer mode network. Cross-correlation processing using the recorded data was performed later. The correlation-period units were set to 3 s. Two types of fringe searches were used in integrating the time-segmented correlation data. One was a normal fringe search in which only the linear-phase change with respect to time was compensated for. The other one was a fringe search using a third-order polynomial function with respect to time.

The coarse delay search functions obtained using these fringe searches are shown in Fig. 8. The received radio source was 3C273B, and the integration period was 90 s. Only one channel in the 8-GHz band is shown in the figure. There was a scattered structure in the delay rate direction for the normal fringe search (Fig. 8(left)) due to a higher-order phase change that could not be compensated for by the linear phase-change correction. There was a simple peak structure and a larger correlation amplitude when a third-order polynomial function was applied (Fig. 8(right)).

To compare these results with those for conventional VLBI observation, we conducted the same observation two days later and using H-maser clocks at both stations. The relation between the correlation amplitude and integration period for both observations is shown in Fig. 9. A third-degree polynomial search was used for the observation made using the GPS clock. For the H-maser experiment, no difference was observed between search methods. For the GPS experiment, the correlation amplitude fell when the integration period exceeded 100 s. In other words, we can say, a GPS time-and-frequency reference receiver can be used to supply a standard frequency for VLBI for frequencies up to 8 GHz if a third-order fringe search is used and the integration period is less than 100 s.

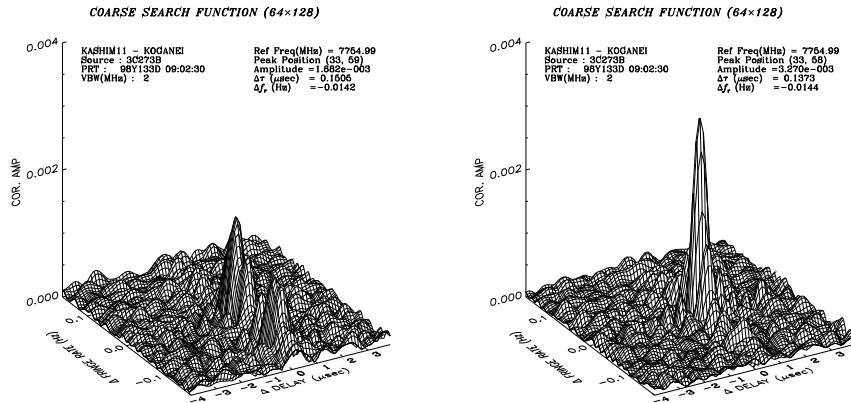


Figure 8. Coarse delay search function for normal (left panel) and third-order (right panel) fringe search.

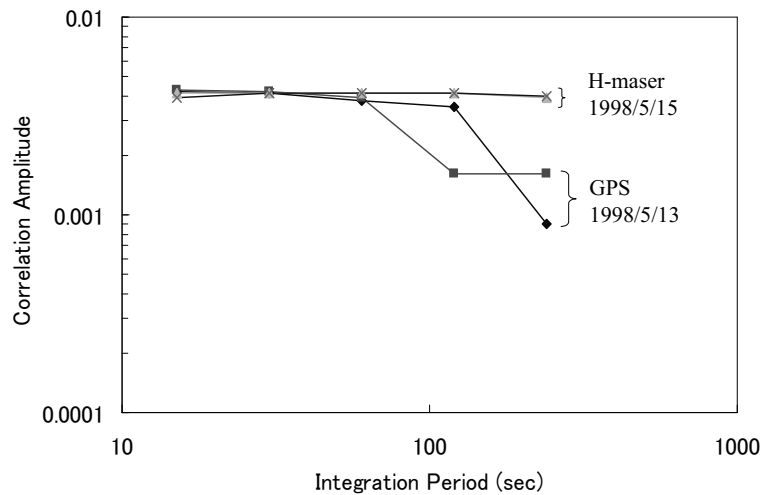


Figure 9. Relation between correlation amplitude and integration period for two test observations: in one H-maser clocks were used at both stations, and in the other a GPS reference receiver was used at one station.

## Acknowledgments

A real-time VLBI technique for the KSP has been developed in cooperation with the Telecommunication Network Laboratory Group of Nippon Telegraph and Telephone Corporation (NTT). We thank all staff members of NTT involved in the real-time VLBI Project for their efforts to maintain the high speed network of the KSP. The large virtual radio telescope project has been promoted in collaboration with the Institute of Space and Astronautical Science (ISAS), National Astronomical Observatory (NAO), and NTT. The Giga-bit VLBI system has been developed under a cooperative efforts by Communications Research Laboratory, NAO, Tokyo University, Toshiba Corporation, Yamashita Engineering Manufacture Inc., and Oki Electric Industry Co., Ltd. We would like to express deep appreciations to colleagues in these organizations.

## References

- Amagai, J., H. Kunimori, and H. Kiuchi, Preliminary experiments of improved optical-linked RF interferometer, Technical Development Center News CRL, No.12, 20-23, 1998.
- Kiuchi, H., T. Kondo, M. Sekido, Y. Koyama, M. Imae, Hoshino, Uose, Real-Time VLBI Data Transfer and Correlation System, *J. Commun. Res. Lab.*, 1999.
- Kondo, T., N. Kurihara, Y. Koyama, M. Sekido, R. Ichikawa, T. Yoshino, J. Amagai, K. Sebata, M. Furuya, Y. Takahashi, H. Kiuchi, and A. Kaneko, Evaluation of repeatability of baseline lengths in the VLBI network around the Tokyo metropolitan area, *Geophys. Res. Lett.*, 25, 1047-1050, 1998.
- Koyama, Y., N. Kurihara, T. Kondo, M. Sekido, Y. Takahashi, H. Kiuchi, and K. Heki, Automated geodetic very long baseline interferometry observation and data analysis system, *Earth Planets Space*, 50, 709-722, 1998.
- Koyama, Y., J. Nakajima, M. Sekido, and M. Kimura, The first fringes from the Giga-bit VLBI system, Technical Development Center News CRL, No.13, 14-16, 1998.
- Takahashi, Y., H. Kiuchi, A. Kaneko, S. Hama, J. Nakajima, N. Kurihara, T. Yoshino, T. Kondo, Y. Koyama, M. Sekido, J. Amagai, K. Sebata, N. Kawaguchi, H. Kobayashi, M. Iguchi, T. Miyaji, H. Uose, and T. Hoshino, The plan of the big virtual telescope using the high speed communications network, Technical Development Center News CRL, No.13, 17-19, 1998.

## **Status Report of Geographical Survey Institute Japan**

*Shoichi OGI: GSI VLBI Group  
Geodetic Department  
Geographical Survey Institute (GSI)  
Ministry of Construction, Japan*

### **Abstract**

We briefly present a history of VLBI activities and the status of Geographical Survey Institute (GSI). Firstly GSI developed three mobile VLBI systems and had repeated observations with CRL. On the other hand, GSI installed 1000 permanent GSP stations all over Japan (GEONET). Then our VLBI strategy has been shifted from domestic mobile VLBI observation to permanent VLBI stations and international VLBI service. Last year GSI finished constructing GSI domestic VLBI network with five permanent VLBI stations and Tsukuba VLBI center with three baseline K-4 correlator. A main station of the network is Tsukuba VLBI station (32m). Tsukuba VLBI station also becomes a key station in the international VLBI networks. Now GSI analyzing survey results comparing with the data from GEONET.

### **1. History of VLBI activities at GSI**

The Communications Research Laboratory (CRL) is a pioneer of VLBI in Japan. CRL established K series VLBI standard. With support of CRL, Geographical Survey Institute (GSI) started to introduce K series VLBI techniques in 1981. The first system is a mobile system with a 5m-diameter antenna. In 1984, GSI had the first VLBI experiment with Kashima VLBI station of CRL. From 1986, GSI participated in a project named 'VLBI Experiment for Geodetic Application' (VEGA) using the mobile system. The purposes of the VEGA project were the detection of crustal deformation, accuracy improvement of the Japanese precise geodetic network, and contribution to determination of GPS satellite orbit. From 1986 to 1994, GSI repeated mobile VLBI experiments at 8 sites in Japan. By comparing with the survey results in 1987 and 1989, GSI succeeded in detecting a velocity of the Philippine plate relative to Kashima as 3.7cm per year. This plate motion is asserted to be the main force of earthquakes in the Tokai area. The main station of these mobile VLBI experiments was Kashima VLBI station (26m).

GSI developed three mobile systems. Diameters of these antennas were 5-m, 2.4-m (with CRL) and 3.8-m. In 1995 GSI had a cooperative VLBI experiment with National Geography Institute of Korea using the 3.8-m diameter mobile VLBI system.

Through these experiences GSI became a mastery of skills in VLBI operation. In 1992, GSI started international VLBI experiments participating in the DOSE project with Kashima VLBI station. In 1992, the ownership of Kashima VLBI station (26m) was transferred from CRL, and GSI became proprietary of it. Since 1997, GSI has been participating in CORE (Continuous Observation of the Rotation of the Earth). The Japanese geodetic network was connected to global geocentric reference frames such as ITRF (International Terrestrial Reference Frame) by series of the international VLBI experiments.

In parallel with a growth of the number of the permanent GPS stations, VLBI strategy was shifted from mobile VLBI systems to permanent VLBI stations. On the ground monument of Shintotukawa mobile VLBI station, a 3.8m-diameter permanent VLBI station was installed in 1995. Near Chichijima VLBI-SLR collocation site, a 10m-diameter permanent VLBI station was installed in 1997. A 10m-diameter permanent VLBI station was installed in 1997 at Aira. GSI also installed a set of correlator for three stations and three baselines. In 1998 GSI opened Tsukuba VLBI Center as an operation, correlation and analysis center for domestic VLBI experiments. This means that GSI have full facilities for independent VLBI survey.

Installation of Tsukuba VLBI station (32m) was completed on 26 March 1998. Tsukuba VLBI station has taken place in Kashima VLBI station since June 1998. A performance of Tsukuba VLBI station is the top of the world VLBI standards. Tsukuba VLBI station is a key station in the GSI domestic VLBI network and in the international VLBI networks. In 1999, GSI nominated Tsukuba VLBI station as a network station and Tsukuba VLBI center as a correlation center of IVS (International VLBI Service for Geodesy and Astrometry).

## **2. Tsukuba VLBI station (32m)**

GSI finish constructing Tsukuba VLBI station (32m) on 26<sup>th</sup> March 1998. Tsukuba VLBI station had first (official) experiment in June 1998. To realize a high performance, we introduced some ideas. The back panels and ventilation system keeps shape of the antenna surface. Antenna structure is covered with sunshade panels. GPS antenna is settled on the top of the VLBI antenna for collocation. Helium cooling system is installed for front-end receiver. The front-end and Back-end are connected with optical transmission devices to improve the SNR. Back-end room is shielded from radio noise and H-maser room is shielded from electromagnetic noise. Mark-IV and K-4 type recording is available. GSI also is developing a dubbing machine from K-4 to Mark-IV. Tsukuba VLBI station is settled near TSKB (IGS station). Soon IGS network and VLBI network will be collocated at Tsukuba.

In 1999, Tsukuba VLBI Station will participate in CORE, Japan-German Cooperative Experiments for UT1, Japan Tie with CRL, APSG (Asia Pacific Space Geodesy), Direct Tie with Antarctic Station (Showa) and collocation survey with IGS, etc.

Specifications of Tsukuba VLBI station are shown in the following table.

**Specifications (Tsukuba VLBI station)**

Installation	March 1998	Surface smoothness	better than 0.5mm
First (official) experiment	6 June 1998	Axes crossing error	less than 1mm
Diameter	32m	Maximum speed	3 degree / sec
Antenna Type	Cassegrain Az-El Mount		
S band	2.1 - 2.5 GHz	SEFD	X band : 297 Jy    S band : 322 Jy
X band	7.78 – 8.98 GHz	(average value of five quasars : Orion-a, Cas-a, Cygnus-a, Taurus-a, Virgo-a)	
K band (receiver is not installed)	19.5 – 25.0 GHz	Tsys	X band : 55.03 K S band : 61.09 K

**3. GSI Domestic VLBI Network**

GSI operates a domestic VLBI network with total five stations. Aira VLBI station and Chichijima VLBI station were installed in 1997. Recording system of the network is K-4 system. GSI carried out the first simultaneous experiment operating the five stations in June 1998. The coordinates of each stations were decided with precision of 2-5mm (one sigma) horizontally and 9-16mm (one sigma) vertically. GSI is planning to have four domestic experiments with the network to detect crustal movement in 1999. GSI is also planning to have some research experiments to improve accuracy and to test new automation techniques.

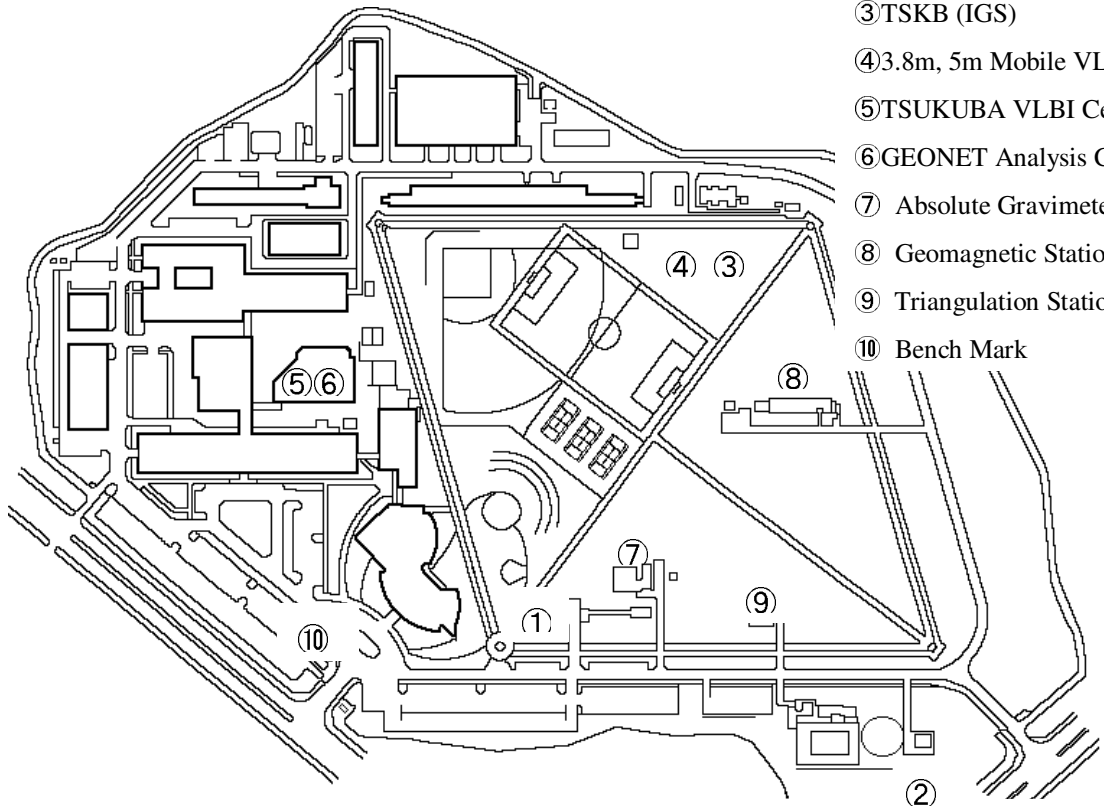
**4. Tsukuba VLBI Center**

In 1998 GSI opened Tsukuba VLBI Center as an operation, correlation and analysis center. GSI installed a new correlator system for three stations three baselines. Cosmo Research Corp makes the correlator unit. Kety Corp. Ltd. makes the software that controls the each unit. Software for Bandwidth Synthesis and database producing is developed by CRL. SOLVE of NASA/GSFC is working as a baseline analysis software.

**5. JGD2000**

GSI is preparing a new geodetic framework named JGD2000 (Japanese Geodetic Datum 2000), planning to publish in 2000. GSI VLBI group is contributing to JGD2000. JGD2000 is being built by VLBI experiments and GPS campaign. Coordinates of the JGD2000 are based on ITRF94 and GRS80. JGD2000 is connected at the Kashima VLBI station to ITRF94 by international VLBI experiments. VLBI group determined three baselines precisely by mobile VLBI experiments. These baselines and permanent GPS stations are the backbone of JGD2000.

## Site Map Geographical Survey Institute



- ① GEONET
- ② TSUKUBA VLBI Station
- ③ TSKB (IGS)
- ④ 3.8m, 5m Mobile VLBI
- ⑤ TSUKUBA VLBI Center
- ⑥ GEONET Analysis Center
- ⑦ Absolute Gravimeter
- ⑧ Geomagnetic Station
- ⑨ Triangulation Station
- ⑩ Bench Mark



① GEONET



④ 5m mobile VLBI



② Tsukuba 32m VLBI

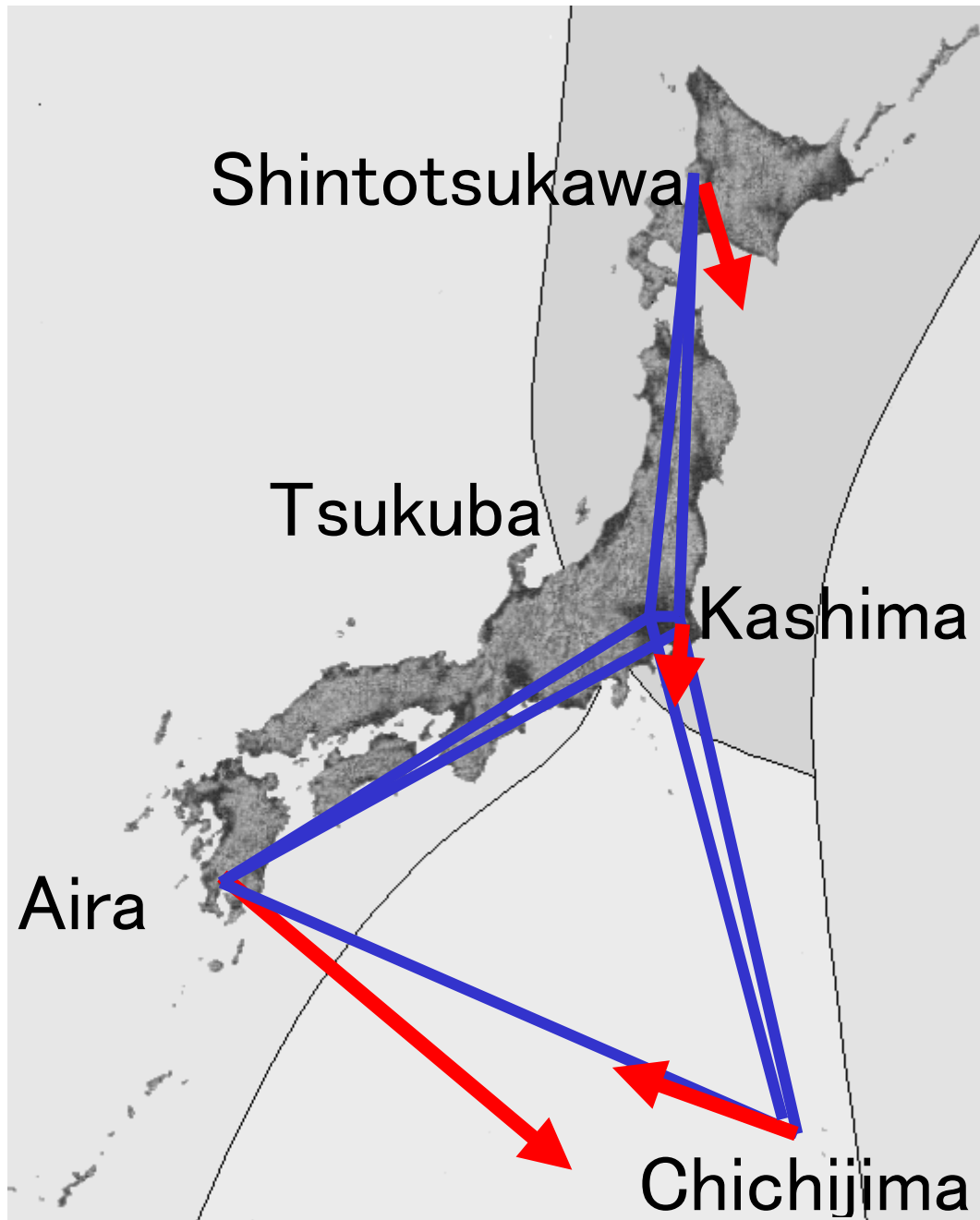


⑥ GEONET analysis center

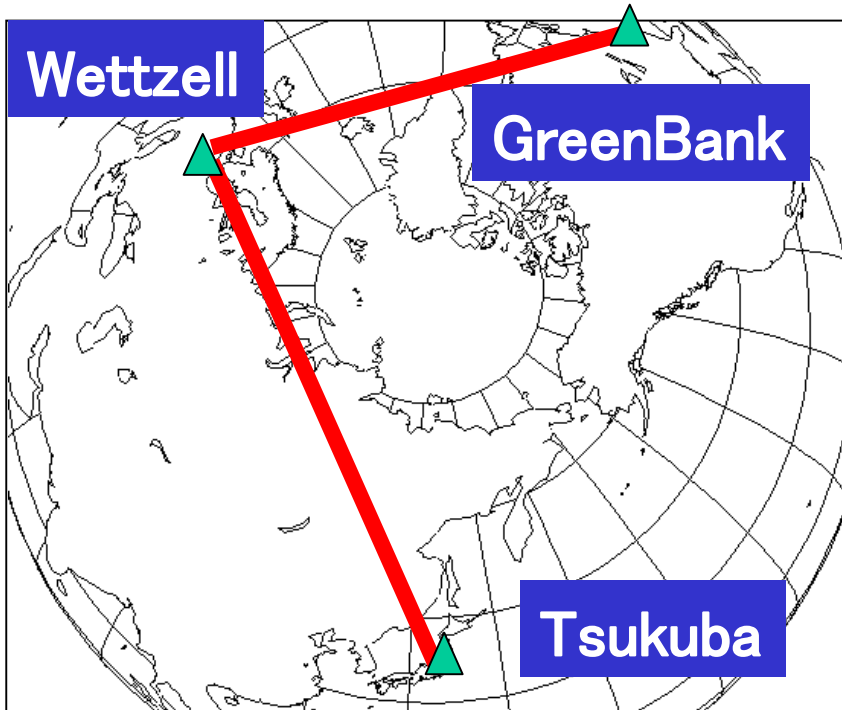


⑤ VLBI center

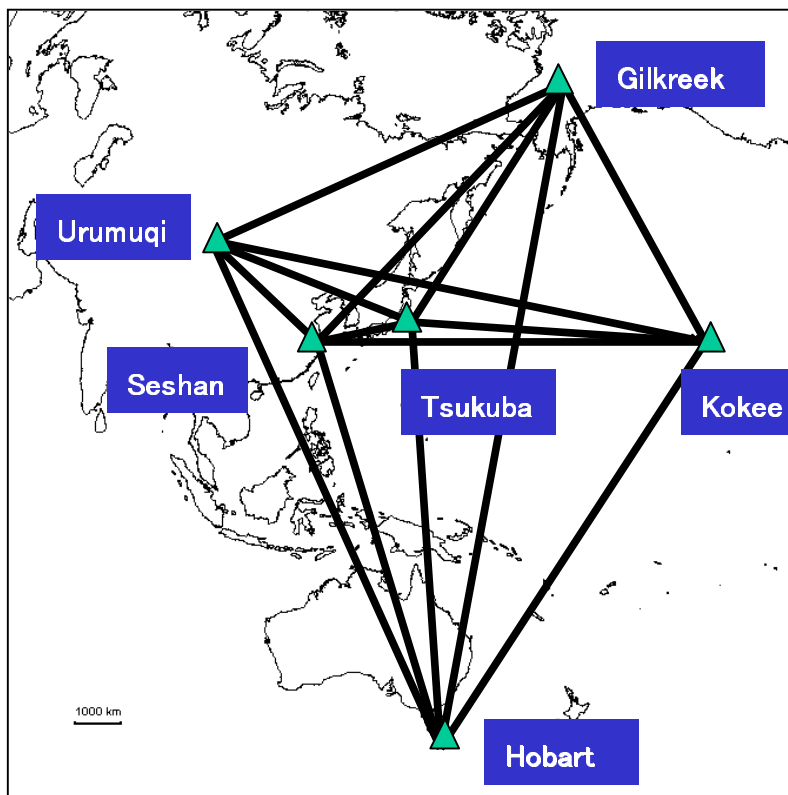
**GSI Domestic VLBI Network and  
Detected Velocities of Plates**



→ 20mm/Year



Japan German Cooperative Experiments for UT1



APSG(Asia Pacific Space Geodesy)

# Overview of performance of European VLBI Geodetic Network in the Europe campaigns in 1998

MAURO SORGENTE AND LEONID PETROV

*Geodetic Institute of the University of Bonn (GIUB), Germany*

E-mail: sorgente@hp138.mpifr-bonn.mpg.de, petrov@kuestner.geod.uni-bonn.de

## Abstract:

*Six VLBI sessions have been carried out in 1998 under the program "Measurement of Vertical Crustal Motion in Europe by VLBI". From 6 to 9 stations took part in each experiment. The data were correlated at the Bonn correlator. This report summarize the problem disclosed during analysis of these experiments. The range of variation of the system temperature at zenith for each antenna is shown and our judgment about the system performance is presented. An analysis of the presence of spurious signals in the phase calibration signal is made.*

## 1 Introduction

Six VLBI sessions have been carried out in 1998 under the program "Measurement of Vertical Crustal Motion in Europe by VLBI". From 6 to 9 stations took part in each experiment. Transportable 6 meter antenna TIGO has been included in this network since December 1997 for testing its performances before it will be moved to another place. The radiotelescope Yeibes did not participate in observations in 1998 due to malfunction of the formatter. Magnetic tapes with recorded signal were sent to Bonn for processing at the correlator of Max-Plank-Institut für Radioastronomie and for consecutive parametric analysis using CALC/SOLVE software.

Dates of the experiments during 1998 and the list of stations successfully participated in observations are presented in table 1.

Experiment	Date	Stations
Europe41	02-Feb-98	Cri-Mad-Mat-Med-Not-Nya-Ons-Tig-Wet
Europe42	20-Apr-98	Cri-Mat-Med-Not-Nya-Ons-Tig
Europe43	22-Jun-98	Cri-Mat-Not-Nya-Ons-Tig-Wet
Europe44	17-Aug-98	Cri-Mat-Med-Nya-Ons-Tig-Wet
Europe45	12-Oct-98	Cri-Mad-Mat-Med-Not-Nya-Ons-Wet
Europe46	14-Dec-98	Cri-Eff-Mad-Mat-Med-Not-Nya-Tig-Wet

Table 1: Experiments under program "Europe" in 1998.

Detailed reports about each experiment are available at Web:

<http://giub.geod.uni-bonn.de/vlbi/experiments/experiments.html>

## 2 Summary of the problems

The following problems were detected during the correlation and parametric data analysis:

- No fringes were found in some channels. Some experiments had massive channels losses what led to appearance of group delay subambiguities due a false detection of sidelobes in delay

resolution function. Such data were processed by a special procedure REFRINGE developed by A. Nothnagel what allowed to recover substantial part of data.

- Phase calibration amplitude recorded at some stations was sometimes too weak. If the phase calibration amplitude is lower than 1% of the noise level then it cannot be used in data analysis. Manual phase calibration is used in such cases as a last resort. When manual phase calibration is applied we lose information about phase fluctuations in individual video converters what may considerably degrade accuracy of measurements of group and phase delays.
- Local radio interference affected S-band at some stations.
- Incorrect frequency setup before the beginning the session due to mistake of an operator. It is an expensive mistake! It is absolutely impossible to use such data.
- Incorrect heads setup before the beginning the session. Sometimes it was possible partly to recover the data by the price of substantial degradation of the performance.
- Some channels have fringe amplitude lower than 50% the average fringe amplitude probably due to radio interference?
- Unfortunately all station are affected by spurious signals in phase calibration. This problem was reported in early MARK-III observations in late 70-s and is not yet solved.

Influence of spurious signals is seen in the plots of dependence of normalized phase calibration amplitude versus phase of phase calibration signal (in rad). We can classify a pattern on these plots according to three main categories: one cycle periodicity (fig. 1) due to the presence of an additive coherent signal; two cycle periodicity due to a band filter imperfection (fig. 2) and peculiar variability (fig. 3). Spurious signal in phase calibration results in appearance of systematic errors in group and phase delay.

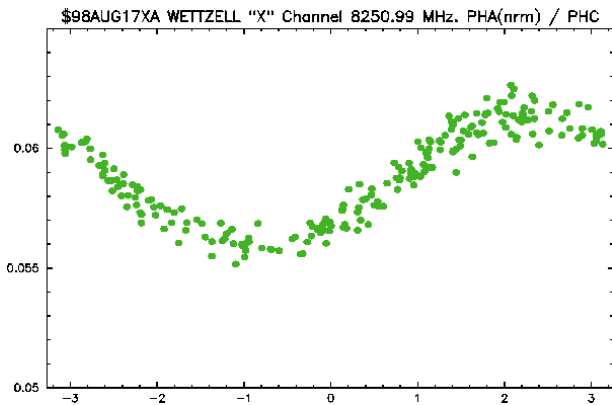


fig. 1

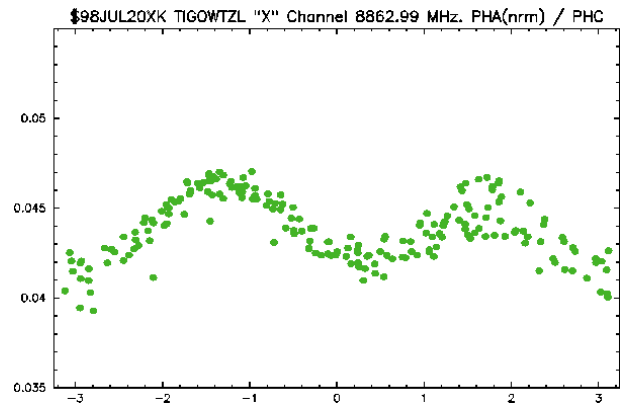


fig. 2

- Considerable variations of system temperature were found for some stations during experiments.
- Cable calibration was not available for some stations or was unrealistic.

### 3 Particular problems of stations

#### CRIMEA<sup>1</sup>

No fringes were found at all scans at channel  $\nu=2292.99$  MHz in Europe42, Europe43 and Europe44 sessions due to a wrong frequency setup.

<sup>1</sup>Alternative name: Simeiz.

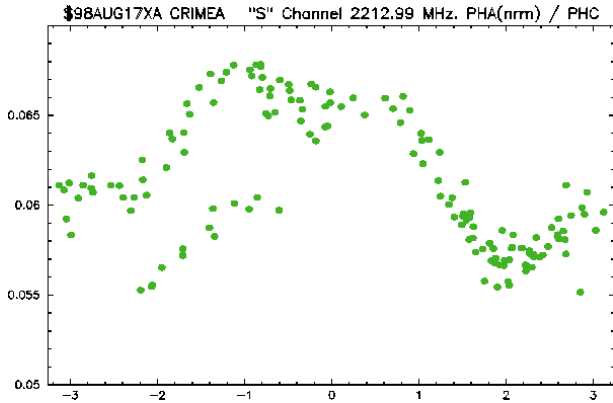


fig. 3

The single band delay was not stable in Europe41 and Europe45 sessions. Jumps in both single band and multi band group delay during Europe41 experiment occurred during power breaks. To find jumps in single band delay larger than 400 nsec requires substantial additional correlator resources.

System temperature records frequently had values in overflow at one or more channels, f.e. at the vc05 and vc06 ( $\nu=8420.99$ ,  $8500.99$  MHz) at X-band and at the vc12 ( $\nu=2267.99$  MHz) at S-Band, although fringe amplitude were normal what allows us to conclude that it was a failure in recording system temperature values.

Cable calibration unit was not switched on for all experiments and therefore cable calibration is not available.

## DSS65<sup>2</sup>

Station did not participate in Europe42, Europe43 and Europe44 experiments. Only 4 hours of good data were collected in Europe46.

The phase calibration amplitude was generally too weak and lower than the minimum acceptable threshold. It was generally necessary to introduce a manual phase calibration.

There were two jumps in amplitude of phase calibration signal at X-band and at S-Band during Europe45 experiment.

No fringes were found at  $\nu=2292.99$ ,  $8570.99$  MHz for all scan in Europe41 session.

Cable calibration unit was not switched on for all experiments.

System temperature was not recorded in all experiments.

## EFLSBERG<sup>3</sup>

This station took part only in Europe46 experiment. Sensitivity at S-band was 50% of expected.

Antenna failed to reach sources in time for 10 scans due to a wrong schedule setup.

## MATERA

A fringe amplitude lower than the average was found at the channels  $\nu=2212.99$ ,  $2227.99$  and  $2237.99$  MHz. It was due to the presence of emitter of a television company RAI close to the station at azimuth 240 degree. A diagram of the distribution of all sources affected by a radio interference during Europe41 session is shown in fig 4. Letters are the source codes. Azimuths of

<sup>2</sup>Alternative name: Madrid.

<sup>3</sup>Alternative name: Effelsberg.

the sources seen from Matera are put at the horizontal axis and elevations are put at the vertical axis. It was noted that the amplitude of this interference was weaker in Europe44, Europe45, Europe46 experiments. The radio interference affected 10–20% scans.

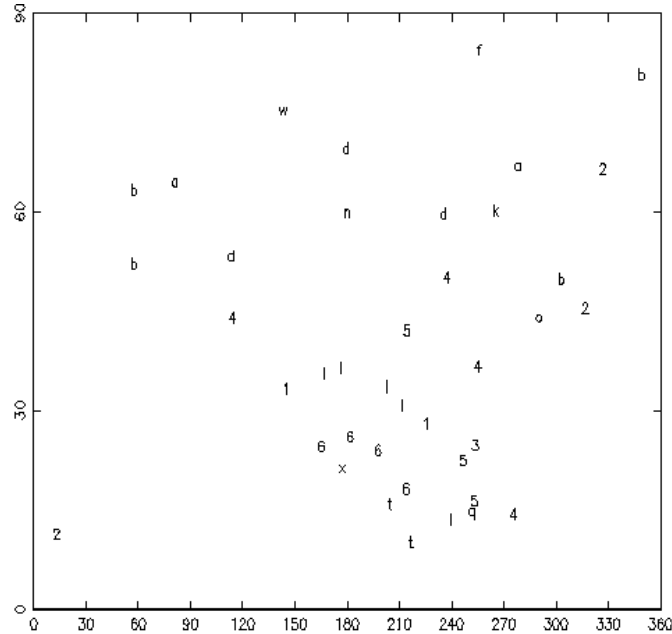


fig. 4 Interference in Matera due to TV emitter

Another source of radio interference was noticed in Europe44, Europe45 and Europe46 at the channel  $\nu=2287.99$  MHz. The average fringe amplitude at this channel was more than 50% lower than the average fringe amplitude in all scans. The origin of this new interference is not yet identified. Probably it doesn't have azimuth dependence. System temperature for this channel was in overflow.

## MEDICINA

High error rate in data recording was found in Europe45 experiment. The higher threshold of allowable fraction of bytes in error was used for processing the data (0.1 instead of 0.01) what resulted in increasing scattering in fringe phases.

Cable calibration was wrong for all experiments and its usage would degrade fit considerably.

## NOTO

The main problem which still is not solved is that phase calibration has a constant systematic offset about  $+25^\circ$  and  $-10^\circ$  at channels  $\nu=8420.99$  and  $8570.99$  MHz respectively. Additional phase offsets were introduced in fringing in order to compensate this error.

Incorrect triple cap heads setup in Europe41 and Europe42 experiments did not allow to register data correctly and high parity error rate was detected in reading the tapes. The threshold of allowable fraction of bytes in error was raised during fringing (0.1 instead of 0.01).

A tape with poor quality was used in Europe45. Probably checking the tape before the experiment was not adequate.

## NYALES20<sup>4</sup>

Error parity rate was detected: ( $10^{-3}$ – $10^{-4}$ ) in all experiments except Europe41 instead of  $10^{-5}$ . No fringe and no phase calibration amplitude at frequencies  $\nu=2212.99$ ,  $2287.99$  MHz were found in Europe42 and Europe43 sessions in 60 scans. All these scans were recorded in forward passes. Observed SNR at S-band was only 30% of expected in Europe46 experiment.

A big difference in the phase calibration amplitude at three channels:  $\nu=2212.99$ ,  $2227.99$  and  $2237.99$  MHz (about 150, 120 and 100 units arbitrary units respectively) with respect to three another channels  $\nu=2267.99$ ,  $2287.99$  and  $2292.99$  MHz (about 40, 60 and 60 units) was found.

## ONSALA60<sup>5</sup>

Heads had wrong setup before the Europe42, Europe43 and Europe44 experiments and the signal was written in forward and reverse passes on the same tracks. The threshold of allowable fraction of bytes in error was raised from 0.01 to 0.1, but even this trick didn't help to recover all data.

The station did not take part in Europe46 experiment because the head assembly and the driver unit was under repair.

System temperature varies up to 50% during experiments.

## TIGOWTZL<sup>6</sup>

SEFD of TIGOWTZL at S-band is 13 000 Jy what is at one order of magnitude less than SEFD for other stations.

Not all baselines with TIGOWTZL were correlated in earlier experiments since predicted SNR was too low.

A peculiar interference was found during correlation the data of 60 meters baseline TIGOWTZL-WETTZELL at channel 2212.99 MHz when the antennas looked in direction at azimuth about 0 and 180 degrees. The fringe amplitude was more than 80 higher than the average fringe amplitude. This frequency was discarded in the final fringing of this baseline. Since this problem affected only a short baseline its origin is probably some local source of coherent interference.

## WETTZELL

The presence of strong additive spurious signals in phase calibration signal at some channels at X-band was detected.

## 4 System temperature performance

System temperature is written in log file and is available for analysis<sup>7</sup>. Measured system temperature varies with time and with elevation angle. The following model was used to represent system temperature:

$$T_{sys} = T_o (1 + a t)(1 + b_1 m + b_2 m^2 + b_3 m^3)$$

here  $T_o$ ,  $a$ ,  $b_1$ ,  $b_2$ ,  $b_3$  — parameters obtained in non-linear least square adjustments,  $m(E)$  — is a number of air masses as a function of elevation. Chao wet mapping function [1] was used for computation of  $m(E)$ . Two typical cases of dependence of system temperature (in K) in zenith direction on time during an experiment are shown in plots 5–6.

---

<sup>4</sup>Alternative name: Ny Alesund.

<sup>5</sup>Alternative name: Onsala.

<sup>6</sup>Alternative name: TIGO.

<sup>7</sup>DSS65 and NYALES20 not always recorded system temperature.

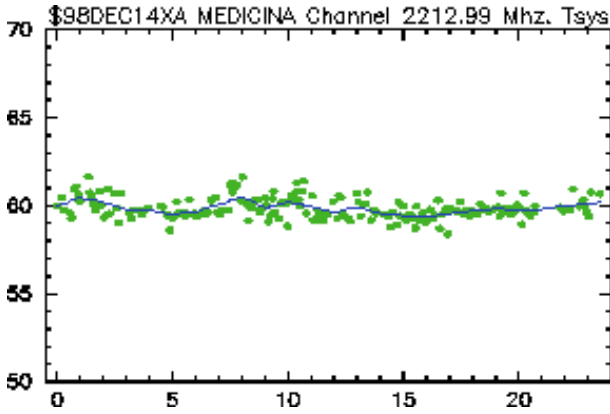


fig. 5

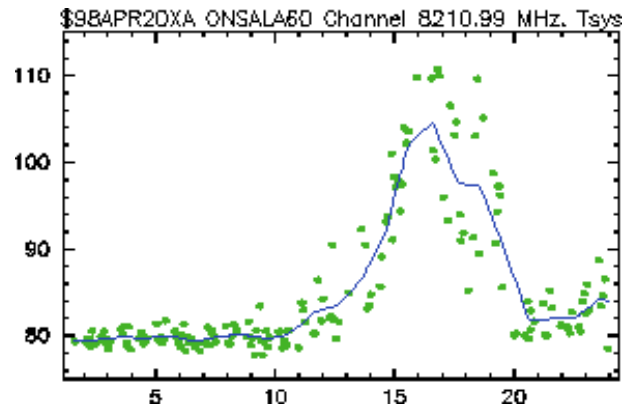


fig. 6

The lowest and the highest values of system temperature in zenith direction for each station are presented in table 2.

Station	$T_{SYS}$ 8.2 GHz lower values	$T_{SYS}$ 8.2 GHz higher values	$T_{SYS}$ 2.3 GHz lower values	$T_{SYS}$ 2.3 GHz higher values
CRIMEA	45	100	80	160
DSS65	45	90	50	120
EFLSBERG	40	55	140	160
MATERA	45	180	55	200
MEDICINA	40	45	60	85
NOTO	105	120	110	160
NYALES20	55	80	30	200
ONSALA60	75	140	55	120
TIGOWTZL	65	80	70	90
WETTZELL	55	90	40	50

Table 2: System temperature at zenith direction.

We see that system temperatures 40K are achievable but unfortunately rather higher values were obtained during the experiments. It is a reserve for improving performance.

## 5 Conclusions

Performance of the station is still far from ideal. In order to get the best performance a special care should be taken by personal before and during the experiment. Efforts for making correct frequency setup, correct heads setup, tapes checking, elimination of the sources of spurious signals in phase calibration, proper cooling receivers don't cost too much but may give considerable improvement in accuracy of the final results.

## References

- [1] Chao, C.C.: A model for tropospheric calibration from daily surface and radiosonde balloon measurements. Technical Memo, 391-350, Jet Propulsion Laboratory, 1972.

## The CGS VLBI EUR98 Geodetic solution and comparison with the CGS GPS results.

R. Lanotte<sup>1</sup>, C. Ferraro<sup>1</sup>, A. Nardi<sup>2</sup>, C. Sciarretta<sup>2</sup>, F. Vespe<sup>3</sup>

- 1) Telespazio SpA, Centro di Geodesia Spaziale "G.Colombo", Matera, Italy
- 2) Telespazio SpA, Via Tiburtina 167, Rome, Italy
- 3) Agenzia Spaziale Italiana, Centro di Geodesia Spaziale "G.Colombo", Matera, Italy

**Abstract.** Nine years of VLBI data acquired within the EUROPE campaign have been analysed to estimate the motion of the stations participating to this campaign. The estimated site velocities and baseline time series are compared to those obtained from the GPS solution carried out at CGS as contribution to EUREF. Both the solutions have been expressed in the ITRF96 reference frame in order to compare them in a unique reference system.

### 1. Introduction

Data acquired from 1990 up to the beginning of 1998 in the VLBI EUROPE campaign have been analysed in the CGS VLBI EUR98 solution, including 42 sessions each lasting 24 hours. Figure 1 shows the network under investigation. Two VLBI solutions, using the CALC/f-SOLVE software system [Rogers et al., 1983; Clark et al., 1985, Petrov 1999], are computed. The first one is an arc solution which provides, for each observing session, estimation of the site coordinates, that is the time series of the baselines. In the following this solution is referenced as "the baseline solution". The second solution is a global solution where site positions and velocities are estimated using all sessions. This solution will be referenced as "the velocity solution". Both the solutions were compared to the GPS solution computed at the CGS as contribution to EUREF.

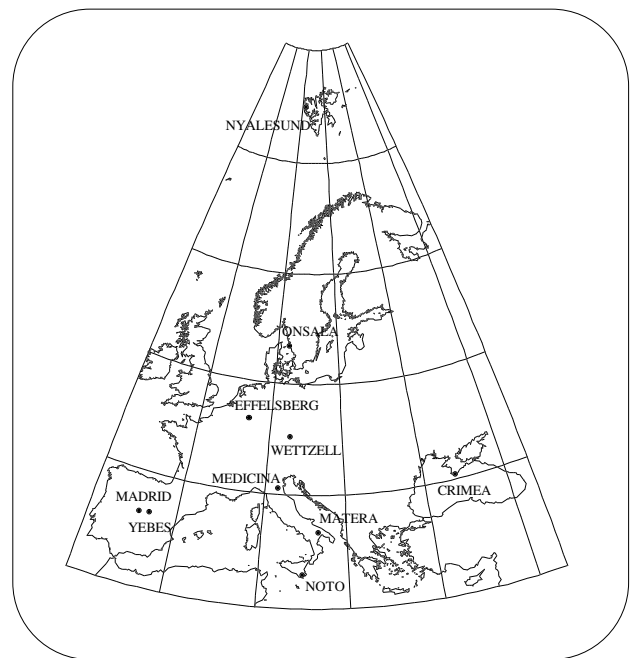


**Figure 1:** The network of the fixed VLBI stations participating to the EUROPE campaign.

## 2. The CGS VLBI EUR98 solution

### The baseline solution

In the baseline solution the so called "reweighting process" is performed for each session by estimating a constant formal error. This constant added to the variance of the observations (derived in the correlation process) has to satisfy the condition that the overall reduced  $\chi^2$  of the residual delays in the session was equal to unity. The baseline solution, using the reweighted observations, provides the time series of the geodetic parameters and in particular the baseline vector components.

Clocks were estimated using a reference station and modelling the differences between the reference clock and the others with an unconstrained second order polynomial plus a continuous piecewise linear function with duration of the linear sections of 60 minutes and  $5 \cdot 10^{-14}$  constrained in slope.

To take into account the tropospheric delay we have to separate it into its dry and wet components. The dry delay for each observation was estimated at the zenith using the Saastamoinen model and then mapped to the elevation of the observation with the Niell dry mapping function [Niell, 1996]. Wet tropospheric zenith delay was estimated using a continuous, piecewise linear function with duration of the linear sections of 60 minutes and 50 ps/h constrained in slope and then mapped to the elevation of the observation with the Niell wet mapping function [Niell, 1996].

The regional extension of the network under investigation does not allow to reliably determine parameters such as the celestial source positions as well as Earth rotation parameters. For this reason they have been kept fixed using: the IERS celestial reference frame ICRF95 [IERS, 1997] for the source coordinates, the IERS series 97 C 04 for the Earth Orientation Parameter and nutation series [IERS A.R., 1997]. For precession the J2000.0 model has been used.

Figure 2 shows the baseline length variations for all the baselines relevant to Wettzell. These baselines can be considered as representatives for all the baselines in the baseline solution. The baselines are divided in two groups, the first contains the baselines with a rate not significantly different from zero, except for the baseline Wettzell-Yebes that has a vary high error rate. In the second group are the baselines with rate different from zero and these are the baselines containing the Italian sites.

### The velocity solution

In the velocity solution station positions and velocities have been estimated as global parameters, i.e. common to all the analysed sessions. In this solution the previously obtained arc weights are applied. The same parameterization described in the baseline solution has been used, moreover this solution is constrained fixing position and velocity of Wettzell at the value of ITRF96 [Boucher et Al., 1998] for the epoch 1997.0. In order to compare the estimated velocities to those provided by the ITRF96 a four parameters transformation was determined to take in to account for rotation and scale factor time derivatives. Table 1 reports the estimated station velocities and the ones provided by the ITRF96 in the topocentric Up, East and North reference frame. The horizontal components are in good agreement, some discrepancies are in the Up component in particular for Medicina and Noto.

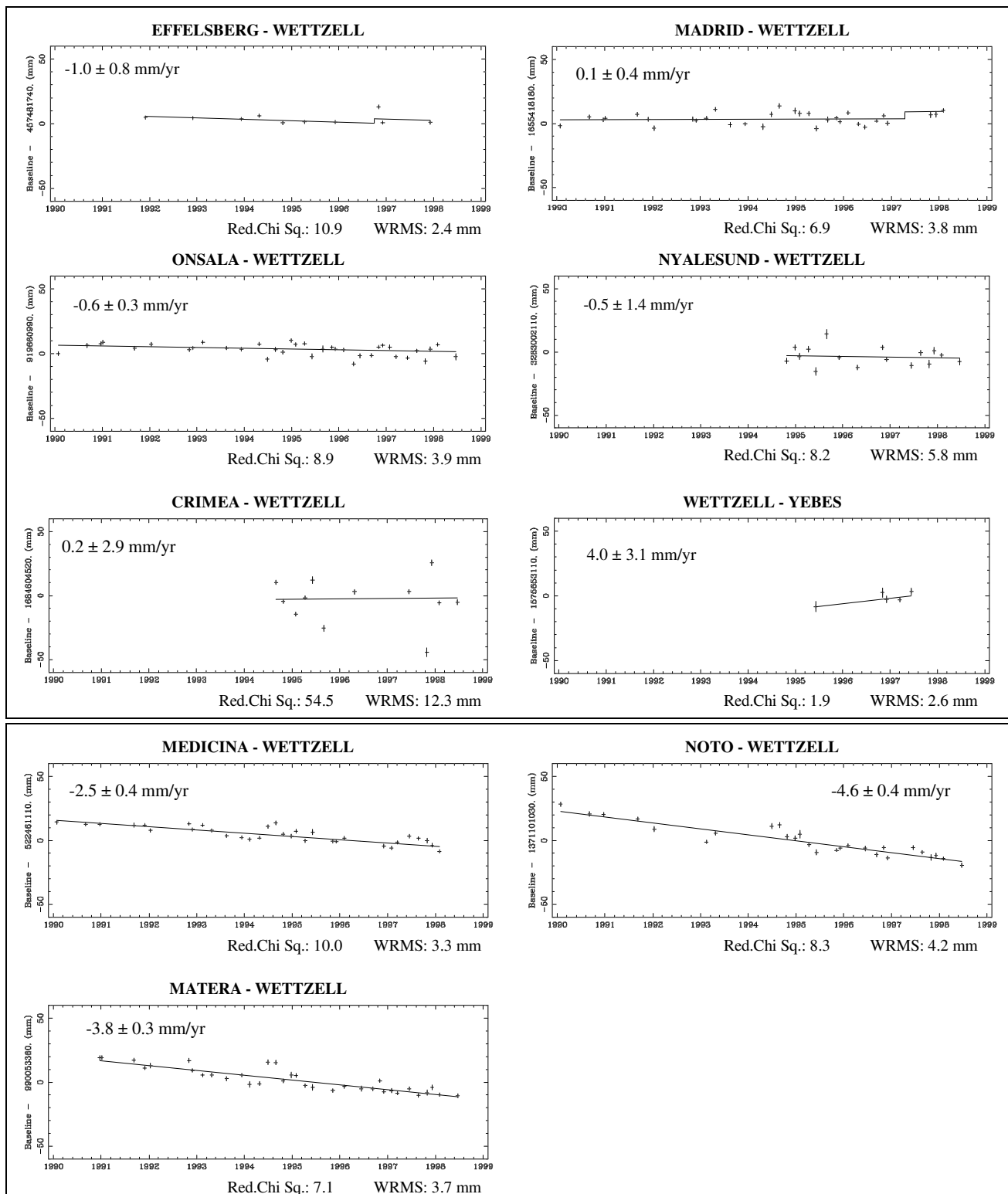


**Figure 2:** Length variation of the baselines including the Wettzell site. The points are the calculated value of the baseline at an epoch with one sigma formal error bar. The straight line on the plots is the line of best fit by least squares. The rate, error rate, reduced chi square and WRMS fit is reported on each plot.

		VLBI (mm/yr)	ITRF96 (mm/yr)
CRIMEA	U	4.0 ± 1.8	-1.8 ± 11.3
	E	26.1 ± .3	24.1 ± 2.5
	N	10.0 ± .3	8.5 ± 3.1
EFFELSBURG	U	-1.6 ± 1.0	-3.7 ± 2.5
	E	18.9 ± .2	19.2 ± .7
	N	12.9 ± .2	13.9 ± .6
MADRID	U	2.8 ± .5	3.9 ± .3
	E	18.9 ± .1	19.6 ± .4
	N	15.2 ± .1	15.1 ± .4
MATERA	U	-.4 ± .5	-.7 ± .2
	E	23.9 ± .1	23.8 ± .4
	N	17.0 ± .1	18.5 ± .4
MEDICINA	U	-4.4 ± .6	1.4 ± .1
	E	23.2 ± .1	23.8 ± .3
	N	15.3 ± .1	15.1 ± .3
NOTO	U	-2.2 ± .5	.7 ± .2
	E	22.4 ± .1	22.4 ± .5
	N	17.2 ± .1	19.1 ± .5
NYALESUND	U	2.7 ± 1.4	-2.0 ± .6
	E	9.2 ± .3	10.9 ± .6
	N	13.5 ± .4	14.8 ± .6
ONSALA	U	1.6 ± .5	.1 ± .2
	E	17.6 ± .1	17.4 ± .2
	N	12.8 ± .1	13.1 ± .2
WETTZELL	U	-2.2 ± .0	-2.4 ± .1
	E	20.5 ± .0	20.5 ± .0
	N	13.5 ± .0	13.3 ± .1
YEBES	U	-31.5 ± 9.2	.5 ± .1
	E	17.2 ± 1.7	18.5 ± 5.4
	N	12.2 ± 1.7	14.3 ± 5.8

Table 1: Site velocities in the local topocentric reference frame estimated using the VLBI and comparison with the values provided by the ITRF96.

### 3. The CGS GPS solution

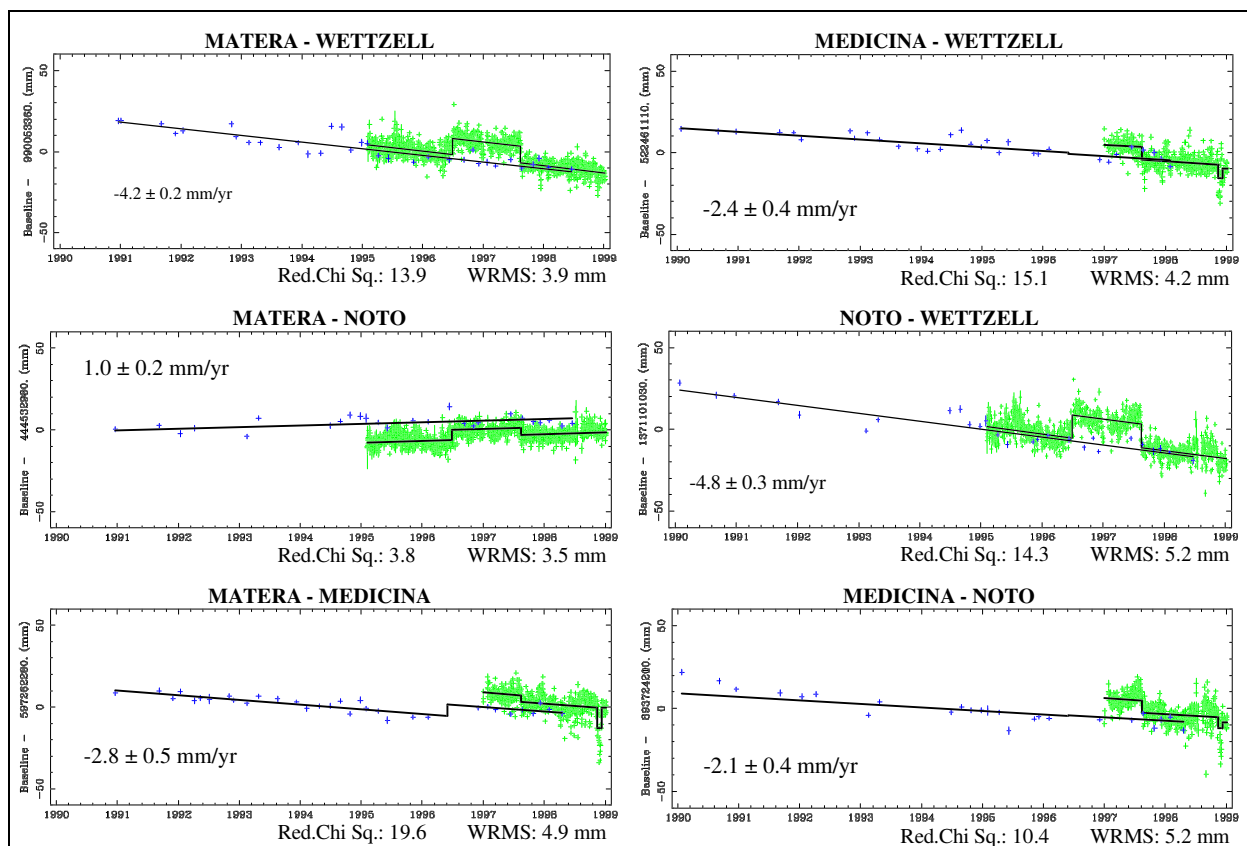
The ASI/CGS participates to EUREF [Bruyninx et al. 1996] as Local Analysis Center providing weekly solutions of the Italian GPS Fiducial Network (IGFN) [Fermi et al., 1997] plus other European sites. The CGS GPS solution has been performed using the software MicroCosm. It is based on four years of daily station coordinates, starting from 1995. Only few stations have data covering the full time span (see table 2). Figure 3 shows the GPS network. The solution is constrained by fixing the position and velocity of Wettzell to the values from ITRF96, satellite ephemerides and EOP to the IGS final values.



Figure 3:

#### 4. Comparison of the VLBI and GPS baselines

The two solutions have co-located sites: Madrid, Wettzell, Medicina, Matera and Noto. Data from Madrid are not used in this comparison, due to poor quality of GPS acquisitions. The estimated GPS site coordinates have been reported to the VLBI geodetic marker using the eccentricity vectors from ITRF96. A least square linear fit has been performed on the baselines to estimate a common rate for both VLBI and GPS. As the GPS estimates accumulate in time to be submitted to EUREF, they suffer of upgrading of models in the IGS products (orbits, EOP, ITRF) on which they rely on. To take into account these changes, plus other known receivers problem, “jumps” have been inserted into the linear fit estimation. Figure 4 shows the comparison among the time series of the baselines.



**Figure 4:** Baselines among Wettzell, Matera, Medicina and Noto. VLBI and GPS results are used to estimate a combined rate. The solid line is the combined linear fit.

#### 5. Comparison of the VLBI and GPS site velocities

The velocities used in the comparison have been obtained in different ways: for the VLBI directly from the velocity solution while for GPS from a linear fit of the site positions. They have been compared by estimating a 4 parameters transformation using the estimated rates of Noto, Matera and Medicina. In table 2 the two velocity fields in the local topocentric reference frame, Up, East and North components are reported, while in figure 5 the horizontal velocities are plotted.

		GPS mm/yr	VLBI mm/yr	Time span of the GPS data in years
MATERA	U	-0.6 ± 0.8	-0.5 ± 0.5	4.0
	E	24.1 ± 0.4	24.0 ± 0.1	
	N	17.4 ± 0.2	16.9 ± 0.1	
MEDICINA	U	0.4 ± 1.6	-4.5 ± 0.6	3.5
	E	24.5 ± 0.9	23.2 ± 0.1	
	N	14.9 ± 0.5	15.2 ± 0.1	
NOTO	U	-4.2 ± 1.0	-2.3 ± 0.5	4.0
	E	21.8 ± 0.6	22.5 ± 0.1	
	N	16.6 ± 0.3	17.1 ± 0.1	
BOLZANO	U	5.8 ± 2.4		1.0
	E	15.4 ± 1.3		
	N	16.2 ± 0.7		
CAGLIARI	U	-0.6 ± 1.0		4.0
	E	22.9 ± 0.5		
	N	12.6 ± 0.3		
COSENZA	U	-4.4 ± 6.5		0.6
	E	21.2 ± 3.5		
	N	19.3 ± 2.0		
GENOVA	U	0.7 ± 9.2		0.4
	E	31.4 ± 4.9		
	N	23.7 ± 2.4		
TORINO	U	12.4 ± 3.1		1.6
	E	20.5 ± 1.4		
	N	16.9 ± 0.7		
PERUGIA	U	-3.5 ± 3.1		1.2
	E	21.1 ± 1.7		
	N	16.8 ± 0.9		
PADOVA	U	-10.1 ± 2.6		1.0
	E	20.3 ± 1.5		
	N	17.5 ± 0.8		
VENEZIA	U	3.0 ± 0.7		4.0
	E	21.7 ± 0.4		
	N	14.9 ± 0.2		

Table 2: Site velocities in the local topocentric reference frame estimated using the GPS and comparison with the values estimated using the VLBI.

## 6. Conclusions

The comparison between the VLBI and GPS results appear to be very consistent both in terms of baselines rate and horizontal velocities (cfr. baselines to Wettzell in Fig. 2 and table 2). The baseline rates enlighten a non completely eurasiatic nor rigidly coherent motion of Italian sites: Matera and Noto show a significant rate w.r.t. Wettzell and are not motionless w.r.t. each other; Medicina show smaller, but not insignificant, motion w.r.t. Eurasia (Wettzell) and w.r.t. the other two Italian sites.

The origin of some small inconsistencies (within 1 cm in the worst case) in the relative positions of the colocated systems have to be investigated.

The results for most of the GPS Italian sites cannot be considered reliable due to the short time series of the data acquired by these stations.

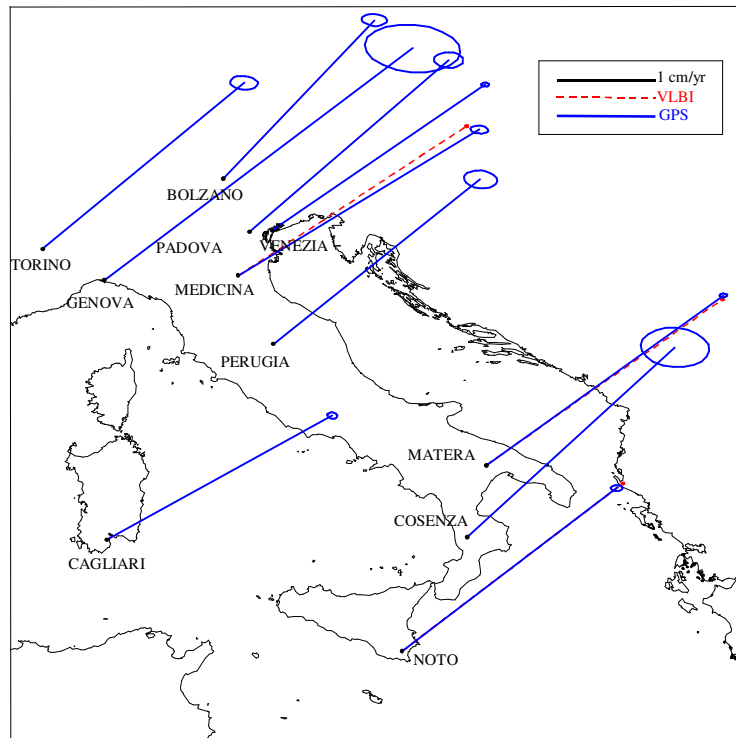


Figure 5: Absolute horizontal velocities of the Italian sites of the Italian GPS Fiducial Network. For Matera, Medicina and Noto, the VLBI horizontal velocities are also showed.

## References

- Boucher, C., Z. Altamini, and P. Sillard, Results and Analysis of the ITRF96, IERS Technical note 23, Central Bureau of IERS, Paris Observatory, May 1998.
- Bruyninx, C., W. Gurtner, and A. Muls, The EUREF Permanent GPS Network, Proceedings of EUREF symposium, Ankara, May 1996.
- Fermi, M., C. Ferraro, A. Nardi, C. Sciarretta, G. Bianco, F. Vespe, First results of the Italian GPS Fiducial Network, Proceedings of the 4th International Seminar "GPS in Central Europe", Penc, 7-9 May 1997, Warsaw University of Technology, Institute of Geodesy and Astronomy, ISBN 83-85287-26-4, Warsaw 1997.
- IERS Annual Report 1997, Central Bureau of IERS, Paris Observatory, July 1998.
- IERS Technical note 23, Definition and Realization of the International Celestial Reference System by VLBI Astrometry of Extragalactic Objects Central Bureau of IERS, Paris Observatory, June 1997.
- Ma, C., J.M. Sauber, L.J. Bell, T.A. Clark, D. Gordon, W.E. Himwich, and J.W. Ryan, Measurement of Horizontal motions in Alaska Using Very Long Baseline Interferometry, *J. Geophys. Res.*, 95, 21,991-22,011, 1990.
- Niell, A. E., Global mapping functions for the atmosphere delay at radio wavelengths, *J. Geophys. Res.*, 101, 3227-3246, 1996.
- Petrov, L., Fast version of VLBI software SOLVE (f-SOLVE), unpublished, 1999, <http://giub.geod.uni-bonn.de/vlbi/development/f-SOLVE/f-SOLVE.html>.
- Rogers, A.E.E., R.J. Cappallo, H.F. Hinteregger, J.I. Levine, E.F. Nesman, J.C. Webber, A.R. Whitney, T.A. Clark, C. Ma, J.R. Ryan, B.E. Corey, C.C. Counselman, T.A. Herring, I.I. Shapiro, C.A. Knight, D.B. Shaffer, N.R. Vandenberg, R. Lacasse, R. Mauzy, B. Rayhrer, B.R. Schupler, and J.C. Pigg, Very Long Baseline Radio Interferometry: The Mark III system for geodesy, astrometry, and aperture synthesis, *Science*, 219, 51-54, 1983.

# A two-step approach to analyze European geodetic Very Long Baseline Interferometry (VLBI) data

Rüdiger Haas<sup>1</sup> and Axel Nothnagel<sup>2</sup>

<sup>1</sup> Onsala Space Observatory (OSO), SE-439 92 Onsala, Sweden, (haas@oso.chalmers.se)

<sup>2</sup> Geodätisches Institut der Universität Bonn (GIUB), DE-53115 Bonn, Germany, (nothnagel@uni-bonn.de)

## Abstract

Since 1990 the European fixed station geodetic Very Long Baseline Interferometry (VLBI) network has been observing on a regular basis in order to determine crustal motion in Europe. Usually the analyses of geodetic VLBI data are set up in two different ways: a) to produce station coordinates for each observation epoch from independent parameter adjustments and b) to compute station coordinates at a reference epoch together with drift rate components simultaneously from solutions where station drifts are modeled directly using vector representation. In this paper we present an alternative analysis strategy which uses a two step approach. In a first step all station coordinates are estimated as independent parameters for each session. Then in a second step topocentric drift rate vectors are computed from the individual series of station coordinates and their covariance matrices.

## 1 Introduction

The first purely European geodetic Very Long Baseline Interferometry (VLBI) session was observed in January 1990. With this initial session the European geodetic VLBI group started a routine observing program with usually 6 observing sessions per year in the European fixed station geodetic VLBI network. Until the end of 1998 a total number of 46 sessions was carried out. The analyses of geodetic VLBI data are usually set up to produce two different representations of the station coordinates from a least-squares or Kalman Filter adjustment of the observations. In the first type of solutions each observing session is adjusted independently and a series of station coordinates with respect to a reference station in the network is determined. In geodetic VLBI a reference station or some type of constraint is always needed in order to resolve the translational degrees of freedom of the network. Adopted from satellite orbit determinations this type of solutions is a so-called ‘arc solution’ with station coordinates as ‘arc parameters’.

The second type of adjustment estimates station coordinates at a reference epoch plus station drift parameters in the form  $dx/dt$ ,  $dy/dt$ ,  $dz/dt$ . Since these parameters are determined from all observation sessions together they are called ‘global parameters’ determined in a so-called ‘vector solution’. Additionally, in both types of solutions a number of parameters have to be estimated in each session which model effects valid only within the individual sessions. These are mostly parameters which describe the behavior of the station clocks, the refraction of the atmosphere and some or possibly all Earth orientation parameters (EOP).

The arc solution gives a good insight into the quality of the individual observing sessions since the individual results may be displayed graphically on an epoch by epoch basis. Currently it is common use to depict these in three dimensional baseline components [e.g. RYAN et al. 1993]. The repeatability of baseline length measurements which are invariant against any rotations are a useful measure to derive the measurement accuracy. Here, the rotational degrees of freedom of the network are fixed by using an external EOP series.

The vector solution directly produces station related annual displacement vectors. For its central location and the good agreement of its annual motion due to continental drift with the NNR-Nuvel-1A model [DE METS et al., 1994] most often the coordinates and drift rate of Wettzell are held fixed in adjustments of European VLBI data. Earth orientation parameters may be estimated if the first epoch EOP are fixed. Subtracting the NNR-Nuvel-1A model drift from station motions estimated in vector solutions thus yields annual displacement vectors in a European/Wettzell fixed frame.

## 2 Modified Analysis Strategy

In the least squares adjustment of a vector solution the scatter of the individual sessions as it is present in the arc solutions is constrained into one single vector for each station. Any large deviations of individual sessions and stations in particular are not discernable any more. In addition, from our experience with vector solutions the annual drift vectors of the European regional network with Wettzell as a fixed reference station and fixed EOP has a tendency to display a small spurious rotation about the central station. The reason of this is still unknown but deficiencies of stations in the earlier sessions may be suspected.

In order to overcome these deficits and to have a better way of visualizing the session to session evolution of a station's coordinates we devised a third analysis strategy which consists of two steps. In a first step we perform an usual arc solution, i.e. we determine relative station coordinates for all stations with respect to a reference station in the network which moves according to the NNR-Nuvel-1A [DE METS et al., 1994]. The results are series of geocentric station coordinates but also the full covariance matrices for each observing session which are saved for further use. In order to create a European plate fixed frame plate motion according to the NNR-Nuvel-1A model is subtracted.

With the parameters of the WGS84/GRS80 ellipsoid the geocentric Cartesian station coordinates are transformed into geocentric ellipsoidal ones with a conventional transformation procedure. In order to also transform the formal errors of the Cartesian station coordinates the full covariance matrix between all station coordinates of the solution, i.e. between the three dimensional coordinates of each individual station and between the coordinates of all participating stations, is transformed into the ellipsoidal system as well. The results of the transformations are ellipsoidal station coordinates for each participating station in the session and the covariance matrix between the ellipsoidal coordinates of all stations in the specific session.

In the second step the series of station latitude and longitude together with the geocentric height is used to determine the topocentric annual station drift in the respective tangential plane. In order to express the motions of the stations in mm per year a mean value for longitude, latitude and height for each station is subtracted and the angular positions are transformed into metric North and East components. Finally, least squares adjustments are performed to estimate offsets and rates of linear regressions for each station. Again the whole covariance information for each session is applied, so e.g. the rate for the height component depends on the results for the east and north components according to the covariance matrix, too.

In the series some of the stations suffered abrupt changes in the station position due to track and wheel repairs. At epochs where we have good evidence for these changes we introduce discontinuities in the linear trends. In these cases the same linear rate before and after the discontinuity but two different absolute values, one before and one after the modification, is estimated in the least squares adjustments.

## 3 Topocentric station drift rate results

The European geodetic VLBI session from January 1990 to October 1998 were analyzed with the two-step analysis approach described in the previous section. In the first step we performed an 'arc-solution' using the CALC/SOLVE/GLOBL VLBI data analysis software package [MA et al., 1990]. Clock parameters with respect to a reference clock in each session were estimated with second order polynomials and additional piecewise linear components every 6 hours. Atmospheric wet zenith path delays were estimated as piecewise linear functions every 60 minutes using the NMF 2.0 mapping function [NIELL, 1996]. Additionally, horizontal delay gradient parameters in North and East direction were estimated in a piecewise linear mode every 8 hours. Relative station coordinates with respect to a reference station were estimated for each station except for the reference station itself which we chose to be Wettzell. Since we wanted to refer to a single reference station we had to leave out three sessions

in 1992 and one in 1998 where Wettzell did not participate. Coordinates of radio sources were kept fixed at values of the International Celestial Reference Frame (ICRF) 1995 and a priori coordinates for the observing sites were introduced according to the International Terrestrial Reference Frame (ITRF) 1996. Earth orientation parameters (EOP) were adopted from a recent global VLBI solution by the GSFC VLBI group [MA and RYAN, 1998] while daily nutation offsets with respect to the IAU 1980 nutation model were estimated for each session.

In the second step we used the results of the first step transforming the coordinates of the stations and determining topocentric station drift rates using the strategy described before. Table 1 displays the results for horizontal and vertical station drift rates and figures 1 and 2 show these results in a graphic representation. Ny Ålesund, Simeiz and Yebes were not considered in the second step because of their short observational history which produces fairly insignificant and unreliable results.

Tab. 1: Topocentric station drift rates of six stations in the network.

station	East [mm/y]	wrms [mm]	North [mm/y]	wrms [mm]	height [mm/y]	wrms [mm]
Effelsberg	$+1.45 \pm 1.27$	3.26	$-0.36 \pm 0.89$	2.68	$-0.21 \pm 3.16$	9.21
Madrid	$+0.01 \pm 0.48$	4.36	$+0.17 \pm 0.37$	3.10	$+2.57 \pm 1.35$	13.29
Matera	$+1.95 \pm 0.29$	3.07	$+4.14 \pm 0.25$	4.00	$+0.55 \pm 0.87$	11.56
Medicina	$+2.82 \pm 0.41$	2.93	$+2.05 \pm 0.31$	2.16	$-4.39 \pm 1.12$	7.75
Noto	$-0.81 \pm 0.38$	4.32	$+4.45 \pm 0.36$	4.38	$-1.05 \pm 1.21$	10.63
Onsala	$-1.89 \pm 0.45$	3.93	$-0.55 \pm 0.29$	3.81	$+2.34 \pm 0.98$	14.63

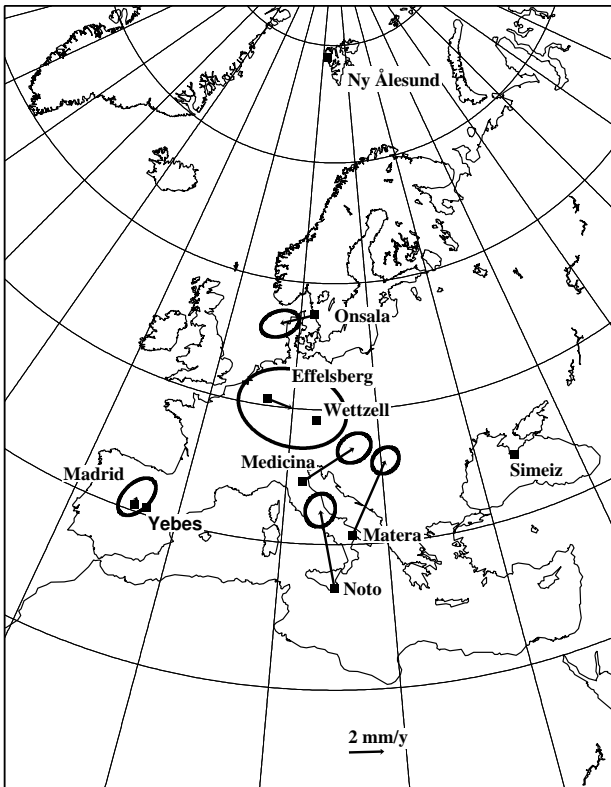


Fig. 1: Horizontal station drift rates in a European plate fixed frame with respect to Wettzell.

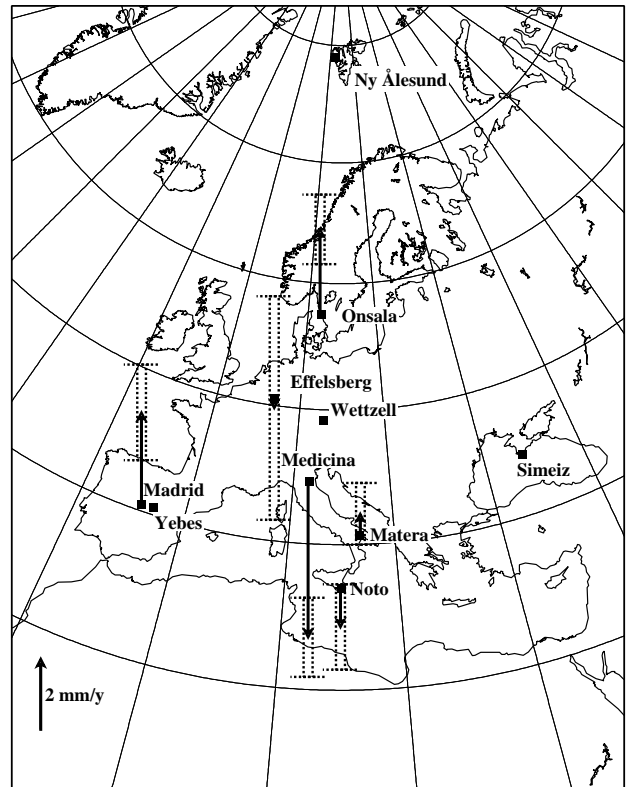


Fig. 2: Vertical station drift rates in a European plate fixed frame with respect to Wettzell.

As mentioned already the annual horizontal motion of Wettzell agrees very well with the NNR-Nuvel-1A continental drift model. Thus, fixing the motion of Wettzell to this model and using high accuracy Earth rotation parameters from external sources places a reliable bound on the long term drift of the European continent as represented by the observing sites. Only the EOP have an effect on the determination of the drifts of the stations relative to Wettzell. Since the long term stability is extremely reliable and the short term variations only increase the scatter of the results, the drift vectors determined up to date deserve a high level of confidence.

The estimated vertical motions are linked directly to the vertical rate of Wettzell which is set to zero in our analysis. Thus, these rates can only be considered relative to Wettzell which may not have a constant height over the years. Although global solutions of the world-wide VLBI data set suggest a small subsidence of Wettzell [e.g. MA and RYAN, 1998] local and regional surveys have not confirmed this [SCHLÜTER, pers. communication].

For the three stations Effelsberg, Madrid and Medicina we introduced discontinuities in their positions due to track and wheel replacements at those stations. Table 2 displays the resulting station offsets with their formal errors. The latter are computed applying the error propagation law to the differences of the positions before and after the displacements. Since the observation epochs after track repairs are relatively short for all three stations the magnitudes of the resulting offsets have to be considered very preliminary. More observations are needed to compare the VLBI estimates of the height changes with local geodetic measurements which are currently underway.

Tab. 2: Displacements due to track and wheel replacements

station	date	East offset [mm]	North offset [mm]	height offset [mm]
Medicina	96/07/01	$-5.69 \pm 3.73$	$+2.50 \pm 2.85$	$+14.36 \pm 10.19$
Effelsberg	96/10/01	$-6.61 \pm 7.99$	$+0.22 \pm 5.55$	$+17.35 \pm 19.85$
Madrid	97/04/30	$-2.64 \pm 4.98$	$-11.03 \pm 4.01$	$-9.61 \pm 14.02$

## 4 Discussion

The advantage of the two-step analysis approach is that from the graphical representation of the individual station coordinate series any abnormal results are discernable. In addition, the scatter of the results as presented in a topocentric systems gives an impression of the repeatability of the coordinate series of a station rather than a baseline component representation. Since the separation between horizontal and vertical components is much easier than in a geocentric Cartesian system an easier interpretation is permitted.

It should be emphasized here that the significance of the station drift components are the more obvious the larger the annual drift. On the contrary stations with hardly any motion suffer from the fact that the results will arbitrarily scatter about an average position before the number of sessions is large enough to establish stability. Consequently the azimuth of the drift vector will take up arbitrary values when additional sessions are added but the magnitude will become smaller and smaller eventually.

From the session by session display of the horizontal coordinate results it is clear that the scatter in most cases will inhibit a suitable visual impression (e.g. Fig. 3). In order to give the display a higher degree of significance annual averages were calculated and plotted in the same fashion (e.g. Fig. 4). Especially in the years since 1993 when 6 sessions per year were observed the averages are a good representation of the respective station positions. On the other hand the averages of the earlier

years are often computed from three or less sessions and thus lack the required stability. It should be noted again that from all series a constant drift component according to the NNR-Nuvel-1A model is subtracted already.

Since the least squares solution setup selected here relies on fixed coordinates of the station Wettzell and on an external series of Earth orientation parameters (EOP) the coordinate results of the individual session days are affected by the Earth orientation parameters. Although any uncertainties in the ERP series may create additional noise in the components of the coordinates the long-term trend of the station drifts should not be disturbed.

Figure 3 shows the individual coordinate results for the station of Noto as determined from the solution with the drift of Wettzell and the apriori EOP fixed. In the representation of the annual averages (Fig. 4) the visual impression becomes much clearer. It can be seen that the results of the earlier session which are those in the South lack the stability as seen in the later sessions.

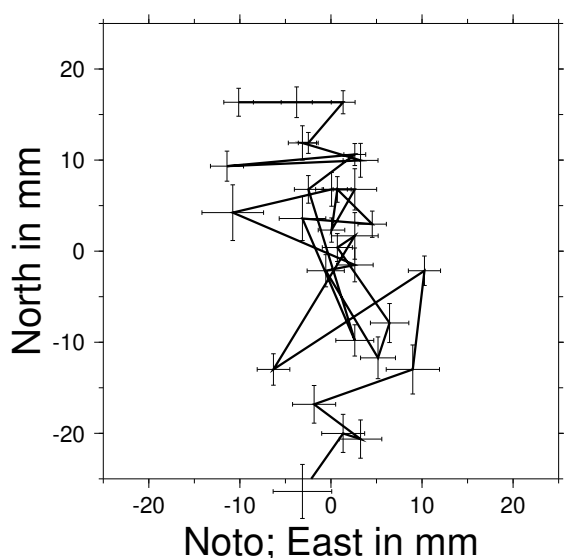


Fig. 3: Session by session results in the horizontal components with a constant part subtracted.

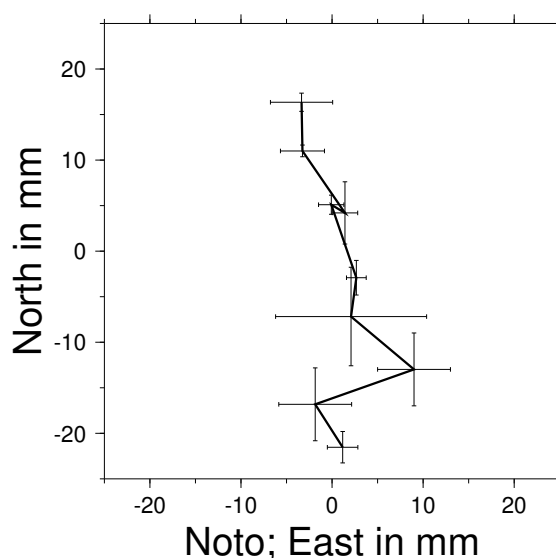


Fig. 4: Annual session averages in the horizontal components with a constant part subtracted.

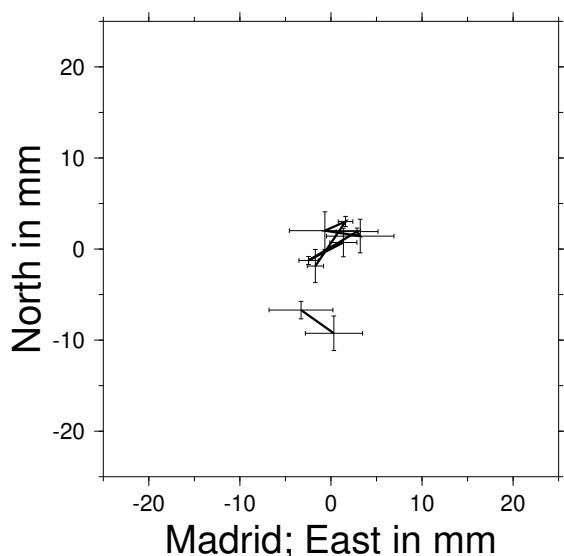


Fig. 5: Annual session averages in the horizontal components with results of the years 1997 and 1998 disconnected due to mechanical displacement of the VLBI reference point.

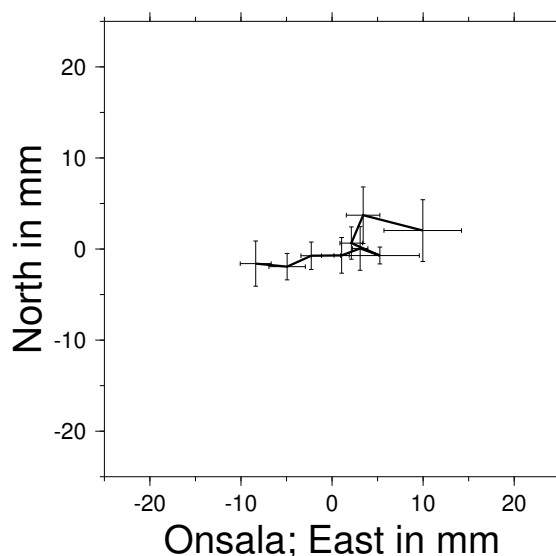


Fig. 6: Annual session averages in the horizontal components with a constant part subtracted.

In Figure 5 the annual averages of the Madrid horizontal components are displayed. The results of the years 1997 and 1998 are disconnected from the earlier years due to the fact that local modifications for track repairs have shifted the VLBI reference point to the South. The remaining series of points shows only very little scatter and no significant trend.

The evolution of the station coordinates of Onsala suggests a significant westward motion of the site (Fig. 6). However, this motion only stabilized in the years since 1993. If a displacement rate is computed with all the data a smaller magnitude can be expected than if only the data since 1993 would be used.

The graphical representation of the vertical components displays a much larger scatter than the horizontal components (e.g. Fig. 7) and thus significant vertical rate determinations will need a longer time base. The example of Matera in this figure represents the current situation at most of the European stations where the scatter of the individual results still inhibits a definite conclusion whether or not there is a significant height change.

Only Medicina (Fig. 8) already shows a significant subsidence, a fact which is supported by the information of heavy ground water extraction in the Po Valley. Unfortunately, the continuous series is interrupted by a telescope uplift due to necessary modifications of the antenna track as can be seen in figure 8. Even though there is this discontinuity in the series, the Medicina height results produce the least scatter in the network which is also obvious in the weighted RMS results (see table 1). The superior quality of these height results may in part be a consequence of the fact that Medicina has the shortest distance to Wettzell.

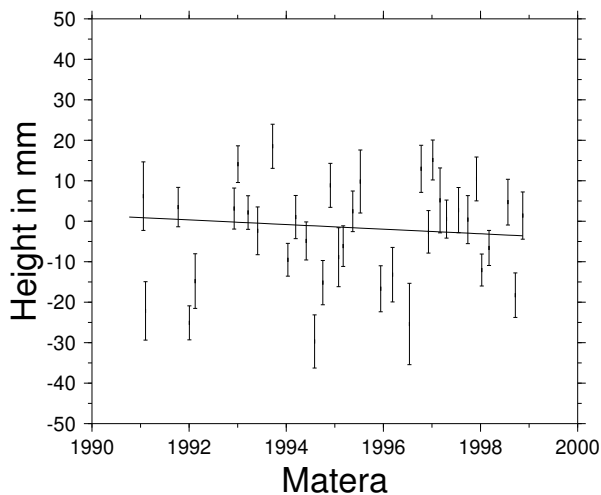


Fig. 7: Vertical components with a constant part subtracted.

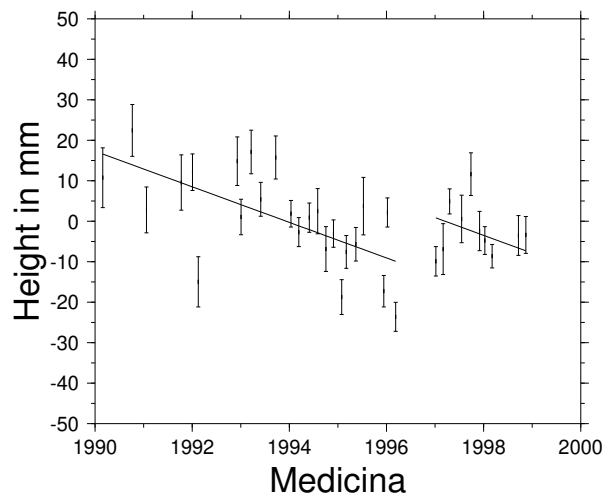


Fig. 8: Vertical components with a constant part subtracted.

Concerning the quoted formal errors of the results it should be emphasized that the inverse squared of the formal errors of the individual topocentric coordinate components were used as the weights for the linear regressions. Taking into account that the  $\chi^2$  per degree of freedom ranged between 4 and 6, the sigmas of the coordinate components are too optimistic by a factor of 2 to 3. However, the errors quoted for the annual rates are based on the scatter of the individual results of the series and thus represent the overall repeatability from session to session. They are, therefore, rather more realistic than those from batch vector solutions [see e.g. LANOTTE et al., 1999 this issue] where the large number of delay observables heavily affects the formal errors of all parameters.

## 5 Conclusions and Outlook

We developed an alternative two-step analysis strategy to derive station drift rates from the analysis of individual VLBI sessions. This method permits a visual inspection of the series of coordinate results and it reduces any cross-talk of station deficiencies in individual sessions with annual drift rates of ‘healthy’ stations. In order to end up with reliable drift vectors from time series, results from individual sessions for a single station may be selected for exclusion if obvious deficiencies suggest to do so. The advantage of this as compared to vector solutions is that deviations are made obvious and that not the whole session has to be discarded. The disadvantage of the method is that it has to rely on a single station whose coordinates and drift rate have to be fixed in the analysis. Any necessity for a new fixed station in sessions added to series, for example due to a failure of the initial reference station, would impose a shift onto the results of the other stations. Therefore, applications of this two-step method to the combination of different networks are not readily available. Only in confined series where one single site can be fixed for the majority of the sessions this method provides a good basis for scrutinizing the data on a station by station basis. Currently a method is being developed which permits the inclusion of additional sessions where the initial reference station is for any reason not part of the session. A further extension of the method would be the combination of different networks.

**Acknowledgements.** We thank the staff members of all observatories participating in the series and the staff at the Bonn correlator for their hard work. Rüdiger Haas is supported by the European Union within the TMR programme under contract FMRX-CT960071. This research has made use of NASA Goddard Space Flight Center’s VLBI terrestrial reference frame solution 1102g, 1998 August. Figures were produced with the GMT software package [WESSELS and SMITH, 1995].

## References

- De Mets, C., R.G. Gordon, D.F. Argus and S. Stein: *Effect of recent revision to the geomagnetic reversal time scale on estimates of current plate motions*, GRL 21(20), 2191–2194, 1994
- Ma, C., J.M. Sauber, L.J. Bell, T.A. Clark, D. Gordon and W.E. Himwich: *Measurement of horizontal motions in Alaska using very long baseline interferometry*, JGR 95, 21991–22011, 1990
- Ma, C. and J.W. Ryan: *NASA Space Geodesy Program – GSFC DATA Analysis – 1998, VLBI Geodetic Results 1997 – 1998, August, 1998*, <http://lupus.gsfc.nasa.gov/global/glb.html>, 1998
- Niell, A.E.: *Global mapping functions for the atmosphere delay at radio wavelength*, JGR 101(B2), 3227–3246, 1996
- Ryan J.W., C. Ma, D.S. Caprette: *NASA Space Geodesy Program - GSFC Data Analysis - 1992, Final Report of the Crustal Dynamics Project VLBI Geodetic Results 1979-91*, NASA Technical Memorandum 104572, Greenbelt, 1993
- Wessels, P. and W.H.F. Smith: *New version of the Generic Mapping Tool released*, EOS 76, 329, 1995

# A geocentric relativistic VLBI-Model

Klaus Börger, Geodetic Institute, University of Bonn, Nussallee 17, 53115 Bonn  
e-mail: boerger@uni-bonn.de

February 1999

## Abstract:

Three relativistic models are available in the data analysis software CALC/SOLVE, that is to say the Shapiro-, the Hellings- and the Consensus-Model. They all have in common the same starting point, i.e. the motion of a photon is described in a barycentric spacetime and only the subsequent transformation into a geocentric spacetime finally provides the relation between observation and model-quantities. Further these models only supply an observation equation, but an adequate stellar model for the radio sources is missing. Based on this a geocentric modelling with a relativistic stellar model is presented. In order to investigate the new model, different analyses were made, which finally confirm the general validity of the geocentric relativistic model. Comparing parameter estimations shows that the new model actually yields improved results.

## 1 Introduction

At present three relativistic VLBI-models are implemented in the data analysis software CALC-SOLVE. These models – considered as a series – reflect the continuous development and improvement of theory and practice. Specified there are the Shapiro-Model, which is the original relativistic VLBI-Model, further the Hellings-Model as an enlargement and adaption to improved observation accuracies and finally the Consensus-Model, which is the standard relativistic VLBI-model, recommended for use by the IERS. As a matter of principle there is no substantial difference between these models, although they are different in derivation [*Eubanks (1991)*]. These models all have in common a primary barycentric reference and they all do not have a stellar model, i.e. a general relativistic transformation from the celestial system to the geocentric system. Starting from these states, a new approach, especially regarding geodetic aspects, is opposed to the customary models.

## 2 Intentions and features of the new model

The purpose is to develop an **alternative approach**, which does not only supply an observation equation, but also demonstrates a method, which shows new aspects and perspectives by a comprehensive consideration of the matter. The new model is characterized by the inclusion of a stellar model and a **geocentric approach**. Concerning this, at a first glance it is true, that both procedures, the geocentric one as well as the barycentric one, are equivalent, but from a geodetic point of view a geocentric modelling is better qualified, because all observation and estimation parameters are related to earth, except the radio source positions. Further relativistic effects w.r.t. the earth are smaller than those related to the sun. And a final argument for a geocentric modelling is the general possibility of transferring the results to other space geodetic methods which have the delay as principal observable, too. In order to connect theory and experiment data analysis using the new model is necessary. The performed investigations mainly serve two aspects, that is to say the verification and classification of the quality of the new model.

### 3 Modelling

Four aspects are significant for modelling, which are shown in figure 1. At the telescopes a signal-stream is observed and a time information is assigned. In relativity one distinguishes between coordinate time and proper time, which for example is realized by a clock on the surface of the Earth, i.e. each station clock provides a proper time. Therefore an exact **definition of the observable**, which is the difference between two points of time, is absolutely necessary. From this follows the proper time of arrival is the **primary measuring quantity**

$$\tau_a \text{ in station } a \qquad \qquad \qquad \tau_b \text{ in station } b . \qquad (3-1a)$$

It is not possible to synchronize different positioned clocks, for this purpose one has to compare the corresponding coordinate times. Assumed a negligible station velocity and ignoring a clock correction the coordinate times belonging to (3-1a) are determined by

$$t_a = (g_{00})_a^{-\frac{1}{2}} \tau_a , \qquad \qquad \qquad t_b = (g_{00})_b^{-\frac{1}{2}} \tau_b . \qquad (3-1b)$$

$g_{00}$  is the time component of the metric tensor  $g_{\alpha\beta}$ . With this preliminary the **observable of the geodetic VLBI** is obtained from the difference of the quantities in (3-1b) [see *Börger (1998)*]

$$\begin{aligned} \Delta t &= t_b - t_a \\ &= \Delta\tau - \left\{ [1 - (g_{00})_b^{-\frac{1}{2}}] \tau_b - [1 - (g_{00})_a^{-\frac{1}{2}}] \tau_a \right\} \end{aligned} \qquad (3-2a)$$

$$= \Delta\tau - \left\{ [(g_{00})_a^{-\frac{1}{2}} - (g_{00})_b^{-\frac{1}{2}}] \tau_a + [1 - (g_{00})_b^{-\frac{1}{2}}] \Delta\tau \right\} ,$$

$$\Delta\tau = \tau_b - \tau_a . \qquad (3-2b)$$

The first expression in the brace on the right side of the last equation (3-2a) is the **difference in geometry** and the second one is the classical **relation between coordinate- and proper time**.

Further the introduction of different systems is necessary, because parameters and vectors are presented in different systems. I.e. in the language of relativity one has to **define different spacetimes**, and it is distinguished between three spacetimes, that is to say the catalog-spacetime  $\hat{\Sigma}$  in which the radio source positions are tabled; the geocentric spacetime  $\Sigma$ , which is the basis of this approach and local spacetimes  $\bar{\Sigma}$ , which are connected to the telescopes. In addition to this one has to determine the relations between these spacetimes, i.e. one has to determine the transformations. For this purpose the concept of tetrads is applied [see *Börger (1998)*].

Finally the **determination of the signal-path** as well as the **determination of the signal-velocity** are needed. Concerning the last aspect one has to deal with electrodynamics. The determination of the signal-path has to be explained in more detail. The signal-path depends on geometry, because geometry defines geodetic lines and therewith those lines on which electromagnetic signals travel. Within the Einstein theory of gravitation the determination of geometry results from the solution of the field equations. These field equations require an adequate model of matter, which should contain all forms of energy and momentum as shown in figure 1. This of course is an interesting methodical aspect. The **solution of the Einstein's field equations**, i.e. the determination of expressions for the metric coefficients is described in e.g. *Börger (1996)*.

The next step is to express all these ideas and thoughts in mathematical terms in order to get a model and an observation equation. A detailed description of the relations and the derivation of the basic equations is given in *Börger (1998)*.

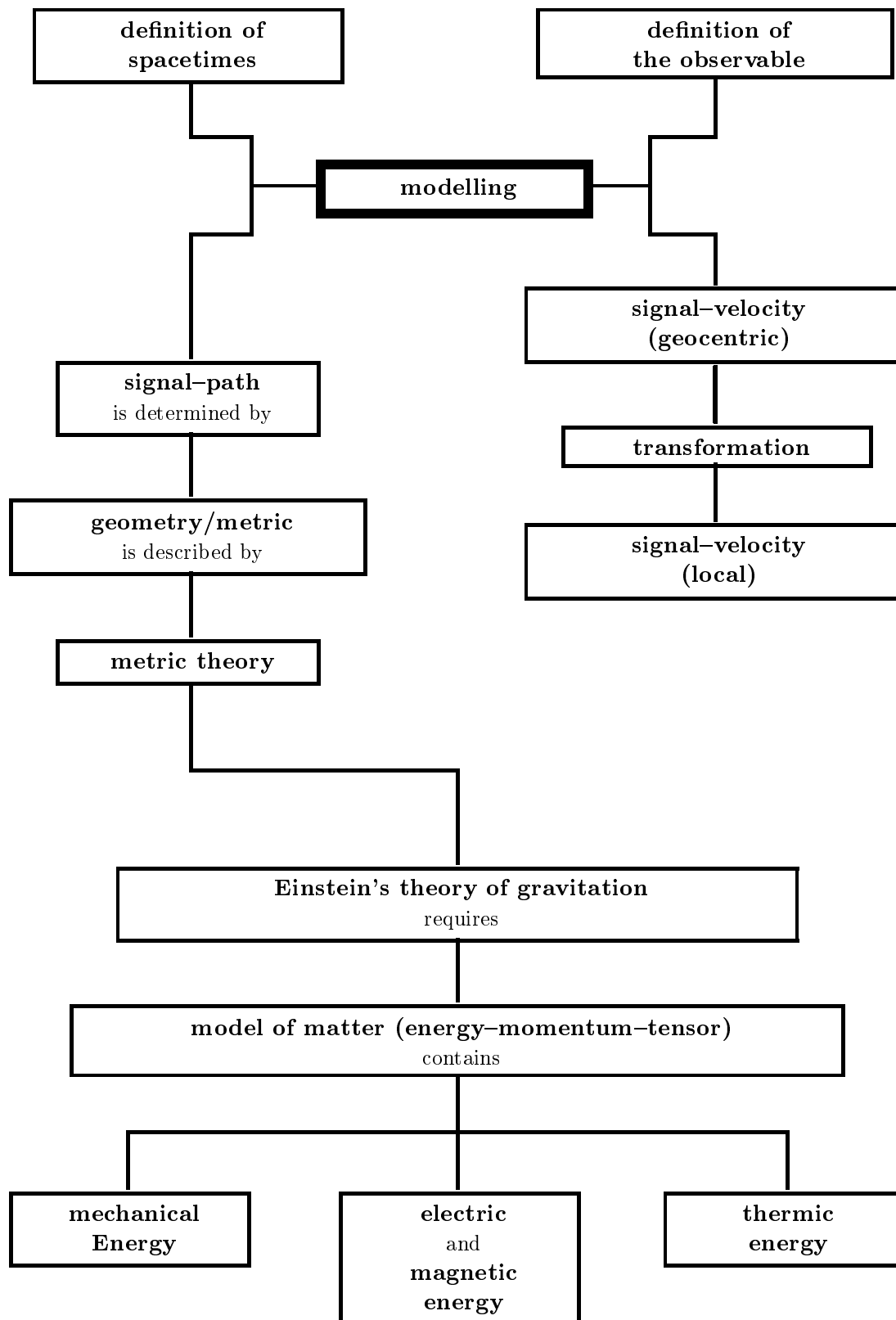


Fig. 1: procedure of modelling

Due to *Börger (1998) (3.6-6)* the **geocentric relativistic observation equation of the geodetic VLBI** reads:

$$\Delta t = \frac{s}{v_H} \left\{ 1 + \frac{1}{v_H^2} \sum_{n=1}^{\infty} \sum_{m=2}^{\infty} \frac{1}{n! m!} (\Delta_{ij} D_n^i D_m^j) \Delta t^{(n+m-2)} \right\}^{-\frac{1}{2}}, \quad (3-3a)$$

an expression, which determines the delay in an iterative mode. The first term on the right side is a first approximation, the so-called **Newtonian delay**. Up to the order  $n = 4$ , the  $D_n^i$  are determined as follows:

$$D_1^i = \left( \frac{dx_H^i}{dt} \right)_b = c \left( \frac{k^i}{k^0} \right)_b = v_{Hb}^i \quad (3-3b)$$

$$\begin{aligned} D_2^i &= \left( \frac{d^2 x^i}{dt^2} \right)_b \\ &= \left( \frac{1}{c} \Gamma_{\beta\gamma}^0 v_{Hb}^i - \Gamma_{\beta\gamma}^i \right)_b v_{Hb}^\beta v_{Hb}^\gamma + \left( P^i - \frac{1}{c} P^0 v_{Hb}^i \right)_b \end{aligned} \quad (3-3c)$$

$$\begin{aligned} D_3^i &= \left\{ \left( \frac{1}{c} \Gamma_{\alpha\beta,\gamma}^0 + \frac{3}{c^2} \Gamma_{\alpha\beta}^0 \Gamma_{\gamma\delta}^0 v_H^\delta - \frac{2}{c} \Gamma_{\alpha\mu}^0 \Gamma_{\beta\gamma}^\mu \right) v_{Hb}^i \right. \\ &\quad \left. - \left( \Gamma_{\alpha\beta,\gamma}^i - 2 \Gamma_{\alpha\mu}^i \Gamma_{\beta\gamma}^\mu + \frac{3}{c} \Gamma_{\alpha\beta}^0 \Gamma_{\gamma\delta}^i v_H^\delta \right) \right\}_b v_{Hb}^\alpha v_{Hb}^\beta v_{Hb}^\gamma \end{aligned} \quad (3-3d)$$

$$\begin{aligned} D_4^i &= \left\{ \left( \frac{1}{c} \Gamma_{\alpha\beta,\gamma\delta}^0 - \frac{2}{c} \Gamma_{\alpha\mu,\delta}^0 \Gamma_{\beta\gamma}^\mu - \frac{2}{c} \Gamma_{\alpha\mu}^0 \Gamma_{\beta\gamma,\delta}^\mu \right. \right. \\ &\quad \left. - \frac{2}{c} \Gamma_{\epsilon\alpha,\beta}^0 \Gamma_{\gamma\delta}^\epsilon - \frac{1}{c} \Gamma_{\alpha\beta,\mu}^0 \Gamma_{\gamma\delta}^\mu + \frac{2}{c} \Gamma_{\mu\nu}^0 \Gamma_{\alpha\beta}^\nu \Gamma_{\gamma\delta}^\mu \right. \\ &\quad \left. + \frac{4}{c} \Gamma_{\alpha\mu}^0 \Gamma_{\nu\beta}^\mu \Gamma_{\gamma\delta}^\nu + \frac{10}{c^2} \Gamma_{\alpha\beta}^0 \Gamma_{\gamma\delta,\nu}^0 v_{Hb}^\nu \right. \\ &\quad \left. - \frac{20}{c^2} \Gamma_{\alpha\beta}^0 \Gamma_{\mu\gamma}^0 \Gamma_{\nu\delta}^\mu v_{Hb}^\nu + \frac{15}{c^3} \Gamma_{\alpha\beta}^0 \Gamma_{\gamma\delta}^0 \Gamma_{\mu\nu}^0 v_{Hb}^\mu v_{Hb}^\nu \right) v_{Hb}^i \\ &\quad - \Gamma_{\alpha\beta,\gamma\delta}^i + 2 \Gamma_{\alpha\mu,\delta}^i \Gamma_{\beta\gamma}^\mu + 2 \Gamma_{\alpha\mu}^i \Gamma_{\beta\gamma,\delta}^\mu \\ &\quad + 2 \Gamma_{\mu\alpha,\beta}^i \Gamma_{\gamma\delta}^\mu + \Gamma_{\alpha\beta,\mu}^i \Gamma_{\gamma\delta}^\mu - 2 \Gamma_{\mu\nu}^i \Gamma_{\alpha\beta}^\mu \Gamma_{\gamma\delta}^\nu \\ &\quad - 4 \Gamma_{\alpha\mu}^i \Gamma_{\nu\beta}^\mu \Gamma_{\gamma\delta}^\nu - \frac{4}{c} \Gamma_{\alpha\beta,\gamma}^0 \Gamma_{\delta\mu}^i v_{Hb}^\mu - \frac{6}{c} \Gamma_{\alpha\beta,\gamma}^i \Gamma_{\delta\mu}^0 v_{Hb}^\mu \\ &\quad - \frac{15}{c^2} \Gamma_{\alpha\beta}^0 \Gamma_{\gamma\delta}^0 \Gamma_{\mu\nu}^i v_{Hb}^\mu v_{Hb}^\nu + \frac{8}{c} \Gamma_{\alpha\mu}^0 \Gamma_{\beta\gamma}^\mu \Gamma_{\delta\mu}^i v_{Hb}^\mu \\ &\quad \left. + \frac{12}{c} \Gamma_{\alpha\mu}^i \Gamma_{\beta\gamma}^\mu \Gamma_{\delta\nu}^0 v_{Hb}^\nu \right\}_b v_{Hb}^\alpha v_{Hb}^\beta v_{Hb}^\gamma v_{Hb}^\delta. \end{aligned} \quad (3-3e)$$

The index  $b$  means that all calculations have to be done at the position of the station  $b$ , which receives the signal as second.  $k_H^i$  is the spatial component of the **wave-vector** of a radio source  $H$  and  $v_H^i$  is the **3-coordinate-velocity** of an emitted signal, which is the spatial component of the so-called **4-coordinate-velocity**  $v_H^\alpha$ , that appears in (3-3c-e). The  $\Gamma_{\beta\gamma}^\alpha$  are the **Christoffel-symbols**, partial derivatives of the metric coefficients  $g_{\alpha\beta}$ .  $P^\alpha$  in (3-3c) pays attention to the influence of refraction.

For computation of the **theoretical delay** due to (3-3a) the radio source positions are needed in the geocentric spacetime  $\Sigma$  and the developed **stellar model** provides the necessary transformation from the catalog-spacetime  $\hat{\Sigma}$  to the geocentric spacetime  $\Sigma$ . This **general-relativistic transformation of the source position** reads:

$$r_H^i = (e_k^i \tilde{e}_j^k \hat{r}_H^j) + (\delta r^i)_1 + (\delta r^i)_2 + (\delta r^i)_3 + (\delta r^i)_4 \quad (3-4a)$$

with

$$(\delta r^i)_1 = \frac{1}{2} h_{00(2)} (e_k^i \tilde{e}_j^k \hat{r}_H^j) + \frac{1}{2} h_{im(2)} e_k^m \tilde{e}_j^k \hat{r}_H^j \quad (3-4b)$$

$$\approx h_{00(2)} (e_k^i \tilde{e}_j^k \hat{r}_H^j)$$

$$(\delta r^i)_2 = \frac{v^i}{c} - \frac{v^m}{c} \left\{ \left( \frac{1}{2} \frac{v^i}{c} + e_k^i \tilde{e}_j^k \hat{r}_H^j \right) (e_k^m \tilde{e}_j^k \hat{r}_H^j) \right\} - \frac{1}{2} \frac{v^2}{c^2} (e_k^i \tilde{e}_j^k \hat{r}_H^j) \quad (3-4c)$$

$$(\delta r^i)_3 = -\frac{1}{2} h_{0i(1)} h_{0m(1)} e_k^m \tilde{e}_j^k \hat{r}_H^j + (h_{0m(1)} e_k^m \tilde{e}_j^k \hat{r}_H^j) (e_k^i \tilde{e}_j^k \hat{r}_H^j) \quad (3-4d)$$

$$(\delta r^i)_4 = (h_{0m(1)} e_k^m \tilde{e}_j^k \hat{r}_H^j) \frac{v^i}{c} + \left( h_{0m(1)} \frac{v^m}{c} \right) (e_k^i \tilde{e}_j^k \hat{r}_H^j) . \quad (3-4e)$$

$e_j^i$  is the classical rotation matrix between the catalog-system and the geocentric system.  $\tilde{e}_j^i$  is an additional rotation matrix containing relativistic precession terms. The  $(\delta r^i)$  are corrections due to gravitation and relative motion of the two systems. As a matter of principle the supplements of the classical transformation are rather small and for this reason they are negligible except the aberration. A valuation of the terms is to find in *Börger (1998)*.

## 4 Numerical investigations

This section deals with data analysis using the new model, whereat these investigations mainly serve two aspects, that is to say the verification and classification of the quality of the geocentric relativistic model. For this purpose eleven experiments were analyzed and one batch solution was performed. Because four different relativistic models are available here four types of solution were created, but all with the same parametrization. With these given odds the quality of a solution is characterized first by the **WRMS of the observed delay**. Table 1 shows the results. The WRMS is the same

Experiment (database)	(3-3a)	HELLINGS	SHAPIRO	CONSENS
	WRMS [ps]	WRMS [ps]	WRMS [ps]	WRMS [ps]
96MAR04XH	39,744	39,718	39,746	39,748
96APR15XH	49,869	49,854	49,855	49,873
96MAY20XH	64,061	64,088	64,062	64,015
96JUN10XH	44,746	44,822	44,743	44,742
96JUL15XH	61,512	61,556	61,487	61,509
96AUG12XH	60,844	60,954	60,871	60,878
96SEP11XH	58,970	59,015	58,935	58,966
96OCT21XH	51,358	51,417	51,412	51,357
96NOV20XH	32,459	32,410	32,402	32,440
97FEB10XH	31,548	31,581	31,532	31,535
97FEB20XH	23,504	23,506	23,502	23,475
batch solution	40,888	40,911	40,878	40,881

Tab. 1: WRMS of the observed delay

for all models. Only within the sub-pico-seconds differences appear, but they do not have any level of

significance. Based on this first investigation one statement results: the new model is valid and well arranged in the order of accuracy as is easily recognized in the results of the batch solution.

To obtain further statements the parameter estimation of a single representative experiment is considered, i.e. station coordinates respectively baseline lengths are compared. For ease of comparison in table 2 the estimated baseline lengths are divided into a constant part and a rest. The formal errors

		(3-3a)		HELLINGS		SHAPIRO		CONSENS	
baseline	length	rest	Sigma	rest	Sigma	rest	Sigma	rest	Sigma
(name)	[mm]	[mm]	[mm]	[mm]	[mm]	[mm]	[mm]	[mm]	[mm]
Fortaleza-HartRAO	7025279700,00	0,15	10,51	2,65	10,51	2,36	10,51	2,60	10,51
Fortaleza-Miami20	5402898100,00	38,03	13,04	39,01	13,03	39,47	13,03	39,72	13,04
Fortaleza-Westford	5897126000,00	94,36	8,17	95,98	8,17	95,99	8,17	96,18	8,17
Fortaleza-Wettzell	7215409500,00	15,42	10,30	18,14	10,30	17,54	10,30	17,94	10,30
HartRAO-Miami20	10814594300,00	58,89	27,11	61,27	27,10	62,20	27,10	62,10	27,11
HartRAO-Westford	10658658500,00	16,78	12,91	19,78	12,90	20,21	12,90	19,89	12,91
HartRAO-Wettzell	7832322500,00	6,12	8,74	8,62	8,74	8,68	8,74	8,53	8,74
Miami20-Westford	2044503900,00	80,67	9,30	80,96	9,30	81,16	9,30	81,10	9,30
Miami20-Wettzell	7588401900,00	91,37	18,17	93,06	18,17	93,55	18,17	93,54	18,17
Westford-Wettzell	5998325500,00	31,61	4,09	33,37	4,09	33,49	4,09	33,38	4,09

Tab. 2: Baseline lengths from 96APR15XH

are the same for all models and the estimated lengths of the conventional models are nearly the same for the conventional models. The results of the new model differ significantly (max. 2mm). If these differences are interpreted as a result of a higher order modelling of the series expansions (3-3a) one may say that these differences represent a model refinement and should lead to slightly better results in the sense of being closer to reality. To show this the new geocentric model (3-3a) was applied in a reduced form, so that the resulting baselines are less close to reality than those resulting from the complete model. This reduced model, i.e. the neglecting of extensions and supplements, leads to results, that converge to the conventional ones. Of course further investigations have to be done to consolidate these findings.

## 5 References

- Börger K (1996)** , Determination of metric coefficients with VLBI, Proceedings of the 11th working meeting on european VLBI for Geodesy and Astrometry, Chalmers University of Technology, Research Report No. 177, Göteborg 1996
- Börger K (1998)** , Untersuchungen zur geozentrischen Modellbildung der relativistischen Langbasisinterferometrie, Mitteilungen aus den Geodätischen Instituten der Rheinischen Friedrich-Wilhelms-Universität Bonn, Nr. 84
- Eubanks T M (editor) (1991)** , A Consensus Model for Relativistic Effects in Geodetic VLBI, Proceedings of the USNO Workshop on Relativistic Models for Use in Space Geodesy, United States Naval Observatory, Washington

# Comparison of european network solutions

Klaus Börger, Geodetic Institute, University of Bonn, Nussallee 17, 53115 Bonn  
e-mail: boerger@uni-bonn.de

February 1999

## Abstract:

In the last years European VLBI arrived at high efficiency. The number of stations increased and the frequency of campaigns was forced. The accuracy of station coordinates is about several millimeters and the formal errors of the horizontal motions are less than 1 mm per year. In Europe different groups analyse the observed data and provide results, which should in fact converge. In order to investigate this question an analysis was performed, which compares the analysis strategies and the results of the different groups in order to assess the consequences of the individual approaches.

## 1 Introduction

In Europe different groups work on the data analysis of VLBI-observations and all these groups use their own strategy and method of data analysis. Independent of these different procedures the result should remain the same. Thus one requires to comply with the

### Principle:

*The determination of a parameter by different methods  
has to lead to the same result.*

Object of this presentation is to check, whether the different european network solutions fulfil this requirement. Surely contradictions are of special interest, because these need an exact explanation and therewith a detailed investigation.

## 2 Comparison

In order to make a comparison possible at all a common basis is needed. For this purpose the following odds were given. The NNR-NUVEL-1a should be used as drift model and the ITRF 1996 should serve as a priori station coordinates. The parameter estimation especially should provide and submit the station velocities of european stations with respect to NNR-NUVEL-1a in Up, East, North. The other aspects concerning the parameter estimation respectively solution were at disposal.

The following tables show the frame and general design of this comparison. In general the used software is CALC/SOLVE, but *Titov* used OCCAM. The session types as well as the time span are nearly the same, except for *Tomasi*, who used not only Europe-campaigns, but all experiments with at least three european stations from December 1987 to October 1998.

Table 2 shows, that the source coordinates are different, but this should have no significant influence on the parameter estimation, because the coordinates only slightly differ. On the contrary the different choice of the earth orientation series could cause a small rotation of the network.

The setup of the parameter estimation is nearly the same, but the modes of determination of the station velocity are different. Two methods were applied. The **direct method**, which determines the delay in the adjustment by immediate estimation and the **indirect method**, which is a two step

procedure. In a first step the station coordinates are estimated for each epoch and in a second step the station velocities are derived from this time series of station coordinates.

The differences of these two procedures as well as the advantages and disadvantages will become evident especially in the solution of *Tomasi*, who used the direct method, and *Nothnagel & Haas*, who used the indirect method.

	LANOTTE	TITOV	TOMASI	NOTHNAGEL & HAAS
USED SOFTWARE	F-SOLVE V98/08/09	OCCAM 3.4	F-SOLVE V98/11/25	CALC8.2/SOLVE
SESSION TYPES	EUROPE campaigns	EUROPE campaigns	all exp. with 3 european stations	EUROPE campaigns
TIME SPAN	Jan 1990 to Jun 1998	Jan 1990 to Jul 1998	Dec 1987 to Oct 1998	Jan 1990 to Oct 1998

*Tab. 1: Software, sessions and time span*

Before comparing the results a further note is necessary. The estimated station velocities of *Titov* have to be considered as preliminary ones, because it seems, that there is a mistake in his NUVEL-code, and this possible error sometimes causes great deviations from the other results.

	LANOTTE	TITOV	TOMASI	NOTHNAGEL & HAAS
STATION COORDINATES	ITRF 1996 (required)	ITRF 1996 (required)	ITRF 1996 (required)	ITRF 1996 (required)
SOURCE COORDINATES	ICRF 1995	ICRF 1996	GODDARD	ICRF 1995
EOP	IERS 97C04	IERS C04	GODDARD	GODDARD

*Tab. 2: Aprioris*

Object of the comparison are estimated station velocities and these motions are presented as velocity plots in *section 4*, so that the following considerations refer to this section. First the horizontal motion and then the height evolution is discussed.

The first that is remarkable in the velocity plot for **Ny Ålesund** is the great error ellipse of *Nothnagel & Haas* in relation to the error ellipse of *Tomasi*. Concerning this one has to take into account that different methods were used to determine the station velocity. When using the direct method the formal errors result from simultaneous adjustment in the batch solution. As a matter of principle in a batch solution a great number of observations is used, what means to deal with a great number of degrees of freedom. For this reason the formal errors and therewith the error ellipses will be small.

When applying the indirect method the number of degrees of freedom only depends on the number of coordinate triplets, which contribute to determine the station velocity. Thus in relation to the direct method the number of degrees of freedom will be smaller and therefore one obtains greater error ellipses. This "scaling effect" occurs in all plots.

The reference system for the velocities is the european plate with Wettzell fixed to NNR-NUVEL-1a motion. With that Ny Ålesund moves to west, but the great error ellipse points at a great scattering of the vector. For this reason the great error ellipse is a hint for a small number of observations or vice versa more observations have to be done in order to confirm this motion.

**Onsala** shows a clear motion to west with respect to Wettzell, too. Again to recognize the "scaling effect" of the error ellipse.

The results of **Effelsberg** contradict, in particular the vector of *Nothnagel & Haas* and the one of *Lanotte*. The comparison provides this statement and the error ellipse explains this phenomenon, because the size of the error ellipse directs attention to a non-significant motion. Thus the different solutions show arbitrary velocities.

The italian stations **Medicina** and **Matera** both show a clear and agreeing motion to east. **Noto** in South-Italy moves in northern direction, but it is not clear.

The last station in the network to be considered is **Madrid (DSS65)**. Remembering that the solution of *Titov* is preliminary, then a nearly zero velocity remains.

With regard to the height evolution of the stations the behaviour is similar to the horizontal motion and therewith the interpretations are similar. **Ny Ålesund** and **Onsala** both show an uplift, whereat the motion of Ny Ålesund is not significant due to the great error ellipse. As the horizontal motion the results of the height evolution of **Effelsberg** are inconsistent, i.e. there is no real vertical motion. **Medicina** shows a clear sinking motion. **Matera** and **Noto** do not really move in vertical direction due to great error ellipses. **Madrid** shows a clear uplift, which is in accordance with the lifting rate Antonius Rius presented at the last meeting in Oslo and which is about  $2mm$  per year.

### 3 Final remarks

First of all it turned out, that a comparison is useful, because only by a comparison the results and statements become more certain, and only a comparison reveals contradictions, which then are an occasion for a detailed investigation. With regard to the results it is right to say, that at the present level of accuracy there is a general agreement.

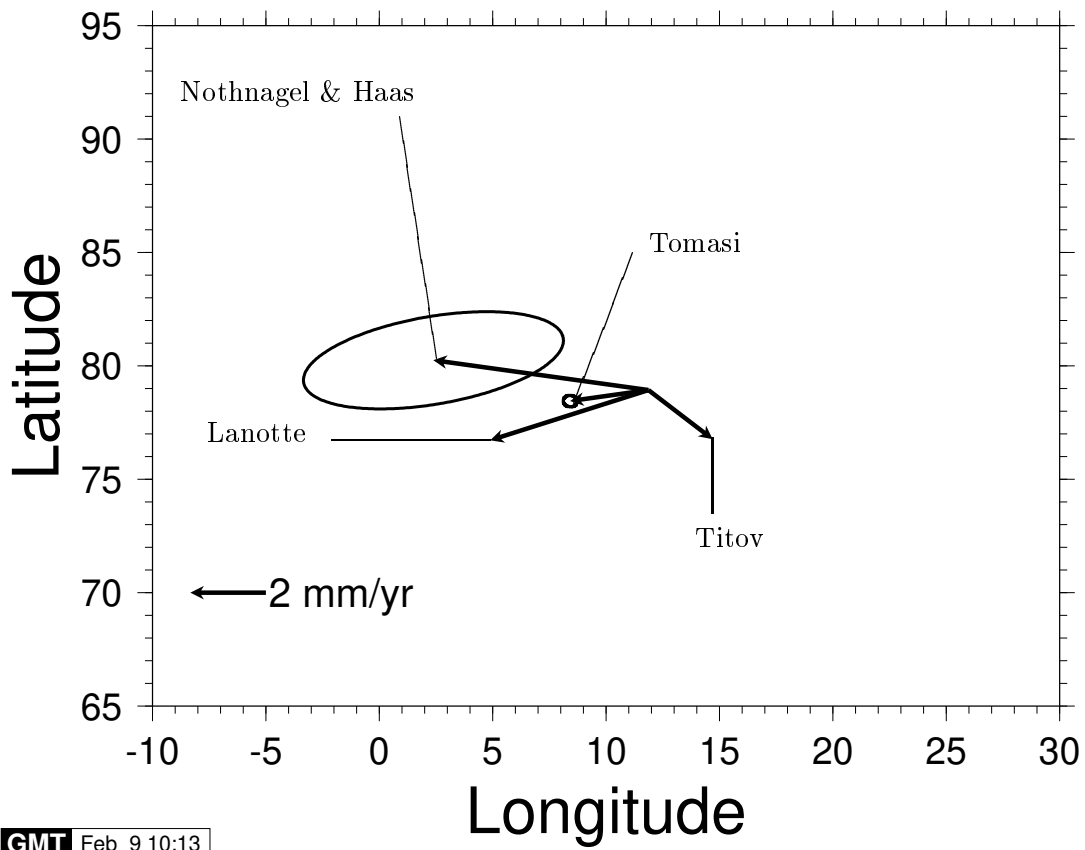
### 4 Acknowledgements

Thanks to *Rüdiger Haas*, *Roberto Lanotte*, *Axel Nothnagel*, *Oleg Titov* and *Paolo Tomasi* for submitting the solutions and thanks for a good cooperation.

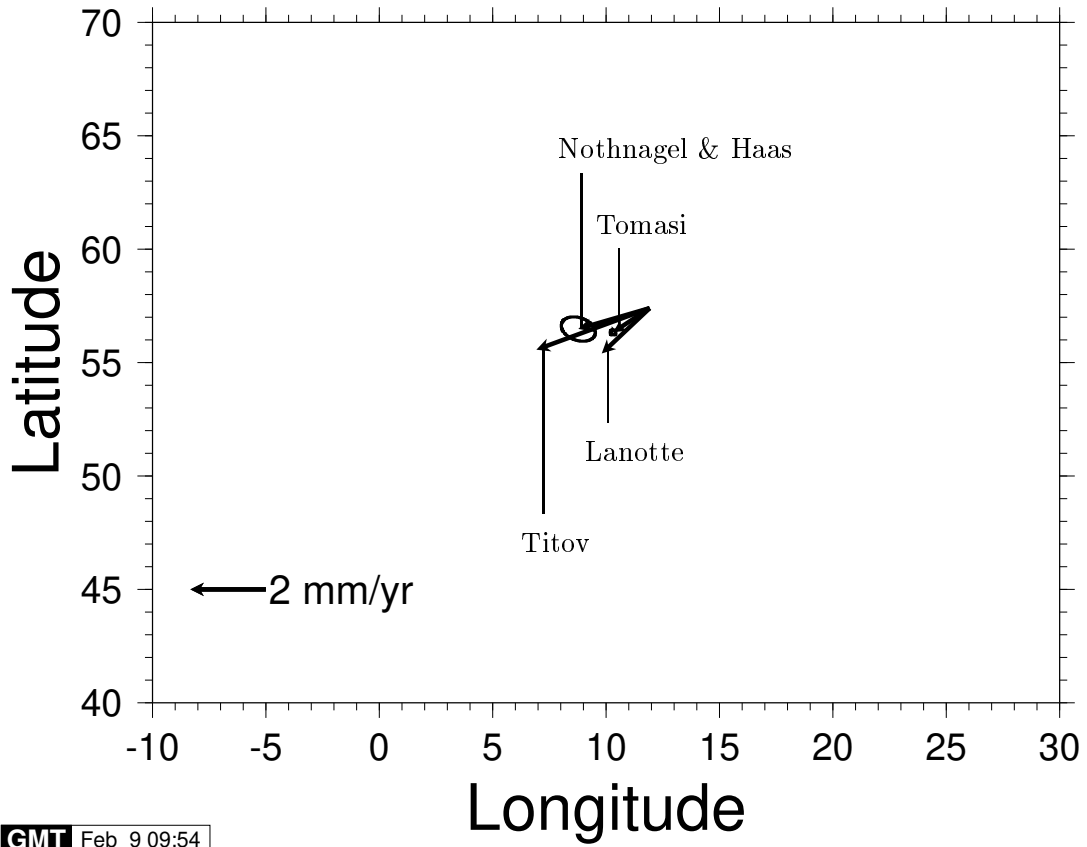
### 5 Plots

The following pages show the velocity plots for all mentioned stations.

# Velocity for NY ÅLESUND

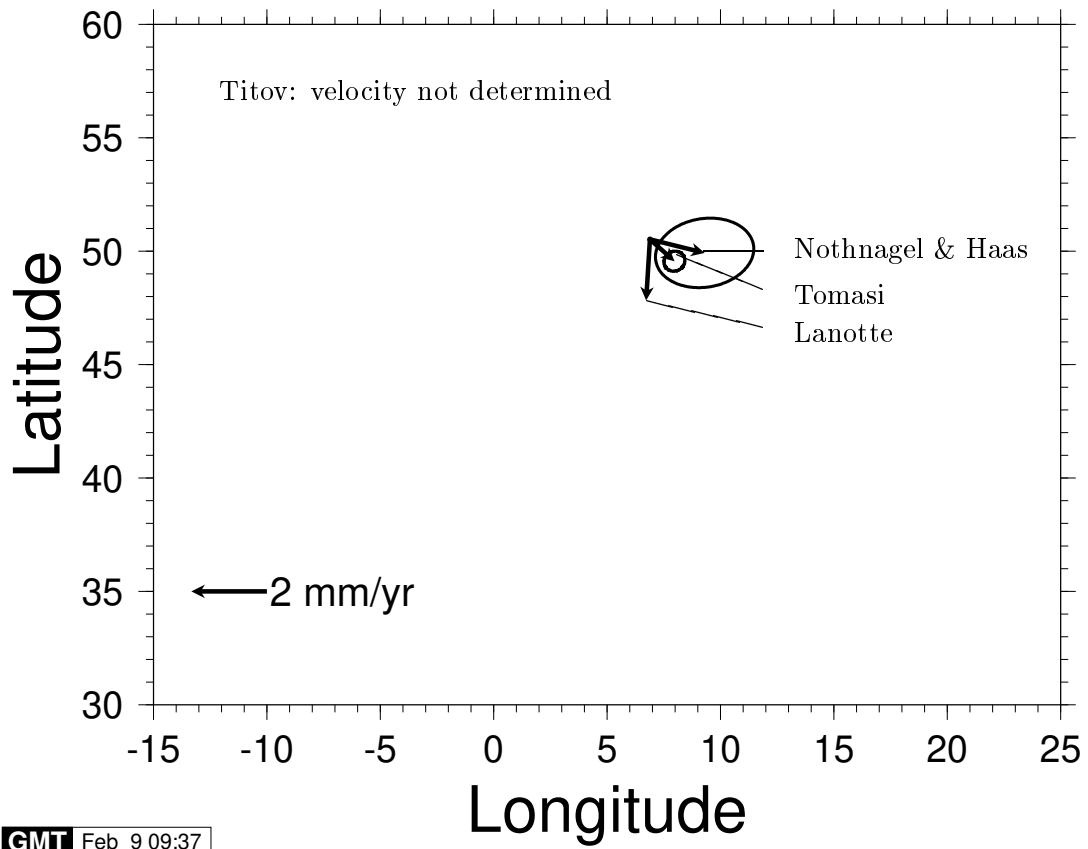


# Velocity for ONSALA



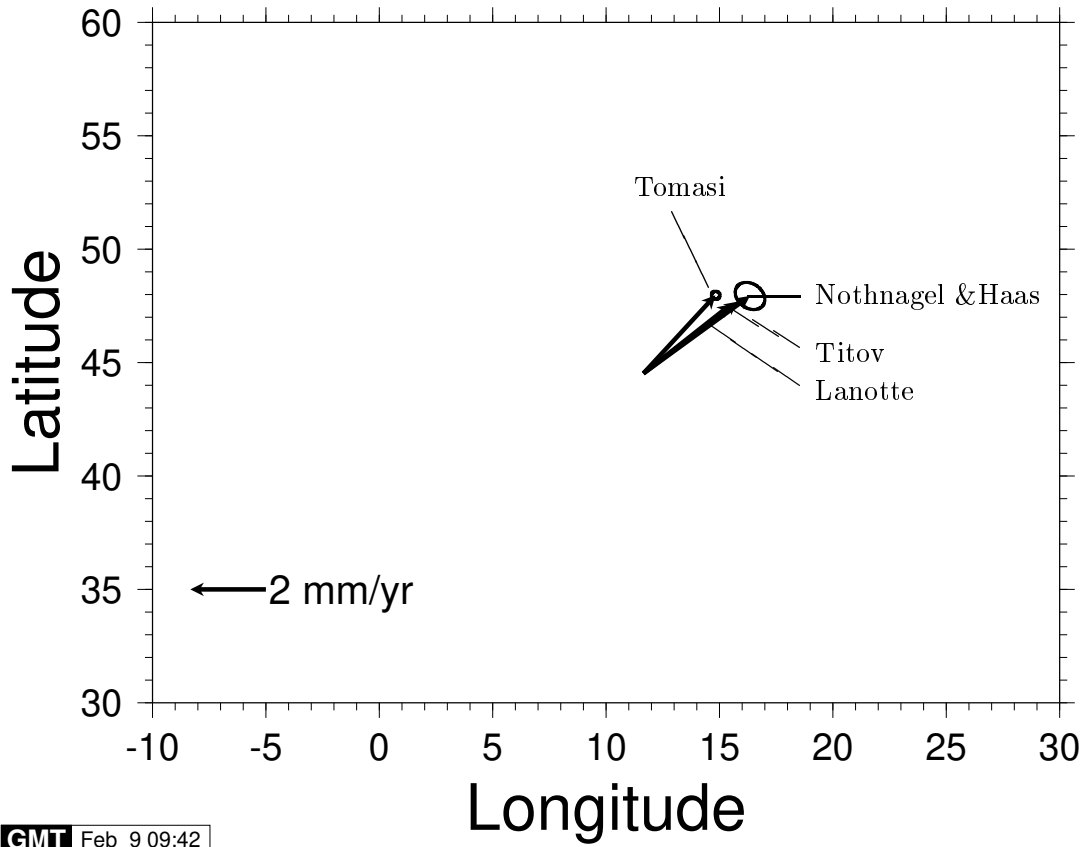
GMT Feb 9 09:54

# Velocity for EFFELSBURG

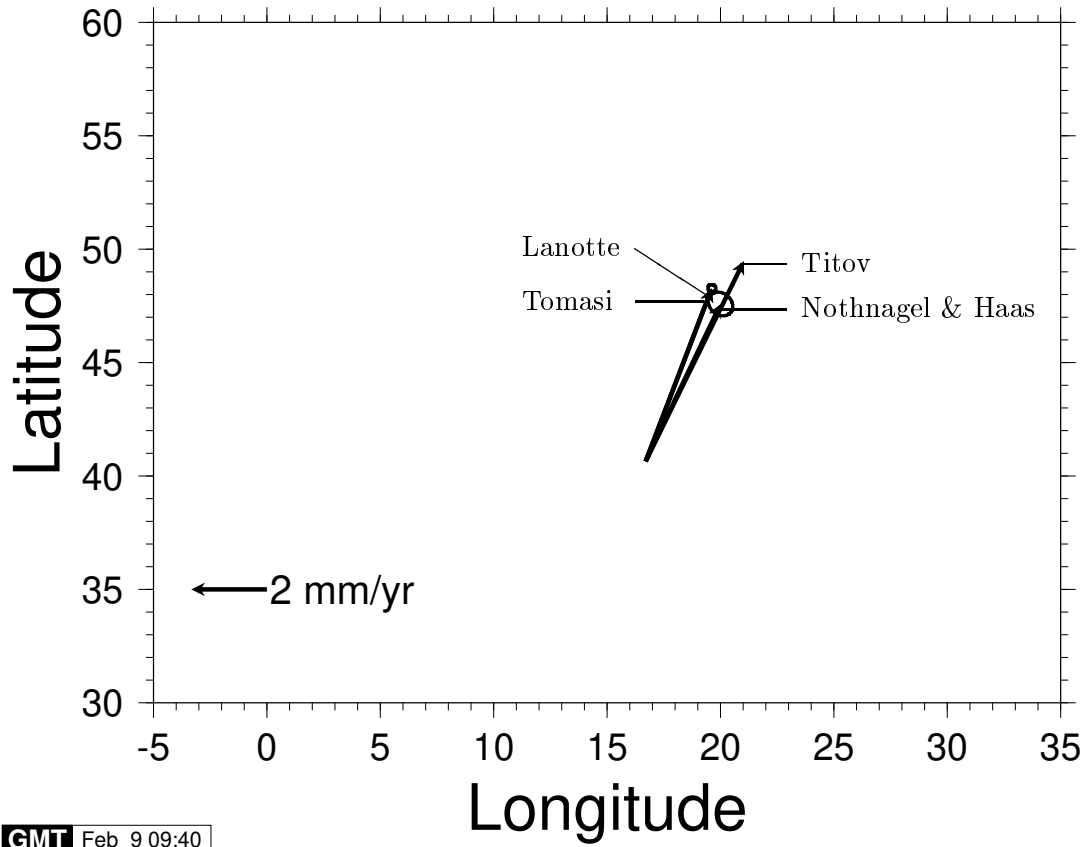


GMT Feb 9 09:37

# Velocity for MEDICINA

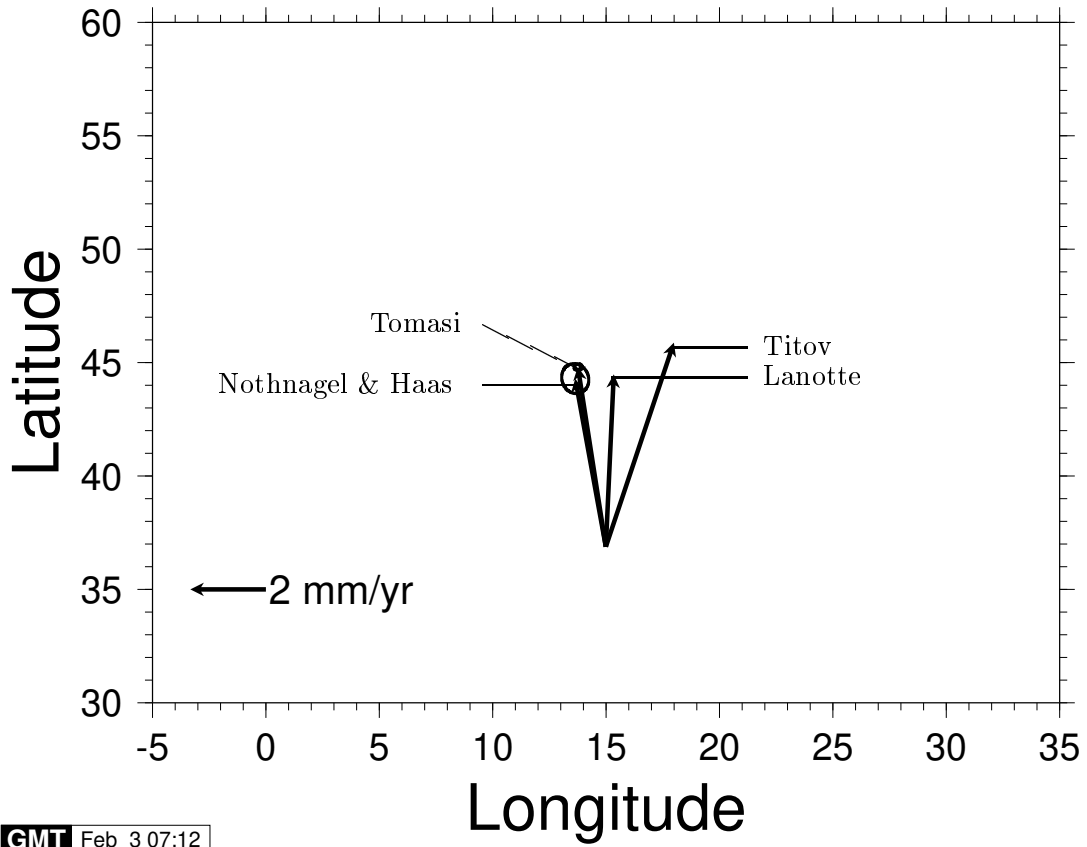


# Velocity for MATERA

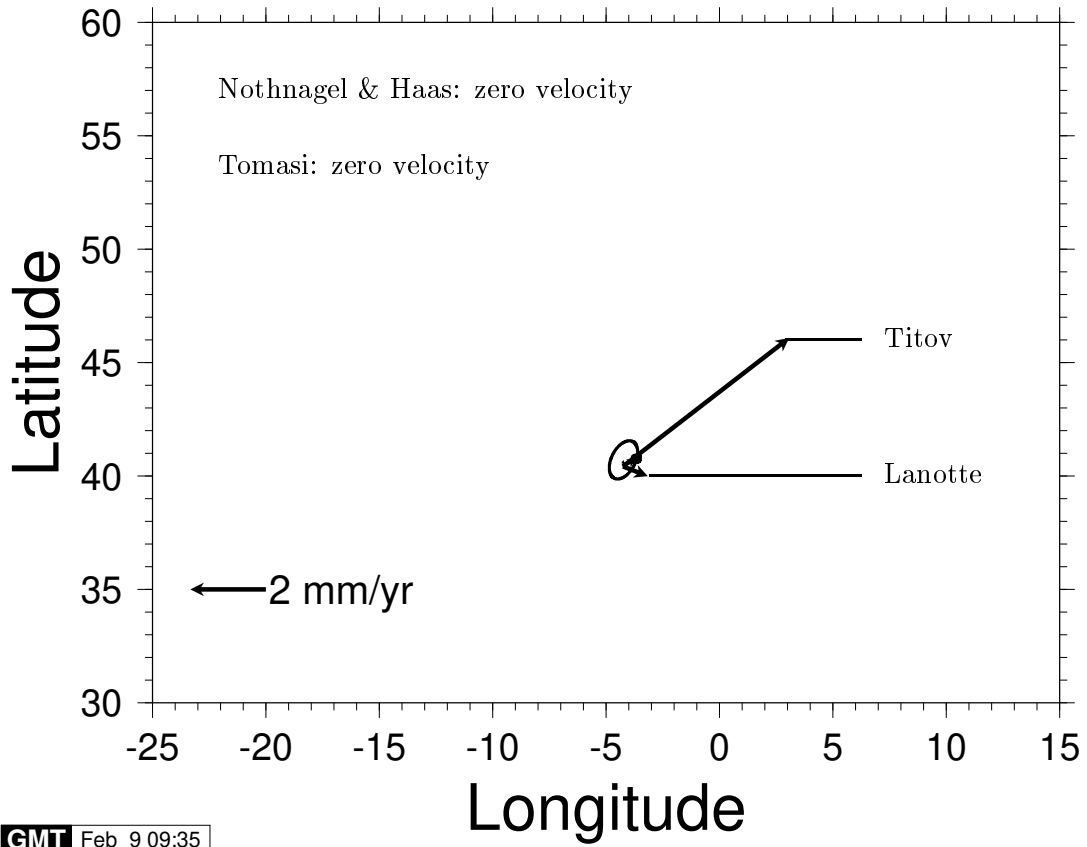


GMT Feb 9 09:40

# Velocity for NOTO

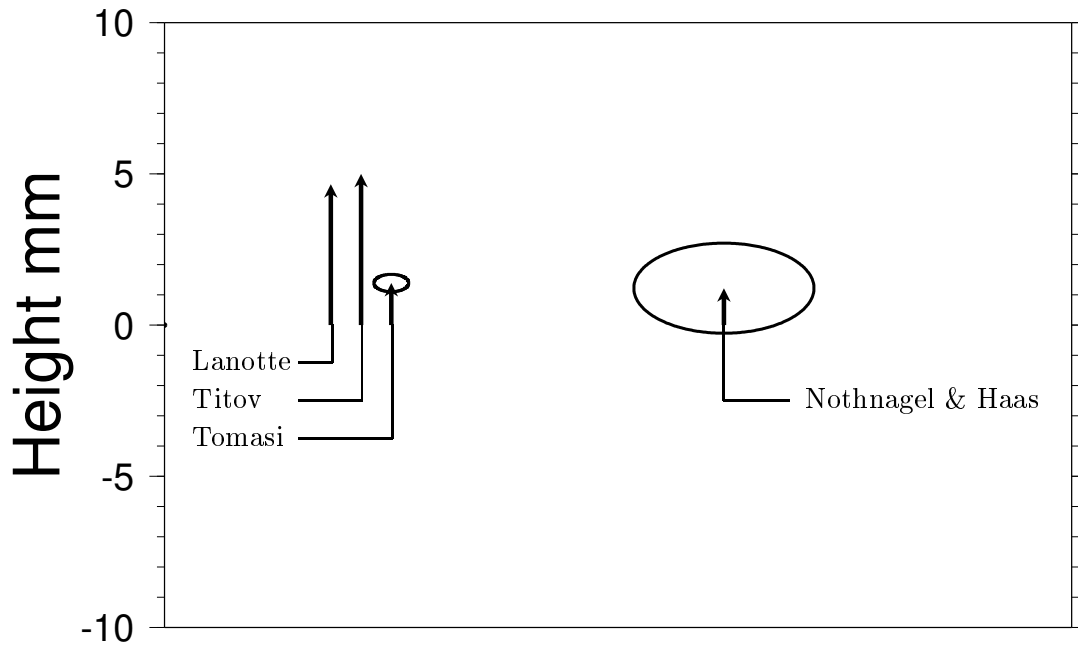


# Velocity for DSS65



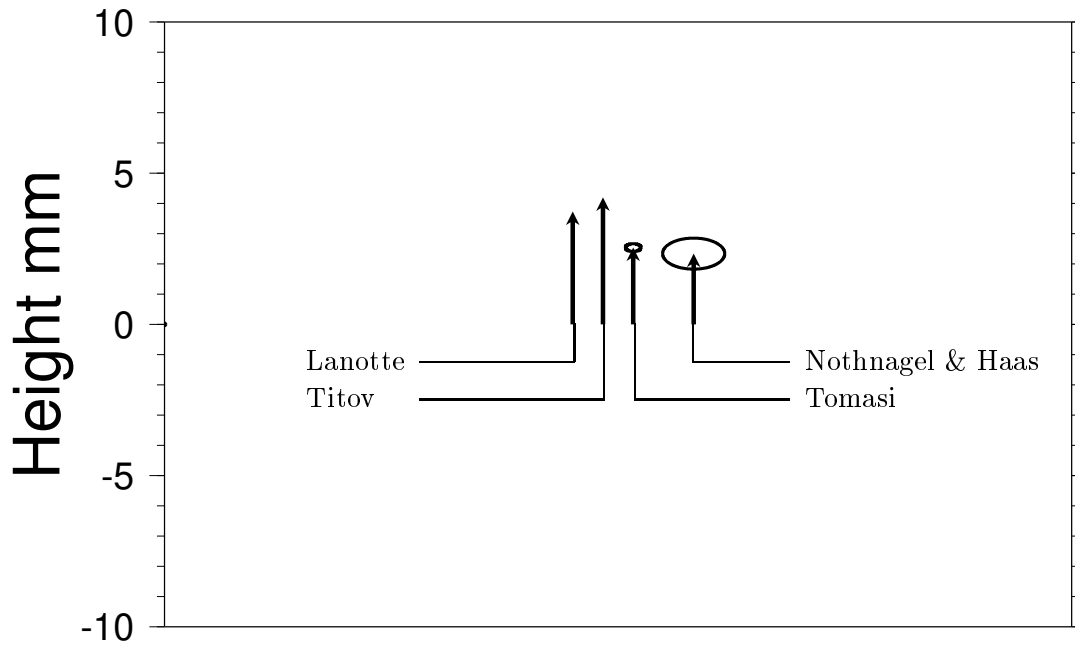
GMT Feb 9 09:35

# Height evolution for Ny ÅLESUND:



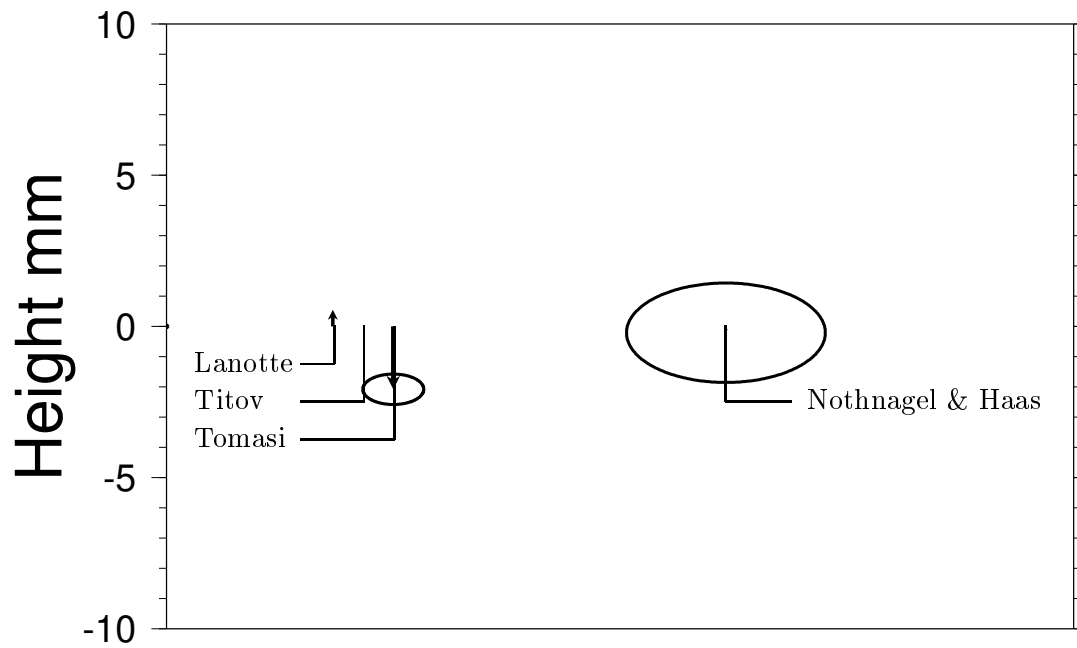
GMT Feb 9 10:43

# Height evolution for ONSALA:



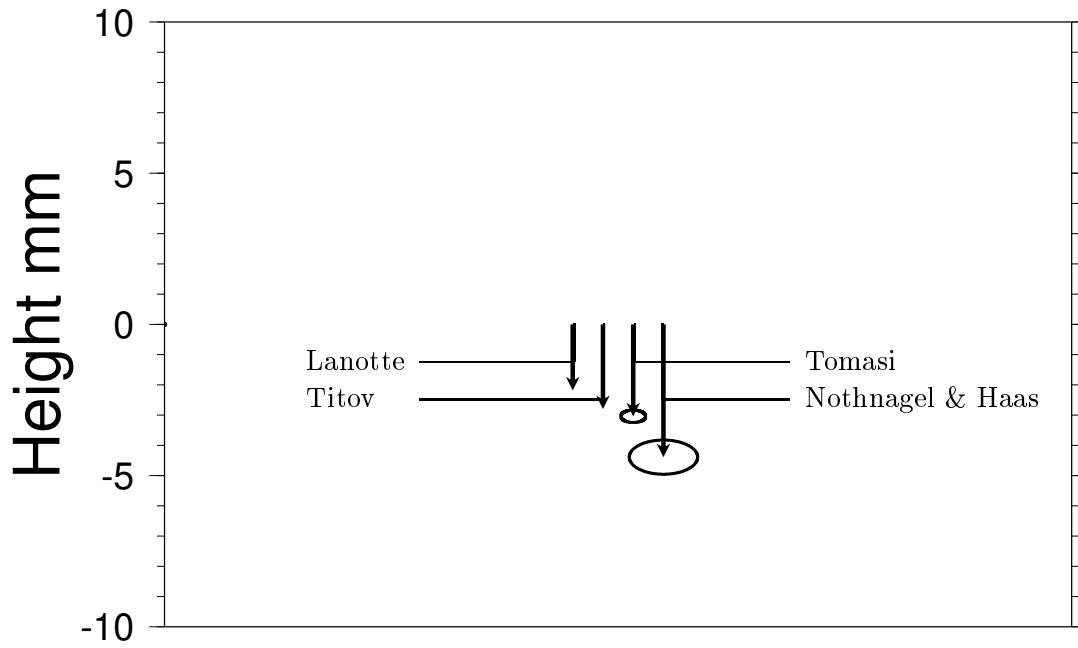
GMT Feb 9 10:44

# Height evolution for EFFELSBURG:



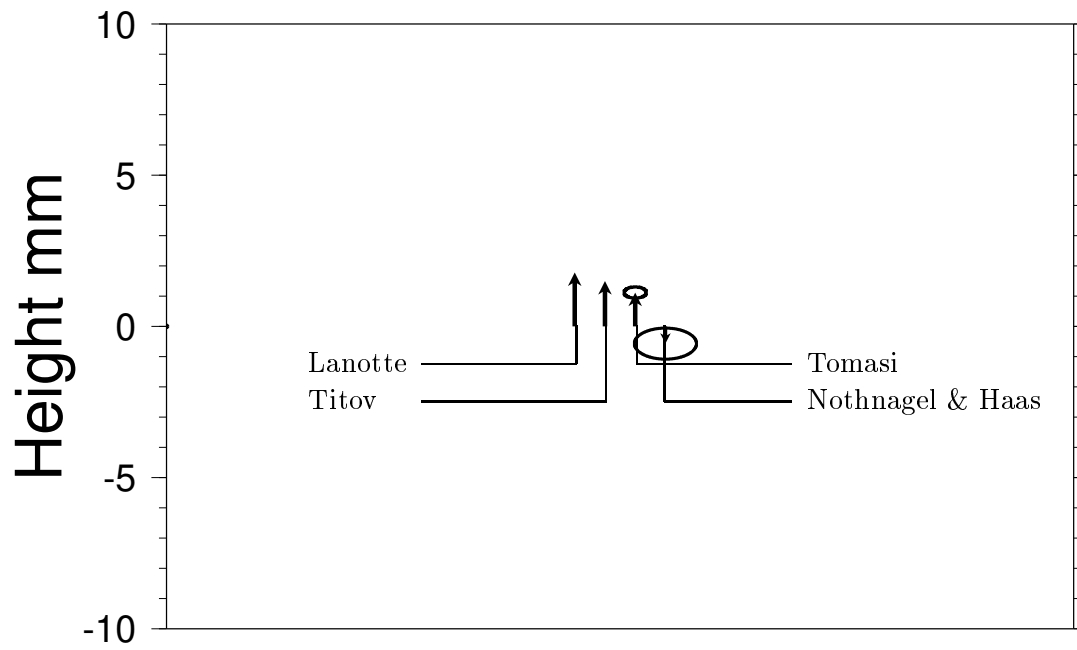
GMT Feb 9 10:39

# Height evolution for MEDICINA:



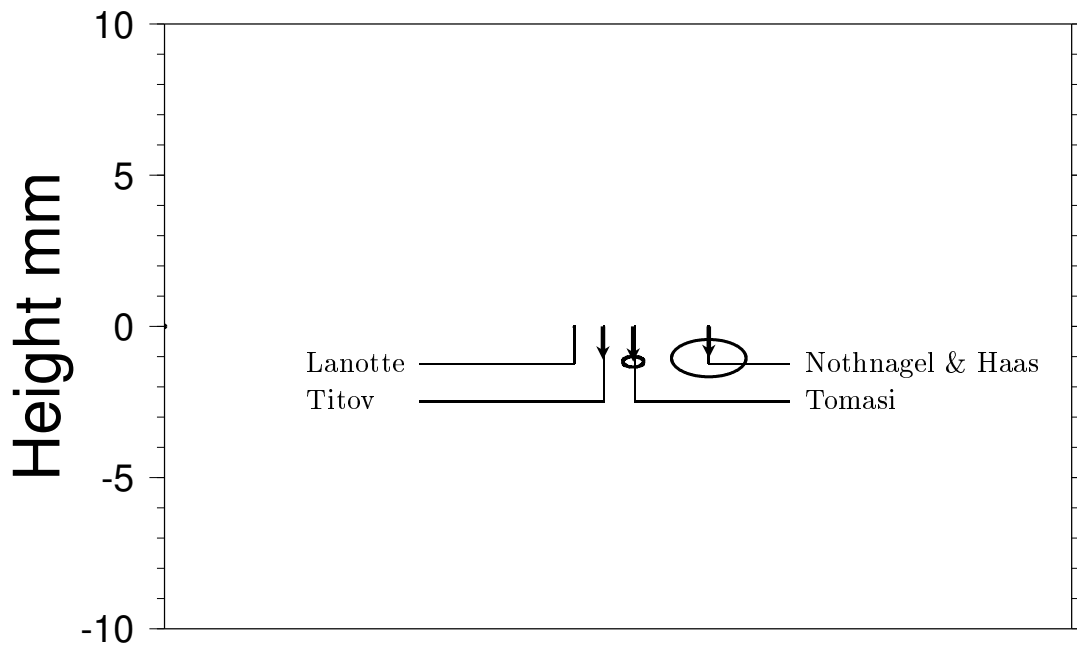
GMT Feb 9 10:41

# Height evolution for MATERA:



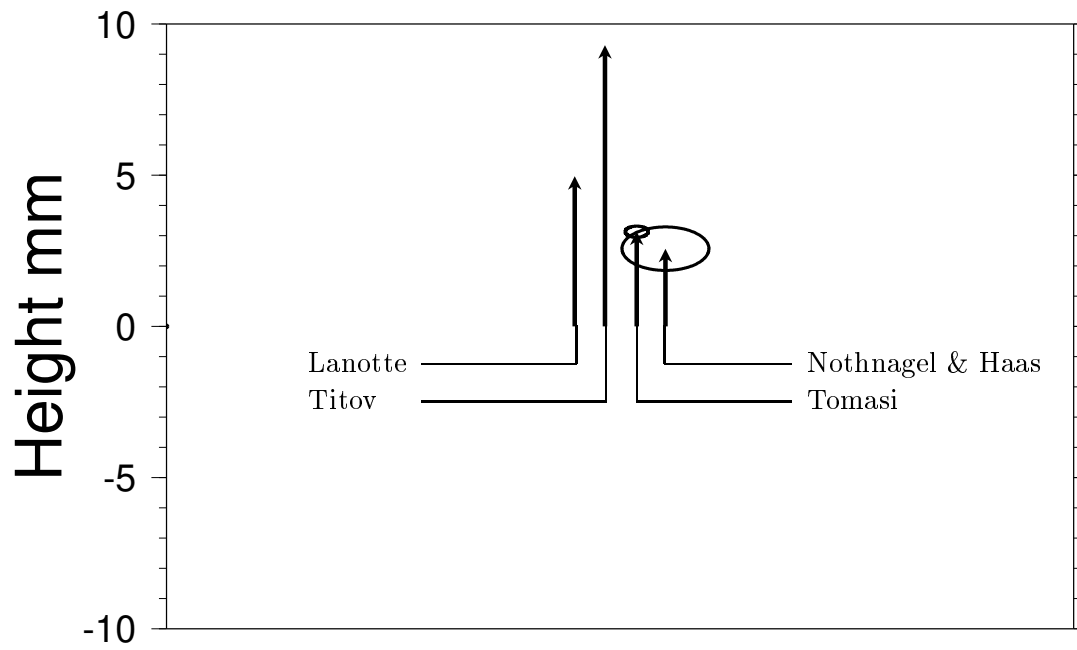
GMT Feb 9 10:40

# Height evolution for NOTO:



GMT Feb 9 10:42

# Height evolution for DSS65:



GMT Feb 9 10:36

# Absolute methods for determination of reference system from VLBI observations.

L. PETROV

*Geodetic Institute of the University of Bonn\**

petrov@kuestner.geod.uni-bonn.de

## Abstract:

*There are two principal approaches to derivation of a reference system from various types of observations. Positions of stations and sources can be determined with respect to the reference frame taken as a fiducial one in differential approaches. Positions of a subset of some fiducial stations/sources which “hold” the system are fixed and are not estimated in the framework of this approach. The catalogues built by this way depend on the values of a priori positions of fiducial objects and therefore we call them “differential catalogues”. However method of VLBI allows us to derive positions of all stations/sources from the observations up to a set of arbitrary constants. Since the reference system obtained by this way does not depend on the a priori catalogues it is called “absolute” reference system. Approaches for the development of such absolute catalogues of stations/sources using VLBI observations are discussed. Consequences on separation vertical component of station velocities from horizontal components are emphasized.*

## 1 Introduction

The method of VLBI is purely geometric. Equation for an observed time delay may be written in the first approximation as

$$\tau = \frac{1}{c} \hat{\mathcal{E}} (\vec{r}_1 - \vec{r}_2) \cdot \hat{\mathcal{H}} \vec{s} \quad (1)$$

where  $\hat{\mathcal{E}}$  — a rotation matrix which takes into account diurnal Earth rotation and pole motion,  $\vec{r}$  — a station position vector in geocentric coordinate system,  $\hat{\mathcal{H}}$  — a rotation matrix which takes into account precession and nutation and  $\vec{s}$  — a unit vector of source position in barycentric reference system. Time delay is proportional to a projection of the baseline vector on the source vector. Having observed different sources at different baselines we are in principle able to get adjustments to the station positions, source coordinates and parameters of the matrices  $\mathcal{E}$  and  $\mathcal{H}$  using estimation technique like LSQ [1].

Two estimation strategies are possible. We can determine positions of some subset of stations and sources while leaving positions of other stations and sources fixed. This approach is called “differential”. Estimates of positions of the targeted objects depend on the values of positions of the fixed objects. Errors in a priori values of positions of fixed objects as well as the errors in the Earth orientation parameters (EOP) if they are not estimated propagate to the estimates of positions of the targeted objects. We can use differential approach when the expected precision in determination of positions of targeted objects is less than the precision of positions of the fixed objects. In this case an additional error due to the uncertainty in positions of fixed objects does not bring substantial contribution to the general error budget. It is plausible to apply the differential method in estimation of positions of mobile VLBI stations.

---

\*On leave from Pulkovo observatory.

However using the differential approach we have to get a good input catalogue of positions of the objects which are to be used as fixed. VLBI nowadays is the most precise technique and we are unable to get EOP, station and source positions determined by other techniques without substantial degradation of precision. Thus, we have to have tools for estimation of positions and velocities of all stations, coordinates of all sources as well as EOP series from a single global solution. This approach we call “absolute”.

## 2 Discussion

We encounter a specific difficulty in making a global solution. The design matrix of this problem turns out to be a matrix of incomplete rank and the normal matrix which corresponds to it be singular. The reason of it stems from the fact that the equation (1) is invariant with respect to a group of linear transformations and therefore the columns of the design matrix are linearly dependent.

- Time delay is invariant with respect to a translation of terrestrial reference system. If we add an arbitrary vector to all vectors of station positions, the time delay remains the same.
- Time delay is invariant with respect to a turn of terrestrial reference system. If we multiply all vectors of station positions by an arbitrary rotation matrix and multiply matrix  $\hat{\mathcal{E}}$  by the matrix to be reciprocal to this matrix, the time delay remain the same.
- Time delay is invariant with respect to a translation of terrestrial velocities field. If we add an arbitrary vector to all vectors of station velocities, the time delay remains the same.
- Time delay is invariant with respect to a rotation of terrestrial reference system. If we multiply all vectors of station velocities by an arbitrary rotation matrix and multiply matrix  $\hat{\mathcal{E}}$  by the matrix to be reciprocal to this arbitrary matrix, the time delay remains the same.
- Time delay is invariant with respect to a turn of celestial reference system. If we multiply all vectors of source positions by an arbitrary rotation matrix and multiply matrix  $\hat{\mathcal{H}}$  by the matrix to be reciprocal to this matrix, the time delay remain the same.

We have 5 vector invariance conditions, each of them depends on 3 parameters. Thus, the equation (1) is invariant with respect to a 15-parameters linear transformation when we determine positions and velocities of all stations, EOP series and positions of all sources.

Invariance conditions can be written as

$$\left\{ \begin{array}{l} \sum_i^m \Delta \vec{r}_i = \text{const} \\ \sum_i^m \frac{\vec{r}_i \times \Delta \vec{r}_i}{r_i^2} = \text{const} \\ \sum_i^m \Delta \vec{v}_i = \text{const} \\ \sum_i^m \frac{\vec{r}_i \times \Delta \vec{v}_i}{r_i^2} = \text{const} \\ \sum_j^n \sin \alpha_j \cdot \Delta \delta_j - \cos \delta_j \cos \alpha_j \sin \delta_j \cdot \Delta \alpha_j = \text{const} \\ \sum_j^n -\cos \alpha_j \cdot \Delta \delta_j - \cos \delta_j \sin \alpha_j \sin \delta_j \cdot \Delta \alpha_j = \text{const} \\ \sum_j^n \cos^2 \delta_j \Delta \alpha_j = \text{const} \end{array} \right. \quad (2)$$

where  $m$  is the number of stations and  $n$  is the number of sources.

To solve equations of conditions of incomplete rank we can either use equations (2) as equations of constraints or to use conditional LSQ (i.e to find estimates of the parameters which provides minimum to a weighted sum of residuals under condition that equations (2) are exactly fulfilled, refer [2] for details). Adjustments depend on the choice of constants in (2) and implicitly depend on the values of a priori positions of stations and sources and EOP series. We can compute values of these constants by the manner which provide getting adjustments which would satisfy to explicitly specified boundary conditions. Another way is to get a solution using arbitrary values of these constants and then fulfill transformation of preliminary output catalogues and EOP series. The meaning of the solution with constants equal to zero (“zero solution”) is that the output catalogues of station positions, station velocities, source positions don’t have net translation net turn and net rotation.

It is worth noting that equations (2) may be written in alternative forms. In general, the matrix of the equations (2) can be multiplied by an arbitrary non-singular matrix. Implicit form of imposing some invariance conditions may be also used: for example, not estimation of some parameters.

The transformation of terrestrial and celestial reference systems, EOP series which conserves time delay (1) may be written in the form:

$$\begin{aligned}\vec{r}_n &= \vec{r}_o + \Delta\vec{r}_e + \vec{T} + \vec{\Phi} \times \vec{r}_o \\ \vec{v}_n &= \vec{v}_o + \Delta\vec{v}_e + \vec{V} + \vec{\Omega} \times \vec{r}_o \\ \vec{s}_n &= \vec{s}_o + \Delta\vec{s}_e + \vec{\Psi} \times \vec{s}_o\end{aligned}\quad (3)$$

where  $\vec{r}_n$  — a vector of station position in a new reference system,  $\vec{r}_o$  — a vector of station position in an old reference system,  $\Delta\vec{r}_e$  — a vector of adjustments to the station position obtained from the solution,  $\vec{T}$  — a translation vector of terrestrial reference system,  $\vec{\Phi}$  — a small turn vector of terrestrial reference system. Analogously,  $\vec{V}$  and  $\vec{\Omega}$  are a translation and a small turn vectors of station velocities field and  $\vec{\Psi}$  is a small turn vector of celestial reference system.

EOP series are transformed by the following way:

$$\begin{aligned}Yp_n &= Yp_o + \Delta Yp_e + \vec{\Phi}_1 + \vec{\Omega}_1 \cdot (t - t_o) \\ Xp_n &= Xp_o + \Delta Xp_e + \vec{\Phi}_2 + \vec{\Omega}_2 \cdot (t - t_o) \\ UT1_n &= UT1_o + \Delta UT1_e - k(\vec{\Phi}_3 - \vec{\Psi}_3) - k\vec{\Omega}_3 \cdot (t - t_o) \\ \frac{\partial}{\partial t}UT1_n &= \frac{\partial}{\partial t}UT1_o + \Delta \frac{\partial}{\partial t}UT1_e - k\vec{\Omega}_3 \\ \varepsilon_n &= \varepsilon_o + \Delta\varepsilon_e - \vec{\Psi}_1 \\ \psi_n &= \psi_o + \Delta\psi_e + \frac{1}{\sin\varepsilon_0}\vec{\Psi}_2\end{aligned}\quad (4)$$

where  $t_o$  is the epoch of station coordinates,  $k = 1.002\,737\,909$  and  $\varepsilon_0$  is a mean obliquity of ecliptic to equator.

As it was previously mentioned equation (1) is an approximation. Time delay is computed with a relative precision  $10^{-11}$  on the basis of a refined model [3]. The two major omitted terms are

$$\frac{1}{c^2} \left( \hat{\mathcal{E}}(\vec{r}_1 - \vec{r}_2) \cdot \vec{V}_\oplus \right) - \frac{1}{c^2} \left( \hat{\mathcal{E}}(\vec{r}_1 - \vec{r}_2) \cdot \hat{\mathcal{H}}\vec{s} \right) \left( \vec{V}_\oplus \cdot \vec{s} \right)\quad (5)$$

where  $\vec{V}_\oplus$  is barycentric Earth velocity.

The vector of barycentric Earth velocity usually is not an estimated parameter and therefore these terms are not invariant with respect to a turn of celestial reference frame. Barycentric Earth velocity is taken from ephemerides which provide it with a precision rather better than it can be determined from VLBI observations. Ephemerides keep the orientation of the dynamic reference frame in which they are defined and are not undergone transformation. Therefore, applying transformation (3) and (4) may cause an error. We can neglect this error provided the vector  $\vec{\Psi}$  is small enough:

$$\frac{\|\sigma(\vec{s})\|}{\|\vec{\Psi}\|} \ll \frac{\|\vec{V}_\oplus\|}{c}\quad (6)$$

where  $c$  is light velocity,  $\sigma(\vec{s})$  — an uncertainty of source vector adjustments. Since  $\frac{\|\vec{V}_{\oplus}\|}{c} \approx 10^{-4}$  this condition is usually fulfilled. Influence of other omitted terms is less and can be wholly ignored.

We have a freedom of choice of  $\vec{T}$ ,  $\vec{V}$ ,  $\vec{\Phi}$ ,  $\vec{\Omega}$ ,  $\vec{\Psi}$ . Freedom in choice of translation vector  $\vec{T}$  leads to the fact that separation vertical and horizontal components in vectors of station positions is up to some degree arbitrary. Let we have 6 stations as it seen in fig. 1. Having added a translation vector  $\vec{T}$  we change positions of stations so that the stations  $a$  and  $b$  are uplifting, the stations  $e$  and  $d$  are sinking and no additional vertical motion is added to the stations  $c$  and  $d$ . If we change direction of the vector  $\vec{T}$  at  $90^\circ$  as it shown in fig. 2 then the station  $c$  will be uplifting,  $d$  sinking and vertical positions of the stations  $a$ ,  $b$ ,  $d$  and  $e$  remain the same. Applying a turn of the reference system makes the whole picture more complicated due to an additional horizontal displacement caused by the turn of reference system which depends on the relative positions of the station coordinates vectors and the vector  $\vec{\Phi}$  (fig 3). Applying different vectors  $\vec{T}$  and  $\vec{\Phi}$  we get different vertical positions of the stations. Analogously, applying different vectors  $\vec{V}$  and  $\vec{\Omega}$  we get different values of vertical and horizontal velocities of the stations. One choice  $\vec{V}$  and  $\vec{\Omega}$  may reveal an uplift of the targeted station while another choice of  $\vec{V}$  and  $\vec{\Omega}$  may reveal sinking the same station. And both solutions satisfy observations!

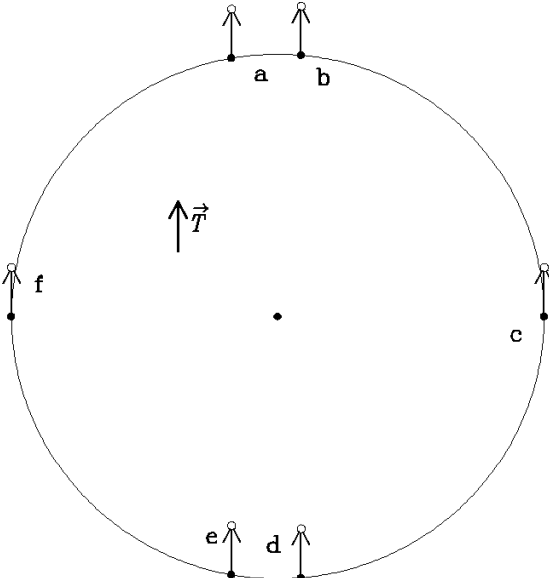


fig. 1

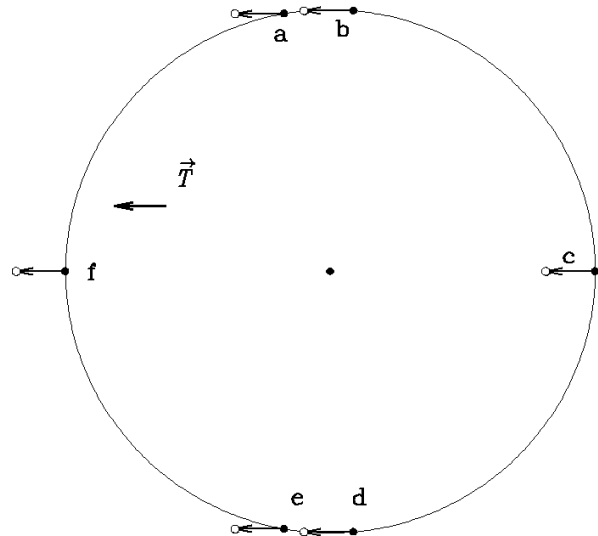


fig. 2

I would like to emphasize that we are in principle unable to determine parameters of this transformation from VLBI observations. Therefore one possible way is not to worry about some arbitrariness of the output solutions. However a raw solution *implicitly* depends on used equations of invariance conditions and a priori catalogues. Changes in a priori catalogues, changes in equations of invariance conditions, addition or removal some observations from analysis may lead to considerable changes in values of the output coordinates and EOP series what may cause an illusion of “instability” of solution. In order to avoid these problems we can transform our raw solution on the basis of *explicitly* specified boundary conditions using external information.

Several strategies for obtaining parameters of the transformation can be used.

- Vectors of the transformation can be usually chosen to make a new solution compliant with catalogues of stations and sources and EOP series determined by other techniques. We explicitly formulate boundary conditions of compliance. These conditions set equality of some coordinates of stations, sources and/or EOP series to the values from the external catalogues. As an example

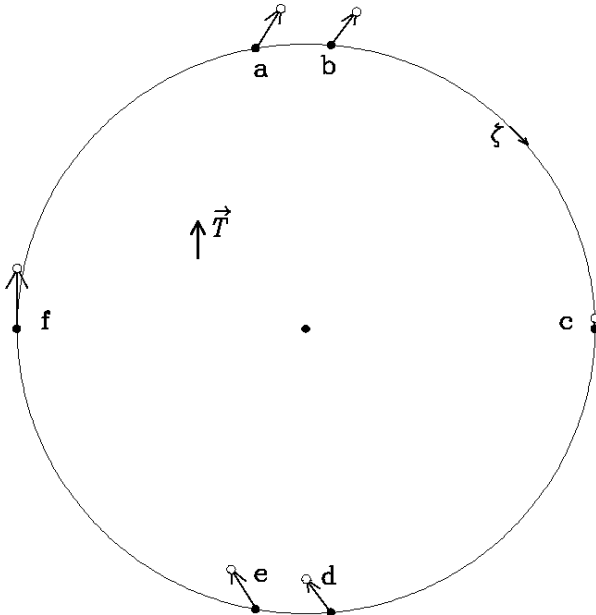


fig. 3

we can demand equality of final EOP to the values from USNO concrete EOP series on the specific date.

- We can modify boundary condition and to require not rigorous equality of the values but minimization of a norm of differences of the new catalogues and the old external catalogues. For example, we can demand that a sum of squares of differences between the new sources catalogue and the IERS sources catalogue would be minimal.
- Boundary conditions can be set for compliance with some physical considerations. For example, we can require that our new field of velocities would not have rotation with respect to some model of plate tectonic or we can require that some subset of stations has minimal deviation from the model of post-glacial rebound or we can require that the pole coordinates don't have secular trend.

Boundary conditions set a system of linear equations which ties parameters of the transformation (3), (4), external catalogues or model with zero solution. Having solved these equations we find parameters of the transformation. After applying this transformation we get the final catalogues and EOP series.

### 3 Conclusion

The VLBI output catalogues and EOP series contains both information which is *derived from the measurements* and external information which is *imposed*. The fact that terrestrial reference frame and velocities field can be determined only up to transformation (3), (4) puts some restrictions on interpretation of the results obtained from VLBI.

- Earth Orientation parameters and positions of all stations cannot be unambiguously determined from a single 24 hours VLBI experiment. However baseline lengths are invariant with respect to translation and rotation and can be determined without applying external conditions.
- Secular trend in Earth orientation parameters series cannot be in principle measured by VLBI.

- If we analyze VLBI data only from the region small with respect to the Earth radius we can determine vertical and horizontal component of station positions and station velocities only up to a common arbitrary vector. But we still can determine relative vertical and horizontal position and velocities.
- If we compare two different VLBI solutions they should be first undergone a transformation: rotation and translation to fit the same boundary conditions.

## References

- [1] L. Petrov, The methods of determination of geodynamical parameters using VLBI. Ph.D. thesis, Saint-Petersburg, 1995 (*in Russian*)
- [2] G. Scheffe, Dispersion analysis, N.Y., p. 512, 1977
- [3] O. Sovers, Fanselow, J., and Jacobs, C. , Astronomy and geodesy with radio interferometry: experiments, models, results. Reviews of Modern Physics, Vol. 70, N4, p. 1393–1454, 1998

# Steps towards phase delay VLBI

L. PETROV

*Geodetic Institute of the University of Bonn\**

petrov@kuestner.geod.uni-bonn.de

## Abstract:

*One of the promising ways for improving precision of estimation of the targeted parameters of geodetic VLBI is to use phase delay measurements which are roughly 40-fold more precise than group delay observables. However phase delay ambiguities should be resolved before using these observables in LSQ adjustments. This problem is solved almost always for the case of relatively short baselines (1–10 km) where we are able to ignore an atmosphere contribution to time delay, but it is still a challenge for the case of longer baselines.*

*A procedure for resolving phase delay ambiguity is presented. It exploits the fact that phase misclosures are usually a small fraction of phase ambiguity spacings. Phase delay measurements made in the network consisting of three or more stations provide some redundancy.*

*It is shown that the proposed approach allows to resolve phase delay ambiguities for a subset of observations. Some results of phase delay solutions of EUROPE, IRIS-S and VLBA networks are presented. It was found that the success rate of phase delay ambiguity resolution for intercontinental baselines depends on the system sensitivity, the level of instrumental noise and the number of observations. Phase delay ambiguities can be resolved for up to 90% observations for the best, state-of-art VLBI experiments, although a success rate 40-70% is more typical.*

## 1 Introduction

Phase spectrum of cross-correlation function within a band of registration is produced by a correlator in processing very long baseline interferometry measurements [1]. The correlator output is used for

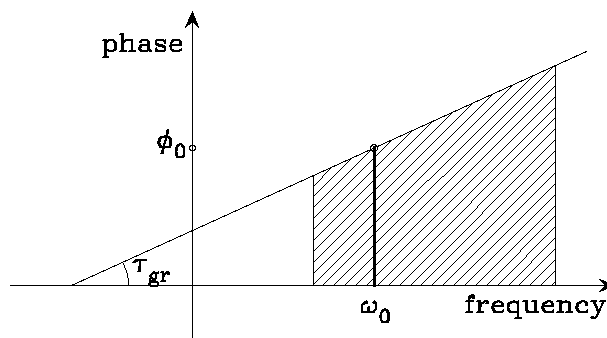


fig. 1

obtaining two basic quantities: group delay and phase delay:

$$\tau_{group} = \frac{\partial \varphi}{\partial \omega} \quad \tau_{phase} = \frac{\varphi}{\omega_o} + \frac{2\pi}{\omega_o} N \quad (1)$$

where  $\varphi$  is a phase of cross-spectrum,  $\omega_o$  is a circular reference frequency and  $N$  — an integer number of ambiguities. Precision of measurement of these quantities is:

$$\sigma(\tau_{group}) \sim \frac{1}{SNR \cdot \Delta\omega} \quad \sigma(\tau_{phase}) \sim \frac{1}{SNR \cdot \omega_o} \quad (2)$$

---

\*On leave from Pulkovo observatory.

where  $\text{SNR}$  is a signal to noise ratio of fringe detection,  $\Delta\omega$  — effective bandwidth. The bandwidth of registration is considerably less than the reference frequency and therefore the precision of measurement of phase delays is much higher than the precision of measurements of group delays. But there is a substantial obstacle before direct use of phase delay: it is measured only up to an unknown integer number of phase turns. We are able to use phase delays in a parameter adjustment process only after resolving phase delay ambiguities. Early experiments showed [2], [3] that the phase delays may be successfully used for analysis of observations made at very short baselines of 0.1–1.0 km where phase delay ambiguities are resolved rather easy. Now we try to resolve phase delay ambiguities for baselines of arbitrary length.

## 2 Phase delay observables

Group and phase delays at X ( $\sim 8.4\text{GHz}$ ) and S ( $\sim 2.3\text{GHz}$ ) bands are measured in geodetic VLBI observations. Properties of these observables are presented in table 1.

Tab. 1

	<b>Group delay</b>	<b>Phase delay</b>
Precision	X-band: 0.02–0.04 nsec S-band: 0.01–0.2 nsec	X-band: 0.0005–0.001 nsec S-band: 0.002–0.005 nsec
Ionosphere contribution	X-band: 0.2–2.0 nsec S-band: 2.5–30.0 nsec	X-band: 0.2–2.0 nsec S-band: 2.5–30.0 nsec
Ambiguity	X-band: 28–100 nsec S-band: 50–200 nsec	X-band: 0.12 nsec S-band: 0.45 nsec
postfit rms	0.02–0.03 nsec	0.005–0.010 nsec

We see that a scatter of post-fit residuals of group delays has a magnitude 2–5 times less than phase delay ambiguity spacings at X-band and 5–20 times less than ambiguity spacings at S-band. In principle, phase delay ambiguities can be resolved by using model values of phase delay derived from a group delay solution provided the following conditions are true:

- Theoretical model for group and phase delay differs by no more than 0.2–0.3 phase turns;
- Instrumental difference between group and phase delay does not exceed 0.2–0.3 phase turns;

However, both these conditions are usually not fulfilled. Three contributions to time delay are different for phase and group delays: feed horn rotation, source structure correction and ionosphere contribution. The first term can be precisely calculated. Difference in source structure correction is usually less than 0.1 phase turns. Unfortunately, ionosphere contribution is substantially different for group and for phase delay observables what puts serious problems before a phase delay ambiguity resolution.

Ionosphere contribution to time delay can be written in the form

$$\tau_{group}^{iono} = \frac{q}{f_g^2} \quad \tau_{phase}^{iono} = -\frac{q}{f_p^2} \quad (3)$$

where  $q$  is a quantity proportional to the difference of integral electron content over the ray paths from the source to the site 1 and the site 2,  $f_g$  and  $f_p$  — effective frequencies for group and phase delays which are within 3–5% from the reference frequency. Difference in the ionosphere contribution as it is seen in table 1 is about 3–15 phase turns and we unable to ignore this effect in a phase delay ambiguity resolution process.

To take into account the ionosphere contribution we use ionosphere free linear combinations of

observables. The most important combinations are:

$$\begin{aligned}
\tau_g^{if} &= \frac{f_{gx}^2}{f_{gx}^2 - f_{gs}^2} \tau_{gx} - \frac{f_{gs}^2}{f_{gx}^2 - f_{gs}^2} \tau_{gs} \\
\tau_p^{if} &= \frac{f_{px}^2}{f_{px}^2 - f_{ps}^2} \tau_{px} - \frac{f_{ps}^2}{f_{px}^2 - f_{ps}^2} \tau_{ps} \\
\tau_{p_x g_s}^{if} &= \frac{f_{px}^2}{f_{px}^2 + f_{gs}^2} \tau_{px} + \frac{f_{gs}^2}{f_{px}^2 + f_{gs}^2} \tau_{gs} \\
\tau_{p_s g_s}^{if} &= \frac{f_{ps}^2}{f_{ps}^2 + f_{gs}^2} \tau_{ps} + \frac{f_{gs}^2}{f_{ps}^2 + f_{gs}^2} \tau_{gs}
\end{aligned} \tag{4}$$

where  $f_{gx}$ ,  $f_{gs}$  are effective frequencies for group delay ionosphere contribution at the bands X and S and  $f_{px}$ ,  $f_{ps}$  are effective frequencies for phase ionosphere contribution. Having substituted typical values of the effective frequencies we can write (4) in this form:

$$\begin{aligned}
\tau_g^{if} &\approx 1.08 \tau_{gx} - 0.08 \tau_{gs} \\
\tau_p^{if} &\approx 1.08 \tau_{px} - 0.08 \tau_{ps} \\
\tau_{p_x g_s}^{if} &\approx 0.94 \tau_{px} + 0.06 \tau_{gs} \\
\tau_{p_s g_s}^{if} &\approx 0.51 \tau_{ps} + 0.49 \tau_{gs}
\end{aligned} \tag{5}$$

where index  $p$ , or  $g$  denotes phase or group delays,  $x$  and  $s$  denotes a band. The first ionosphere free linear combination is used in group delay solutions. The second combination is called pure phase delay ionosphere free linear combination and the latter two are called semi-phase delay ionosphere free linear combinations.

### 3 Phase delay ambiguity resolution

In general, the problem of phase delay resolution has more than one solution. To provide a unique solution we have to postulate some additional conditions. The following principles are formulated:

- *Group delay ionosphere free linear combinations and phase delay ionosphere free linear combinations don't have considerable differences.* In the absence of source structure contribution and instrumental errors these two quantities should coincide. Thus, this assumption is equivalent to the assumption that instrumental noise is small.
- *Misclosures in phase delays are considerably less than phase delay ambiguity spacings.* It was found that misclosures in phases are at the level of 0.05–0.15 phase turns for the sources to be observed under geodetic programs. It means that the instrumental noise is primarily station-dependent but not baseline-dependent.
- *There exist a smooth function of a difference between group delay ionosphere free linear combination and ionosphere free combination of phase delays.* We assume that a random component in differences is small. We have to somehow model this difference and the number of parameters of such a model should be small enough to secure uniqueness of the solution. We are unable to resolve correctly phase delay ambiguities if we allow considerable fluctuations of the differences. We cannot say beforehand whether this assumption is correct or not. When this condition is not valid then a phase delay ambiguity resolution process fails and we have to exclude such baselines from the list of baselines eligible for phase delay solutions.

Method of ambiguity resolution functions (ARF) is proposed to resolve phase delay ambiguities. The following baseline-dependent quantities are introduced:

$$\begin{aligned} X_{ARF}^{pa} &= -(t_{pxgs}^{if} - (\tau_c + \tau_a)) \cdot \frac{2\pi}{\omega_o} \\ S_{ARF}^{pa} &= -(t_{psgs}^{if} - (\tau_c + \tau_a)) \cdot \frac{2\pi}{\omega_o} \end{aligned} \quad (6)$$

where,  $t_{pxgs}^{if}$ ,  $t_{psgs}^{if}$  are ionosphere free linear combinations of group and phase delay observables from (4),  $\tau_c$  — theoretical ionosphere free time delay,  $\tau_a$  — contribution to time delay from adjustments obtained in the previous solution. Analogously, a station-dependent ARF can be introduced, so that the ARF for the specified baseline is a difference of the ARF for the stations forming the baseline. Values of station-dependent ARF are computed for each scan by solving equations which tie ARF with observed phase and group delays. ARF for one station among the stations participated in this scan is not determined and is considered as a reference one. Usage of station-dependent ARF instead of baseline-dependent ARF brings considerable merit if more than two stations participated in the observations of the scan. Each scan has  $\frac{n(n-1)}{2}$  baseline-dependent ambiguities, but only  $n-1$  are independent since they should satisfy to a closure conservation condition for each triplet of stations:

$$\frac{1}{2\pi}(\varphi_{12} + \varphi_{23} - \varphi_{13}) - \frac{\dot{\tau}_{23}\tau_{12}}{\omega_o} + N_{12} + N_{23} - N_{13} = 0 \quad (7)$$

ARF would have only integer values in the absence of instrumental errors. Phase delay ambiguity resolution is reduced in this case to elimination of an integer part from ARF and redistribution of baseline-dependent phase delay ambiguities. Instrumental errors which are intrinsic to phase delays enter ARF directly. Instrumental errors which are intrinsic only to the group delays enter ARF directly and indirectly via bias in  $\tau_a$  which is obtained in group delay solution. Thus, ARF is contaminated by both integer phase delay ambiguities and instrumental noise of measurement of group and phase delays in realistic case. Raw ARF is undergone by a filtering process. It is modeled as a sum of three components:

$$ARF_i = r_i + h_i + N_i \quad (8)$$

where,  $r_i$  — is a regular slowly varying smooth function,  $h_i$  — is a noise-like high frequency varying quantity and  $N_i$  — is a discontinuous ambiguity function which can have only integer values.

The regular component is modeled by a linear spline with imposing constraints on its rate of change. Parameters of the filter: duration of the segments (usually 1–2 hours) and the level of constraints (reciprocal weights are usually in the range 0.01–0.1 1/hour) control behavior of the regular component. The high frequency component is restricted by imposing an upper limit (usually 0.2–0.3) for its maximal in modulo value. Then station dependent phase delay ambiguities are determined as an integer part of the difference of the ARF value and the regular component. If a remnant in ARF after subtraction the regular part and the integer ambiguity exceeds the upper limit for the high-frequency component then that value of ARF is treated as an outlier.

Algorithm of phase delay ambiguity resolution can be described as follows:

1. Obtain the best group delay solution.
2. Form phase delays from measured wide-band fringe phases by applying a feed horn rotation correction. Obtain preliminary phase delay ambiguities from baseline-dependent ARF. Eliminate ambiguities in misclosures.
3. Compute post-adjustment station-dependent X-band ARF.
4. Filter station-dependent ARF with resolving station-dependent ambiguities;

5. Compute baseline-dependent ambiguities using station-dependent ambiguities;
6. Refine a PxGs (X-band semi-phase) delay solution by
  - (a) Consecutive elimination of outliers from the solution up to the specified limit;
  - (b) Backward restoration of the previously suppressed observations up to the specified limit;

Errors made in phase delay ambiguity resolution during filtering ARF can be corrected in refinement of the initial solution provided the error rate was not high (no more than 10–20%).

7. Compute post-adjustment station-dependent S-band ARF;
8. Repeat steps 4, 5, then refine PsGs delay solution;
9. Produce PxPs combinations and refine pure phase delay solution;

The process of phase delay ambiguity resolution works satisfactory if the following assumptions are correct:

- Short periodic fluctuations of ARF (periods  $< 3^h$ ) are less than 0.3 phase turn;
- Low frequency ARF rate is less than 0.3 turn/hour;
- Baseline-dependent systematic errors are negligible;

## 4 Results

Typical ARF before and after filtering are presented in the fig. 2–5. Argument in plots is time in hours elapsed since beginning of the experiment.

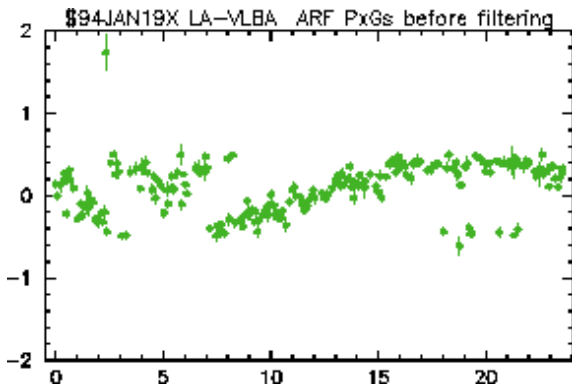


fig. 2

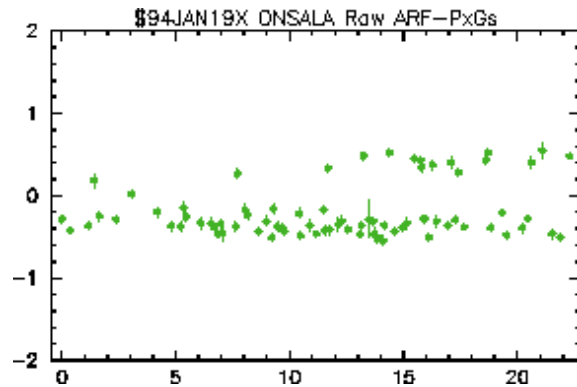


fig. 3

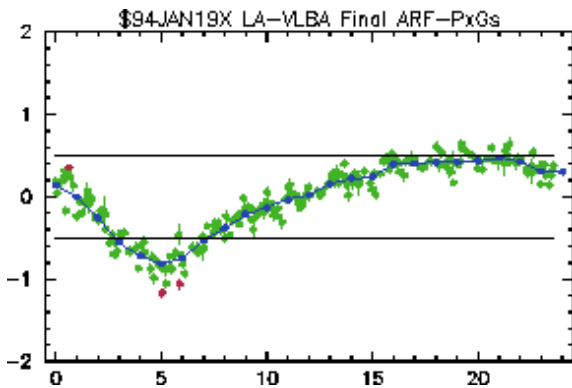


fig. 4

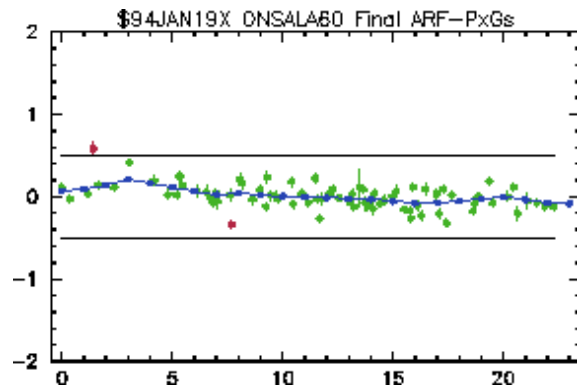


fig. 5

Solid line in fig. 4–5 represents adjustments of the regular component of ARF.

About 100 sessions were processed by algorithms of phase delay ambiguity resolution: experiments carried under programs EUROPE, IRIS-S, geo-VLBA, NEOS-A, NAVEX. I found that

- Phase delay ambiguities can be resolved for the baselines up to 10 thousand km. It is difficult to resolve ambiguity for the longer baselines since there are too few common observations at the baselines with length more than 85% of the Earth diameter.
- The most important factors which influence on the possibility to resolve phase delay ambiguities are station sensitivity and the level of instrumental noise.
- Phase delay ambiguities can be resolved for up to 80–90% of observations in geo-VLBA and R&D experiments, 60–80% of IRIS-S experiments and 40-70% of EUROPE and NEOS-A experiments.
- It is more difficult to resolve phase delay ambiguities at S-band than at X-band.
- There are stations which are not eligible for phase delay ambiguity resolution.

After resolving phase delay ambiguities we are able to use several types of linear combinations of phase and group observables. Properties of different types of solutions are presented in the table 2.

Tab. 2

<b>Group delay combination</b>			
Used combination:	$1.08\tau_{gx}$	$-0.08\tau_{gs}$	$+\tau_n$
Uncertainty (VLBA mode)	15ps	6ps	12ps
Uncertainty (best Mark-III)	25ps	10ps	15ps
Ambiguity spacings:	>15ns		
<b>X-band semi-phase delay combination</b>			
Used combination:	$0.94\tau_{px}$	$+0.06\tau_{gs}$	$+\tau_n$
Uncertainty (VLBA mode)	0.5ps	4ps	8ps
Uncertainty (best Mark-III)	1.0ps	8ps	8ps
Ambiguity spacings:	114ps		
<b>Phase delay solution</b>			
Used combination:	$1.08\tau_{px}$	$-0.08\tau_{ps}$	$+\tau_n$
Uncertainty (VLBA mode)	0.5ps	0.2ps	8ps
Uncertainty (best Mark-III)	1.0ps	0.3ps	8ps
Ambiguity spacings:	131ps and 34ps		

It is remarkable that there is a noise floor  $\tau_n$ . Existence of this floor makes pure phase delay solutions not so attractive. We see that the advantages of a solution made by using a combination of phase and group delay observables called semi-phase with respect to a group delay solution are substantial. At the same time a pure phase delay solution brings only marginal improvement with respect to a semi-phase delay solution due to existence of the noise floor. Moreover, the pure phase delay solution is less reliable than the semi-phase delay solution, since it has two ambiguity spacings: 131 psec and 34 psec while the semi-phase delay solution has the only ambiguity spacing 114 psec. It is difficult to detect observations with wrongly resolved ambiguities with spacings 34 psec when the noise floor is only 4 times less, while it is rather more easy to guarantee a correctness of a phase delay ambiguity resolution when the ambiguity spacing is 15 times wider than the noise floor.

A continuous set of 22 sessions carried out under program CONT94 at the VLBA and NAVEX networks was analyzed. 13 stations participated. Baseline lengths were in the range 0.6–10.4 thousands

km. 60315 out of 66857 observations were used in the group delay solutions. Weighted sum of root mean squares of postfit residuals was 18 psec. 53049 phase delay observables were used in the semi-phase delay solutions. Weighted sum of root mean squares of postfit residuals was 8.1 psec. Precision of determination of geodynamical parameters improved by the factor 2. At the same time increasing precision didn't result in improving accuracy.

Baseline length repeatability is presented in the table 3.  $L$  is the baseline length. Differences are

Tab. 3

$$\begin{aligned} \text{Phase delay solutions:} & \quad R(L) = 0.11 \text{ mm} + 9.6 \cdot 10^{-10} \times L \\ \text{Group delay solutions:} & \quad R(L) = 0.19 \text{ mm} + 8.7 \cdot 10^{-10} \times L \end{aligned}$$

not statistically significant. Detailed analysis of a baseline evolution reveals substantial variations in baseline lengths of unknown origin which affects both phase and group delay solutions. Plots in fig. 6–7 shows typical case. Left plot presents daily estimates of baseline length in mm obtained from semi-phase delay solutions and the right plot shows the baseline evolution obtained from group delay solutions. Average baseline length (5040 km) is removed in both plots. Argument in plots is time in days elapsed from 01-JAN-94. Error bars are  $1\sigma$  formal uncertainties.

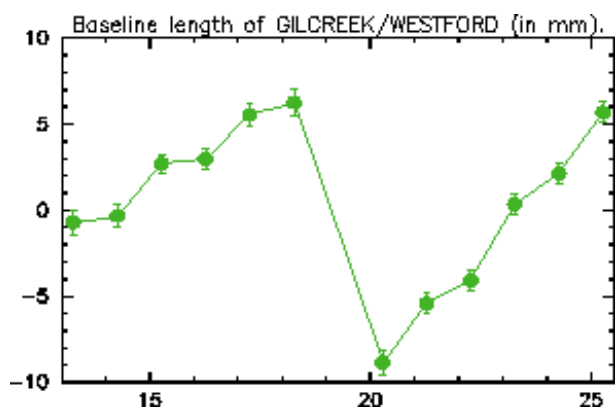


fig. 6

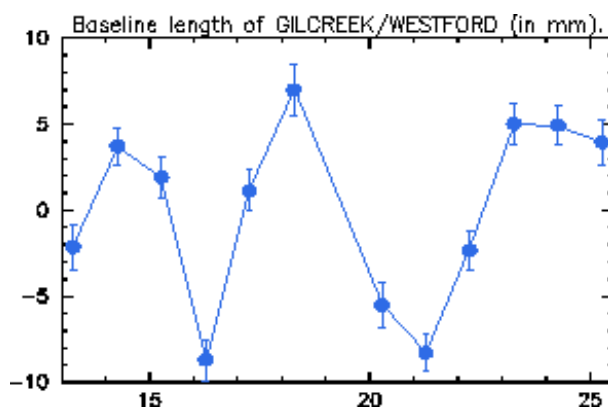


fig. 7

Hourly values of UT1 and pole motion were also obtained. UT1 was modeled by a sum of global offset, global rate and linear spline with 1 hour segment. Rate of change between adjacent segments was constrained with weights to be reciprocal to the constant 0.3 msec/day. The estimates from the phase delay solutions are less noisy and deviate less from the empirical model than the estimates obtained in group delay solutions although an improvement is not conclusive. Results of determination of UT1 for hour intervals using semi-phase and group delay solutions are presented in fig. 8–9 respectively. Argument is time in hours. Mean value and linear trend were removed. A thin solid line represents empirical model derived using a whole set of VLBI group delay observables for 20 years [4]. A grey bar represents  $1\sigma$  formal uncertainties.

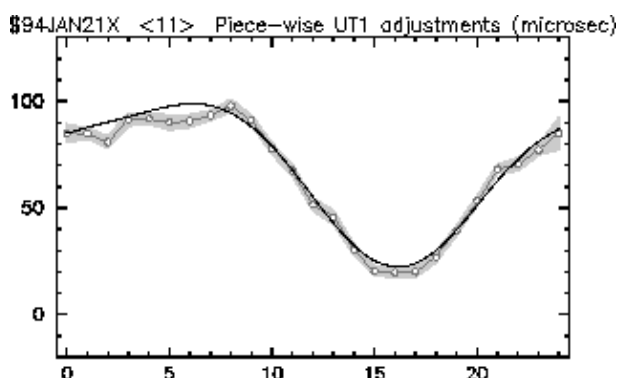


fig. 8

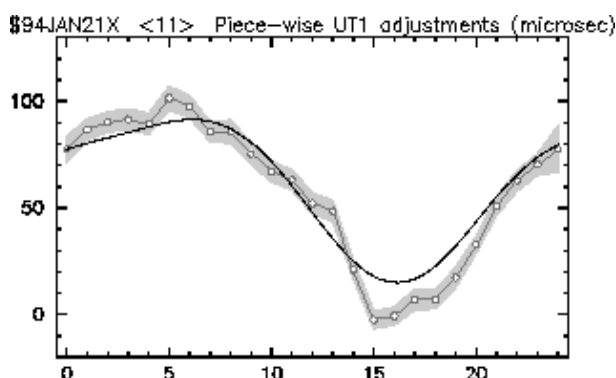


fig. 9

Result of determination of hourly estimates of pole coordinates (in microarcseconds) from semi-phase and group delay solutions are shown in fig. 10–11 respectively.

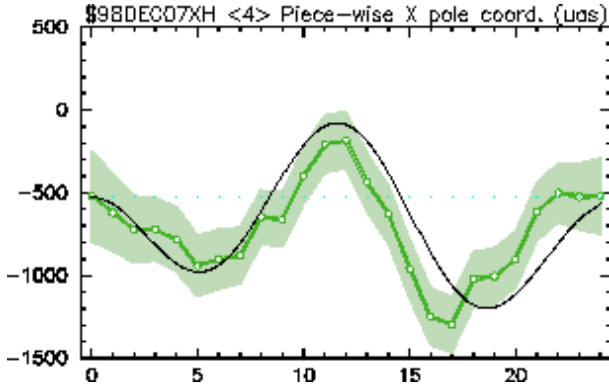


fig. 10

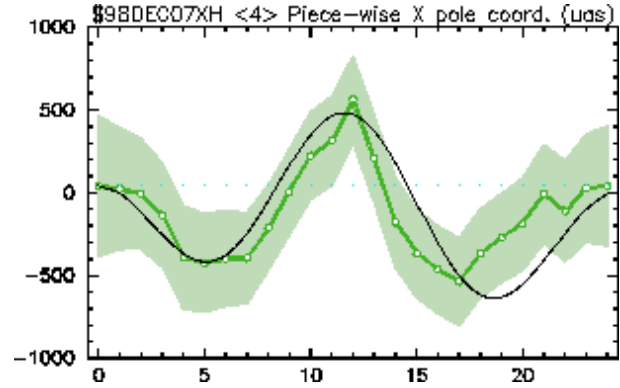


fig. 11

## 5 Conclusion

- Phase delay ambiguities can be successfully resolved for 80–90% of VLBA observations and for 40–70% of Mark-III data at the baselines with length up to 85% Earth diameter;
- Critically important factors for resolving phase delay ambiguities:
  - High sensitivity: X-band:  $\sigma(\tau_{gr}) < 20\text{psec}$ , S-band:  $\sigma(\tau_{gr}) < 100\text{psec}$  (properly cooled receiver);
  - Low level of instrumental errors (excellent performance of phase calibration).
- Semi-phase delay solutions have not worse precision than pure phase delay solutions, but are more reliable;
- The precision of semi-phase delay solutions is better than the precision of group delay solutions, but an improvement in accuracy is not significant.

## 6 Acknowledgments

This work is supported by DFG (Deutsche Forschungsgemeinschaft), research grant CA 92/7-1.

## References

- [1] T.A. Clark, et al.: Precision geodesy using the MARK-III very long baseline interferometric systems, IEEE Trans. Geoscience and Remote Sensing, 23, 438–449, 1985
- [2] T.A. Herring: Submillimeter horizontal position determinations using very long baseline interferometry, Journ. Geophys. Res., Vol. 97, p. 1981–1990, 1992.
- [3] J.R.Ray, Himwich W.E., and Knight C.A.: Radio interferometric survey between the GRAS and VLBA antennas, Ft. Davis, TX, Contributions of Space Geodesy to Geodynamics: Technology Ed., Smith, D.E. and Turcotte, D.L., American Geophys. Union, Geodynamics Series, Vol. 25, Washington, D.C., p. 115–124, 1993
- [4] J. M. Gipson: Very long baseline interferometry determination of neglected tidal terms in high-frequency Earth orientation variations, Journ. of Geophys. Res., Vol. 101, No B12, p. 28051–28064, December 10, 1996

## Integrating GPS zenith path-delay measurements into the analysis of geodetic VLBI observations from the European network

M. Rioja<sup>1,2</sup>, P. Tomasi<sup>1,3</sup>

<sup>1</sup> *Istituto di Radioastronomia del C.N.R. Via Gobetti 101 - 40129 Bologna, Italy*

<sup>2</sup> *Now, at Observatorio Astronomico Nacional - Alcala de Henares, Madrid, Spain*

<sup>3</sup> *Istituto di Tecnologia informatica spaziale del C.N.R - Matera, Italy*

### Abstract

Estimates of vertical components of site coordinates from 'standard' geodesy techniques of analysis of VLBI observations have uncertainties about 3-4 times larger than the other components. This is a consequence of the large correlation between the zenith path delay and the vertical component of the stations. We want to contribute to the effort of investigating the potential of new routes, combining the products of different geodesy techniques, to lighten that situation. We present preliminary results from a 'hybrid' route of analysis which implements external GPS tropospheric estimates into the VLBI analysis, along with a comparison with results from the 'standard' route. At this early stage of our project the 'hybrid' route appears as a very promising approach, with first time clear evidence of improvement with respect to the 'standard' route.

### 1. Introduction

Since 1990 an European geodetic network consisting of fixed VLBI antennas has regularly performed simultaneous S/X observations at a rate of six 24-hour experiments per year. The participating stations are located at Onsala (Sweden), Wettzell (Germany), Medicina (Italy), Madrid (Spain), Matera (Italy), Noto (Italy), also, since 1994, Ny-Alesund (Norway) and Crimea (Ukraine). The Effelsberg 100 m. antenna near Bonn (Germany) take part once a year to an European VLBI geodetic experiment. During 1997 the new mobile VLBI antenna, part of the TIGO project, has been installed at the Wettzell station and was regularly inserted in European VLBI experiments during 1998.

In the meantime the IGS GPS network has been established throughout the world, and it is regionally enhanced with more permanent GPS sites. At present all European VLBI geodetic stations, except Crimea, are equipped with permanent GPS receivers.

The processing of the european geodesy observations is regularly performed at the correlator centre at MPIFR, in Bonn (Germany). The geodetic observables are accessed by different groups to proceed with the data analysis, using distinct software tools and/or strategies. It is a general aspect in all analysis that the uncertainty in the estimated values of the vertical components of the sites, or baseline vectors, is about 4 times larger than for the rest of components. The vertical components are largely affected by the propagation of elevation dependent errors in the group delay model, for example in the formulation of the tropospheric contribution.

We are currently investigating the potential of a novel route, which combines both VLBI and GPS techniques, as a way to improve the estimates of vertical components for the sites. In principle, the simultaneous multi-directional nature of GPS observations could yield an advantageous configuration for the modelling of tropospheric contributions into the observables. Our aim is to make a systematic comparison of the results obtained following the "standard route" of analysis of VLBI observations, and a "hybrid route" which implements simultaneous GPS tropospheric estimates. We present comparative preliminary results from the implementation of external GPS tropospheric estimates, computed every hour, in the VLBI analysis with CALC/SOLVE package. We are also presenting an easy way to introduce zenith path delays derived from GPS, into the CALC/SOLVE standard software, with few modifications in the program DBCAL. Previous attempts have been done by other authors (Carlsson et al. 1995) with no conclusive results.

## 2. Data Analysis

We have started to work on a novel route to disentangle the coupling between the values for the vertical coordinates of the stations (or baselines) and the tropospheric contributions at each site, estimated from VLBI analysis. In the past, many attempts have been made to use water vapor radiometers (WVR) in order to produce the same results. Due to the large cost of the equipment, an advanced algorithm has been introduced into the CALC/SOLVE package in order to determine the zenith path delay, or more specifically the wet contribution, at each station. In this case we are using, as produced by a WVR, the zenith path delay produced by the International GPS Service for Geodynamics (IGS) at the Berna center, in the analysis of the VLBI observations from the European geodesy network during 1998.

Our final working database will consist of the six European VLBI observations from 1998, and the simultaneous standard IGS products for the 1-hourly tropospheric zenith-delay estimates, whenever available, for each participating site. The results presented in this contribution comprise a subset of the complete database which consists of the first 4 epochs of VLBI observations.

We have performed parallel analysis, with CALC/SOLVE, following (1) the 'standard route', and (2) a 'hybrid route' which implements external tropospheric zenith delay values from GPS. In both cases we have used an identical configuration of parameters, except for the sub-section concerned with the troposphere. In the 'standard route' we have used a piece-wise linear function to estimate 1-hourly residuals, to the *a priori* values, with typical values to constraint the rate and atmospheric gradients. In the 'hybrid route' we used the tropospheric zenith delays resulting from linear interpolation of the 1-hourly estimates from IGS, whenever available, at each site, and no further adjustment in the analysis. The tropospheric contribution from sites with missing IGS entries (such as Medicina, Madrid and Crimea) were estimated following an identical procedure as in the 'standard route'. In all cases we used the corresponding Nielt mapping functions for the dry and wet components of the neutral atmosphere.

The IGS delivers total values of the zenith path delay. We have extracted the wet component contribution for our comparative studies by subtracting the dry Saastamoinen component, which is used in both VLBI and GPS data analysis.

We present a comparison of the achievements from both routes attending at repeatability results for the length and vertical components of the participating baselines.

We have also performed individual analysis and cutoff elevation angle tests of each VLBI session of observations, in February, April, June and August. If these sessions may be taken as representative for a certain epoch of the year, the results reflect interesting seasonal effects of the impact of elevation dependent errors, we believe that largely associated with the wet component of the troposphere, in the analysis.

## 3. Preliminary Results - Repeatability tests

Figure 1 shows plots of baseline length repeatability versus baseline length, corresponding to a series of 'standard' analysis using different cutoff elevation angles, in SOLVE, from 5 to 25 degrees, in steps of 5 degrees. The database includes the first 4 epochs of VLBI observations in 1998. Best linear fits have been estimated for each solution. Among them, the fit with the minimum slope corresponds to the analysis with a cutoff elevation angle of 5 degrees. Figure 2 shows the same information as figure 1, corresponding to a parallel 'hybrid' analysis including external GPS tropospheric zenith-delay values. The fit with minimum slope in figure 2 corresponds to a cutoff elevation angle in SOLVE equal to 10 degrees. For comparison, figure 3 shows the results derived using most favourable parameter configuration from both analysis routes.

It should be pointed out that, in principle, the 2 cutoff tests presented in figures 1 and 2 are quite different, and that might explain, at least in large extent, the different results. In the case of the 'standard' analysis, we are computing both the baseline length and the tropospheric zenith delay at the 2 ends of the baseline. In the case of 'hybrid' analysis, we are just computing the baseline length. This can explain the rapid "degradation" of the results shown in figure 1, going from lower to an upper cutoff. In addition to the fact that the number of data points used in the analysis is decreasing, and hence producing a larger statistical uncertainty, there is a large correlation between zenith path delay and vertical component of the stations, almost equal to 100% when using a cutoff elevation angle larger than about 15 degrees.

We have made a comparison of the tropospheric zenith delay estimates from VLBI and GPS techniques for the participating stations and at the time of the VLBI observations. We find a systematic

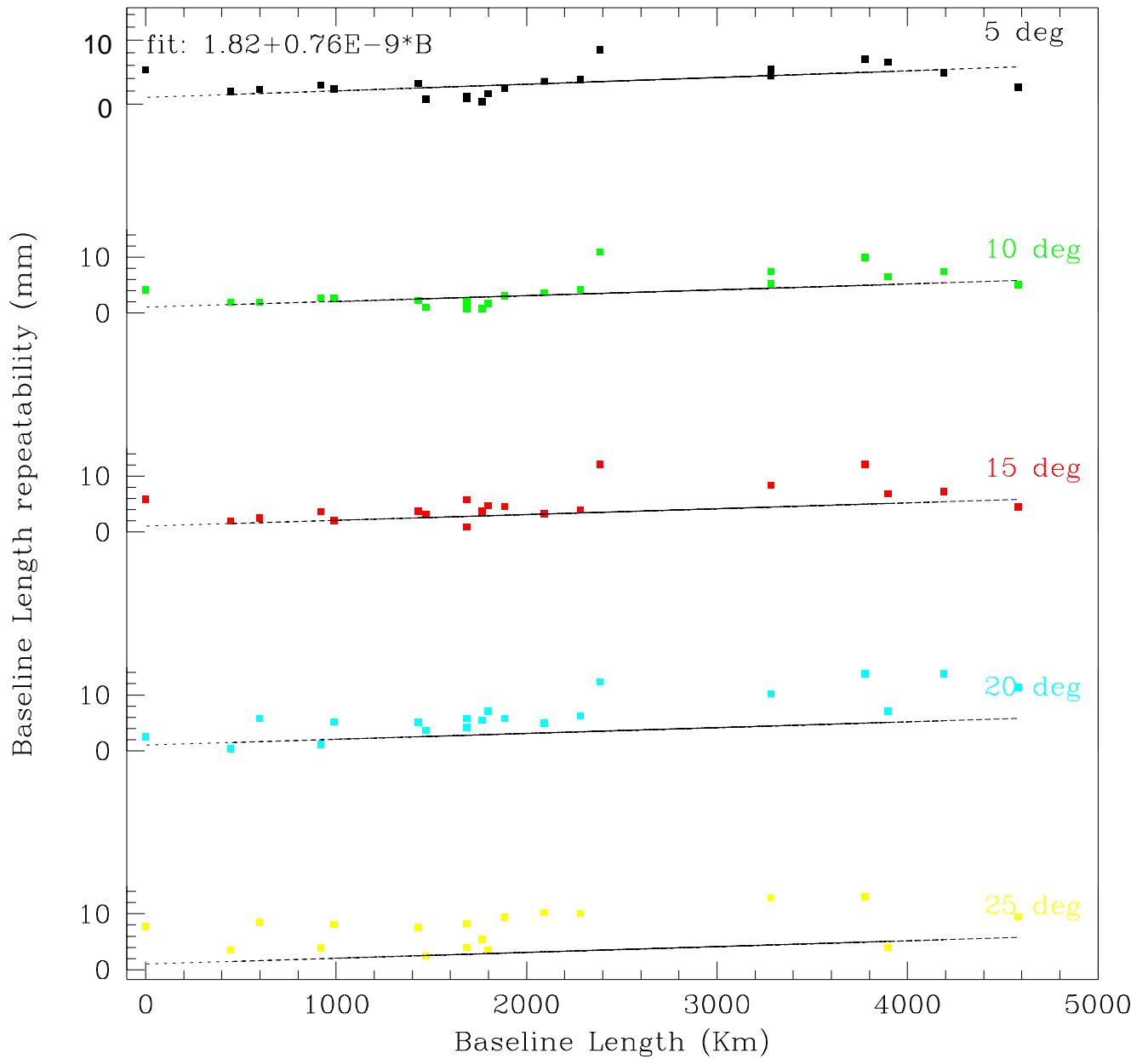


Figure 1: Repeatability of the baseline length estimates, using a 'standard route' in the analysis of 4 24-hours european VLBI sessions in 1998, with different cutoff elevation angles in SOLVE (see upper right corner of each plot). The solid line represents the best-fit with the minimum slope, corresponding to a cutoff elevation angle of  $5^{\circ}$ . It is inserted in all subplots for visual cross-checking. The fitted coefficients appear written above the  $5^{\circ}$  plot.

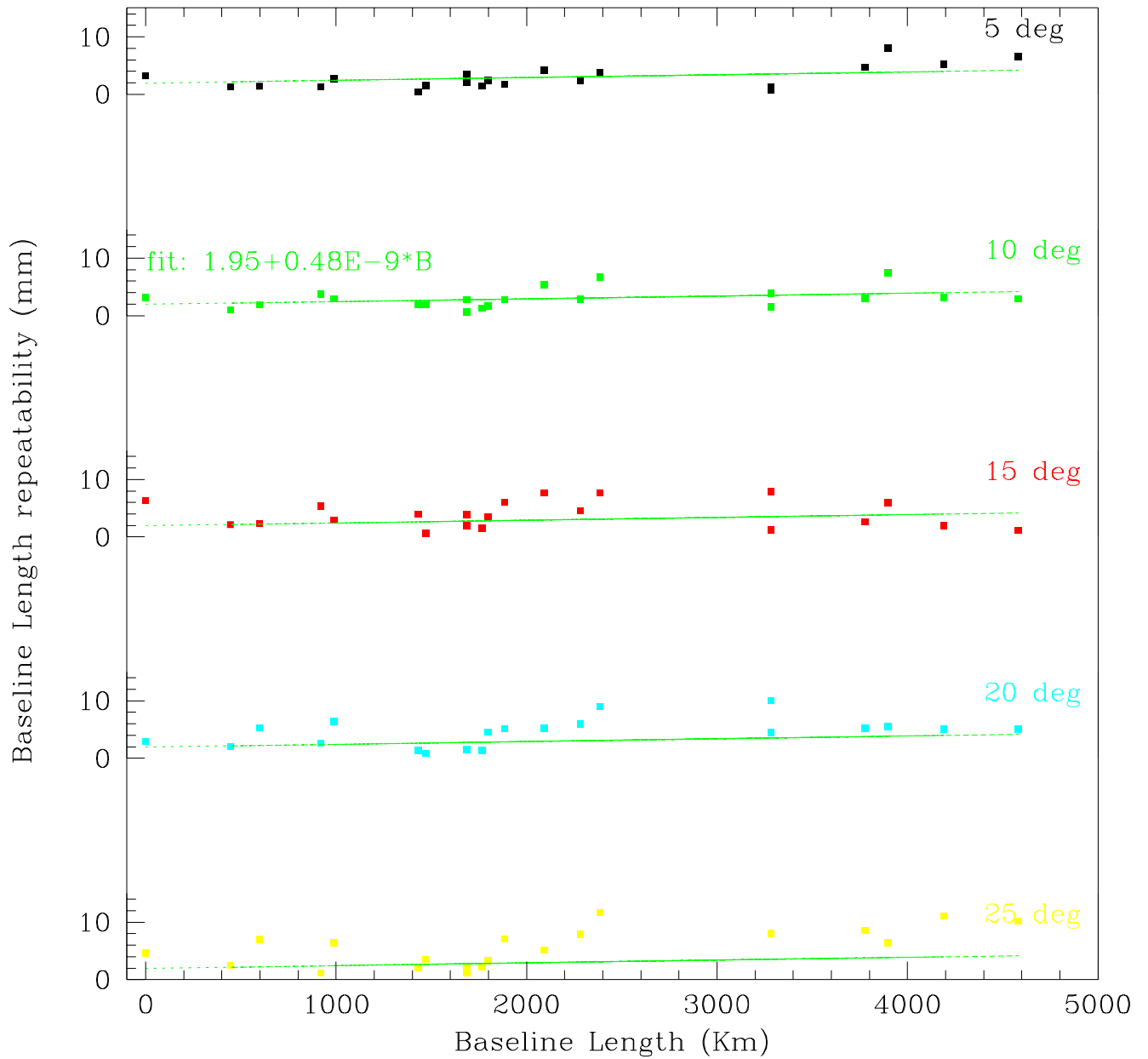
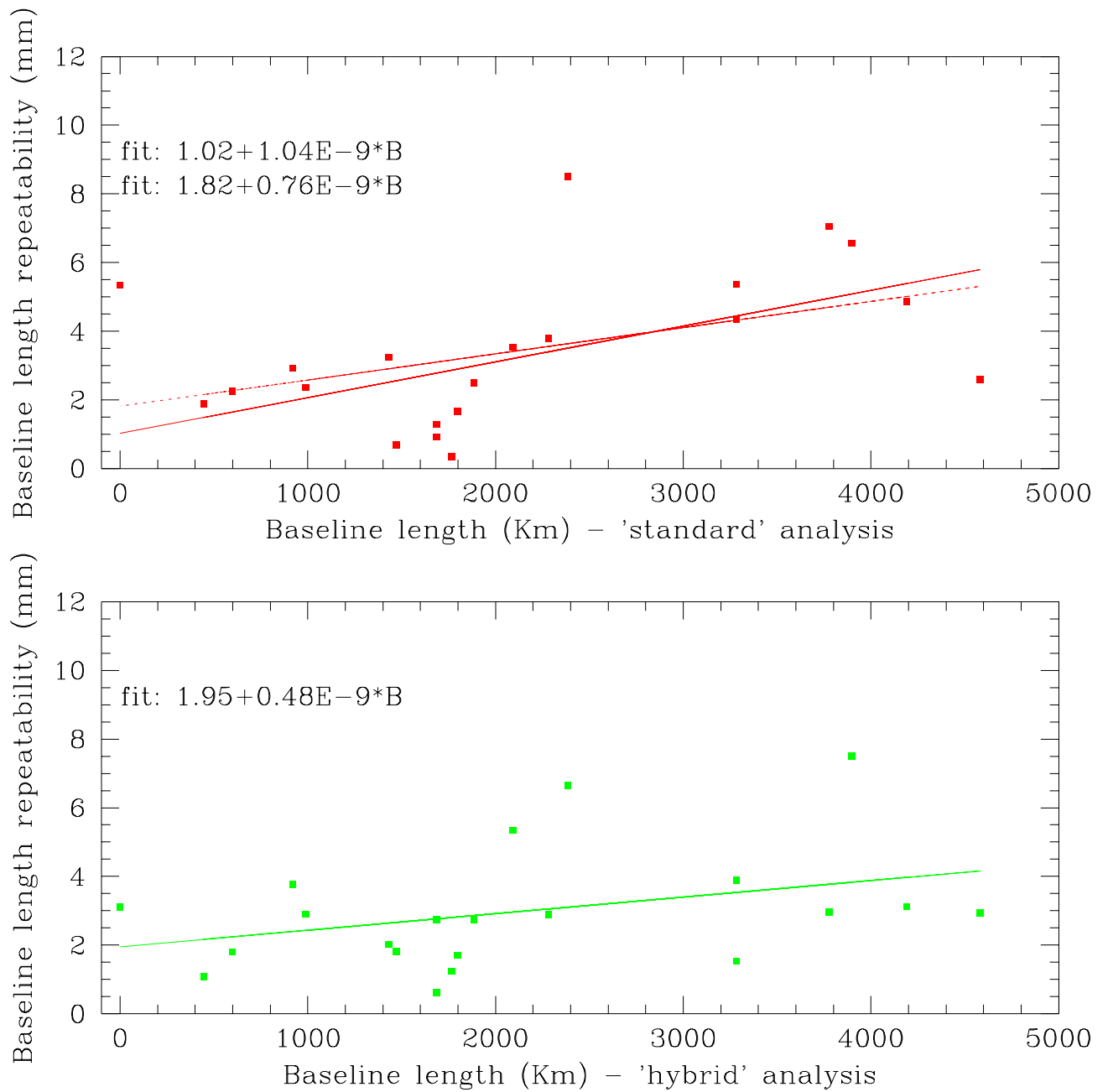


Figure 2: Repeatability of the baseline length estimates, using a 'hybrid route' in the analysis of 4 24-hours european VLBI sessions in 1998, with different cutoff elevation angles in SOLVE (see upper right corner of each plot). The solid line represents the best-fit with the minimum slope, corresponding to a cutoff elevation angle of  $10^0$ . It is inserted in all subplots for visual cross-checking. The fitted coefficients appear written above the  $10^0$  plot.



**Figure 3: Repeatability of the baseline length estimates, using an 'standard' analysis (upper), and a 'hybrid' analysis (lower) of 4 24-hours european VLBI sessions in 1998, with cutoff elevation angles of  $5^{\circ}$  and  $10^{\circ}$ , respectively, in SOLVE. Solid lines are best linear fits. The 2 fits in the upper plot differ in the inclusion in the fit of the shortest baseline (Tigo-Wettzell). See text for explanation of 'standard' and 'hybrid' nomenclature.**

bias between the estimates of both techniques, the VLBI values always smaller than the GPS values, variable with time. Figure 4 shows a comparison of the tropospheric total zenith delays from VLBI (our analysis) and GPS (IGS product) techniques for the station of Wettzell, at 3 epochs.

Exploiting the temporal span of our database along 1 year, we have also attempted to investigate the impact of potential “seasonal” aspects onto the geodetic parameters. We have carried on comparative analysis using different cutoff elevation angles, at 10 and 5 degrees. Figure 5 shows the differences between baseline length estimates from individual ‘standard’ analysis of 4 VLBI observations in 1998. The plots corresponding to the observations from June and August show larger differences for the longest baselines, instead, in February and April, there is no significant dependence with baseline length. This can be explained in terms of the wet component of the troposphere being most difficult to model in summer periods.

At present, we are trying to make a sensible comparison of the vertical estimates derived from the 2 analysis routes considered in this presentation. Figure 6 shows repeatability plots for the vertical components of the baselines, as estimated from the ‘standard’ and ‘hybrid’ analysis routes. The configuration of the parameters involved in both analysis is identical to the one corresponding to the results presented in figure 3.

#### 4. Conclusions and Future work

We have established a working interface that integrates external tropospheric data in the analysis of VLBI observations with SOLVE. Our goal is to make a systematic comparison between the results obtained from an standard VLBI analysis and those from a ‘hybrid route’ which implement simultaneous GPS tropospheric estimates. The results presented here are preliminary and constitute a progress report on that project. Nevertheless, we want to point out some interesting facts that are worth mentioning. We confirm the evidence found by other authors too, that the inferred wet delay contributions estimated from GPS and VLBI techniques exhibit similar short term variations, but with an apparent long term bias. Our results from repeatability tests and cutoff elevation angle tests indicate a promising perspective for the combination of both geodetic techniques. In fact it is the first time such a clear evidence is found. Inferring from the improvement found in VLBI, we believe that a reduction of the current 10 deg cutoff elevation angle in GPS observations, might be a non-negligible factor for further improvement of results.

We intend to extend our analysis to include the 2 remaining 24-hours sessions of European VLBI observations from 1998. There are many interesting aspects that remain to be understood and investigated, just to mention here a few of them: the effect of decreasing the solution interval of tropospheric estimates, try new strategies in the analysis, understanding the systematic bias between estimates from both techniques...

#### 5. References

Carlsson T.R., Elgered, G., and Johansson, J., 1995, *Proc. 10th Working Meeting on European VLBI for Geodesy and Astrometry*, Eds. R. Lanotte and G. Bianco, pp. 148-153

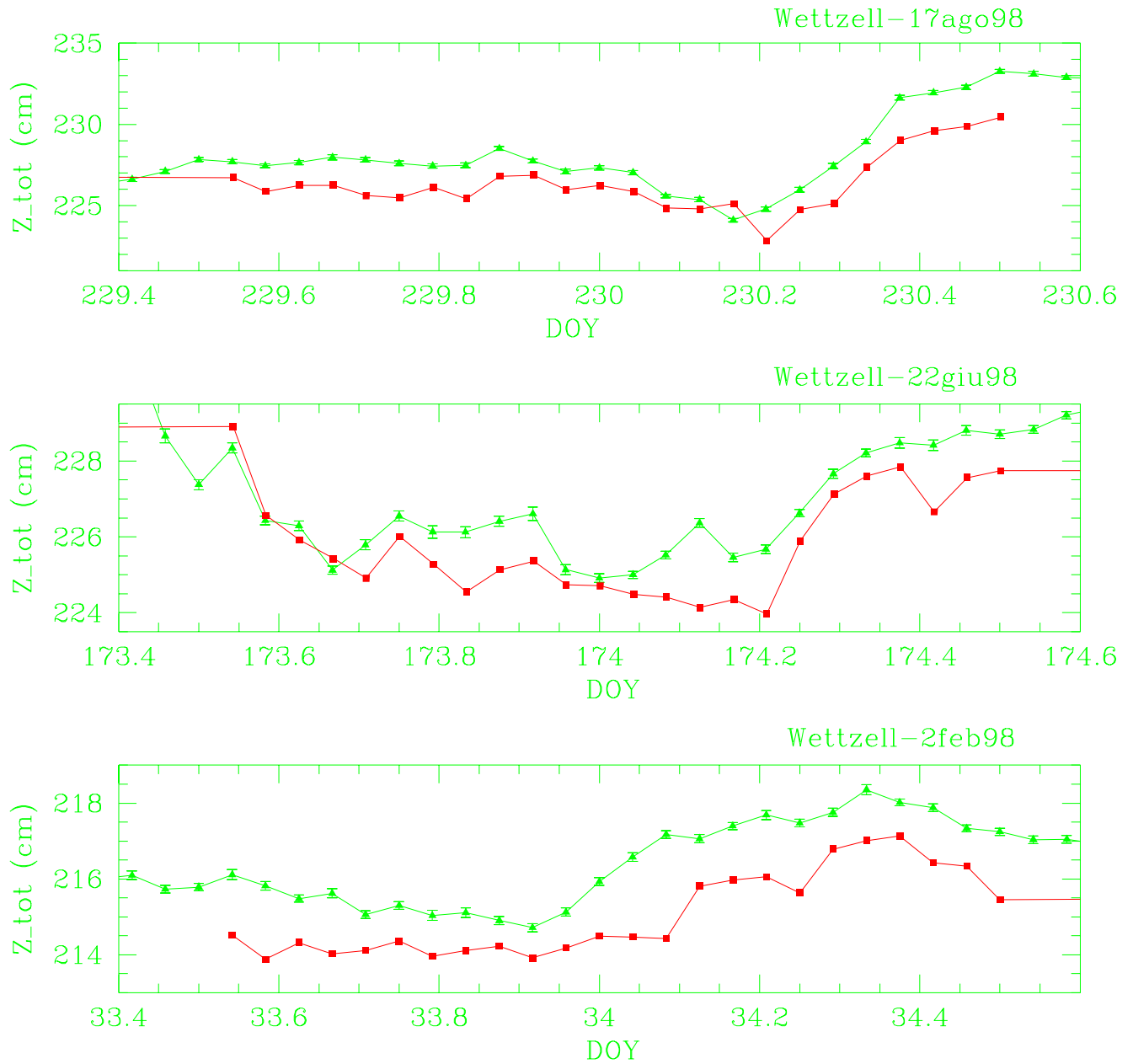


Figure 4: Comparison of 1-hourly tropospheric zenith delay estimates for Wettzell, along 3 days in 1998, using VLBI (filled squares) and GPS (filled triangles) techniques.

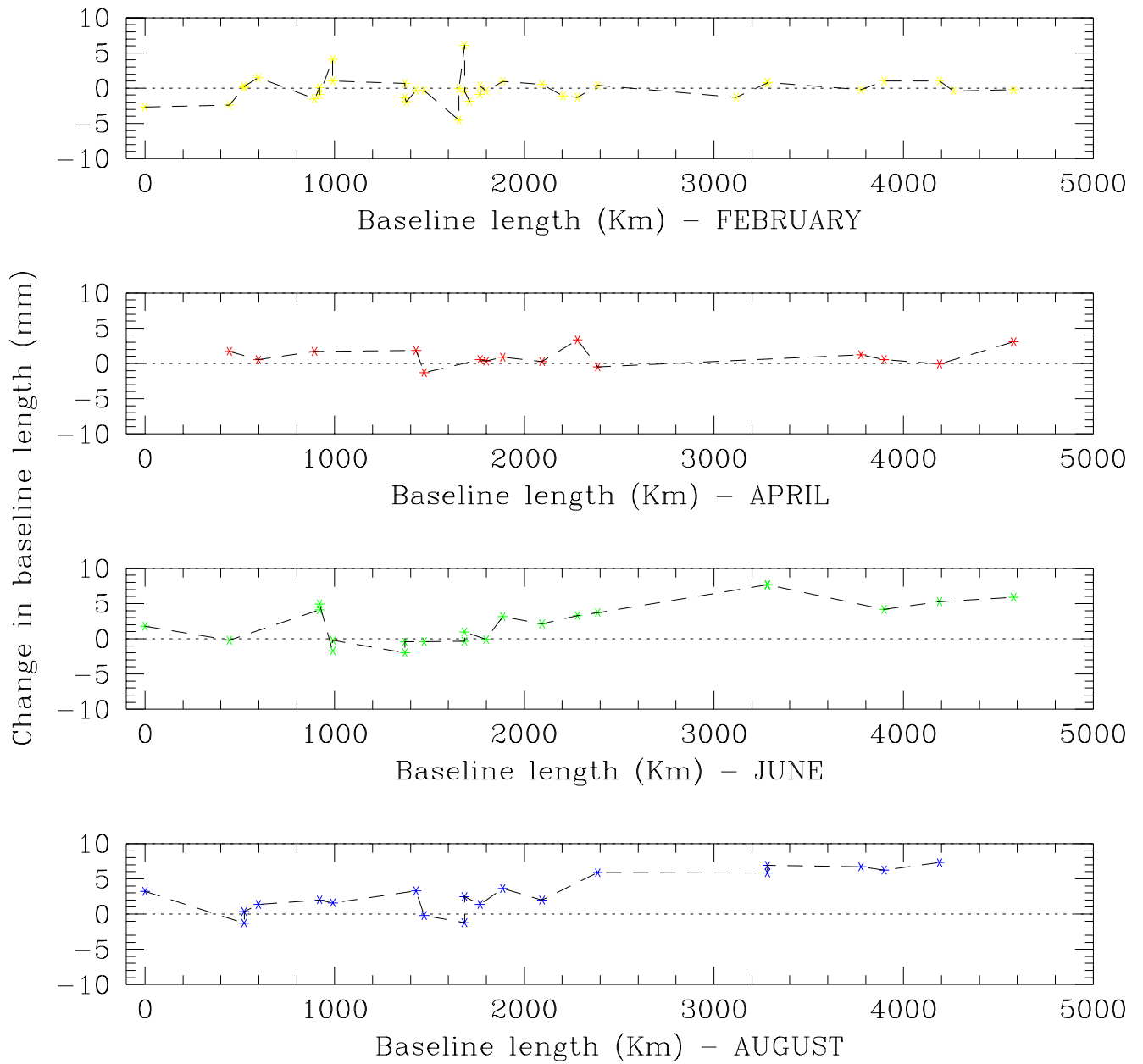


Figure 5: Differences in the baseline length estimates with SOLVE, using two different cutoff angles, 10 and 5 deg. Some sort of "seasonal" dependence is visible.

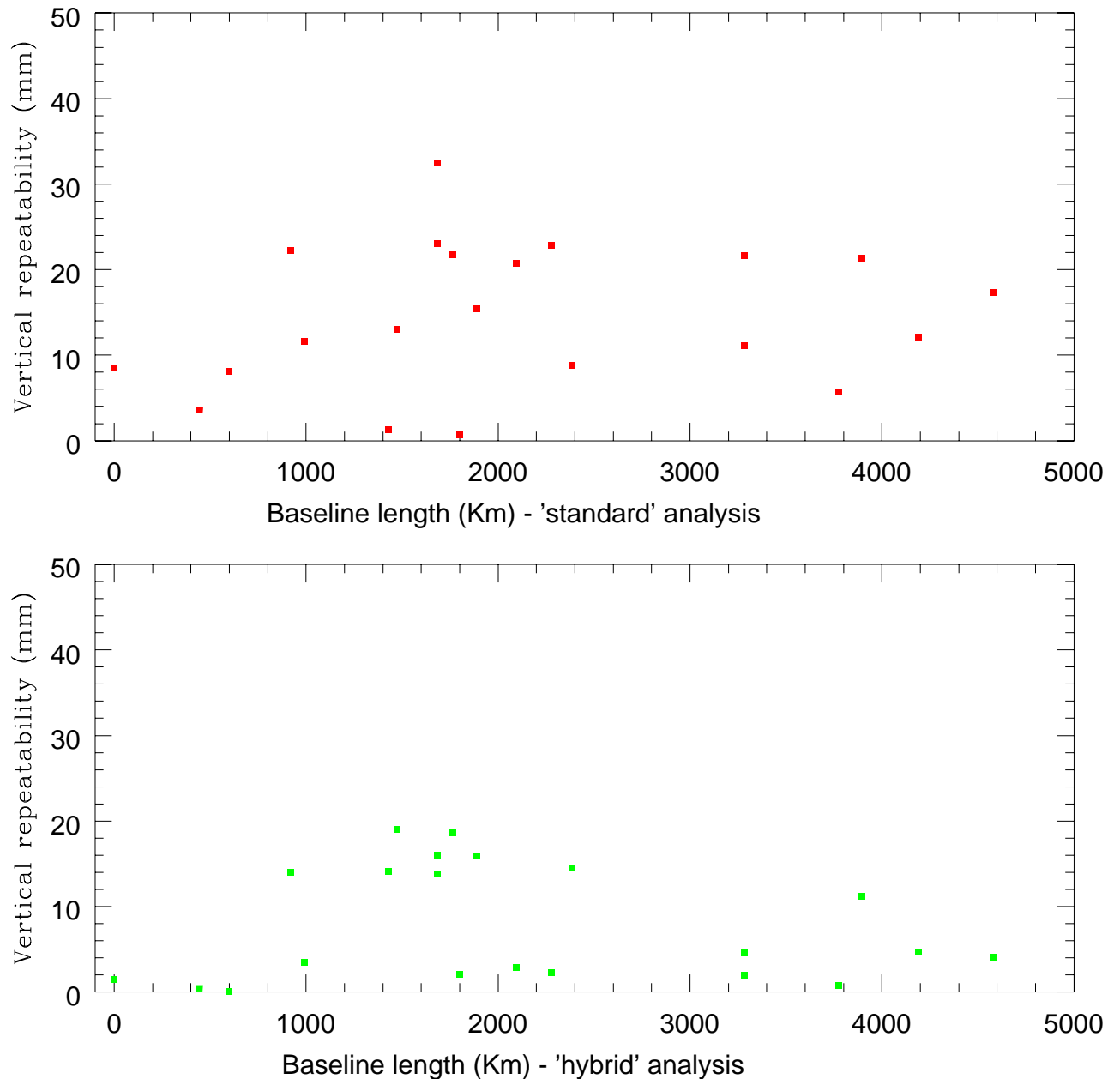


Figure 6: Repeatability of the baseline vertical component estimates, using a 'standard route' analysis (upper), and a 'hybrid route' analysis (lower) of 3 24-hours european VLBI sessions in 1998, with cutoff elevation angles of  $5^{\circ}$  and  $10^{\circ}$ , respectively, in SOLVE. See text for explanation of 'standard route' and 'hybrid route' nomenclature.

# Comparison of atmospheric parameters estimated from VLBI, GPS and microwave radiometer data

Lubomir P. Gradinarsky, Rüdiger Haas,  
Jan M. Johansson, Gunnar Elgered

Onsala Space Observatory, Chalmers University of  
Technology, Onsala, Sweden

## Abstract

Very Long Baseline Interferometry (VLBI) is colocated with a permanent Global Positioning System (GPS) receiver and a Water Vapour Radiometer (WVR) at the Onsala Space Observatory (OSO). Both VLBI and GPS data are affected by the propagation delay of radio waves in the atmosphere, while the WVR is sensitive to the atmospheric emission close to the center of the 22 GHz water vapour emission line and provides wet delay estimates. We present a comparison of estimated atmospheric parameters (equivalent zenith wet delay and linear horizontal delay gradients) derived from an independent analysis of simultaneous VLBI, GPS and WVR observations. We study and compare the estimated parameters using different elevation cut off angles for the analysis of VLBI data with those obtained from the GPS and the WVR data analyses. The parameters are estimated for 90, 180 and 360 minutes long intervals, which allows us to study the averaging effect on the integrated parameters of the turbulent atmosphere.

## 1. Objectives

Variations in the atmospheric refractive index are a major error source for the space based geodetic techniques. Symmetry and the elevation dependence of the propagation delay are used in the VLBI and GPS processing for estimating the total zenith delay. It has been realized [MacMillan, 1995] that azimuthal asymmetries in the atmospheric refractive index could be present leading to errors in the horizontal and the vertical station coordinates. Including a horizontal gradient estimation into the data processing leads to an improved repeatability of the site coordinate estimates for

both VLBI and GPS [Rothacher *et al.*, 1998; Bar-Sever *et al.*, 1998; MacMillan, 1995]. The objective of this work is to compare estimated wet delay and linear atmospheric gradients from the different techniques, study the differences and discuss the effect of the different processing strategies on the estimated atmospheric parameters. A better estimation of the horizontal gradients should lead to improved geodetic estimates.

## 2. Colocated techniques

The 20 m radome enclosed telescope at the Onsala Space Observatory is used for geodetic Very Long Baseline Interferometry (VLBI). In 1997 Onsala participated in 18 geodetic VLBI sessions, from the EURO, the CORE-B-100 and the RD-VLBA series [Haas *et al.*, 1999]. In our study 14 such 24 hour long sessions covering all seasons of the year 1997 were processed.

The permanent GPS site at Onsala is a part of the International GPS Service (IGS) [Beutler *et al.*, 1995] and is equipped with two receivers: a Turbo Rogue 8-channel and an Ashtech Z12 channel connected to a Dorne–Margolin B type antenna with a conically shaped radome. The receivers are connected to a 5 MHz reference frequency from the hydrogen maser which is also used in the VLBI observations.

The water vapour radiometer measures the sky emission at two frequencies – 21.0 GHz and 31.4 GHz. The sky emission (equivalent temperature) at those frequencies depends on the cosmic background emission, the amounts of water vapour, liquid water, and oxygen. By using algorithms described in [Elgered, 1993] the measured temperatures can be related to the wet path delay.

## 3. Atmospheric parameters of interest

The elevation dependencies of the wet and the hydrostatic component of the delay is used to estimate a total zenith delay (VLBI and GPS). The hydrostatic part can be estimated with good accuracy in the zenith direction based on the ground pressure measurements. Subtracting the hydrostatic component from the total delay yields the wet delay component.

The other parameter of interest is the horizontal wet delay gradient. Figure 1 displays an example of presence of a wet delay gradient in the WVR data. The first plot (1a) displays the measured delay, the second (1b) shows the zenith delay values for one scan at elevation the elevation 33.4 degrees (taken at time indicated with the vertical line in (1a)) and the third (1c) displays a 3D view of the mapped delay, where an obvious tilt in the delay values is present<sup>1</sup>.

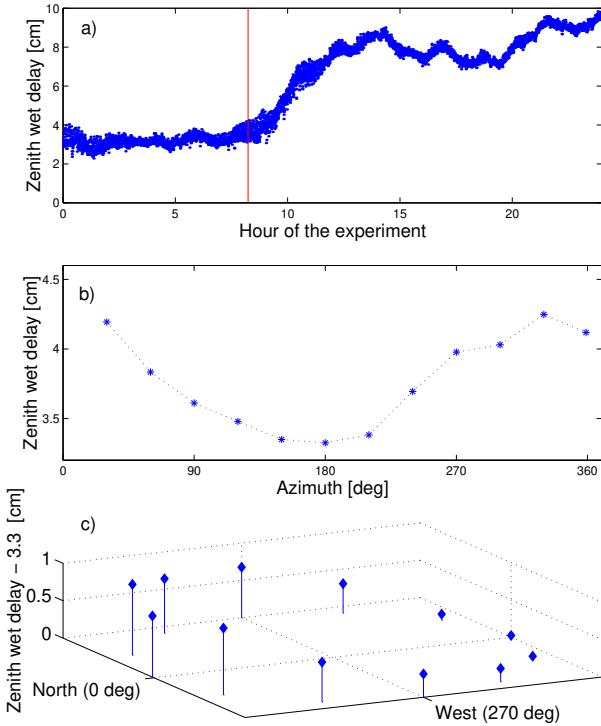


**Figure 1:** Example of wet delay gradient:  
a) 24 hours of WVR data, August 31, 1998;  
b) azimuth scan at the constant elevation 33.4 degrees at the time indicated by the line in 1a;  
c) 3-D view of the wet delay for the azimuth scan.

A linear azimuthal asymmetry in the troposphere can be described using the model [Davis et al., 1993]:

$$\begin{aligned} \Delta \tilde{L}^z(\epsilon, \phi, \Delta t) &= \Delta L^z + V_L \Delta t \\ &+ \cot \epsilon \left[ 1 - 10^{-6} N_s \csc^2 \epsilon \right] \\ &\times [\Xi_n \cos \phi + \Xi_e \sin \phi] \end{aligned}$$

where  $\epsilon$  and  $\phi$  are the azimuth and the elevation angles,  $\Delta t$  the time (from the first epoch

<sup>1</sup>note the constant 3.3 cm wet delay subtracted from the total value for better visibility

for which the model is derived),  $\Delta \tilde{L}^z(\epsilon, \phi) = \Delta L/m_o(\epsilon)$  is the equivalent zenith wet delay,  $\Delta L^z$  – mean zenith delay,  $V_L$  – zenith delay rate  $\Xi_i$  – north /east delay gradient components,  $10^{-6} N_s \csc^2 \epsilon$  – correction for bending ( $0.2^\circ$  for  $\epsilon = 5^\circ$  at sea level [Davis et al., 1993]).

In our study we compare the wet delay estimates from WVR observations with the wet delay estimates from VLBI and GPS data. Note, however, that the horizontal gradient estimates from WVR are for the wet part only, whereas VLBI and GPS estimates are the total horizontal gradients. We assume that the main gradient contribution is due to the wet part, which is not completely true in situations when large pressure or temperature gradients exist at the site.

#### 4. Data acquisition and processing strategies

The data of the three techniques were processed for 3 different time intervals 90, 180, and 360 minutes, producing estimates of delay and horizontal gradients. The VLBI data were processed using the SOLVE software. The constraints for the total delay and the delay gradients were 36 cm/day and 4 mm/day, respectively. The mapping functions derived by Niell, [1996] were used. Several solutions were produced using different cut-off angles of 5, 10, 15 and 20 degrees.

The GPS data at OSO are acquired in a continuous mode where a sampling frequency of 1 s is used. The data are resampled to 300 s during processing. JPL provided the orbits, the earth orientation, and the clock correction parameters. Using the GIPSY [Webb and Zumberge, 1996] processing package with fixed orbits, earth orientation, clock correction parameters and station coordinates provides the opportunity to use the Precise Point Positioning [Zumberge et al., 1997] technique, where the zenith delay and linear gradients at the site are estimated. The Niell mapping functions and constraints equivalent to those used in the VLBI analysis were used for the specification of the Kalman filter used in GIPSY.

The WVR operates in a continuous sky scanning mode. The zenith wet delay estimates are obtained using an automated editing procedure

for the sun<sup>2</sup>, the horizon mask<sup>3</sup> and rain<sup>4</sup>. After the wet delay was obtained the gradient model was fit to the data in a least squares sense to estimate the north and the east gradient parts.

## 5. Intercomparison results

Before presenting the comparisons it is worth to mention some features for each of the techniques. The VLBI estimates, especially the gradients might be affected by the source distribution on the sky. The GPS estimates will also be affected to some extent by the location of Onsala being  $57^\circ$  in latitude, resulting in a poorer satellite coverage in the north. The WVR estimates are affected by rain and heavy clouds, and during those periods the data have larger uncertainties if they were not removed by the editing.

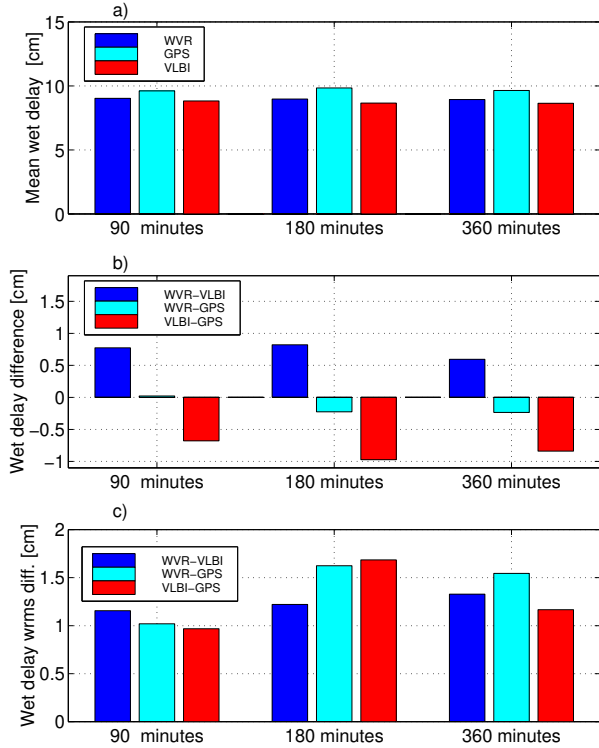


**Figure 2:** Wet delay statistics: a) weighted means; b) weighted differences; c) wrms differences.

First we present results for the zenith wet delay estimated from VLBI, GPS and WVR. Figure 2 displays a statistical comparison. Plot

<sup>2</sup>points obtained within  $15^\circ$  of the sun are removed

<sup>3</sup>the 20 m antenna radome obscures the horizon between NE and E

<sup>4</sup>the wet delay algorithm brakes down during rain

(2a) shows the weighted wet delay means. An agreement at the 1 cm level and no significant dependence on the estimation time interval is observed. The second plot (2b) shows the weighted mean difference between the different techniques. The WVR and the GPS results agree better according to this criterion while VLBI shows an underestimation of the delay. The third plot (2c) shows the weighted RMS (WRMS) differences. Some dependence on the estimation interval is present. The agreement varies between 1.0–1.5 cm for the different combinations of the techniques. Changing the elevation cut-off angle in the VLBI analyses did not affect the agreement. Given these results it is difficult to give any preferences for a better than 1 cm level agreement between any of the techniques.

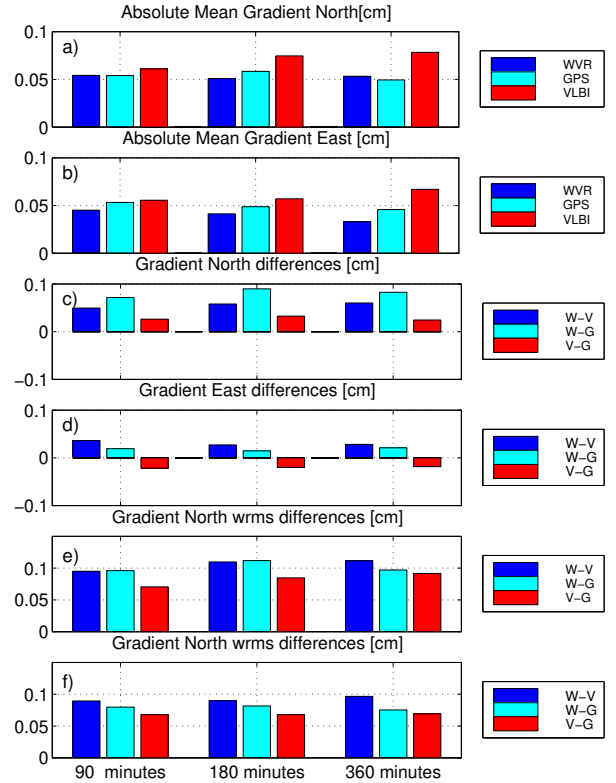


**Figure 3:** Gradient statistics: a) and b) absolute mean north and east; c) and d) differences north and east; e) and f) RMS differences north and east.

Figure 3 presents the results for the north and the east gradient components. The first two rows are the weighted absolute means of the gradient components. The WVR estimates decrease for increased time intervals, which is according to the expectations. The GPS esti-

mates do not show a trend, while VLBI is estimating larger gradients for larger time intervals. This last feature is not physically reasonable and is up to now unexplained. It can be mentioned that looking at the time series of the VLBI gradient estimates shows that in general the VLBI results show less gradient variability, compared to WVR and GPS.

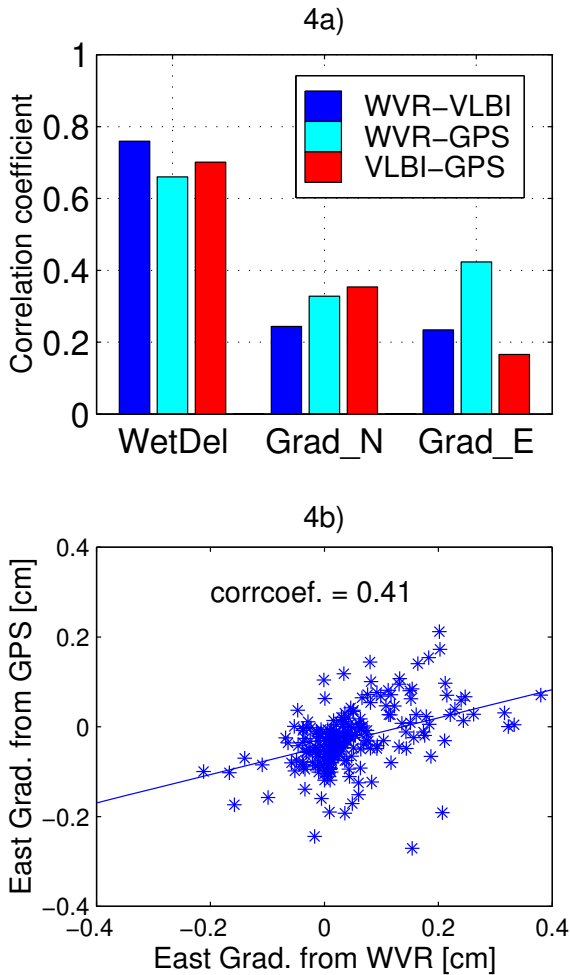


**Figure 4:** a) Cross-Correlation results for the 90 minutes intervals; b) Correlation plot WVR v/s GPS having the largest correlation coefficient.

A possible reason for that might be that the used constraints are too tight. Gradient differences – plots (3c) and (3d) – show that the best agreement is between VLBI and GPS results and that there are larger discrepancies with the WVR results. One possible explanation is that both VLBI and GPS are sensitive to the total gradient. In the eastern component this is not that obvious. The agreement between VLBI and GPS is also best for the WRMS differences

(Fig. 3e and 3f). The dependence of the averaging time is again weak. Since there is no consistent trend we may be seeing random variations due to the limited data set. It is interesting to mention that choosing higher cut-off angles increased the differences due to larger estimated gradients from the VLBI data. This is in agreement with the expectation of larger tropospheric inhomogeneity for smaller scales.

Finally the correlation coefficients for the 90 minutes estimates were calculated and the results are shown in Figure 4a. As expected the wet delay correlation is high (at the 0.7 level), while the estimated horizontal gradients are less correlated, which again shows the difficulty of comparing the small gradient components. Figure 4b shows one example correlation plot for the east 90 minutes gradients from the WVR v/s the GPS data set. This was the highest (0.4) correlation coefficient.

## 6. Conclusions and future work

From the presented comparison a good agreement between estimated wet delays from VLBI, GPS and WVR data was shown. The agreement is independent of the averaging time and the VLBI cut-off angle and the WRMS differences are at the 1–1.5 cm level, with correlation coefficients at the 0.7 level. The gradient comparison showed WRMS differences at the level of 1–1.5 mm. This is comparable to the magnitude of the gradients. Week dependence on the estimation time was present and a slightly better agreement between VLBI and GPS on average was evident, possibly related to the fact that both VLBI and GPS data are sensitive to the total gradients. Another possibility is the fact that a major error source of the WVR gradients is the presence of rain or heavy clouds. In the future processing of GPS data with elevation dependent weighting and different cut-off angles might be included. Different tropospheric parameters constrains will also be used. Finally we conclude that the typical size of the estimated horizontal gradient is less than 1 mm. Given that the differences between the estimates using different methods are at the same order, larger data sets are needed in order to study systematic effects.

## References

- Bar-Sever, Y. E., P. M. Kroger, J. A. Borjesson: Estimating horizontal gradients of tropospheric path delay with a single GPS receiver, *Geophys. Res. Lett.*, , **103(B3)**, 5019-5035, 1998
- Beutler, G., I. I. Mueller and R. E. Neilan: The International GPS Service for Geodynamics (IGS): The story, in *GPS Trends in Precise Terrestrial, Airborne, and Spaceborne Applications*, **115**, 3-13, Springer, 1996
- Davis, J. L., G. Elgered, A. E. Niell and C. E. Kuehn: Ground-based measurements of gradients in the "wet" radio refractivity of air, *Radio Science*, **28(6)**, 1003-1018, 1993
- Elgered, G.: Tropospheric radio-path delay from ground-based microwave radiometry, in Janssen, M. A. (ed), *Atmospheric Remote Sensing by Microwave Radiometry*, pp.218-258, Wiley & Sons, Inc, 1993
- Haas, R., L. P. Gradinarsky, J. M. Johansson and G. Elgered: The atmospheric propagation delay: A common error source for Colocated Space Techniques of VLBI and GPS, *Poster paper at GEMSTONE*, Tokyo 1999
- MacMillan, D. S.: Atmospheric gradients from very long baseline interferometry observations, *Geophys. Res. Lett.*, , **22(9)**, 1041-1044, 1995
- Niell, A.: Global mapping functions for the atmosphere delay at radio wavelength, *Journal of Geophysical Research*, **101(B2)**, 3227-3246, 1996
- Rothacher, M., T. A. Springer, S. Schaer, G. Beutler: Processing strategies for regional GPS networks, *International Association of Geodesy Symposia*, **118**, 1998
- Webb, F. H. and J. F. Zumberge: An introduction to GIPSY/OASIS-II, *JPL Publication D-11088*, Jet Propulsion Laboratory, Pasadena, California, 1993
- Zumberge J. F., M. B. Hefflin, D. C. Jefferson, M. M. Watkins, F. H. Webb: Precise point positioning for the efficient and robust analysis of GPS data from large networks, *Geophys. Res. Lett.*, , **102**, 5005-5017, 1997

---

Lubomir P. Gradinarsky, Rüdiger Haas, Jan M. Johansson, Gunnar Elgered, Onsala Space Observatory, Department of Radio and

Space Science, Chalmers University of Technology, SE-439 92 Onsala, Sweden.  
(e-mail:lbjg@oso.chalmers.se)

---

This preprint was prepared with AGU's L<sup>A</sup>T<sub>E</sub>X macros v4. File Wettzell'final formatted February 26, 1999.

## **CORE: Continuous, High-Accuracy Earth Orientation Measurements**

D. S. MacMillan, W. E. Himwich, C. C. Thomas, and N. R. Vandenberg  
NVI, Inc/Goddard Space Flight Center, Greenbelt, Maryland

J. M. Bosworth, B. Chao, T. A. Clark, and C. Ma  
Goddard Space Flight Center, Greenbelt, Maryland

**Abstract.** The international geodetic VLBI community will inaugurate during 1999 a new phase of the program called CORE (Continuous Observations of the Rotation of the Earth). The capabilities of the new Mark IV correlators, available as of mid-1999, will enable greater sensitivity, more frequent observing sessions, and improved system throughput. The CORE program, begun in 1996 with the CONT96 campaign, has gradually increased the number of observing sessions per week. As of early 1999 the average is 2.5 24-hour sessions per week (including the NEOS sessions). This will expand to 3.5 sessions per week beginning in the second half of 1999, with the goal of continuous observing by the year 2001. The concept of CORE requires that Earth orientation measurements will be made with several networks, each operating on a different day. It is therefore important to determine whether there are systematic differences between EOP derived from different networks. We have been acquiring data from different networks observing on the same day or on sequential days in order to validate this concept. Recent analysis comparing data from CORE-A, CORE-B, and NEOS sessions shows that there are systematic differences in EOP, which are now under active investigation.

### **Introduction**

Changes in the Earth Orientation Parameters (EOP) are due to either external torques, or to internal redistribution of angular momentum between the Earth's core, atmosphere, and oceans. Measurements of EOP can therefore place constraints on geophysical models of the solid Earth, the atmosphere, and the oceans. VLBI is one of the most important sources of Earth orientation information that is available. Recognizing the importance of EOP measurements, the international VLBI community is engaged in a program, CORE (Continuous Observations of the Rotation of the Earth) to make continuous EOP measurements beginning in 2001 ramping up from 3.5 24-hour sessions per week during 1999. Two critical elements of the CORE are the Mark-IV correlator that can process much more data and the Mark-IV VLBI hardware that will provide much more precise measurements due to an increase in recorded bandwidth by a factor of 8. The Mark-IV correlator will be capable of supporting continuous data acquisition. The evolution of CORE program is shown in Figure 1. Continuous measurements of EOP will be made with several networks, each operating on a different day. For the CORE program to be successful, EOP derived from the different VLBI networks that will be used need to agree. To investigate this question, we have run a series of VLBI experiments starting in 1997, that are either simultaneous (CORE-A) with the weekly NEOS network or on adjacent days (CORE-B). Here we present results of comparisons of EOP measurements made by these networks.

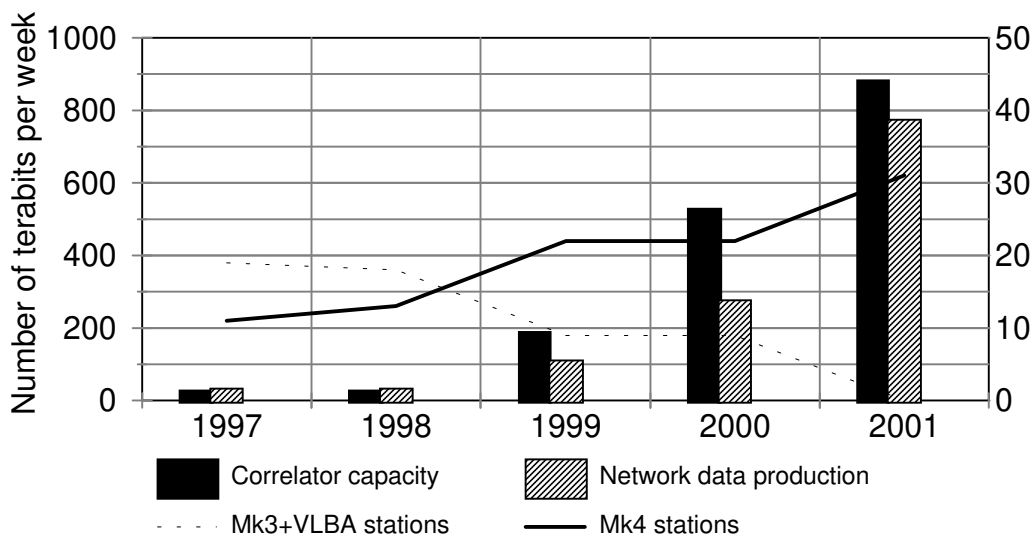


**Figure 1.** Amount of data collected as CORE evolves.

### CORE-NEOS Comparisons

The precision of VLBI measurements has continued to improve by about an order of magnitude each decade. As can be seen in Figure 2, the best UT1 precision has been attained for the NASA R&D experiments. The current best VLBI measurements of UT1 have a precision of about 2  $\mu$ s.

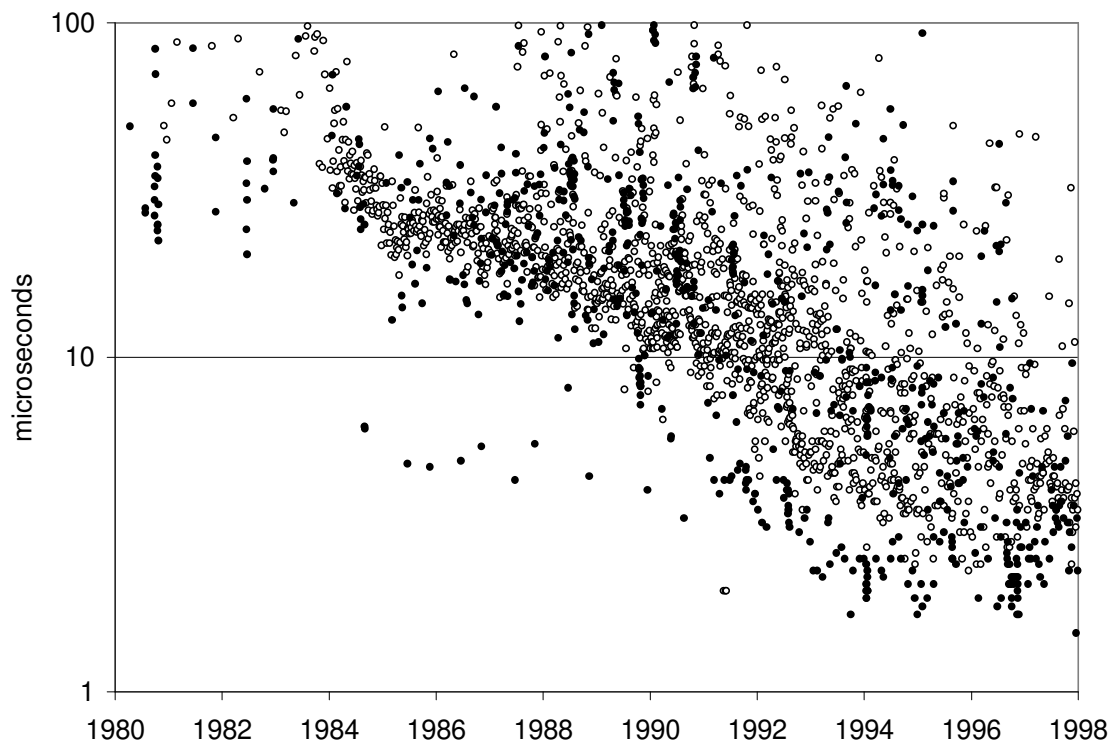


**Figure 2.** Precision of UT1 measured by VLBI. Dark filled circles are NASA R&D sessions and the open circles are all other sessions.

One of the principal problems with high precision VLBI EOP is determining the measurement accuracy. In the CORE program, EOP measurements will be made with several different networks, where each network will operate on a different day. It is therefore important to determine whether there are systematic differences between EOP derived from different networks. Our basic test of accuracy consists of examining the differences between EOP derived from independent VLBI measurements made by different networks.

From the history of VLBI sessions from 1980 to the present, there are about 300 simultaneous sessions. Comparisons of these simultaneous sessions imply that the formal EOP errors should be increased by a factor of 1.5-2.0. As can be seen in Figure 2 for UT1, the EOP precision of these measurements varies over a wide range, which is greater than a factor of ten compared to current precision. This reflects the evolution of the improvement of precision. Therefore it is difficult to determine from this comparison whether the differences are caused by random or systematic errors.

To determine the current EOP accuracy, we have compared measurements made by CORE and NEOS networks. The least squares estimation program (SOLVE) used in the analysis and the theoretical models applies in the analysis are generally described by *Ma et al.* [1990]. The weekly NEOS network uses Kokee, Green Bank, Fortaleza, Nyalesund, and Wettzell. The CORE-A network sessions are simultaneous with NEOS sessions and use antennas at Fairbanks, Westford, Hobart, Hartebeesthoek, and Matera. CORE-A should give the same EOP as NEOS. There are 3 different CORE-B networks: (1) Algonquin, Fortaleza, Fairbanks, Kashima, and Onsala, (2) Crimea, Fairbanks, Kashima, Kokee, Medicina, and Nyalesund, (3) Fairbanks, Kokee, Noto, Green Bank, Seshan, Urumqi, and Yebes. NEOS and CORE-B sessions are on adjacent days. During 1998, CORE-A and CORE-B were also on adjacent days. For comparisons between networks operating on sequential days, we have extrapolated EOP to the midpoint between each of the experiments.

Figure 3 shows the difference between EOP measurements from the CORE-A and the NEOS network. Tables 1-3 summarize the differences between networks. Based on the  $\chi^2/\text{dof}$  of the differences, there are clearly unmodeled sources of random or systematic error. One could argue that the unmodeled error is entirely random and that the formal uncertainties of the EOP estimates are too small by a factor of 1.3-2.0. This is consistent with *Ryan et al.* [1993], who determined that the formal VLBI site velocity uncertainties were too small by a factor of 1.5-2.0 using data decimation tests. There is evidence that there are also systematic EOP errors. The mean differences between networks are also given in Tables 1-3 along with the expected uncertainty of the mean difference assuming that all errors are random. In many cases, the mean difference is significant and is a factor of 4-5 larger than the uncertainty of the mean.

For the NEOS-CORE-A, the differences are significant for X, Y, and UT1. For NEOS-CORE-B, the differences are significant only for UT1. Although the significance of these mean differences is clear from the size of the mean differences compared with the uncertainty of the mean, we have done an F-test to evaluate the significance. We suppose that there is really a systematic difference between networks, given by the mean difference and compute the  $\chi^2/\text{dof}$  about the mean. The F-test simply determines the probability that random error could reduce the  $\chi^2/\text{dof}$  by the observed amount when one parameter (the mean difference) is estimated. This probability is very small for those cases where the mean difference is several times the expected mean error. For NEOS/CORE-A, the probability is less than 0.1% for X and Y and less than 2% for UT1. In the case of NEOS/CORE-B, it is less than 2% for UT1.

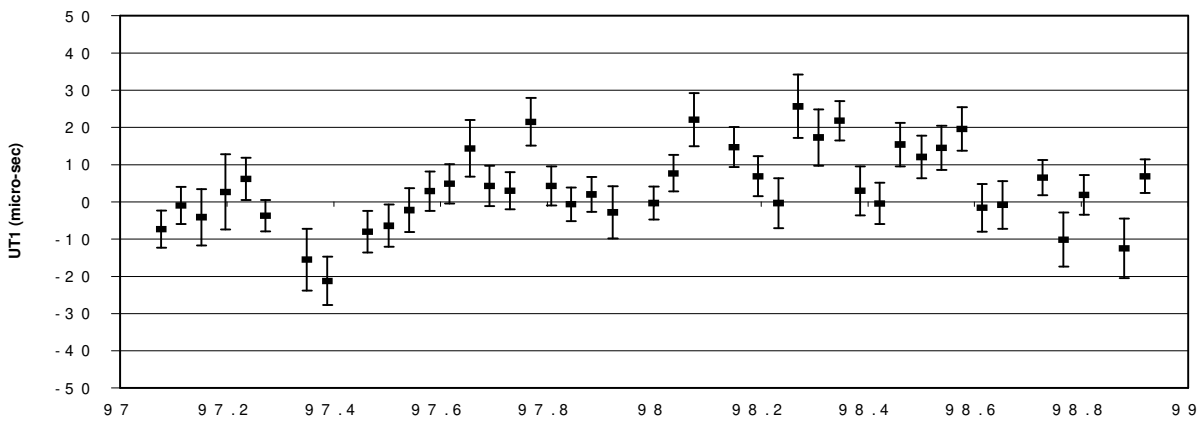
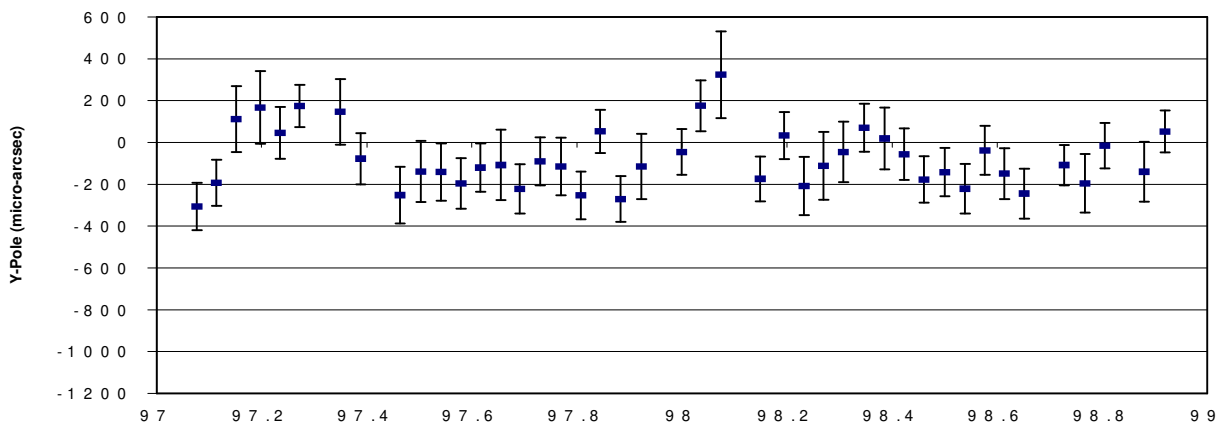
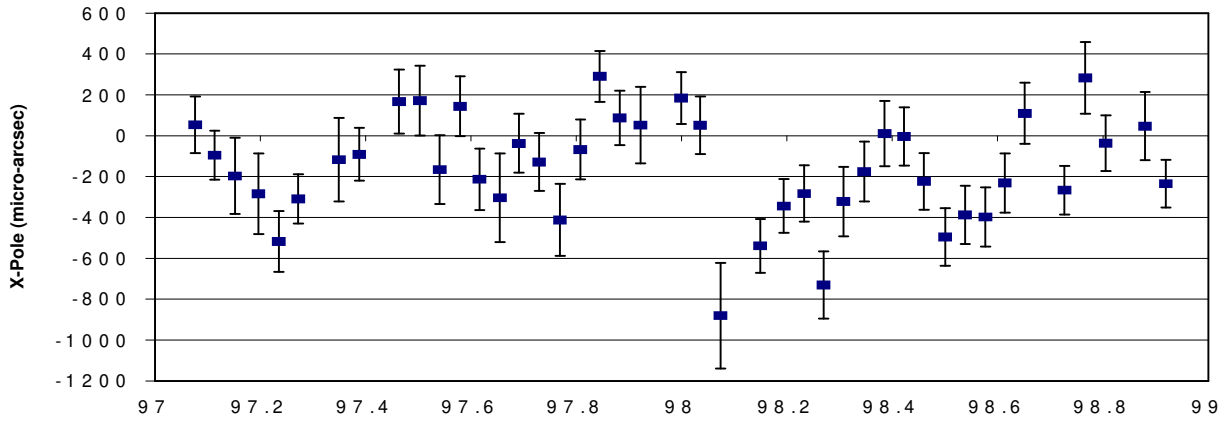


**Figure 3.** NEOS minus CORE-A EOP estimates for 1997-1998

**Table 1.** NEOS - CORE-A Differences

	#sessions	$\chi^2/\text{dof}$	Wrms	$\langle\sigma\rangle$	Mean	$\langle\sigma\rangle/\sqrt{N}$
X( $\mu\text{as}$ )	43	3.6	280	153	-147	23
Y( $\mu\text{as}$ )	43	1.7	280	128	-85	20
UT1( $\mu\text{s}$ )	43	3.0	11.1	6.0	3.7	0.9
LOD( $\mu\text{s}$ )	43	1.9	18.2	14	2.2	2.1

**Table 2.** NEOS - CORE-B Differences

	#sessions	$\chi^2/\text{dof}$	Wrms	$\langle\sigma\rangle$	Mean	$\langle\sigma\rangle/\sqrt{N}$
X( $\mu\text{as}$ )	30	3.9	285	151	-18.2	28
Y( $\mu\text{as}$ )	30	2.6	198	130	-30.1	24
UT1( $\mu\text{s}$ )	30	3.2	15.2	8.9	10.6	1.6
LOD( $\mu\text{s}$ )	30	3.8	24.6	14	-7.4	2.5

**Table 3.** CORE-B - CORE-A Differences

	#sessions	$\chi^2/\text{dof}$	Wrms	$\langle\sigma\rangle$	Mean	$\langle\sigma\rangle/\sqrt{N}$
X( $\mu\text{as}$ )	14	4.4	242	118	-99	33
Y( $\mu\text{as}$ )	14	4.3	206	102	-74	27
UT1( $\mu\text{s}$ )	14	2.3	9.6	6.5	-5.7	1.7
LOD( $\mu\text{s}$ )	14	4.5	21	10	11	2.7

## Summary

Analysis of 73 comparisons between NEOS and CORE networks indicates that formal errors of EOP measurements are too small by a factor of 1.3-2.0. We have found evidence of systematic differences between the EOP measurements made by different networks. These differences appear as a statistically significant mean offsets between the EOP derived from the networks. For networks operating on consecutive days, some of this difference may be due to the interpolation between days. The source of the difference between EOP from the CORE-A and NEOS networks is not clear since these networks operate on the same day. It is possible that network geometry is producing these differences. The cause of these systematic differences is under active investigation.

## References

Ma, C., J. M. Sauber, L. J. Bell, T.A. Clark, D. Gordon, W. E. Himwich, and J. W. Ryan, Measurement of horizontal motions in Alaska using very long baseline interferometry, *J. Geophys. Res.*, 95(B1), 637-651, 1994.

Ryan, J. W., T. A. Clark, C. Ma, D. Gordon, D. S. Caprette, and W. E. Himwich, Global scale tectonic plate motions measured with CDP VLBI Data, in *Contributions of Space Geodesy to Geodynamics: Crustal Dynamics*, Geodyn. Ser., vol. 23, edited by D. E. Smith and D. L. Turcotte, pp. 37-49, AGU, Washington, D. C., 1993.

# Short-period variations of the Earth rotation parameters as seen by VLBI

H. SCHUH

Deutsches Geodätisches Forschungsinstitut (DGFI)  
Marstallplatz 8, D-80539 München, Germany  
schuh@dgfi.badw.de

O. TITOV

Saint-Petersburg State University,  
Bibliotechnayapl. 2, Peterhof, 198904 Saint-Petersburg, Russia  
oleg\_titov@usa.net

## Abstract

Modern geodetic VLBI experiments provide very accurate results of polar motion and UT1-UTC. More than 300 VLBI experiments (NEOS-A from 1993 till 1998, CONT'96, CORE) were analysed by the OCCAM 3.4 VLBI software using the least-squares collocation method (LSCM). The LSCM allows to estimate the Earth rotation parameters with a temporal resolution of 3-7 minutes. Wavelet transformations of the UT1-UTC and polar motion time series obtained by the VLBI solutions were done. Several irregular quasi-periodic variations were found besides the well known diurnal and semidiurnal periods. In many UT1-UTC data sets periods around 8 hours and between 5 and 7 hours can be seen. The results of two parallel VLBI sessions which took place since 1998 were compared in the high-frequency range. The wavelet analysis reveals interesting patterns in polar motion, too.

## 1. Introduction

The geodetic and geophysical interest in VLBI is based on the use of a quasi-inertial reference frame formed by a set of compact extragalactic radio sources. VLBI measures very accurately the angles between the Earth-fixed baseline vectors and the directions to the space-fixed radio sources. Thus, even the most subtle changes of the baseline lengths and of the baseline directions with respect to the inertial system can be detected. Geodynamical phenomena such as polar motion, Universal Time (UT1) variations, precession and nutation, Earth tides, ocean tidal response, and tectonic plate motions can be monitored with highest accuracy.

The UT1 variations are dominated by the seasonal terms, an annual and a semiannual oscillation; but there is also a rich spectrum of tidally induced short-period oscillations (Yoder et al., 1981), which could be seen by VLBI due to its increasing accuracy from mid of the eighties (Robertson et al., 1985; Campbell and Schuh, 1986). Even the short-period tidal influences of the oceans (Brosche et al., 1989) could be detected in the VLBI measurements by analysing a large number of observing sessions (Brosche et al., 1991). Today, a very high temporal resolution of the Earth rotation parameters can be achieved by VLBI using the least-squares collocation method (LSCM) (Titov, 1998). It allows to estimate the Earth rotation parameters every 3-7 minutes. This paper concentrates on short-period variations of the Earth rotation parameters which can be seen when analysing the VLBI results.

## 2. Earth rotation parameters observed by VLBI

More than 300 VLBI experiments (NEOS-A from 1993 till 1998, CONT'96, CORE) were analysed by the OCCAM 3.4 VLBI choosing the LSCM approach. Figure 1 shows UT-UTC1 parameters determined during five days of the VLBI campaign CONT in September 1996. In general there is a good agreement between the results obtained within this study and other VLBI solutions, e.g. the US Naval Observatory (USNO) hourly estimates. From the whole data set, i.e. from more than 300 sessions, the amplitudes of the main diurnal and semidiurnal UT1 variations due to the ocean tides were determined (Titov, 1998). They agree well with other empirical models, e.g. those given in the IERS Conventions (1996). After the ocean tidal influences were removed from the observed UT1-UTC series, the residuals offer the opportunity to search for even smaller variations in the rotation of the Earth. Those are supposed to be due to resonances with modes of the Earth or due to excitation by Earthquakes. Also the VLBI polar motion data sets provide the opportunity to investigate the very short periods.

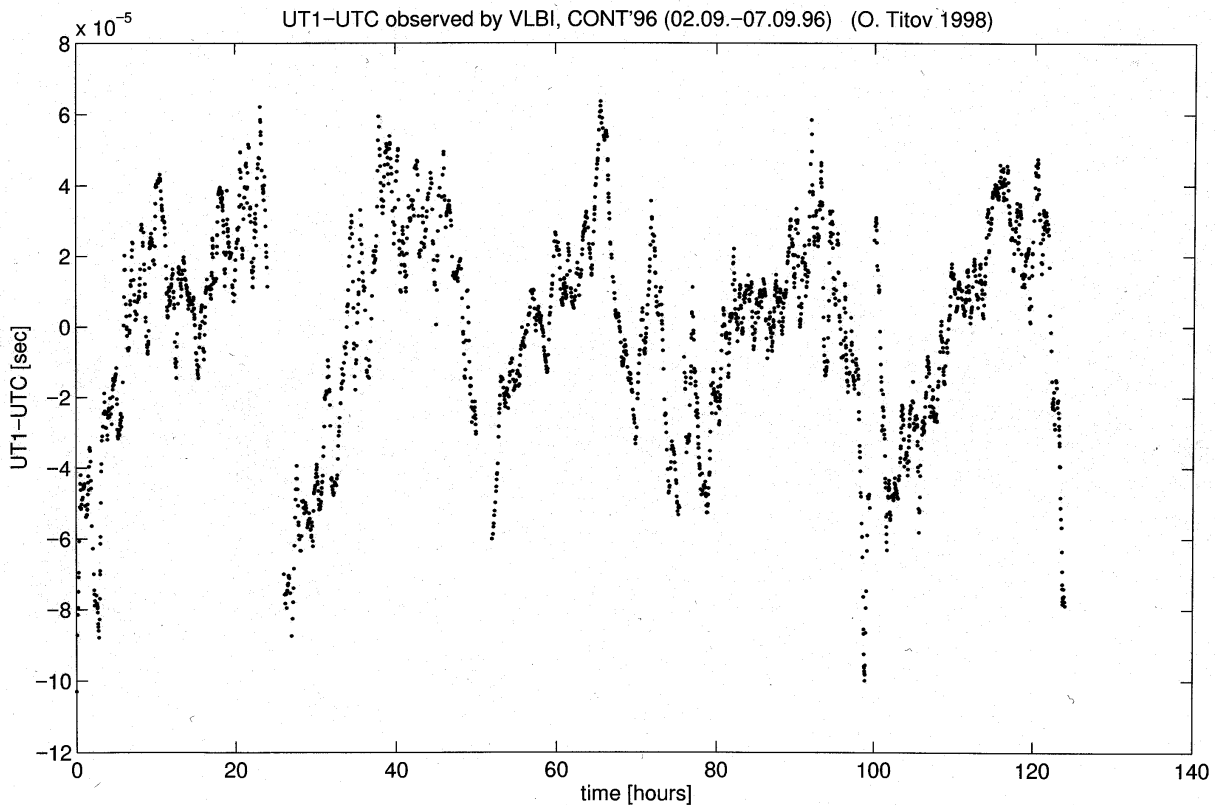


Fig. 1: UT1-UTC parameters with high temporal resolution determined during five days of the VLBI campaign CONT in September 1996.

## 3. Wavelet analysis of Earth rotation parameters

There are several remarkable advantages of the wavelet transform, which was introduced by Grossmann and Morlet (1984), in comparison with 'classical' methods based on the Fourier transform. In the wavelet transform, the harmonic oscillation is replaced by a wavelet function which is adapted to the signal to be analysed by shifting it along the time axis and scaling it along the frequency axis. It allows the time localization of an unstable quasi-periodic signal within a given data set. Hence, the wavelet transform is an excellent tool for analysing signals with time-varying amplitudes and/or periods.

Many of the high-resolution UT1-UTC data series and polar motion data series obtained by the VLBI solutions were analysed with respect to periodic variations. First, the main diurnal and semidiurnal variations due to the ocean tides were removed using the IERS Conventions (1996) correction model. Then, the wavelet transformation was applied. Although ocean tidal influences had been already corrected, many of the wavelet spectra of the UT1 series show residual energy in the diurnal and semidiurnal period range. This can be due to different reasons:

1. The IERS Conventions (1996) correction model is not good enough. It contains only the big diurnal and semidiurnal terms but neglects the smaller ones.
2. The ocean tidal influences on the rotation of the Earth are variable with time for each tide, i.e. they cannot be described by simple trigonometric functions with constant amplitudes and phases. Due to interactions between the ocean currents and the ocean tides it is rather likely that the ocean models have to become refined in the future.
3. There are other influences than ocean tides on the rotation of the Earth with diurnal and semidiurnal periods. These could be caused by the atmosphere for instance.

Additionally, most of the datasets revealed irregular quasi-periodic fluctuations, very often at 20 hours and 40 hours and also with extremely short periods, e.g. around 8 hours, between 5 and 7 hours and even down to 2 to 3 hours. After having subtracted the main ocean tidal terms from the CONT 1996 UT1-UTC series the wavelet spectrum was computed. In figure 2 it is plotted for very short periods below 10 hours.

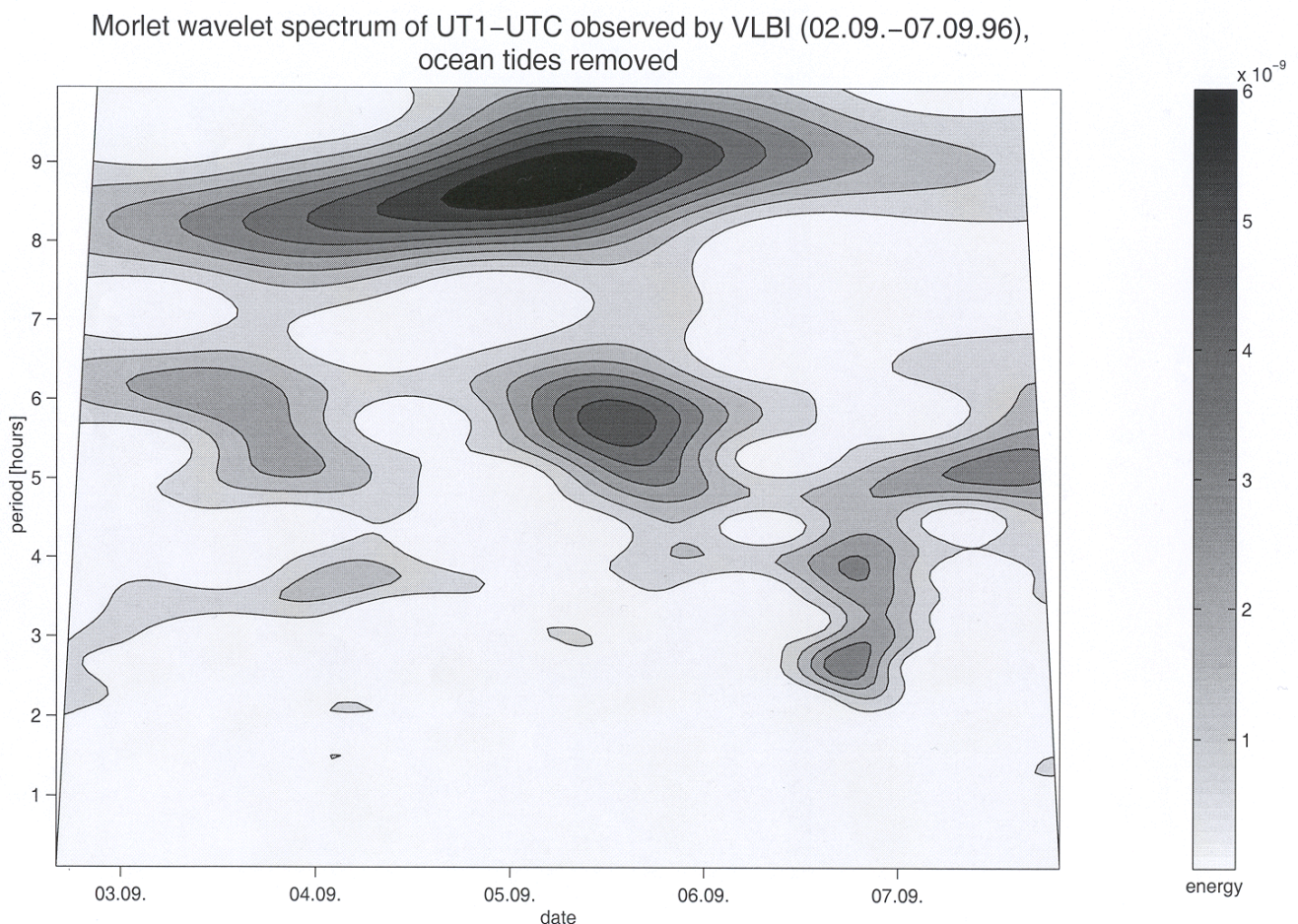


Fig. 2: Wavelet spectrum for periods below 10 hours of the high resolution UT1-UTC series shown in figure 1 (ocean tidal terms removed)

Parallel sessions on different VLBI networks which took place since 1998 offer the opportunity for independent observations of the Earth rotation and hence the wavelet spectra should contain the same variations of the Earth rotation parameters. Figures 3a,b show the results obtained by the VLBI NEOS-A network (Green Bank - Fortaleza - Kokee - Ny Alesund - Tigo) and the CORE-A network (Fairbanks - HartRAO - Hobart - Matera - Westford - Algonquin Park); both started from March, 24th, 1998, 18.00 to observe simultaneously for 24h (NEOS-A256 and CORE-A032). It should be noted that the two networks form two completely different VLBI 'observing systems', i.e. different radiosources were observed by different stations. As we are mainly interested in the short-period variations a comparison in the frequency domain was carried out. Figures 4a,b show the wavelet spectra of the UT1-UTC series obtained by the two VLBI sessions: both agree rather well - in particular a dominant variation around 8 hours can be seen which decreases in the second part of the sessions. As these are the only parallel VLBI sessions which have been analysed so far, further comparisons have to be done.

The VLBI solutions using the LSCM yielded also high-resolution polar motion series. These were analysed as complex values by the wavelet transformation. The wavelet spectra revealed irregular prograde and retrograde short-period fluctuations in polar motion, again very often around 8 hours and even with shorter periods, e.g. at 5-7 hours.

#### **4. Conclusions**

VLBI is unique in its ability to monitor without hypotheses *all* components of Earth orientation. The results of VLBI experiments can be used for scientific research in many areas, such as: tidal deformation of the solid Earth and oceanic and atmospheric tidal loading, excitation of UT1 and polar motion down to periods of a few minutes, investigations of the Earth interior and improvements of the terrestrial reference frame. The Earth rotation data observed by VLBI have begun to reveal hitherto unseen phenomena. Irregular quasi-periodic variations can be seen in the wavelet spectra besides the well known diurnal and semidiurnal periods. Possible excitation mechanisms for the observed variations of the Earth rotation parameters such as terdiurnal variations, the free oscillations of the oceans (10h, 20h, 40h, 50h), atmospheric modes and resonances with free oscillations of the Earth (e.g. the Slichter mode) are under discussion. Careful tests have to be done to check the significance of such tiny variations. In particular, correlations with meteorological parameters at the observing stations are going to be investigated.

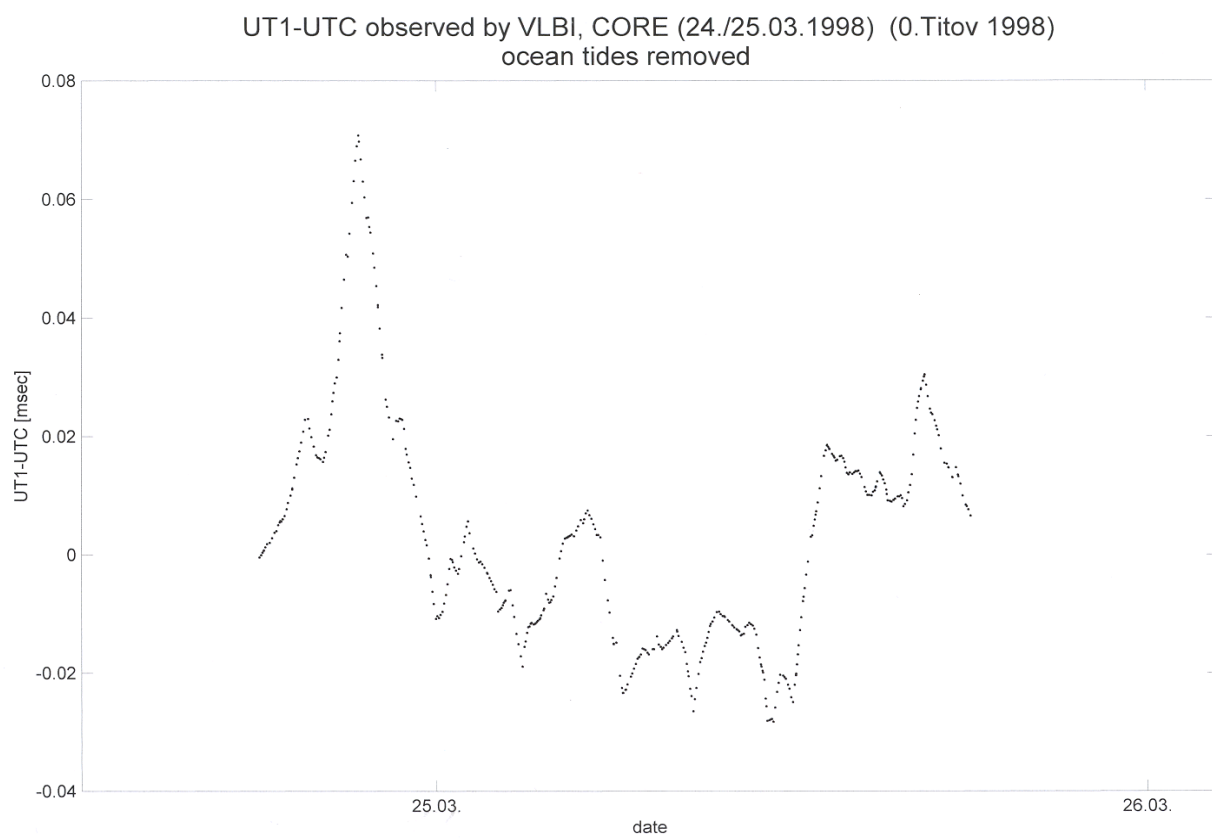
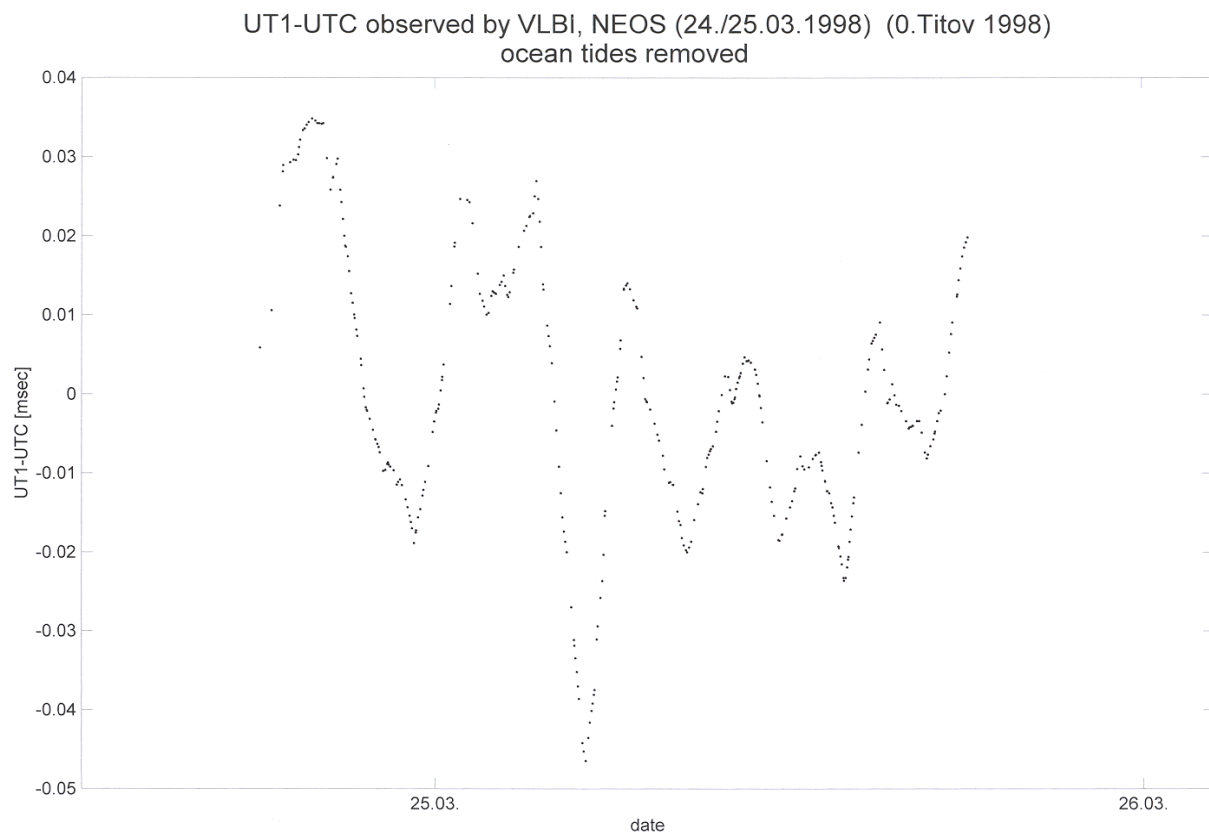


Fig. 3a,b: UT1-UTC parameters with high temporal resolution determined by two parallel VLBI sessions starting on March 24th, 1998 (lower plot: CORE-A032, upper plot: NEOS-A256)

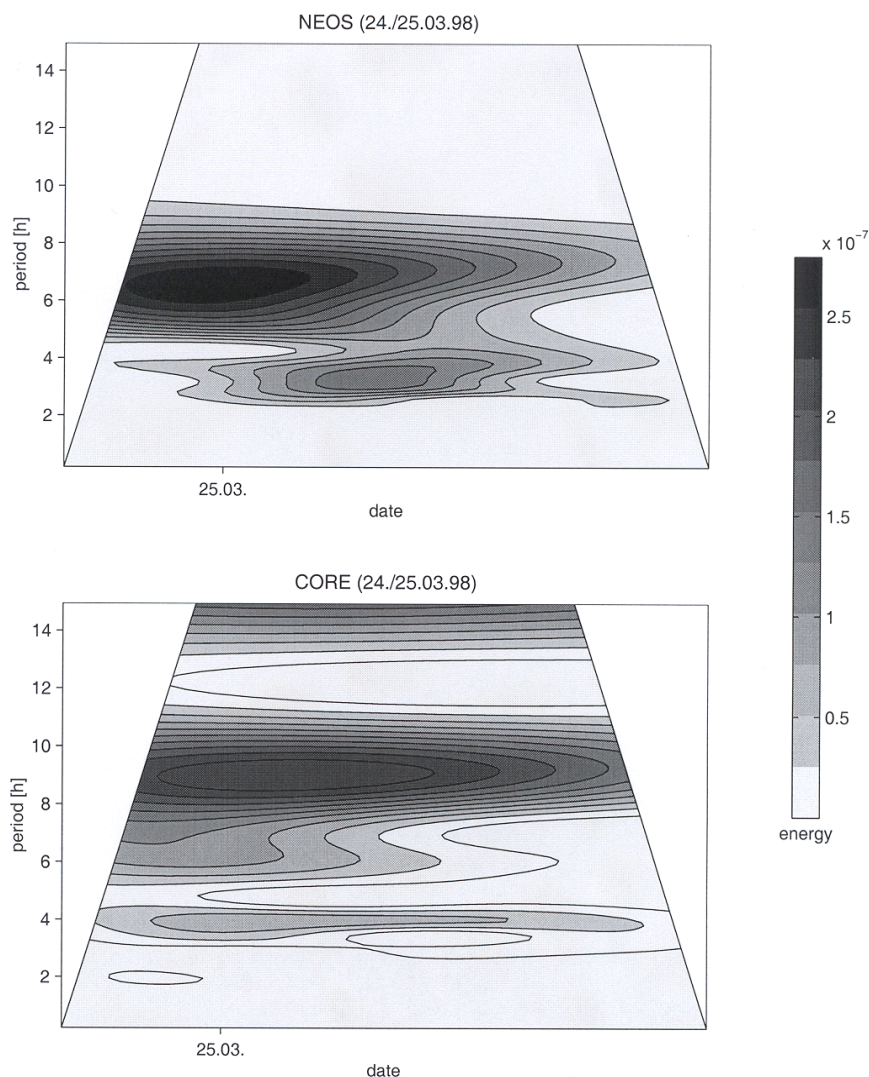


Fig. 4a,b: Wavelet spectra for periods shorter than 15 hours of the two time series shown in figure 3a,b

## 5. References

- Brosche, P., U. Seiler, J. Sündermann and J. Wunsch: Periodic changes in Earth's rotation due to oceanic tides, *Astronomy and Astrophysics*, 220, 318-320, 1989.
- Brosche, P., J. Wunsch, J. Campbell and H. Schuh: Ocean tide effects in Universal Time detected by VLBI, *Astronomy and Astrophysics*, 245, 676-682, 1991.
- Campbell, J. and H. Schuh: Short-period variations of Earth rotation determined by VLBI, *Proc. of the Xth International Symp. on Earth Tides, Madrid, 1985*, ed. by R. Vieira, C.S.I.C., 943-951, 1986.
- Grossmann, A. and J. Morlet: Decomposition of Hardy functions into square integrable wavelets of constant shape, *SIAM J. Math. Anal.*, 15(4), 723-736, 1984.
- Robertson, D.S., W.E. Carter, J. Campbell and H. Schuh: Daily Earth rotation determinations from IRIS very long baseline interferometry, *Nature*, 316, 424-427, 1985.
- Titov, O.: Least squares collocation method (LSCM) for space geodetic data analysis. *Proc. of the IAG Symposium 'Towards an Integrated Global Geodetic Observing System' (IGGOS), Munich, 1998*.
- Yoder, C.E., J.G. Williams and M.E. Parke: Tidal variations of Earth rotation, *J. Geophys. Res.*, 86, 881-891, 1981.
- ... IERS Conventions (1996) ed. by D. D. McCarthy, IERS Technical Note 21, Observatoire de Paris, 1996.

# The effect of ocean tide loading on the determination of earth rotation parameters

Rüdiger Haas and Hans-Georg Scherneck

Onsala Space Observatory (OSO), SE-439 92 Onsala, Sweden, (geo@oso.chalmers.se)

## Abstract

One of the main reasons to do space geodetic observations for instance by using geodetic Very Long Baseline Interferometry (VLBI) is to acquire scientific data for earth rotation studies. The analysis of space geodetic observations requires completeness in the modeling of earth deformation effects. This includes as the largest contributions solid earth tides and ocean tide loading. We concentrate on the effect of modeling errors in ocean tide loading on the estimated earth rotation parameters. Particularly, neglecting the horizontal components of ocean tide loading perturbs the estimated earth rotation parameters on daily and subdaily time scale. Predictions and observations of this influence in the frequency and the time domain are compared and discussed in this paper for different geodetic VLBI networks.

## 1 Introduction

Geodynamic processes deforming the solid earth, displacing masses in the hydrosphere, atmosphere and the earth's core influence the earth's rotational behavior. One way to investigate these processes is to infer the driving mechanisms from studies of earth orientation variations. For this purpose space geodetic techniques like Very Long Baseline Interferometry (VLBI), Global Positioning System (GPS), Satellite Laser Ranging (SLR) and Lunar Laser Ranging (LLR) are used to measure earth rotation parameters.

In the analysis of space geodetic data all known earth deformation effects have to be accounted for. This includes the solid earth tides, and as the second largest effect ocean tide loading, on which we concentrate in this paper. Software packages for the analysis of geodetic VLBI data, e.g. CALC/SOLV/GLOBL [Ma et al., 1990], MODEST [Sovers and Jacobs, 1996], contain modules to compute ocean tide loading effects since many years. But software packages for other techniques, e.g. the Bernese analysis software for GPS data, only recently included this effect [Rothacher, 1998, pers. comm.].

Horizontal ocean tide loading displacements are smaller by a factor of 3 to 10 than the vertical ones but are of special importance for the study of polar motion and UT1 (PMU). Mismodeling of horizontal ocean tide loading in the analysis of space geodetic data introduces a common rotation of the network of space geodetic sites. The determined polar motion and UT1 parameters will be contaminated due to this mismodeling. We call this effect 'virtual PMU variations' (VPMU). These are mainly semidiurnal and diurnal oscillations since ocean tide loading occurs mainly in these frequency bands. The effects are especially important for sparse networks with a small number of participating stations. As the number of stations of the network increases, the common rotation mode becomes more and more rejected and will converge to zero in a continuum situation.

In our paper we predict virtual PMU variations in the frequency and the time domain for the worst case of a complete neglect of horizontal ocean tide loading and compare the predictions to results obtained from the analysis of geodetic VLBI data. We also show that differences in existing ocean tide loading models can introduce 'model dependent virtual PMU variations' (MD-VPMU) with significant magnitude. Regarding expectation of future measurement accuracy in particularly VLBI they appear to be significant.

## 2 Ocean tide loading

The earth's crust is affected by the load of oceanic masses which are redistributed by ocean tides. The crust deforms mainly elastically to this load and site displacement of several centimeters for the vertical and a tenth to a third of it for the horizontal component are induced. Ocean tides are coherent in frequency with the solid earth tides but due to the geometry of the oceanic basins and hydrodynamic resonance effects they show a complicated geographic distribution. So the resulting ocean tide loading effects are strongly site dependent.

Usually this complex hydrodynamic problem is parameterized in a site dependent ocean tide loading model, and a number of amplitude and phase parameters are determined for each site. The loading parameters are computed using tidal amplitudes and phases from ocean tide models and Green's functions. Usually the 11 most important tides are treated individually, and the others can optionally be interpolated on the basis of the admittance spectrum. We will concentrate in the following on the three ocean tide loading models by *Scherneck* [1991, 1996] which are based on the ocean tide models by *Schwiderski* [1980], *Le Provost et al.* [1994] and on the CSR3.0 ocean tide model [*Eanes and Bettadpur*, 1995] and will be called M-S, M-L and M-C, respectively.

Figure 1 shows radial ocean loading amplitudes for the  $M_2$  tide in the Atlantic ocean area according to the ocean loading model M-L based on the ocean tide model by *Le Provost et al.* [1994]. Strong loading effects occur in western Europe, at the east coast of North American and the north-east coast of South America.

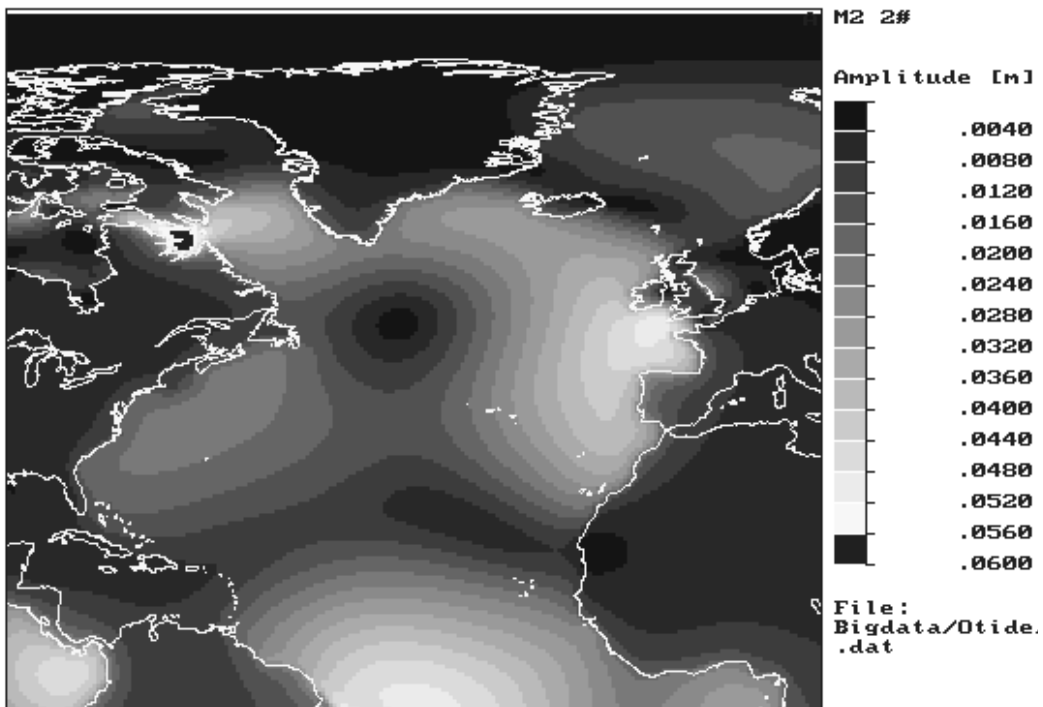


Fig. 1: Vertical ocean tidal loading for the  $M_2$  tide according to the model M-L by *Scherneck* [1996] based on the ocean tide model by *Le Provost et al.* [1994]

Table 1 shows ocean tide loading amplitudes and phases of the strongest tide ( $M_2$ ) for the VLBI stations Fortaleza (Brazil) and Westford (USA). The latter site on the north-east coast of the USA is frequently used in geodetic VLBI observations for Earth rotation studies. The inclusion of the Gulf of Maine in the ocean tide models is an importance difference between the three ocean tide loading

models. The more recent ocean tide models by *Le Provost et al.* [1994] and *Eanes and Bettadpur* [1995] do not include this ocean basin which is strongly resonant near the  $M_2$  tide frequency [*Greenberg, 1987*] while the older ocean tide model by *Schwiderski* [1980] does.

Tab. 1: Ocean tidal loading models for Fortaleza (Brazil) and Westford (USA): (u)p, (e)ast and (n)orth components, amplitudes  $A$  in [mm] and phases  $\Phi$  in  $^\circ$  for the  $M_2$  tide. The models are: 1 Model M-S based on *Schwiderski* [1980], 2 Model M-L based on *Le Provost et al.* [1994], 3 Model M-C based on *Eanes and Bettadpur* [1995].

site	tide	component	M-S <sup>1</sup>		M-L <sup>2</sup>		M-C <sup>3</sup>	
			A [mm]	$\Phi$ [ $^\circ$ ]	A [mm]	$\Phi$ [ $^\circ$ ]	A [mm]	$\Phi$ [ $^\circ$ ]
Fortaleza	$M_2$	u	32.67	39.7	36.01	34.0	37.63	34.3
		e	3.13	28.8	4.69	16.4	4.97	20.8
		n	5.35	62.9	5.08	51.0	5.64	51.9
Westford	$M_2$	u	10.24	185.0	8.24	162.4	8.15	165.4
		e	4.21	215.2	2.58	212.0	2.75	208.3
		n	2.25	324.4	1.62	350.3	1.67	354.9

From the ocean tide loading models M-S, M-L and M-C maximum absolute effects of site displacement can be calculated which is shown in Table 2 for frequently used geodetic VLBI sites. For these stations the maximum peak displacements can reach 70 mm and 12 mm for the vertical and horizontal components, respectively.

Tab. 2: Maximal ocean tide loading effects (u)p, (e)ast and (n)orth in [mm] for frequently used geodetic VLBI sites. See Table 1 for description of the models.

VLBI site	M-S			M-L			M-C		
	u	e	n	u	e	n	u	e	n
Algonquin (Canada)	15.4	5.1	1.5	16.5	4.6	1.2	16.1	4.8	1.4
Fortaleza (Brazil)	61.4	7.0	11.2	67.8	9.1	11.3	70.5	9.6	11.9
Gilmore Creek (USA)	25.0	3.5	10.2	26.9	3.9	10.9	28.6	3.6	10.6
Green Bank (USA)	17.9	5.9	1.4	18.3	5.1	1.0	18.2	5.4	1.0
Hartebeesthoek (South Africa)	32.7	3.4	3.3	36.0	2.5	3.8	33.9	2.9	3.7
Hobart (Australia)	32.4	10.5	6.0	32.9	9.8	6.0	33.1	10.1	5.9
Kokee Park (USA)	41.6	9.5	11.0	43.4	9.5	11.5	48.3	9.8	11.9
Ny Ålesund (Norway)	21.4	5.9	4.2	23.5	5.8	5.1	24.1	6.1	5.2
Onsala (Sweden)	12.0	3.7	2.2	11.6	3.8	2.4	11.8	3.7	2.4
Westford (USA)	25.4	7.5	4.6	22.9	5.1	3.5	23.3	5.5	3.9
Wettzell (Germany)	12.0	3.7	2.2	11.6	3.8	2.4	11.8	3.7	2.4
Yellowknife (Canada)	17.3	7.3	3.9	18.7	7.6	4.1	19.5	7.5	3.7

### 3 Predicting virtual PMU variations

Two realizations of a space geodetic networks consisting of a finite set of observing stations give different results for polar motion and UT1 depending on how the horizontal ocean tide loading is modeled. The differences will be in the frequency spectrum of the ocean tide loading, so the largest effects are to be expected in the semidiurnal and diurnal frequency range. The worst case is the complete neglect of horizontal ocean tide loading while the second worse case is mismodeling of the horizontal ocean tide loading effects.

The effects can be predicted using usual Helmert transforms. We transform the amplitude and phases of horizontal ocean tide loading for the stations participating in a geodetic VLBI network into a common rotation of the network which can be described by three rotation angles corresponding to polar motion and UT1. So for each tide included in ocean tide models a set of three rotation angles can be derived. Usually 11 main tides are included in ocean tide loading models, so 11 times three rotation angles can be derived from the Helmert transforms. From this representation in the frequency domain it is easy to calculate time series of virtual PMU variations for any period of interest.

Table 3 shows as an example amplitudes of prograde and retrograde polar motion and amplitudes of UT1 for the NEOS-A network consisting of the five stations Fortaleza, Green Bank, Kokee Park, Ny Ålesund and Wettzell for the case that ocean tide loading according to model M-S based on the ocean tide model by Schwiderski [1980] is neglected completely. The amplitudes for virtual PMU variations reach values of 50  $\mu\text{as}$  and 1.5  $\mu\text{sec}$ , respectively.

Tab. 3: Frequency domain representation of virtual PMU variations for the NEOS-A geodetic VLBI network. Shown are amplitudes of polar motion (prograde and retrograde) in [ $\mu\text{as}$ ] and UT1 variations in [ $\mu\text{sec}$ ] due to the neglect of horizontal ocean tide loading according to model M-S.

tide	polar motion				UT1	
	prograde		retrograde		$A_1$	$A_2$
	$Ap_1$	$Ap_2$	$Ar_1$	$Ar_2$		
$M_2$	-10.3	24.9	-52.3	19.8	0.8	1.9
$S_2$	1.0	7.4	-19.3	-2.9	0.4	0.6
$N_2$	-4.0	5.1	-9.9	6.4	0.0	0.4
$K_2$	1.0	1.3	-4.8	-1.3	0.0	0.1
$K_1$	3.4	-10.7	-5.6	-8.3	-1.3	1.0
$O_1$	3.5	-5.1	-6.6	-2.2	-1.5	0.1
$P_1$	1.1	-3.3	-1.8	-2.4	-0.4	0.3
$Q_1$	0.7	-1.3	-1.7	-0.2	-0.3	-0.1
$Mf$	0.8	-1.4	1.6	-1.1	0.1	0.0
$Mm$	0.3	-0.7	0.5	-0.4	0.1	0.0
$Ssa$	0.3	0.2	1.2	-1.3	0.2	-0.1

In a similar way model dependent virtual PMU variations (MD-VPMU) can be calculated by Helmert transform. Here we transform the differences in the horizontal ocean tide loading according to the different models into virtual rotations.

Maximum effects for VPMU variations and MD-VPMU variations can be calculated and are shown in Table 4 for different geodetic VLBI networks used for earth rotation studies. The VLBI networks are IRIS-S (Fortaleza, Gilmore Creek, Hartebeesthoek, Westford, Wettzell), NEOS-A (Fortaleza, Green Bank, Kokee Park, Ny Ålesund, Wettzell), CORE-A (Algonquin, Gilmore Creek, Hartebeesthoek, Hobart, Matera, Westford) and CORE-B (Algonquin, Fortaleza, Gilmore Creek, Goldstone, Kashima,

Onsala, Wettzell, Yellowknife). The values are maximum values for a time period of 20 years and assume ideal geometry and parameter estimation. The maximum values for VPMU reach 190  $\mu\text{as}$  and 130  $\mu\text{as}$  for  $x_p$  and  $y_p$ , respectively and 10  $\mu\text{sec}$  for UT1, the maximum values for MD-VPMU reach 40  $\mu\text{as}$  and 25  $\mu\text{as}$  for  $x_p$  and  $y_p$ , respectively, and nearly 3  $\mu\text{sec}$  for UT1. Since hourly estimates for polar motion and UT1 have formal errors of about 120  $\mu\text{as}$  and 8 $\mu\text{sec}$ , respectively [Gipson, 1996], the predicted VPMU are within the resolving power of the observations. The MD-VPMU are small compared to the present day accuracies and so cannot be detected today. However the effects may exceed the detection threshold with the expected increase of accuracy in VLBI in the CORE program [Clark et al., 1997].

Tab. 4: Maximal VPMU and MD-VPMU variations due to the neglect or differences of horizontal ocean tide loading, respectively for different VLBI networks. Polar motion is given in [ $\mu\text{as}$ ], UT1 in [ $\mu\text{sec}$ ]. VPMU variations are calculated from neglect of 1 model M-S, 2 model M-L and 3 model M-C. MD-VPMU variations are calculated exchanging 4 model M-S and M-L, 5 model M-S and M-C and 6 model M-L and M-C. See text for the description of the VLBI networks.

Network		$V_S^1$	$V_L^2$	$V_C^3$	$D_{SL}^4$	$D_{SC}^5$	$D_{LC}^6$
IRIS-S	$x_p$	185.3	187.2	188.6	28.4	24.6	12.4
	$y_p$	67.9	66.7	71.2	11.2	12.1	11.3
	UT1	5.5	7.1	8.1	2.1	2.9	1.1
NEOS-A	$x_p$	110.8	114.8	123.7	23.2	29.5	11.8
	$y_p$	125.8	123.9	130.5	25.2	12.9	16.6
	UT1	6.8	7.0	7.7	2.5	2.4	0.8
CORE-A	$x_p$	116.7	103.9	96.8	40.2	35.7	11.7
	$y_p$	40.7	33.2	32.5	15.7	17.5	5.4
	UT1	5.3	6.3	6.3	1.6	1.3	0.6
CORE-B	$x_p$	135.4	135.0	131.4	32.2	25.4	16.2
	$y_p$	70.6	72.7	81.8	13.0	17.1	17.6
	UT1	8.3	9.7	9.9	2.0	2.0	0.7

## 4 Comparing predictions to results from VLBI analyses

In this chapter we describe the work we did concerning the comparison of predicted and observed VPMU variations. We concentrated on the worst case, the complete neglect of horizontal ocean tide loading. The comparisons were performed in the frequency and in the time domain.

For the comparison in the frequency domain we used the data of IRIS-S network. Since there has been some changes in the network configuration during the years we had to find a set of stations representing the IRIS-S network. We chose the four stations Fortaleza, Hartebeesthoek, Westford and Wettzell because they participated in most of the sessions. With this set of stations we predicted amplitudes of VPMU in the frequency domain according to M-S using Helmert transforms as described before.

We used the IRIS-S data set from 1986 to 1998 to derive high frequent polar motion and UT1 values at tidal frequencies. Radio source coordinates, station coordinates and velocities were fixed to the most recent global VLBI solution by Goddard Space Flight Center [Ma and Ryan, 1998] as well as polar motion UT1 and nutation. Clock and atmosphere parameters were estimated piecewise linearly for each session and high frequent polar motion and UT1 amplitudes as global parameters. We prepared two solutions, one applying horizontal and vertical ocean tide loading according to M-S and one

applying only vertical ocean tide loading according to M-S. Then we calculated the differences of the results for the high frequency polar motion and UT1 amplitudes determined in these two solutions. Table 5 shows predictions and observations for virtual PMU variations due to neglect of horizontal ocean tide loading according to M-S for the 2 strongest tides in the semidiurnal and the diurnal frequency band for the IRIS-S network.

Tab. 5: Predicted and observed VPMU variations in the frequency domain for the two strongest tides in the semidiurnal and diurnal frequency band due to neglect of horizontal ocean tide loading according to model M-S for the IRIS-S network.

polar motion, prograde					polar motion, retrograde			
tide	predicted		observed		predicted		observed	
	$Ap_1$ [ $\mu\text{as}$ ]	$Ap_2$ [ $\mu\text{as}$ ]	$Ap_1$ [ $\mu\text{as}$ ]	$Ap_2$ [ $\mu\text{as}$ ]	$Ar_1$ [ $\mu\text{as}$ ]	$Ar_2$ [ $\mu\text{as}$ ]	$Ar_1$ [ $\mu\text{as}$ ]	$Ar_2$ [ $\mu\text{as}$ ]
$M_2$	-21.2	50.3	$-3.8 \pm 12.1$	$22.9 \pm 12.0$	-43.8	-20.9	$-25.4 \pm 12.2$	$-18.2 \pm 12.3$
$S_2$	2.7	13.3	$5.6 \pm 12.2$	$5.2 \pm 11.6$	-11.0	-14.8	$-6.3 \pm 12.4$	$-14.7 \pm 11.8$
$K_1$	8.9	4.5	$-15.3 \pm 14.0$	$-5.6 \pm 14.9$	-11.1	-8.5	$-13.9 \pm 14.1$	$19.9 \pm 15.0$
$O_1$	4.9	1.4	$-6.0 \pm 14.5$	$6.9 \pm 14.3$	-1.8	-2.8	$-5.3 \pm 14.5$	$-19.0 \pm 14.6$
UT1								
tide	predicted		observed					
	$A_1$ [ $\mu\text{sec}$ ]	$A_2$ [ $\mu\text{sec}$ ]	$A_1$ [ $\mu\text{sec}$ ]	$A_2$ [ $\mu\text{sec}$ ]				
$M_2$	-1.6	1.6	$-3.4 \pm 1.2$	$-0.5 \pm 1.2$				
$S_2$	-0.7	0.6	$-1.7 \pm 1.2$	$-0.4 \pm 1.1$				
$K_1$	0.2	-0.1	$0.2 \pm 1.4$	$0.8 \pm 1.4$				
$O_1$	-0.2	-0.2	$-1.5 \pm 1.4$	$-0.3 \pm 1.4$				

The comparison in the frequency domain shows that the predicted effects can be verified to a large extent. The neglect of horizontal ocean tide loading introduces amplitudes of VPMU variations similar to the predicted values. The semidiurnal tides show a better agreement than the diurnal ones. However, the agreement is not perfect which should not be surprising since the predictions as based on idealized assumptions as to source geometry and independence of estimated parameters. This is not true in the real-world case. The IRIS-S network configuration has been changing over the years and a perfect geometry is not given due to visibility constraints that lead to subnetting in the network observations.

For the comparison in the time domain we used the intensive CONT94 campaign. The results of this comparison have been described in *Scherneck and Haas [1999]* and will only be summarized here briefly. We predicted VPMU variations for the CONT94 observations and compared the predictions to results from VLBI data analysis. For the analysis we estimated hourly polar motion and UT1 values once with vertical and horizontal ocean tide loading and once only with vertical ocean tide loading. The differences between the hourly PMU were compared to the predicted values.

The observed VPMU variations show typical tidal behavior in the semidiurnal and diurnal frequency bands and are similar to the predicted effects. The observed effects are larger than the predicted ones by a factor of 2–3 and appear to have a complicated frequency dependence since diurnal variations are less attenuated than semidiurnal ones. The reason for these discrepancies is most probably again as above, namely idealized conditions in the computation of the predictions.

## 5 Conclusions

This study shows the importance of horizontal ocean tide loading for the determination of polar motion and UT1 (PMU) with space geodetic techniques. A geodetic network consisting of a finite number of participating stations exhibits a common rotation mode due to horizontal ocean tide loading which is not negligible. Neglect of horizontal ocean tide loading in the analysis of space geodetic data contaminates the derived polar motion and UT1 values in form of small periodic rotations that have similar character as the influences coming from matter and motion perturbations in the ocean tide via rotation dynamics.

We predicted virtual PMU variations due to neglect of horizontal ocean tide loading in the frequency and the time domain and verified these predictions by analysis of geodetic VLBI data. Other space geodetic methods, e.g. GPS will be affected in the same way, of course.

Differences in existing ocean tide models have predicted effects on virtual PMU variations of up to 40  $\mu$ as and 3  $\mu$ sec for polar motion and UT1, respectively. They will be of importance for future earth rotation studies considering the expected accuracies of e.g. the CORE program. Today these tiny effects are still too small to be detected, but in the future they are likely to reach the detection threshold.

For the analysis of space geodetic data the best available ocean tide loading models should be used. Comparison of existing theoretical ocean tide loading models to empirical results from VLBI [e.g. *Sovers*, 1994, *Haas* and *Schuh*, 1998] and GPS are useful to verify and/or refine ocean tide loading models.

**Acknowledgements.** Figures in this paper were made with GMT software [*Wessels* and *Smith*, 1995]. This research has made use of NASA Goddard Space Flight Center's VLBI terrestrial reference frame solution number 1102g, 1998 August. Rüdiger Haas is supported by the European Union within the TMR programme under the contract FMRX-CT960071. This project is supported by grants from the Natural Science Research Council of Sweden under account G-AA/GU 03590.

## References

- Clark, T.A., C. Ma, J.W. Ryan, B.F. Chao, J.M. Gipson, D.S. MacMillan, N.R. Vandenberg, T.M. Eubanks and A.E. Niell, Earth Rotation Measurement Yields Valuable Information About the Dynamics of the Earth System, *EOS Trans., Amer. Geophys. U., Vol. 79(17)*, 1998
- Eanes, R.J., and S. Bettadpur, The CSR 3.0 global ocean tide model, *Technical Memorandum, CSR-TM-95-06*, Center for Space Research, 1995
- Gipson, J.M., Very long baseline interferometry determination of neglected tidal terms in high-frequency Earth orientation variation, *J. Geophys. Res.*, 101, 28051-28064, 1996
- Greenberg, D.A., Modeling tidal power, *Sc. American* 257:5, 106-113, 1987
- Haas, R. and H. Schuh, Ocean Loading Observed by Geodetic VLBI, *Proc. of the XIIIth Int. Symp. on Earth Tides, Brussels, July 1997*, Ducarme (ed.), 111-120, Observatoire Royal de Belgique, 1998
- Le Provost, C., M.L. Genco, F. Lyard, P. Vincent, and P. Canceil, Spectroscopy of the world ocean tides from a finite element hydrodynamic model, *J. Geophys. Res.*, 99, 24777-24797, 1994
- Ma, C. and J.W. Ryan, NASA Space Geodesy Program – GSFC DATA Analysis – 1998, VLBI Geodetic Results 1979-1998, August, 1998
- Ma, C., J.M. Sauber, L.J. Bell, T.A. Clark, D. Gordon, and W.E. Himwich, Measurement of horizontal motions in Alaska using very long baseline interferometry, *J. Geophys. Res.*, 95, 21991-22011, 1990
- Ray, R.D., D.J. Steinberg, B.F. Chao and D.E. Cartwright, Diurnal and Semidiurnal Variations in the Earth's Rotation Rate Induced by Oceanic Tides, *Science*, 264, 830-832, 1994
- Scherneck, H.-G., A parameterized Solid Earth Tide Model and Ocean Tide Loading Effects for Global Geodetic Baseline Measurements, *Geophys. J. Int.*, 106, 677-694, 1991

- Scherneck, H.-G., A comprehensive and tentatively complete summary of oceanic effects in space geodetic baseline measurements, *Proceedings of the 11th Working Meeting on European VLBI for Geodesy and Astrometry*, G. Elgered (ed.), Research Report No 177, Onsala Space Observatory, Chalmers University of Technology, 121-133, 1996
- Scherneck, H.-G. and R. Haas, Effect of horizontal displacements due to ocean tide loading on the determination of polar motion and UT1, *Geophys. Res. Lett.*, 26, 501-504, 1999
- Schwiderski, E.W., On charting global ocean tides, *Rev. Geophys. Space Phys.* 18, 243-268, 1980
- Sovers, O.J., Vertical Ocean Loading Amplitudes from VLBI Measurements, *Geophys. Res. Lett.*, 21, 357-360, 1994
- Sovers, O.J., and C.S. Jacobs, Observation Model and Parameter Partial for the JPL VLBI Parameter Estimation Software "MODEST"-1996, *JPL Publication 83-39, Rev. 6*, JPL, 1996
- Wessels, P., and W.H.F. Smith, Free software helps map and display data, *EOS Trans., Amer. Geophys. U.*, Vol. 55, 293-305, 1991

## TECTONIC MOTION OF EUROPEAN VLBI SITES

*O. Titov*

*Saint-Petersburg State University*

*Bibliotechnaya sq., 2 Peterhof, Saint-Petersburg, 198904, Russia*

*e-mail: oleg\_titov@usa.net*

### 1. Introduction

VLBI sites in Europe show very complex motion due to tectonic processes. Regular VLBI sessions help us to trace a individual drift of each site as well as a general overview of the whole network. The sessions have been processed using OCCAM software [Titov, Zarraoa, 1997]. Evolution of European baselines is resulted. Rates of baselength evolution are compared with GSFC ones obtained using CALC/SOLVE software system [Caprette et al., 1990]. Evolution of Ny-Alesund VLBI site is considered in details. Rates of the station component drift are presented. It is concluded that the motion of some VLBI sites can not be approximated by conventional NNR-NUVEL-1A model [DeMets et al., 1994].

### 2. Observational data and procedure for adjustment

To analyze a tectonic motion of VLBI sites 39 observational sessions on European network (from 26 January 1990 till 17 August 1998) have been processed using OCCAM software. All reductions were made in accordance with IERS Conventions 1996 [McCarthy, 1996]. Kalman filter approach has been used to adjust individual sessions. ICRF 96 system fixed celestial reference frame, IRTF96 positions and NNR-NUVEL-1A velocities approximated the sites motion. VLBI station Wettzell was a reference one for all sessions. Nutation offset to IAU 1980 model, clock offsets and rates as well as wet troposphere delays are estimated. Random walk stochastic model is applied for clock and troposphere parameters approximation.

Next step I analyzed an evolution of baselines using conventional weighted least squares procedure. Baselength for epoch 1999.0 as well as baselength rate were estimated only.

To study a motion of Ny-Alesund VLBI site I have processed 116 observational sessions on different networks (from 04 October 1994 till 01 December 1998) using the same approached as mentioned above. Vertical, latitude and longitude components were estimated for each observational epoch. Temporal evolution of the components is considered.

### 3. Evolution of European baselines

Table 1 shows a velocity rates for 15 European baselines which have long history of observations (more than five years). They are compared with rates from NASA GSFC global solution August, 1998 [Ma, Ryan, 1998]. The GSFC values were obtained using SOLVE software from all VLBI data files (not European network only). Therefore a standard deviations in second column are better. Both set of rates are in perfect agreement. The OCCAM solution also coincides with other ones specially for European network [for example, Tomasi et al., 1997]. Obviously, the velocity rates do not depend on choice of VLBI

network under process. One can make a conclusion that the OCCAM results in Table 1 are reliable.

NNR-NUVEL-1A model considers all VLBI sites on European tectonic plate exception Noto. In accordance with the model almost all baseline rates should be equal to zero. Nevertheless, the observational rates in Table 1 demonstrates a significant deviation from NNR-NUVEL-1A. Only three baselines made up by Wettzell, Onsala and DSS65 sites look close to the model. All Italian VLBI sites (Medicina, Matera, Noto) approaches to Central Europe. South part of Italy (Matera, Noto) approaches to North part (Medicina) as well. NNR-NUVEL-1A model predicts rate -6.6 mm/year for baseline Matera – Noto which looks more stable. It appears that Matera and Noto should be put on the same tectonic plate. Nevertheless, the complex general motion of Adriatic region to be taken into account for correct modeling of International Terrestrial Reference Frame (ITRF). Probably, more adequate to present-day geodetic results Actual Plate Kinematic Model (APKIM) [Drewes, 1998] would be more appropriate for the purpose.

Baseline	Rate and 3 $\sigma$ error from OCCAM (mm/year)	Rate and 3 $\sigma$ error from SOLVE (mm/year)
Wettzell - Onsala	-0.5 +/- 1.0	-0.4 +/- 0.3
Wettzell - Medicina	-2.4 +/- 0.7	-2.6 +/- 0.6
Wettzell - Matera	-4.1 +/- 1.1	-4.0 +/- 0.6
Wettzell - DSS65	0.0 +/- 1.0	0.5 +/- 0.6
Wettzell - Noto	-5.1 +/- 1.0	-5.1 +/- 0.6
Onsala - Medicina	-2.5 +/- 0.9	-2.7 +/- 0.9
Onsala - Matera	-4.5 +/- 1.3	-4.2 +/- 0.9
Onsala - DSS65	0.0 +/- 1.5	0.3 +/- 0.9
Onsala - Noto	-5.1 +/- 1.1	-4.3 +/- 0.9
Medicina - Matera	-1.8 +/- 0.8	-1.6 +/- 0.6
Medicina - DSS65	2.1 +/- 1.4	2.3 +/- 0.6
Medicina - Noto	-3.7 +/- 0.9	-2.9 +/- 0.9
Matera - DSS65	1.7 +/- 2.0	1.4 +/- 1.2
Matera - Noto	0.3 +/- 1.4	0.5 +/- 0.6
DSS65 - Noto	-2.2 +/- 1.6	-2.3 +/- 1.2

Table 1.  
Rates of European baselines from OCCAM  
and SOLVE [Ma, Ryan, 1998]

Moreover, evolution of some baselengths differ from simple linear model. Below you can see the plots of post-fit residuals after removing of trend. For example, baseline DSS65 – Medicina (fig.1) shows slow variations with maximum in 1995. Baseline Wettzell – Matera (fig.2) has 2-cm 'jump' at the beginning of 1994. Post-fit residuals from baseline Medicina – Matera (fig.3) show a negative sign before 1996 and positive after the date. If we divide the baseline history into two subsets (before and after 1996.0), we will obtain two independent solutions. The first part of plot (19 points) provides us the rate  $-3.2 \pm 1.2$  mm/year, the second one (8 points) provides the rate  $0.3 \pm 5.3$  mm/year for the short baseline. The similar picture is for baseline Medicina – Noto (fig.4). Due to limitation of observations after 1996 it is no reasonable to make any final conclusion on evolution of distance between the Italian baselines. Therefore, it is necessary to observe the tendency 3-4 years more.

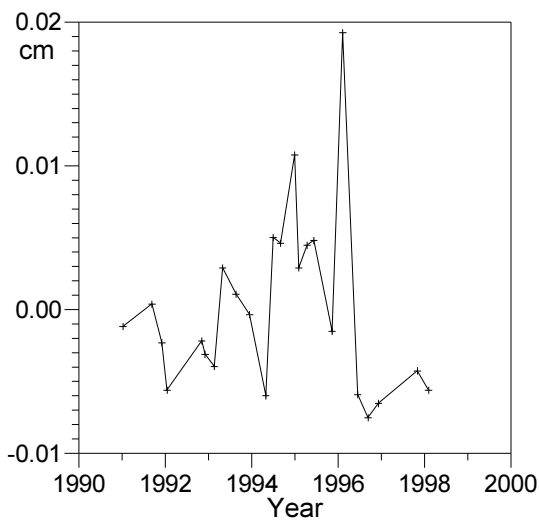


Fig. 1  
Baseline DSS65 – MEDICINA

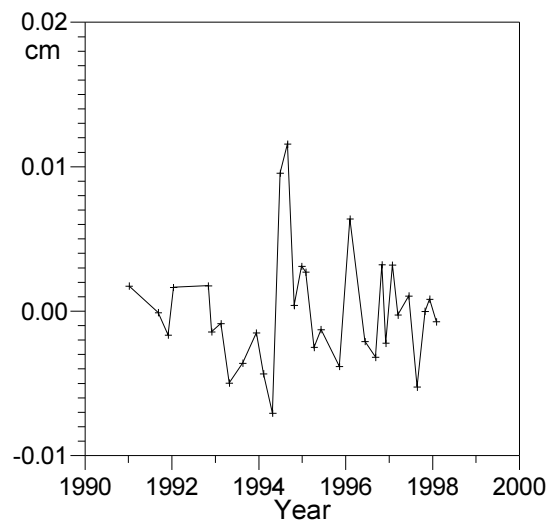


Fig. 2  
Baseline WETTZELL – MATERA

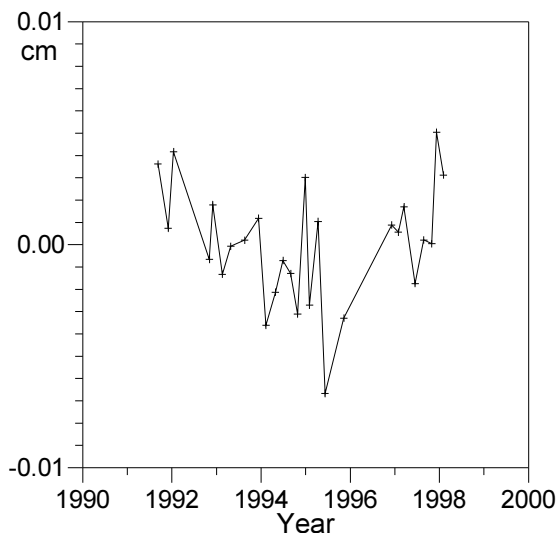


Fig. 3  
Baseline MEDICINA – MATERA

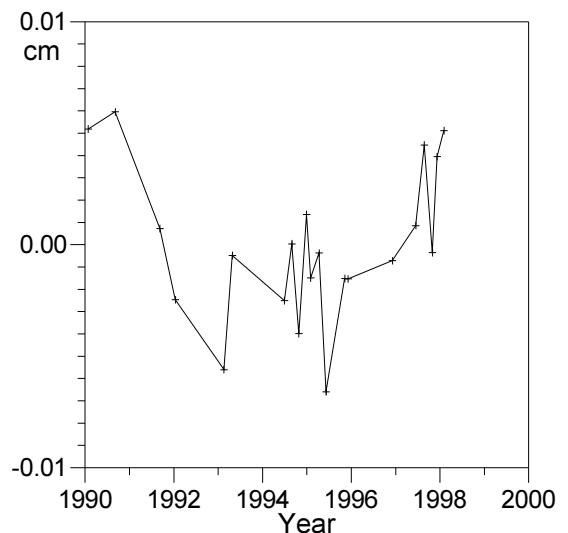


Fig. 4  
Baseline MEDICINA – NOTO

#### 4. Motion of Ny-Alesund VLBI station.

VLBI station Ny-Alesund has been installed in 1994 on Svalbard archipelago [Pettersen, 1995]. Since the year Ny-Alesund actively participates in various observational programs actively. Therefore more detailed analysis of the Ny-Alesund tectonic motion to be made for comparatively short four-years observational history. I have processed 116 VLBI sessions; all of them contain Wettzell (as a reference station) and Ny-Alesund. Evolution of three components is shown on fig. 5-7. Rate estimates of the components are in Table 2. The latitude drift is in good agreement with NNR-NUVEL-1A model. Vertical drift is non-zero and slightly differs from NNR-NUVEL-1A. Longitude component demonstrates significant deviation from model (more than 5 mm/year). Fig. 8 shows a post-fit residual for the component. Obviously, it undergoes a slow variation. To check the suggestion all points on fig. 8 have been divided into two subsets (before and after epoch 1996.5) and two independent rates have been estimated (8.4 +/- 5.4 and 18.3 +/- 3.1 mm/year, correspondingly). The latter rate is almost two times more than the one predicted by NNR-NUVEL-1A. Probably, any deformations at the Svalbard archipelago caused the changes in rates of longitude component motion. It is an active tectonic region near the boundary of the Eurasian plate. Therefore Ny-Alesund VLBI site tectonic motion can be an indicator of tectonic processes at the region.

Component	Rate and $3\sigma$ error from OCCAM (mm/year)	Rate from NNR-NUVEL-1A (mm/year)
Vertical	4.4 +/- 3.3	0.0
Latitude	12.8 +/- 1.5	13.7
Longitude	15.5 +/- 1.7	10.2

Table 2.  
Rates for evolution of Ny-Alesund VLBI station components

## 5. Conclusion

Using the VLBI observations from the European network it is possible to get extremely accurate results for VLBI site velocities. The estimates do not depend on choice of software system or observational network. But it is shown the shift due to tectonic motion sometimes can not be approximated by a straight line. Variations of the motion sometimes are significant even for a short time scale. At least three Italian stations and Ny-Alesund show the effect. All of them are located in unstable tectonic regions. Rather than to consider the site motion as a linear function a more flexible model to be developed for the purpose of comprehensive ITRF making up.

It is known that results obtained by different techniques on short time scales without mutual temporal overlapping show significant disagreement in rates [see, for example, VLBI and GPS results; Bianco et al., 1997]. The disagreement usually is explained by artifacts following from differences in each technique performance. However, real temporal variations of rates will be able to cause the same picture if there is no data span overlapping.

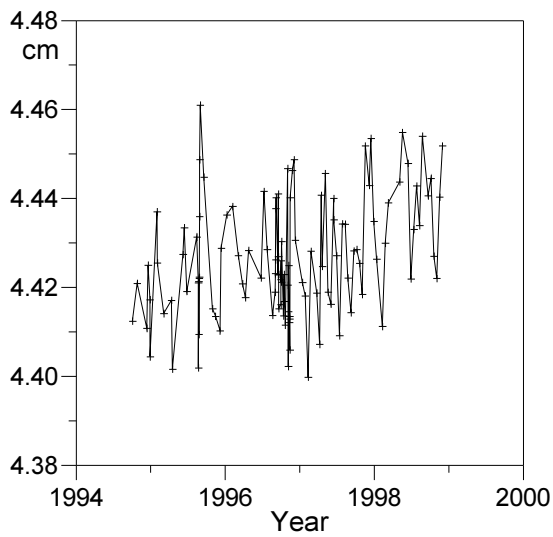


Fig.5  
NY-ALESUND radial component

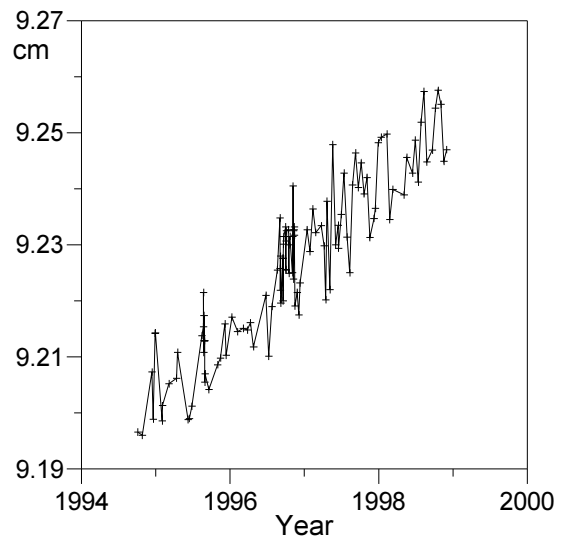


Fig. 6  
NY-ALESUND latitude component

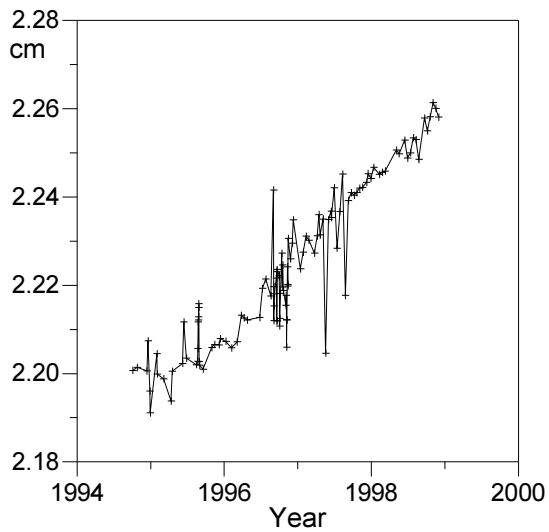


Fig.7  
NY-ALESUND longitude component

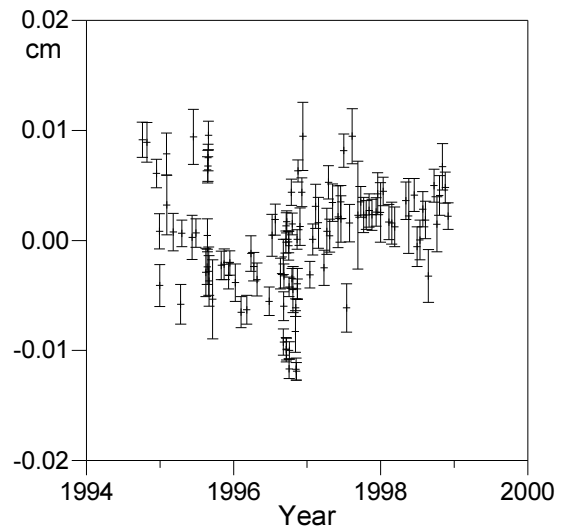


Fig.8  
Post-fit residuals of  
NY-ALESUND longitude component.  
Linear trend and outliers were removed.  
Standard deviations of points are shown.

## 6. References

Bianco G., R. Devoti, M. Fermi, C. Ferraro, R. Lanotte, V. Luceri, H. Nardi, R. Pacione, P. Rutigliano, C. Sciaretta, F. Vespe (1997), *Comparison of Space Geodetic Analysis Results at the CGS*, Proc. of 12<sup>th</sup> Working Meeting on European VLBI for Geodesy and Astrometry (ed. by B. R. Pettersen), Honefoss.

Caprette, D., C. Ma, J.W. Ryan, (1990). *Crustal Dynamics Project data analysis - 1990*. NASA Tech. Mem., 100765, Goddard Space Flight Center, Greenbelt, Md.

DeMets C., R.G. Gordon, D.F. Argus, S. Stein, (1994). *Effect on Recent Revision of the geomagnetic reversal time scale on estimates of current plate motions*. Geophys. Res. Let., 21, 2191-2194.

Drewes H., (1998). *Realization of No Net Rotation Reference Frame*. IERS Workshop, Potsdam, 1998.

Ma, C., J. W. Ryan, *NASA Space Geodesy Program -- GSFC DATA Analysis -- 1998, VLBI Geodetic Results 1979-1998*, August, 1998.

McCarthy D. D. (ed.), (1996). *IERS Conventions 1996*, IERS Tech. Note, 21, Paris Observatory.

Pettersen, B. R., (1995). *Space Geodesy from an Arctic Observatory*, Nordic Space Activities 3, No. 1, p.16.

Titov O., N. Zarraoa, (1997). *OCCAM 3.4. User's guide*. Communications of IAA, 69.

Tomasi P., F. Mantovani, M. Negusini, A. Orfei, P. Santi, (1997). *Activities and recent results in Geodynamics*, Proc. of 12<sup>th</sup> Working Meeting on European VLBI for Geodesy and Astrometry (ed. by B. R. Pettersen), Honefoss.

## **Crustal Deformations in the Central Mediterranean Derived from the WHAT A CAT GPS Project**

*K. Kaniuth, H. Drewes, K. Stuber, H. Tremel*  
Deutsches Geodätisches Forschungsinstitut, München, Germany

*H.-G. Kahle, Y. Peter*  
Eidgenössische Technische Hochschule, Zürich, Switzerland

*S. Zerbini, G. Tonti*  
Università di Bologna, Italy

*G. Veis*  
National Technical University, Athens Greece

*H. Fagard*  
Institut Géographique National, Paris, France

### **Abstract**

The West Hellenic Arc Tectonics and Calabrian Arc Tectonics (WHAT A CAT) project aims at monitoring crustal deformations in the Central Mediterranean by repeated GPS campaigns. The data set acquired so far is rather heterogeneous in terms of availability of GPS satellites, performance of the involved receiver systems and quality of the satellites' orbits. The paper presents the velocity estimates achieved using a modified version of the Bernese GPS software. Main characteristic of the solution strategy is the definition of station velocity parameters already on the observation equation level.

### **Introduction**

Projects aiming at determining crustal deformations along the West Hellenic and the Calabrian Arcs in the Central Mediterranean from repeated GPS observations were established in 1989 and 1987 respectively. Originally initiated independently, both efforts were joined to the West Hellenic Arc Tectonics and Calabrian Arc Tectonics (WHAT A CAT) project in 1992. A first common adjustment of the entire network including several GPS campaigns up to 1994 has been performed in 1995 and established first estimates of site velocities.

This paper describes very briefly the processing characteristics and the results of the latest solution comprising all available data sets from 1988 to 1996. A more extensive analysis including a review of the geophysical background, a detailed discussion of the adjustment approach and an interpretation of the derived velocities will soon be published elsewhere.

## Data Set

The GPS campaigns included in this solution are listed in table 1. As can be seen the data set is extremely heterogeneous with regard to the involved receiver systems:

The first campaigns up to 1992, mainly in the Calabrian Arc area, were observed with the old Texas Instruments 4100 and the Wild Magnavox 102 receivers; in particular the WM 102 experienced many data losses on the L2 frequency.

Even the later campaigns included different receiver types, however with a majority of Leica 200 systems.

Some colocations of different receiver types were performed in order to combine receiver specific subnetworks or baselines with each other. Even then the reliability of the applied antenna phase center models is of great importance. In addition, the number of occupation days per site and epoch varies considerably, and the session length was on the average limited to about eight hours. Moreover, different markers were occupied at a number of sites in the course of the project; consequently, at some sites the results strongly depend on the quality of the observed local ties.

**Table 1** GPS campaigns included in the network adjustment

Epoch	West Hellenic Arc		Calabrian Arc	
	Stat.	Receiver Types	Stat.	Receiver Types
1988, Sept.			7	TI 4100
1989, June			4	TI 4100
1990, June			20	TI 4100 + WM 102
1991, Sept.			6	WM 102
1992, Sept.	16	Leica 200 + WM 102	20	Leica 200 + WM 102
1993, Sept.	20	Leica 200	7	Leica 200
1994, Sept.	15	Leica 200	25	Leica 200
1995, Dec.			2	Leica 200
1996, Sept.	9	Leica 200 + Trimble SST / SSE	24	Leica 200 / 300, Trimble SSE, Ashtech ZXII + Turbo Rogue

## Processing

The data processing was performed using the Bernese GPS software versions 3.4 and 4.0 respectively (Rothacher et al. 1993, Rothacher and Mervart 1996). The subnetwork adjustments generating and saving normal equations for a subsequent combined solution used a modified version of the Bernese program GPSEST. The modifications implemented at DGFI relate mainly to the tropospheric delay modeling and the approach for estimating velocities. The characteristics of the WHAT A CAT solution can be summarized as follows:

Ionosphere free double difference linear phase combination L3, minimum elevation angle 15°, ambiguities partly resolved; day by day variation of network design (baseline definition).

Satellite orbits during 1988 - 1990 based on broadcast ephemerides and a constrained improvement by the regional network itself; precise orbits estimated by the University of California and the University of Berne respectively were available for the campaigns 1991 - 1993; from 1994 on the combined orbits operationally generated by the International GPS Service (IGS) were used.

The tropospheric path delay was predicted using the *Saastamoinen* (1973) model and the mapping functions by *Davis et al.* (1985) or *Niell* (1996); residual zenith delays were estimated for two to three hours intervals using a crude mapping function; the troposphere estimated at antenna colocations were constrained to identity.

Antenna phase center offsets and elevation dependent variations modeled by applying the values recommended by IGS (1996).

The site velocities are not derived by transformation of position parameters using the Bernese program ADDNEQ; instead, the positions at the selected reference epoch 1993.0 and linear annual velocities are already defined on the observation equation level.

Accumulation and solution of normal equations with DGFI's programm ACCSOL (ACCumulate and SOLve) applying the following condition equations:

- Velocities of sites occupied only once = 0,
- Velocities of stations tied by eccentricity vectors = identity.

Local vectors and/or ellipsoidal height differences and/or distances between eccentric markers were introduced as individually weighted observation equations.

The reference frame was defined by introducing the ITRF 96 positions at epoch 1993.0 and the annual velocities as observation equations applying individual weights according to the ITRF standard deviations propagated to 1993.0 (table 2). It is evident from the table that the accuracy of the four Greek stations in ITRF 96 (*Sillard et al.* 1998) is by far too bad as to contribute at all to the reference frame realization.

**Table 2** ITRF 96 fiducials: standard deviations of positions at reference epoch 1993.0 [mm] and of annual velocities [mm/y]

Site	x	y	z	v <sub>x</sub>	v <sub>y</sub>	v <sub>z</sub>
Matera	4.9	4.8	4.9	0.3	0.4	0.3
Cagliari	3.4	2.7	3.4	0.2	0.1	0.2
Noto	3.6	3.4	3.7	0.4	0.5	0.4
Medicina	2.9	2.8	3.3	0.2	0.3	0.3
Dyonysos	31.2	34.8	25.3	4.0	4.4	3.4
Xrisokellaria	40.4	36.8	36.9	5.7	5.2	5.1
Karitsa	49.9	35.4	48.9	6.7	5.2	7.0
Roumeli	99.8	83.6	98.8	10.5	9.3	10.3

## Results

The results of the WHAT A CAT network adjustment following the outlined strategy are given in figures 1 to 4. The absolute horizontal velocities in the ITRF 96 are displayed in figures 1 and 2. Figures 3 and 4 present the velocities remaining after reducing the absolute velocities to the motion of the Eurasian plate as predicted by the NUVEL 1A NNR plate model (*Argus and Gordon 1991*). The precision of the estimated horizontal velocity components ranges between 0.1 mm and 0.3 mm per year mainly depending on the number of occupations. It should be noted that these numbers are precision but not at all accuracy estimates.

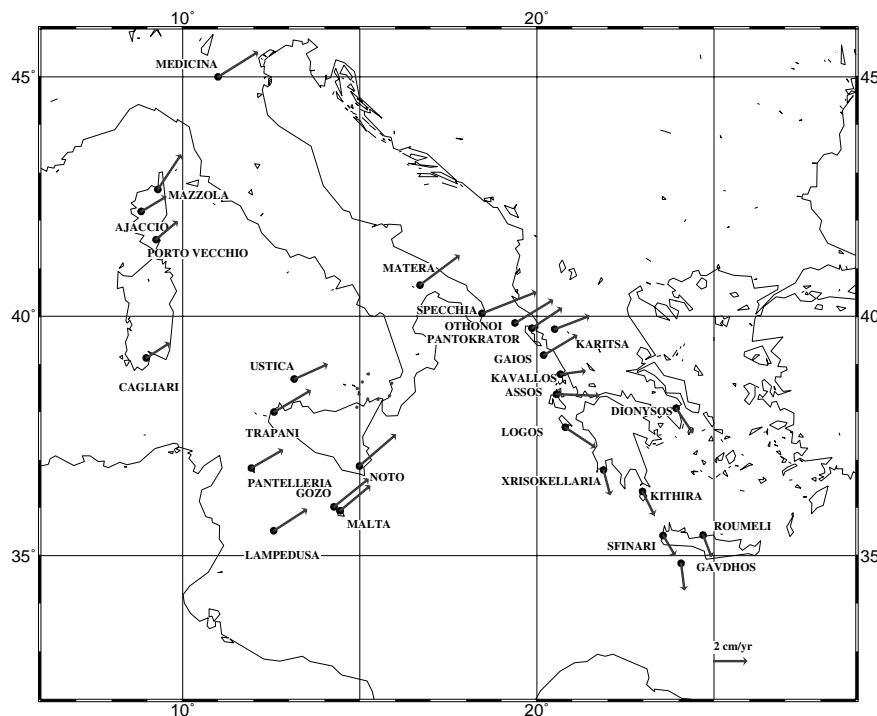


**Fig. 1** Horizontal velocities in the ITRF 96 reference frame

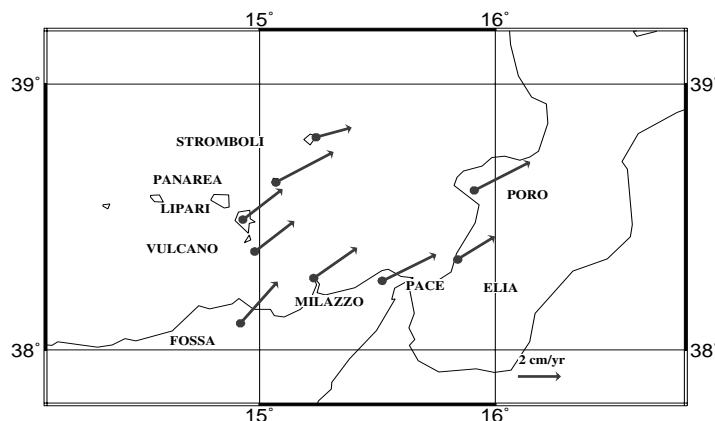


**Fig. 2** Horizontal velocities in the ITRF 96 reference frame (detail)

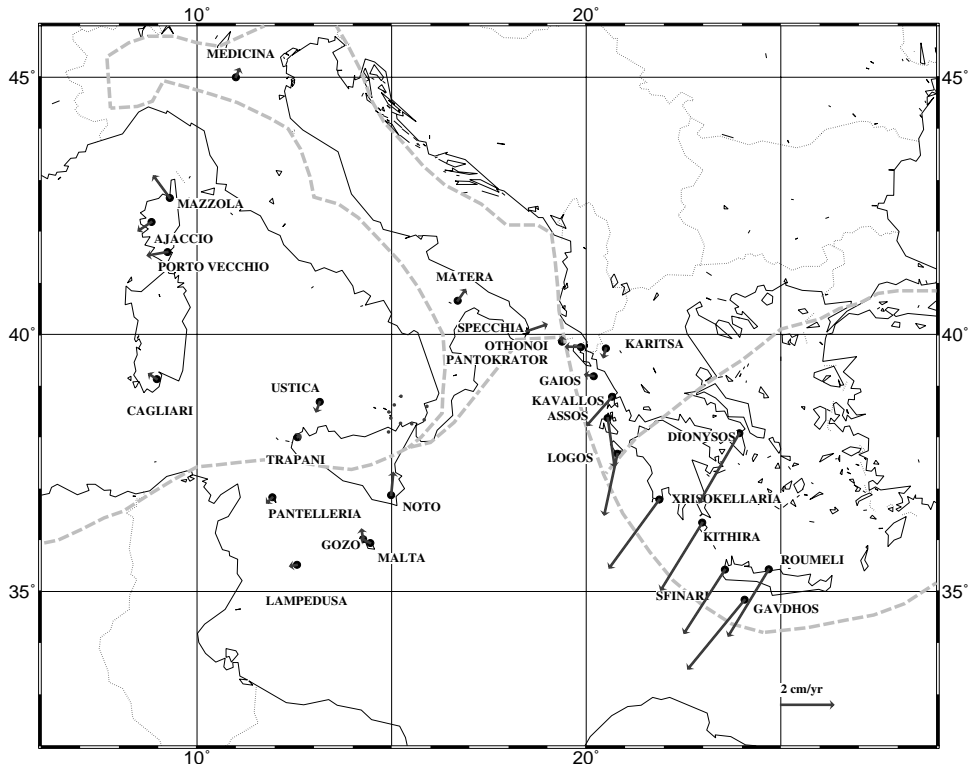


**Fig. 3** Horizontal velocities relative to the NUVEL 1A NNR plate motion model

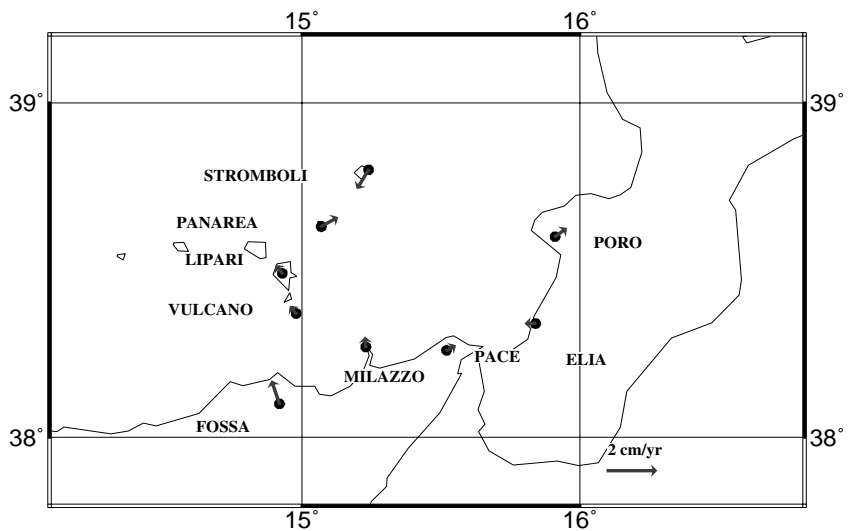


**Fig. 4** Horizontal velocities relative to the NUVEL 1A NNR plate motion model (detail)

## References

- Argus, D.F. and R.G. Gordon* (1991): No-net-rotation model of current plate velocities incorporating plate motion model NUVEL-1. *Geophys. Res. Lett.* 18, 11, 2039-2042.
- Davis, J.C., T.A. Herring, I.I. Shapiro, A.E.E. Rogers and G. Elgered* (1985): Geodesy by radio interferometry: Effects of atmospheric modelling errors on estimates of baseline length. *Radio Sc.*, 20, 1593-1607.
- International GPS Service / IGS (1996): Combination of antenna phase center offsets and variations; antenna calibration set IGS\_01.pcv.  
Ftp://igsb.jpl.nasa.gov/igsb/station/general.
- Rothacher, M., G. Beutler, W. Gurtner, E. Brockmann and L. Mervart* (1993): The Bernese GPS software version 3.4. Astr. Inst. Univ. Berne, Switzerland.
- Rothacher, M. and L. Mervart* (Eds.) (1996): Bernese GPS software version 4.0. Astr. Inst. Univ. Berne, Switzerland.
- Niell, A.E.* (1996): Global mapping functions for the atmospheric delay at radio wavelengths. *J. Geophys. Res.*, 101, B2, 3227-3246.
- Saastamoinen, J.* (1973): Contributions to the theory of atmospheric refraction, part II: Refraction corrections in satellite geodesy. *Bull. Geod.*, 107, 13-34.
- Sillard, P., Z. Altamimi and C. Boucher* (1998): The ITRF 96 realization and its associated velocity field. *Geophys. Res. Lett.* 25, 17, 3223-3226.

## **Geodynamic interpretation of the Central Mediterranean combining geological and VLBI data.**

Erwan Gueguen and Paolo Tomasi  
ITIS-CNR, Centro di Geodesia Spaziale I-75100 Matera (Italy)

### **Abstract**

The Central Mediterranean is a very interesting place to test the use of VLBI data for geodynamics interpretation. It is a very tectonically active area which means that the movements of the different blocks are quite fast. There are three stations distributed over this area and located on the different blocks involved. And finally the geodynamic setting is now quite well known even if there are still some controversies.

In this paper we compare the results of our plate tectonics model with the velocities obtained by VLBI method and we will discuss the geodynamic meaning of the relative motion vectors.

The plate tectonic model show that the rollback of the apenninic subduction hinge slowed down during the evolution the orogen with drastic change when the Southern Apennines front collided with the Puglia swell. The Adriatic plate has to be divided in two sub-plates separated by the Tremiti line.

The results obtained by VLBI method are in good agreement with the velocities derived from the geodynamics model.

### **Introduction**

The Central Mediterranean is a very interesting place to test the use of VLBI data for geodynamics interpretation. It is a very tectonically active area which means that the movements of the different blocks are quite fast. There are three stations distributed over this area and located on the different blocks involved. And finally the geodynamic setting is now quite well known even if there are still some controversies.

The present day geodynamic pattern is a result of the geodynamic evolution of the western mediterranean and thus the velocities obtained from geodetic methods should be close to the velocities observed for the past 5 My.

### **Geodynamic settings**

During the Neogene and Quaternary the western Mediterranean geodynamics was apparently dominated by the 'eastward' migration of the Apenninic arc and the associated back-arc basin opening.

Figure 1 shows the late Oligocene (21 My) paleogeography of the western Mediterranean area. The Corsica-Sardinia block is still attach to the Europe and eastward the Alpine subduction has reached the the collision stage with the thick continental crust of european margin. Whereas in front of the alpine

backthrust belt there is the old oceanic crust of the Tethys Ocean, this will lead to the flip of the subduction zone and thus to the beginning of the evolution of the Apenninic orogen.

During the first 11 My the Apenninic front migrate easily and quickly but around 10 My ago the apenninic front reached the Puglia swell and this has led to a drastic change of the rollback velocities as shown in table 1.

Transect	mean velocity	21 to 10 My	10 to 5 My	5 My to present
Calabria	37 mm/yr.	41 mm/yr.	34 mm/yr.	31 mm/yr.
Southern Apennines	26 mm/yr.	37 mm/yr.	21 mm/yr.	6 mm/yr.
Central Apennines	19 mm/yr.	25 mm/yr.	16 mm/yr.	8mm/yr.
Northern Apennines	9 mm/yr.	12 mm/yr.	7 mm/yr.	6 mm/yr.

Table 1 : Estimate migration velocities of the Apenninic front with respect to fixed Europe during the past 21 My.

Due to the presence of the ionian oceanic crust the calabrian arc continued to rollback quickly. Whereas the most dramatic change concerns the Southern Apennines segment where the migration of the hinge is slowed down by a factor 6 in 10 My. The consequence of this is an inversion of the velocity ratio between the Southern and Central Apennines domains, leading to the formation of the Tremiti Line.

Coevally Africa slowly moving towards Eurasia deforms the southernmost segment of the subduction zone.

### **The present day tectonic settings**

Figure 3 shows a map of the main quaternary structures of the Western Adria/Apennines area.

We can distinguish three main domains characterised by their structural style.

The first one is Tyrrhenian Sea which correspond to the back-arc basin of the Apenninic subduction and all this domain is under a tensional stress field (Bassi and Sabadini, 1994). In the northern part it is formed by stretched relicts of the former alpine orogen, whereas in the central part the deep basins of Marsilli and Vavilov have reached the oceanization stage. It is important to note that the ages of the basin are younger eastward. And now only the basins close to the Italian coast are active (e.g. Salerno, Paola and Catanzaro basins).

The Apennines represents a Neogen roughly E-verging thrust system, which is now affected by a Plio-Quaternary extensional tectonics. All the major compressive features are dislocated by normal faults (Figure 3). For these faults, the seismological data suggest a high angle geometry up to 10-12 km. The compressive tectonic is now located along a very narrow band along the Apenninic front.

The active thrusts are usually visible only on seismic profiles (e.g. CROP3 profile, Barchi *et al.*, 1997) and are blind-thrusts. This is also confirmed by seismological data (Selvaggi and Amato, 1992). The major part of the Apennines is now under an extensional regime.

In the Umbro-marchean Apennines (Central Italy), the compressive tectonic stopped during Lower-Middle Pleistocene (Calamita *et al.*, 1999) and the area is affected by a uplift regime. Coevally the extensional tectonic began to be very active leading to the formation of lacustrine basins.

In the Southern Apennines we find the same tectonic evolution with former compressive features cut by normal faults with formation of intracontinental basins like Potenza and Tolve basins.

The third domain is the Adriatic plate. The lithospheric thickness of Italy (Calcagnile and Panza, 1981) shows that this domain has to be divided in two sub-plates.

The two segments of the western Adriatic are separated by the so-called Tremiti Line which is a roughly E-W trending shear. This lineament lies offshore northward of the Gargano Promontory. It is seismically active and deforms the sea bottom. On the basis of seismicity and geophysical data this structure is interpreted as a lithospheric boundary between two Adriatic subplates, allowing a major rollback of the subduction hinge of northern Adriatic block characterised by a thinner lithosphere.

The northern Adriatic area is formed by thin continental lithosphere (70 km) and is characterised by a faster rollback of the subduction hinge and a high subsidence rate as shown by the thick sedimentary series of the Chieti-Pescara and Ancona basins.

Puglia represents the foreland of both the Apenninic and Dinaric orogens. This foreland is weakly deformed and consists of an emerged domain (Gargano, Murge and Salento areas) and of a submerged area in the Adriatic and Ionian seas. It is formed by a thick continental lithosphere (100 km). Like in the Apenninic domain the Quaternary tectonic activity is characterised by tensional and transtensional faults associated with a horst-and-graben system. But the origin of this tectonic is completely different. In fact it is due to the bulking of the thick Adriatic lithosphere.

The northern boundary of the Adriatic plate is formed by the foredeep of the Southern Alps, which are the backthrust belt of the Alps. It slowly migrates southwards between Late Cretaceous and Pliocene. It is now nearly stopped and according to sediments thickness the subsidence rate is very low (0.3 mm/yr.).

## **Geodynamic interpretation of VLBI results**

In this paper we considered relative European velocities keeping the Wettzell-Madrid baseline fixed in order to compare them with the results of the plate tectonics model. These velocities have been calculated using CALCSOLVE software. In this solution were used all the geodetic experiments with at least three European stations in them.

	Up velocities (mm/yr.)	East velocities (mm/yr.)	North velocities (mm/yr.)
Medicina	$-3.82 \pm 0.397$	$1.91 \pm 0.101$	$2.07 \pm 0.104$
Matera	$0.78 \pm 0.361$	$1.63 \pm 0.093$	$4.34 \pm 0.101$
Noto	$-1.48 \pm 0.340$	$-0.75 \pm 0.082$	$4.72 \pm 0.098$

Table 2 : Relative European velocities keeping the Wettzell-Madrid baseline fixed

#### Horizontal motion

The Matera station is the only one effectively representative of the Adria plate motion. Whereas Medicina is located at the boundary with the Northern Adriatic Block but is still on the Apennines side. Thus we should be very careful when we interpret the Medicina/Matera baseline in terms of tectonics and for example we should not consider that the difference between the motions of the two stations is significant for a rotation of the Adriatic plate.

The Noto station situation is quite ambiguous. It is usually considered as part of the Africa plate. But it is not rigidly linked to Africa as shown by the active extensional tectonics in the Sicily Channel (e.g. Lampedusa graben). And the Hyblean block may slowly rotate clockwise under the indenter effect of northward motion of Africa.

#### Vertical motion

The difference between the two Adriatic segments is underlined by an active subsidence of the Adriatic sea and the coeval uplift of the Bradano Trough and Puglia (Doglioni *et al.*, 1994). Evidence for this uplift is given by uplifted shorelines and Bradanic sediments like the Irsina Conglomerate which is now at about 550 m altitude. These geological data give subsidence rates of about 3.5 mm/yr. for the western Adriatic area (Doglioni and Prosser, 1997) and an uplift of 0.2-0.3 mm/yr. for the Puglia. The uplift rate is in quite good agreement with the  $0.78 \pm 0.361$  mm/yr. Up velocity given by VLBI for the Matera station.

Due to human activities, like intensive pumping of ground water, the Medicina vertical motion is not easily interpretable in terms of tectonic subsidence.

The  $-1.48 \pm 0.340$  mm/yr. Up velocity of the Noto station is also in good agreement with the geological data showing a slow subsidence of the southern margin of the Hyblean plateau.

## Conclusion

The geodynamical regime of the Central Mediterranean dramatically changed between 10 and 5 My ago. Nevertheless the results of the VLBI interpretation are in good agreement with the plate tectonics model for the past 5my. They show that the Apenninic system is still active even if it has slowed down. According to the geological and geophysical data we can consider in a first approximation that the adriatic plate is composed of two almost rigid blocks separated by the Tremiti shear-zone. Whereas the tectonic activity in the Apennines is very diffuse.

To improve these results the next step will be to include the GPS and SLR stations of the Italian network. Larger number of information but moreover a better repartition of the geodetic data over the Apenninic system and the Adriatic plate.

## Acknowledgements

Discussions with E. Festa, P. Pieri, G. Prosser, M. Schiattarella, E. Tavarnelli and M. Tropeano were very helpful. The European Community supported this study (Research Networks, 'Measurement of Vertical Crustal Motion in Europe by VLBI'), grant ERB-FMRX-CT9960071.

## References

- Barchi, M., Minelli, G. & Piali, G. 1997. The Crop 03 profile: a synthesis of results on deep structures of the Northern Apennines. *Memorie della Società Geologica Italiana*.
- Bassi, G., and Sabadini, R. 1994. The importance of subduction for the modern stress field in the Tyrrhenian area ? *Geophys. Res. Lett.*, 21, 5, 329-332.
- Calamita F., Coltorti M., Pieruccini P. and Pizzi A. 1999 Evoluzione strutturale e morfogenesi plio-quadernaria dell'appennino umbro-marchigiano tra il preappennino umbro e la costa adriatica. *Boll. Soc. Geol. It.*, 118, 6pp.
- Calcagnile, G. & Panza, G.F. 1981. The main characteristics of the lithosphere-asthenosphere system in Italy and surrounding regions. *Pure and Applied Geophysics*, 119, 865-879.
- Doglioni, C., Mongelli, F. & Pieri, P. 1994. The Puglia uplift (SE-Italy): an anomaly in the foreland of the Apenninic subduction due to buckling of a thick continental lithosphere. *Tectonics*, 13, 1309-1321.
- Doglioni, C. & Prosser, G. 1997. Fold uplift versus regional subsidence and sedimentation rate. *Marine and Petroleum Geology*, 14, 179-190.
- Gueguen E., Doglioni C. and Fernandez M. (sottomesso a) : On the post 25 Ma geodynamics of the Western Mediterranean. *Tectonophysics*, .
- Selvaggi, G. and Chiarabba, C., 1995. Seismicity and P-wave velocity image of the southern Tyrrhenian subduction zone. *Geophys. J. Int.*, 121, 3, 818-826.
- Selvaggi, G., and Amato, A. 1992. Subcrustal Earthquakes in the Northern Apennines (Italy) : Evidence for a still active subduction ? *Geophys. Res. Lett.*, 19, 21, 2127-2130.
- Spakman, W. 1989. Tomographic images of the upper mantle below central Europe and the Mediterranean, *Terra Nova*, 2, 542-553.

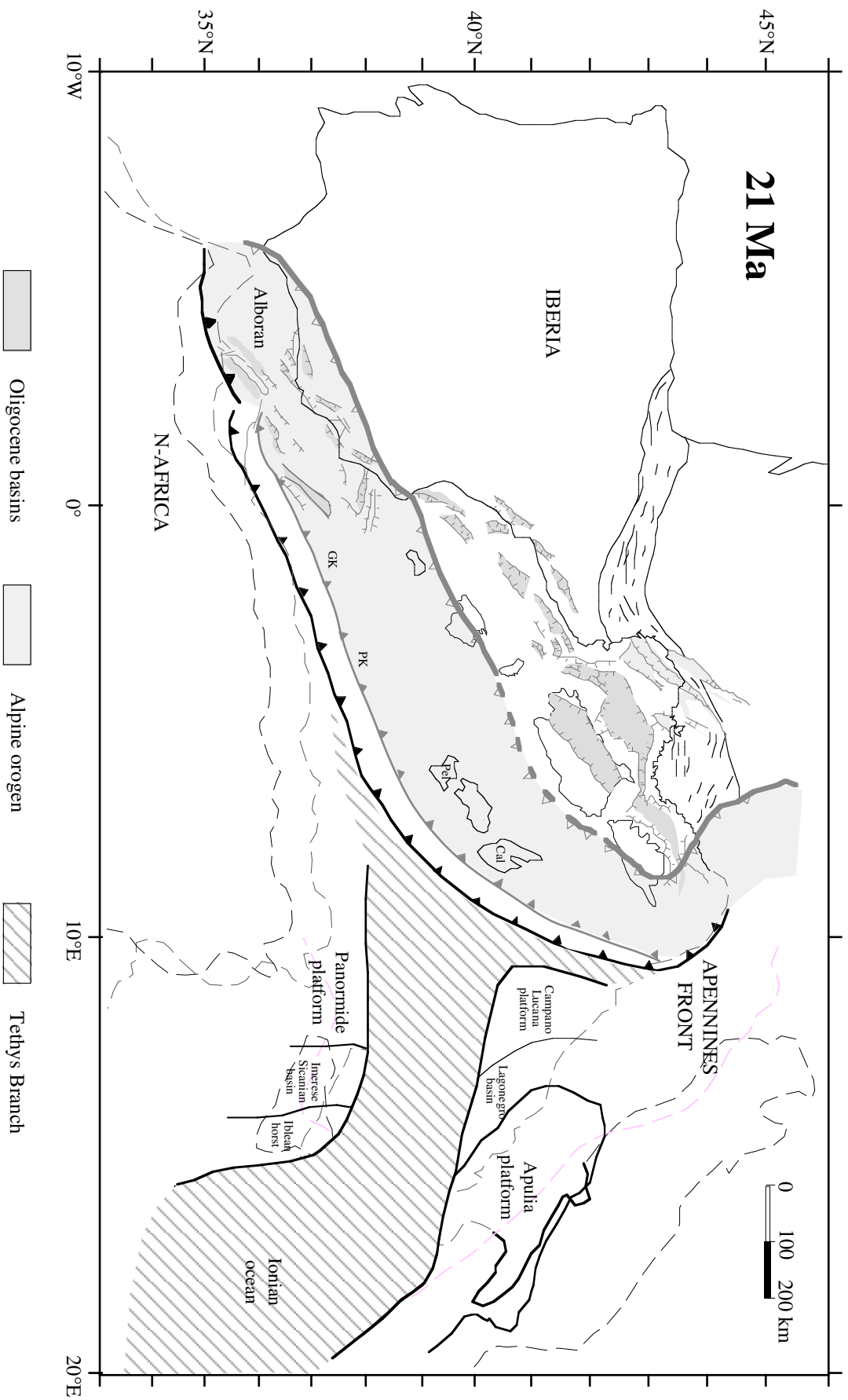


Figure 1 : Late Oligocene paleogeography of the western Mediterranean.

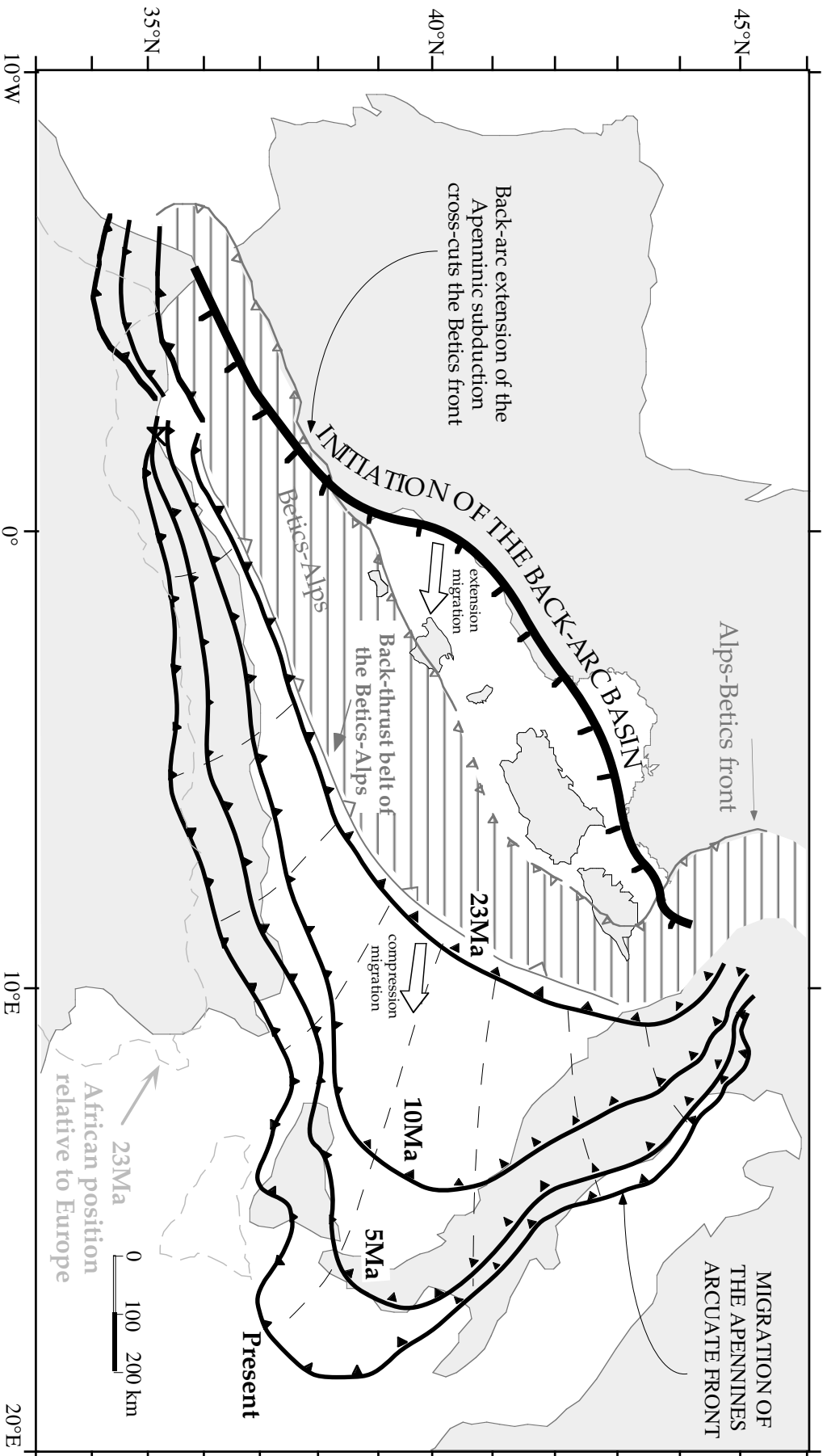


Figure 2 : Migration of the Apenninic front

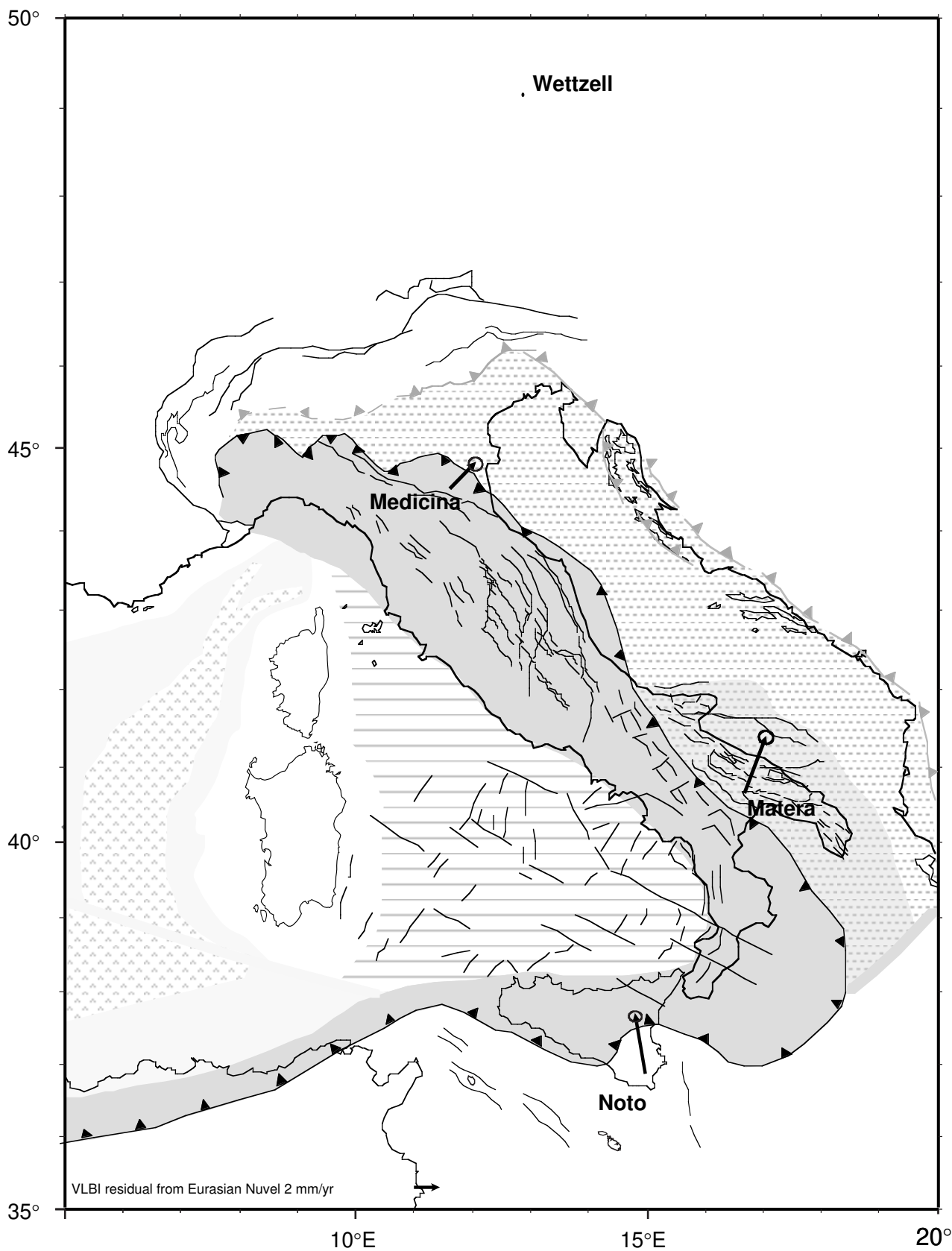


Figure 3 : Structural sketch map of the Central Mediterranean with the VLBI relative European velocities (Wettzell fixed)

# Comparison of deformations resulting from GPS and VLBI data: problems and preliminary results

V. Tornatore<sup>1</sup>, F. Sacerdote<sup>2</sup>, M. Crespi<sup>3</sup>

<sup>1</sup> DIAR-Sezione Rilevamento, Politecnico di Milano

<sup>2</sup> Dip. di Ingegneria Civile, Università degli Studi di Firenze

<sup>3</sup> DITS-Area Topografia, Università degli Studi di Roma "La Sapienza"

## Abstract

This paper discusses preliminary results related to the comparison of long baselines obtained from GPS and VLBI data processing in Europe. This comparison was carried out with the aim to check the agreement of the crustal deformation fields derived by the two techniques. An approach based on the theory of stationary and ergodic stochastic processes is proposed. This approach is able to evaluate temporal correlations of the estimated distances. The results show these correlations are remarkable within each series. The residuals with respect to a linear trend were filtered via least squares collocation but, after having removed the stochastic signal, there is no evidence of significant correlations between the filtered GPS and VLBI residuals.

## 1 Introduction

In the present work we describe the procedure followed to analyse baseline length determinations obtained from GPS and VLBI data in Europe.

The main problems related to the comparison of crustal deformation fields derived by the two techniques and preliminary results have been discussed in a previous paper [Crespi et al. 1997].

The aim of that work was twofold: to underline that the data analysis technique applied to GPS campaigns carried out in small areas cannot be applied to continent-wide campaigns, and to investigate if a statistical analysis more sophisticated than a qualitative comparison could be applied to the two series (GPS and VLBI) of distance determinations.

With the present paper we will describe more in detail the procedure followed to apply the so-called stochastic approach and will present the obtained results at each step.

The approach we have followed is based on the theory of stationary and ergodic stochastic processes. According to this approach one considers data as a realization of a suitable stochastic process defined by some ordering parameter (in our case the time). Applying the classical Wiener filter theory [Papoulis 1965], known in geodesy also as least-squares collocation, it is possible to separate within

output data a part that is correlated, in general not retrievable by deterministic interpolation, that is called *signal* and an uncorrelated part called *noise*. This operation is known as data *filtering*. Then on the base of the available values of the process it allows to predict the most probable values of the signal at instants in which data are not available. This operation is called *prediction*.

This approach requires the covariance function of the process; this usually is not known, but it is empirically determinable and can be interpolated with suitable models.<sup>1</sup> Then the method requires also data devoid of any general systematic distortion and if present it has to be taken out in advance.

## 2 Analysed data set

The GPS series we have used in this comparison are drawn from IGS solutions: in particular they are related to the European part of the IGS series and have been obtained at CODE (Center for Orbit Determination in Europe, Bern University) [Nothnagel 1997].

The VLBI observations come from experiments called EUROPE performed in the European area with a bimonthly duty cycle since 1990. The solutions have been determined at GIUB (Geodetic Institute of University of Bonn).

A first comparison has been recently performed on these two series of distances between couples of stations. A linear regression was applied to both the series for the baseline lengths Wettzell-Madrid, Wettzell-Matera, Wettzell-Onsala finding a substantial agreement concerning the linear trend, even if relevant oscillations among close epochs baseline estimates appear [Nothnagel 1996].

Inspecting these fluctuations a first remark is that a direct comparison of baseline at individual epochs produces different, even opposite, behaviours of the baseline length variation. The second remark is a question: once subtracted the linear trend are such oscillations due to pure observational noise or does it exist any temporal correlation among estimates causing such oscillations ?

## 3 Procedure and description of the results

We investigated in two directions: from one side we looked for systematic effects, superimposed to the general linear trend of the GPS data correlating the values of the time series, and on the other we checked if there exists a significant correlation between the oscillations of the GPS and VLBI series. Under the stationarity hypothesis, once the linear trend has been removed, the empirical covariance function of the residuals has been estimated.

This operation has been performed on GPS data series to obtain more reliable estimates, due to the fact that this series disposes of more numerous data; in fact even if available data span a shorter period (from April 1993 to June 1996) than the VLBI ones, they have a weekly duty cycle.

The results show for all the three baselines considered covariance functions with considerable correlation length of the same order for baselines Wettzell-Madrid and Wettzell-Matera (first zero at about

---

<sup>1</sup>To interpolate the empirical estimates only positive definite functions can be used. A function is positive defined if the corresponding matrix  $Q$  satisfies the relations:

$$\begin{aligned} u'Qu &\geq 0 \quad \forall u \\ u'Qu = 0 &\Rightarrow u = 0, \end{aligned}$$

we are considering the one-dimensional domain.

40 days) and considerably bigger for baseline Wettzell-Onsala (first zero at about 90 days), see Fig. 1, 2 and 3. This is an evidence that oscillations are not due to pure observative noise.

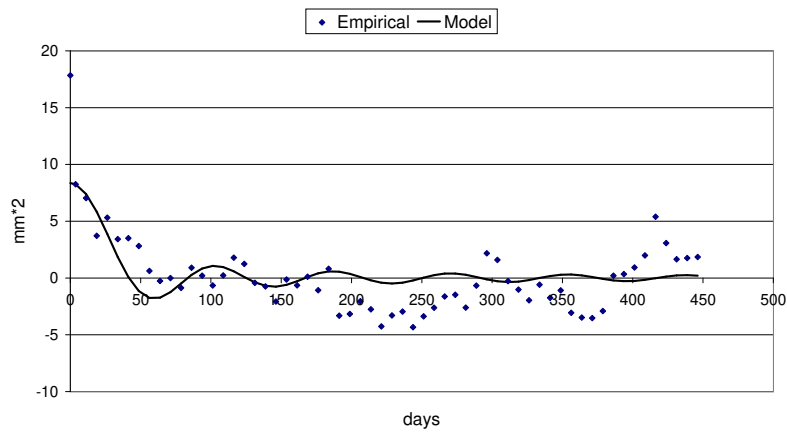


Figure 1: *Autocovariance function of temporal series of GPS distances related to the Wettzell-Madrid baseline after elimination of the linear trend*

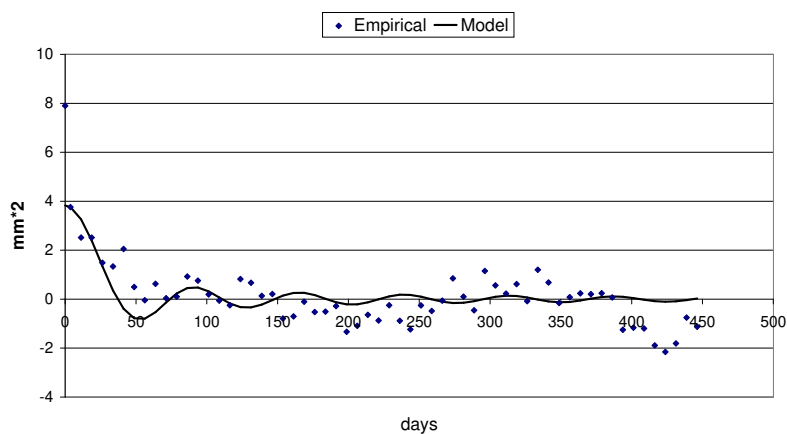


Figure 2: *Autocovariance function of temporal series of GPS distances related to the Wettzell-Matera baseline after elimination of the linear trend*

Using the respective covariance function the filtering of the GPS data for each baseline has been

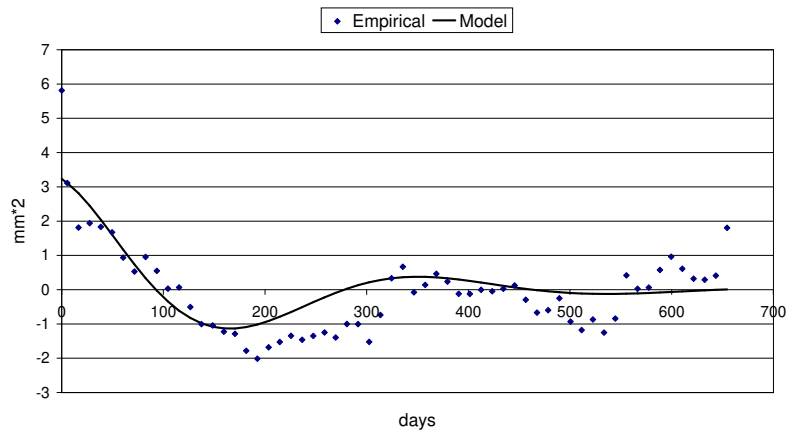


Figure 3: *Autocovariance function of temporal series of GPS distances related to the Wettzell-Onsala baseline after elimination of the linear trend*

performed, the results are in Fig. 4, 5 and 6.

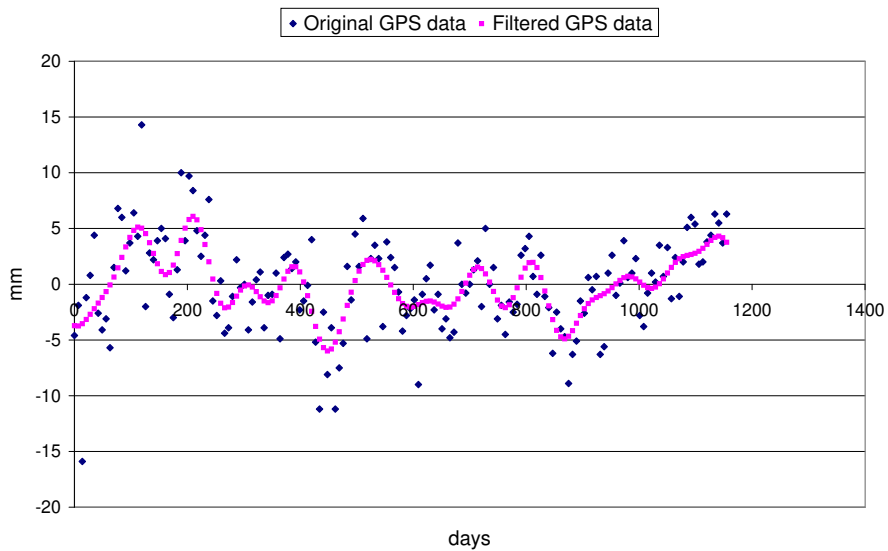


Figure 4: *Filtering of temporal series of GPS distances related to the Wettzell-Madrid baseline after elimination of the linear trend*

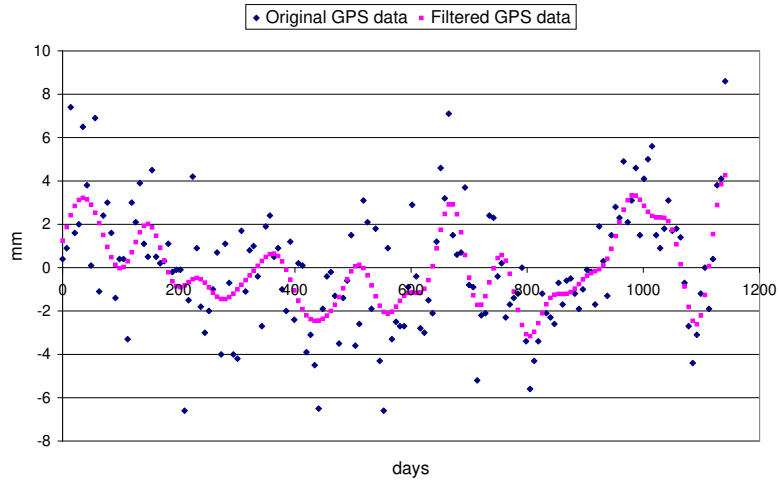


Figure 5: *Filtering of temporal series of GPS distances related to the Wettzell-Matera baseline after elimination of the linear trend*

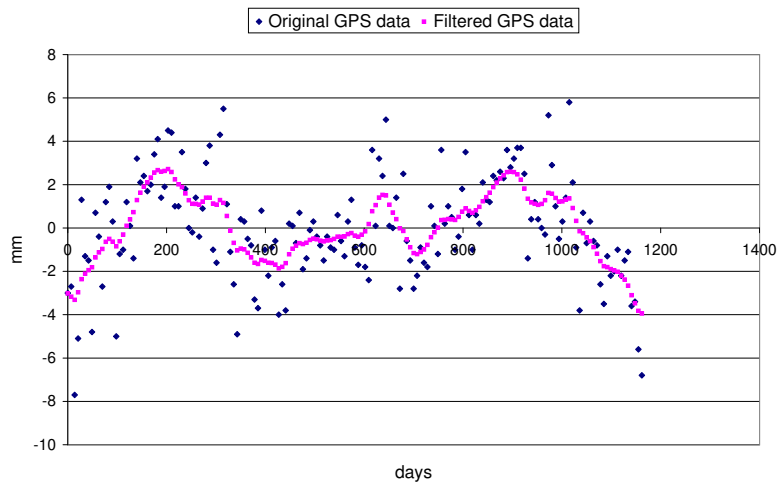


Figure 6: *Filtering of temporal series of GPS distances related to the Wettzell-Onsala baseline after elimination of the linear trend*

Evaluating the residuals between original GPS data set (without trend) and filtered GPS data for each baseline it appears that they do not show significant correlation (see Fig. 7).

## Residuals after filtering GPS data

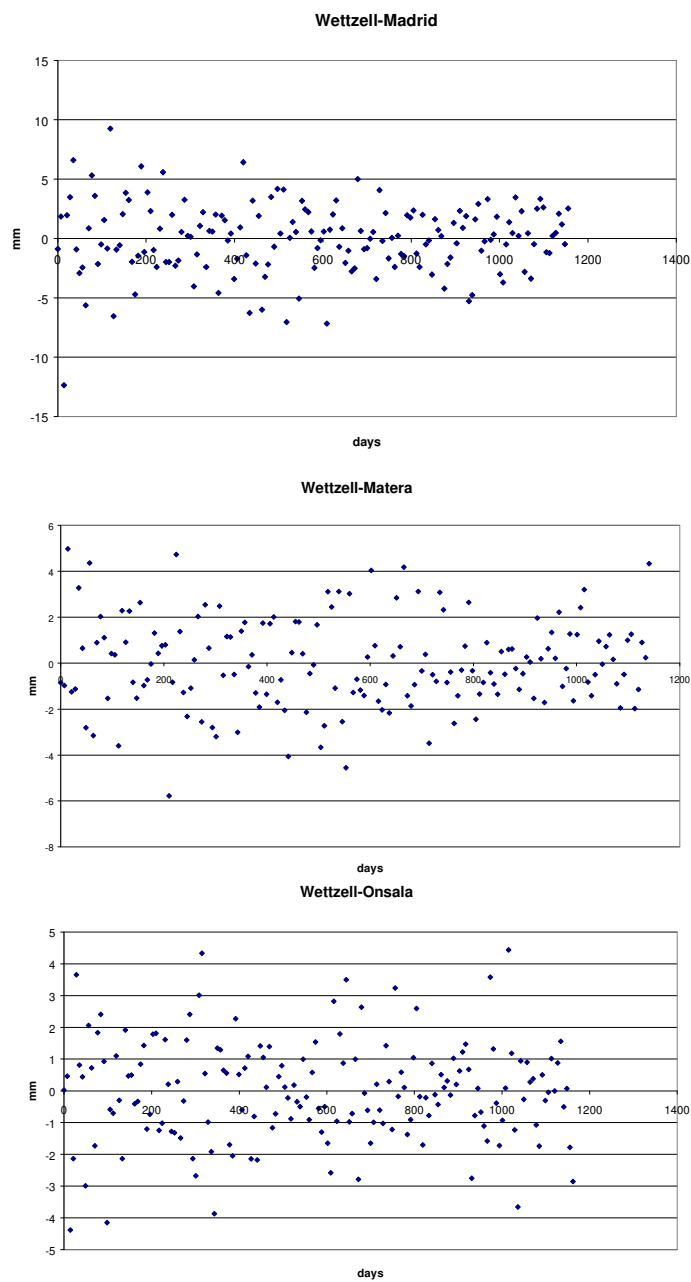


Figure 7: *Residuals for the three baselines*

This is also confirmed by the estimated empirical covariance functions of these residuals which go

immediately to zero.

It is interesting to compare the statistics of the residuals of original GPS data set for the three baselines with residuals obtained after the filtering for the respective GPS baselines. The R.M.S. becomes about  $1mm$  smaller for all the three baselines (see table 1 and table 2).

```

===== Wetzell-Madrid
* * NUMBER OF VALUES = 166
* MEAN = 0.001
* R.M.S. = 4.224
* MINIMUM = -15.900
* MAXIMUM = 14.300
=====
===== Wetzell-Matera
* *NUMBER OF VALUES = 164
* MEAN = 0.000
* R.M.S. = 2.811
* MINIMUM = -6.600
* MAXIMUM = 8.600
=====
===== Wetzell-Onsala
* * NUMBER OF VALUES = 167
* MEAN = 0.010
* R.M.S. = 2.411
* MINIMUM = -7.700
* MAXIMUM = 5.800
=====

```

Table 1: Statistics of residuals of original GPS data (without trend)

```

===== Wetzell-Madrid
* * NUMBER OF VALUES = 166
* MEAN = -0.002
* R.M.S. = 2.938
* MINIMUM = -12.363
* MAXIMUM = 9.268
=====
===== Wetzell-Matera
* *NUMBER OF VALUES = 164
* MEAN = 0.009
* R.M.S. = 1.928
* MINIMUM = -5.784
* MAXIMUM = 4.978
=====
===== Wetzell-Onsala
* NUMBER OF VALUES = 167
* MEAN = -0.009
* R.M.S. = 1.571
* MINIMUM = -4.385
* MAXIMUM = 4.436
=====

```

Table 2: Statistics of residuals obtained after filtering GPS data

Then even considering only the R.M.S of the residuals obtained after the filtering (that is equivalent to the R.M.S of the uncorrelated noise, and that can also be inferred from the autocovariance function), the values obtained of about  $3mm$  for baseline Wetzell-Madrid, about  $2mm$  Wetzell-Matera, and

about  $1.6\text{mm}$  for Wettzell-Onsala are bigger than the respective formal precisions of single solutions. Finally using the covariance functions evaluated for the GPS series the prediction at the VLBI epochs has been performed for the three baselines considered. These prediction values have been compared to the original VLBI values with linear trend removed (see Fig. 8, 9 and 10).

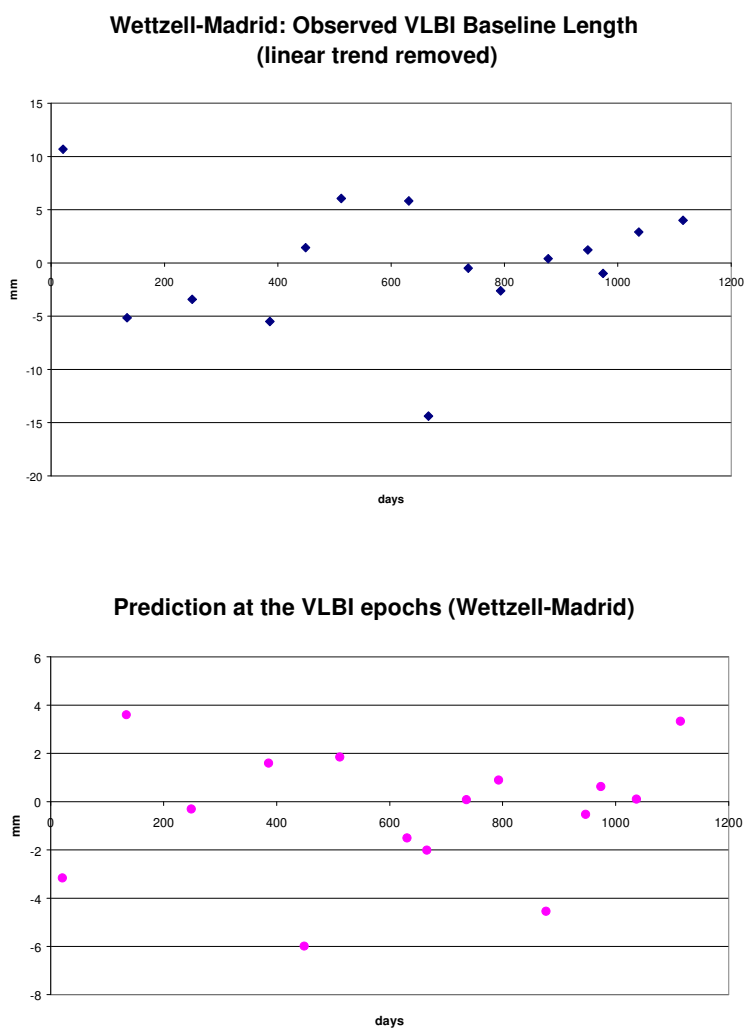


Figure 8: Comparison between observed and predicted values related to the Wettzell-Madrid baseline at the VLBI epochs

As it can be seen from the plots, the two sets of values do not show significant mutual correlation; the evaluation of the correlation coefficient for each couple of the three baselines gives a value near to zero.

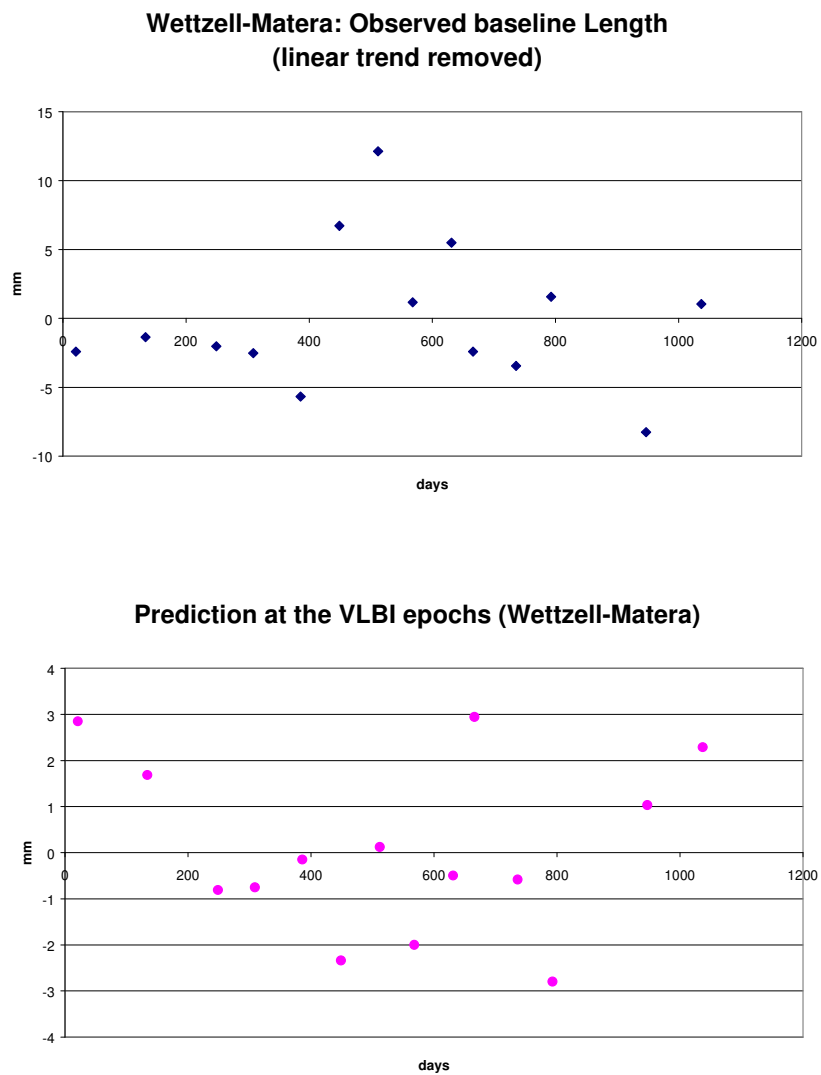


Figure 9: Comparison between observed and predicted values related to the Wettzell-Matera baseline at the VLBI epochs

It is also interesting to note that the amplitude of the oscillations of the predicted values is considerably smaller than the oscillation amplitude of the original VLBI data set. This is an indication that the amplitude of the oscillations one should expect once the correlation among estimates at single epochs has been accounted for, should be remarkably smaller.

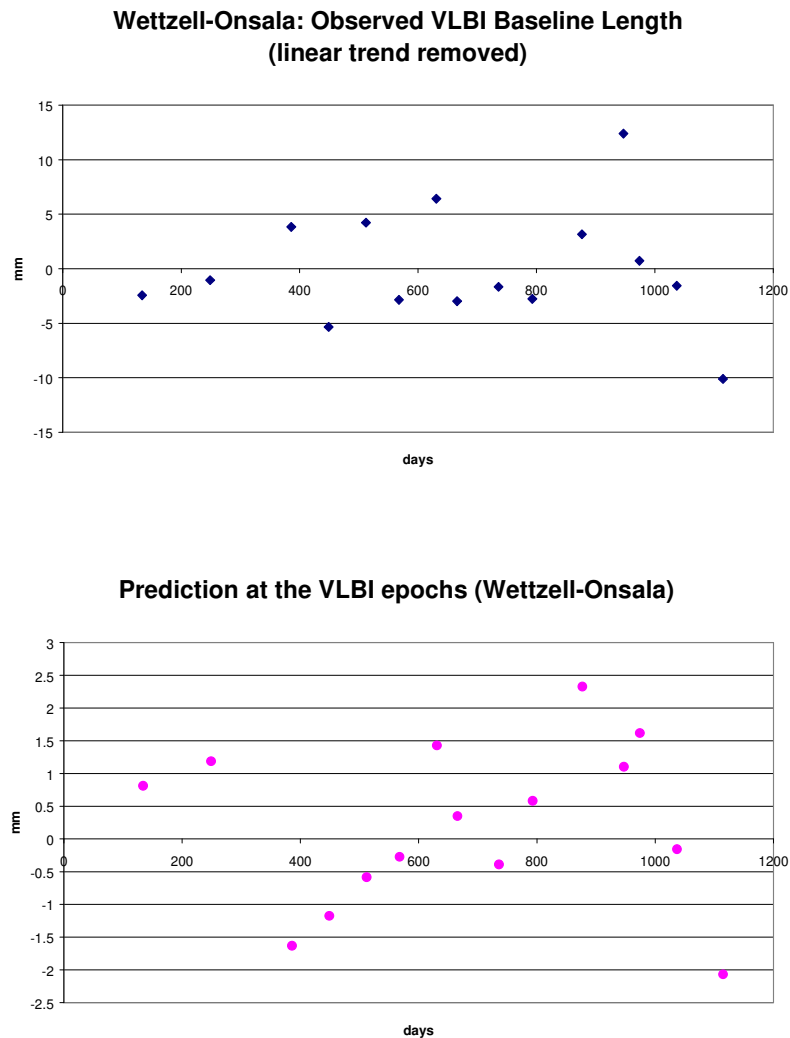


Figure 10: Comparison between observed and predicted values related to the Wettzell-Onsala baseline at the VLBI epochs

#### 4 Conclusions and future developments

This work, even if a preliminary one, has clearly put in evidence that the oscillations appearing in series of GPS and VLBI baseline length determinations are a symptom of the presence of systematic effects not adequately modelled that temporally correlate the solutions.

The fact that the oscillations of the two series have no significant mutual correlation can be an indication that the non properly modelled phenomena can be different for the two techniques.

The procedure we have followed, already successfully applied within the framework of engineering deformation processes [Monti et al. 1978, 1979], seems to be a powerful tool also for the significance analysis of crustal deformation fields.

The nature of the residual stochastic signal that correlates the solutions at single epochs has to be investigated.

Longer series of data (possibly homogeneous from the point of view of the acquisition and analysis of data) including also more recent data have to be examined. Interesting developments of the work could be found by performing independently the estimate of the covariance functions and filtering of data on the VLBI series itself. Other baselines than the three examined in this work have to be investigated for both VLBI and GPS networks. A spectral analysis of the signal for the two series of data could be useful to identify the most significant frequencies.

## Acknowledgements

We acknowledge A. Nothnagel of Geodetic Institute of Bonn University for providing the two series of data.

## References

- [Barzaghi et al. 1983] Barzaghi R., Sansó F. (1983) *Sulla Stima Empirica della Funzione di Covarianza*, Bollettino di Geodesia e Scienze Affini, Anno XLII, No. 4, pp. 389-415.
- [Crespi et al. 1997] Crespi M., Lanotte R., Sacerdote F., Tornatore V. *Confronto di significatività delle deformazioni risultanti da osservazioni GPS e VLBI: problemi e risultati preliminari* presented at XVI Convegno Nazionale GNGTS, Roma 1997, in press
- [Monti et al.1978] Monti, C., F. Sanso' e G. Togliatti (1978) *Analisi autoregressiva di serie temporali di misure altimetriche eseguite sul Duomo di Milano*, Bollettino dell SIFET, n. 2, 1978, 3-47
- [Monti et al.1979] Monti, C., F. Sanso' e G. Togliatti (1979) *Ricerca del modello stocastico previsionale per gli spostamenti di una grande struttura*, L'energia elettrica, n. 2, 1979, 77-83
- [Mussio 1984] Mussio, L. (1984) *Il metodo della collocazione minimi quadrati e le sue applicazioni per l'analisi statistica dei risultati delle compensazioni*, in Ricerche di Geodesia Topografia e Fotogrammetria, vol. 4, CLUP, Milano, 305-338
- [Nothnagel 1996] Nothnagel, A. (1996) - *Update on European Geodetic VLBI Analyses at the Geodetic Institute of the University of Bonn*, in Proc. of the Eleventh Working Meeting on European VLBI for Geodesy and Astrometry (G. Elgered, ed.), Res. Rep. No 177, 110-120
- [Nothnagel 1997] Nothnagel, A. (1997) - Personal communication.
- [Papoulis 1965] Papoulis A. (1965) *Probability, Random Variables and Stochastic Processes*, McGraw-Hill Book Company

# A Classification of ICRF Sources Based on Observed Structure for Ultra-precise VLBI Astrometry and Geodesy

P. Charlot

Observatoire de Bordeaux - CNRS/UMR 5804  
2 Avenue de l'Observatoire, BP 89, 33270 Floirac, France

A. L. Fey

US Naval Observatory  
3450 Massachusetts Avenue, NW, Washington, DC 20392-5420, USA

## Abstract

The intrinsic radio structure of the extragalactic sources is one of the limiting errors in the analysis of astrometric and geodetic VLBI observations. By using VLBI images obtained with the Very Long Baseline Array, we evaluate this effect for 392 sources from the International Celestial Reference Frame (ICRF). Based on this evaluation, we define a “structure index”, ranging from 1 for the very compact sources to 4 for the most extended sources, which can be used as an estimate of the astrometric suitability of the sources. The structure index distribution in each ICRF source category (defining, candidate, other) is presented. We also discuss the correlation between structure index and source position accuracy. This classification is useful to select the most compact sources to observe in future VLBI experiments and to down weight past observations on sources with excessive structure.

## 1 Introduction

The International Celestial Reference Frame (ICRF), the most recent realization of the VLBI celestial frame, is defined by the radio positions of 212 extragalactic sources distributed over the entire sky (Ma *et al.* 1998). These “defining” sources set the initial direction of the ICRF axes and were chosen based on their observing histories with the geodetic networks and the stability and accuracy of their position estimates. The highest quality positions in the ICRF are accurate at the 0.25 milliarcsecond (mas) level. In addition, positions for 294 less observed “candidate” sources and 102 “other” sources with excessive position variation, were also given to densify the frame (Ma *et al.* 1998). Improvements to the ICRF over previous realizations of the celestial frame (e.g. Johnston *et al.* 1995) included modeling of a tropospheric gradient effect which corrected a systematic position offset of nearly 0.3 mas for sources near the celestial equator. The ICRF has been adopted by the International Astronomical Union as the fundamental celestial frame, replacing the FK5 optical frame as of 1998 January 1.

Despite its unprecedented accuracy, the ICRF suffers from errors primarily due to intrinsic source structure. At the milliarcsecond scale, most of the extragalactic sources that form the VLBI celestial frame exhibit spatially-extended structures that are variable in both time and frequency. Such radio structures set limits on the accuracy of source positions estimated with VLBI astrometry unless their effects can be accounted for. Modeling these effects and evaluating their magnitude in the VLBI measurements require knowledge of the brightness distribution of the sources at the epoch of the observations. To this end, an observing program whose goal is to image all the ICRF sources on a regular basis, has been initiated (Fey *et al.* 1996, Fey & Charlot 1997). Based on observations with the Very Long Baseline Array (VLBA), this program has recently reached an important milestone with the completion of first-epoch imaging of approximately 90% of the ICRF sources north  $-20^\circ$  declination.

This paper evaluates the overall impact of source structure effects in the ICRF from the available VLBA images of 392 ICRF sources. The “structure index” defined by Fey & Charlot (1997) is calculated and used to quantify the magnitude of these effects in the band width synthesis (BWS) delay VLBI measurements. We discuss the structure index distribution in each ICRF source category (defining, candidate, other) and the correlation between structure index and source position accuracy. Both of these tests show that the structure index is an appropriate indicator of the compactness of the sources and their astrometric quality. The classification proposed here can therefore be used to identify the most suitable sources for highly-precise VLBI astrometry and geodesy.

## 2 Evaluation of the magnitude of source structure delay effects

The contribution of intrinsic source structure to a BWS delay measurement is derived from the complex visibility measured by a VLBI interferometer. As shown by Charlot (1990), this contribution depends on the brightness distribution of the extended radio source and the coordinates  $u$  and  $v$ , which are the coordinates of the baseline vector projected on the plane of the sky, expressed in units of the observed wavelength. Because of this sole dependence on the  $(u,v)$  coordinates, the overall source structure effect magnitude for a given source is most easily estimated by calculating these effects successively for a range of  $(u,v)$  coordinates. Following such a scheme, Fey & Charlot (1997) defined a “structure index” according to the median of the calculated structure corrections for all projected VLBI baselines that could be possibly observed with Earth-based VLBI (i.e with a  $(u,v)$  length smaller than the diameter of the Earth), separating the sources into four classes as follows:

$$\text{Structure index} = \begin{cases} 1, & \text{if } 0 \text{ ps} \leq \tau_{\text{median}} < 3 \text{ ps}, \\ 2, & \text{if } 3 \text{ ps} \leq \tau_{\text{median}} < 10 \text{ ps}, \\ 3, & \text{if } 10 \text{ ps} \leq \tau_{\text{median}} < 30 \text{ ps}, \\ 4, & \text{if } 30 \text{ ps} \leq \tau_{\text{median}} < \infty. \end{cases}$$

Based on this definition, two structure indices are obtained for each source, one at X band (3.6 cm wavelength) and one at S band (13 cm wavelength), each of which indicating the compactness of the structure at the corresponding frequency band. Dual-frequency observations allow for an accurate calibration of the frequency-dependent propagation delay introduced by the Earth’s ionosphere. For consistency with this calibration, the structure corrections are scaled by 1.08 at X band and 0.08 at S band, prior to the structure index assignment. These scale factors represent the relative contribution of the X- and S-band delay measurements to the dual-frequency-calibrated delay, which is the quantity actually modeled for the determination of astrometric positions. The interested reader is referred to Fey & Charlot (1997) for more details on the structure index definition and Charlot (1990) for a more thorough discussion of the algorithm to calculate source structure effects in the VLBI delay observable.

Shown in Fig. 1 are contour plots of the radio emission at X band of four ICRF sources (0138–097, 0108+388, 0544+273 and 2201+315) representative of each structure index class. The corresponding structure-effect maps showing the magnitude of the corrections to the VLBI delay observable as a function of the interferometer resolution are also represented along with indication of the mean, rms, median and maximum values of these structure corrections. Figure 1 reflects the increase of the magnitude of the structure effects as the brightness distribution becomes more extended. For 0108 + 388, these effects are very large because the source structure is composed of two components of approximately equal strength, causing very low visibility regions in the  $u$ - $v$  plane and consequently large structure corrections (see Charlot [1990] for a detailed study of the case of a two-component model). Fey & Charlot (1997) recommend that only sources with a structure index of either 1 or 2 be used for the most precise astrometric or geodetic work. Sources a structure index of 3 should only be used with caution while those with a structure index of 4 should not be used at all.

The initial classification of Fey & Charlot (1997) included 169 sources. By using the additional VLBA maps now available, we have extended this classification, completing the calculation of the

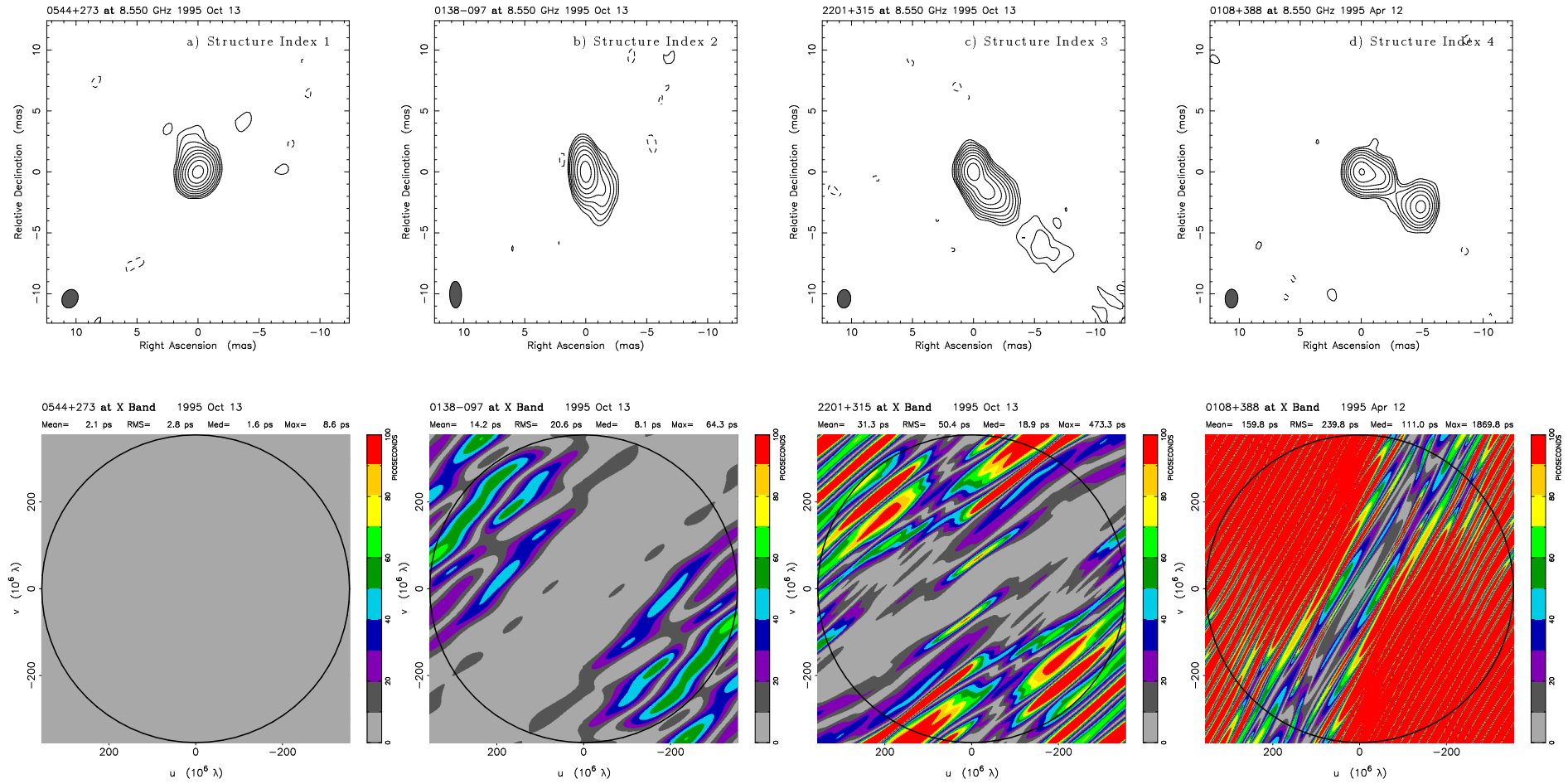


Fig. 1: Top: Contour plots of the radio emission at 3.6 cm wavelength for the four ICRF sources a) 0544 + 273, b) 0138 – 097, c) 2201 + 315 and d) 0108 + 388, representative of each structure index class. The X-band structure index of these sources is indicated in each panel. Bottom: Color plots showing the magnitude of the structure correction (absolute value) induced in the BWS delay by the extended radio emission at X band for the same four sources. The structure correction is plotted as a function of the length and orientation of the VLBI baseline projected onto the sky, expressed in millions of wavelengths ( $u, v$  coordinates). The color scale is identical in each panel and ranges from 0 to 100 picoseconds (ps). All structure corrections larger than 100 ps are plotted as red. The circle drawn in these plots has a radius equal to one Earth diameter, corresponding to the longest baselines that can be theoretically observed with Earth-based VLBI. The mean, rms, median, and maximum values of the structure corrections for all baselines contained within this circle are indicated in each panel.

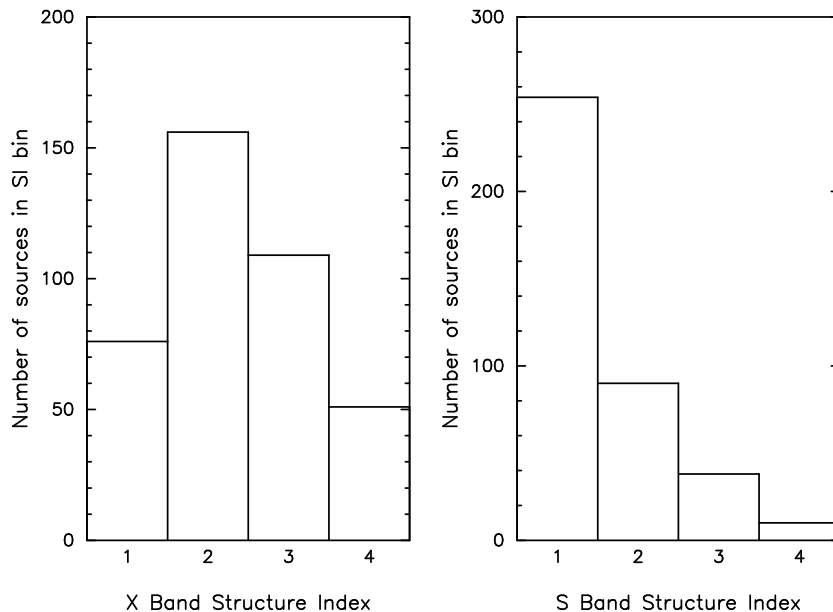


Fig. 2: Distribution of the X- and S-band structure indices for 392 ICRF sources.

X- and S-band structure indices for 392 ICRF sources<sup>1</sup> Such a sample, about two-third of the ICRF catalog, provides a strong basis for evaluating the overall astrometric suitability of the ICRF sources, as discussed in the next section.

### 3 The “structure index” as an indicator for astrometry

In this section, we examine the structure index distribution in the ICRF catalog and discuss the correlation between structure index and ICRF source position accuracy. Figure 2 shows the overall structure index distribution for the 392 ICRF sources which structure corrections have been evaluated. At X band, 232 sources (approximately 60% of the sources in our sample) have a structure index of either 1 or 2, an indication of compact or very compact structures suitable for high-precision VLBI astrometry and geodesy. The remaining 160 sources with a structure index of either 3 or 4 have more extended structures which are likely to affect the observed VLBI delays. Such sources, especially those with a structure index of 4 (approximately 13% of the sources in our sample), should be avoided in VLBI experiments requiring the highest accuracy. At S band, source structure effects appear to be less significant, as reflected by the large number of sources with a S-band structure index of either 1 or 2 (343 sources out of 392). This is a consequence of the S-band structure corrections being scaled by a factor of 0.08 when calculating the dual-frequency calibrated structure delays. Without scaling, the S-band corrections are very large because source structures are generally more extended at S band than at X band. Comparing the X- and S-band structure indices individually for each source indicates that with a few exceptions all sources that have a S-band structure index of either 3 or 4 have also a X-band structure index of either 3 or 4. Therefore, the X-band structure index alone appears to be a good selection criteria for the choice of the most compact sources.

In Fig. 3, the X-band structure index distribution is compared for each ICRF source category. The difference in distribution between the defining-sources and other-sources categories is striking. While two-third of the defining sources (109 sources out of 164) are found to have a structure index of either 1 or 2, only 45% of the “other” sources (37 sources out of 82) have similar structure indices. This confirms that a large fraction of the “other” sources were rejected during the construction of the ICRF because of structure problems. The candidate-sources category appears to have a distribution intermediate

<sup>1</sup>Source images can be obtained from <http://www.usno.navy.mil/RRFID>. Structure-correction maps and structure indices are available from <http://www.observ.u-bordeaux.fr/public/radio/PCharlot/structure.html>.

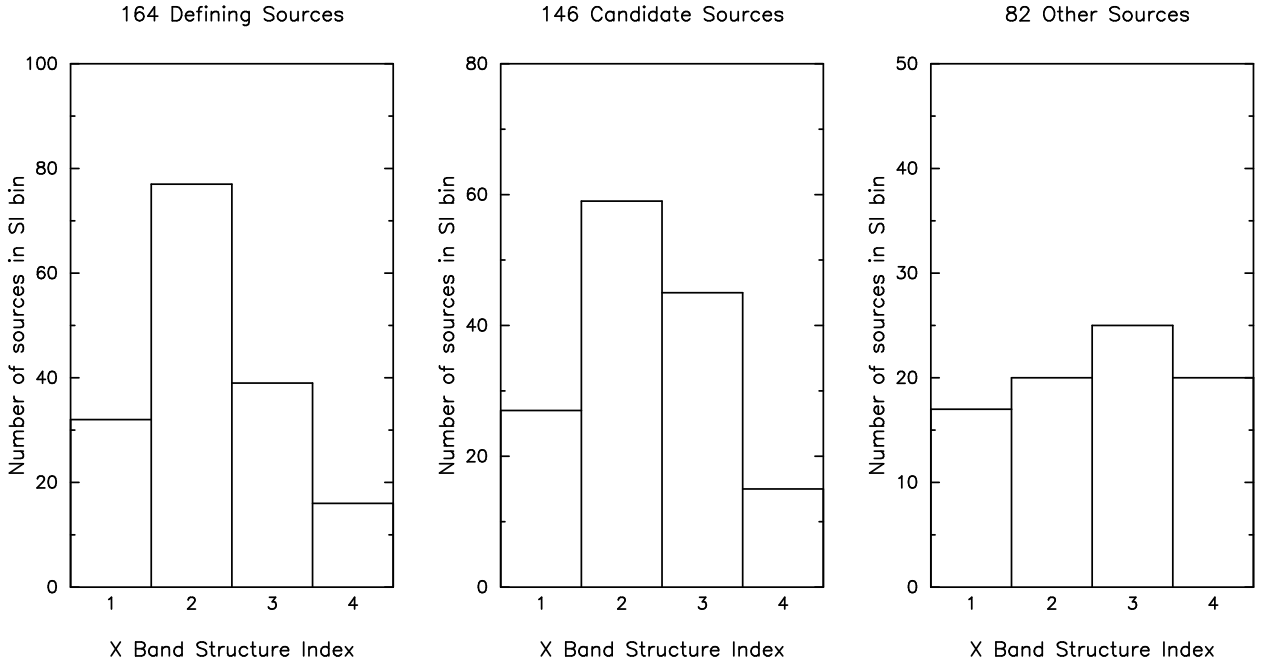


Fig. 3: Distribution of the X-band structure index for the ICRF defining, candidate and “other” sources.

between that of the defining-sources and other-sources categories, with 59% of the candidate sources having a structure index of either 1 or 2. We note that their distribution is almost identical to the overall structure index distribution at X band (Fig. 2), which is consistent with the fact that some of the candidate sources could be designated defining sources in future realization of the ICRF as more data become available or analysis improves, whereas some others would fall into the other-sources category. The defining-sources category includes a majority of compact or very compact sources, as expected from their empirical selection at the time the ICRF was built (see Ma *et al.* 1998). However, despite the stringency of their selection, about one-third of the defining sources are found to have a structure index of either 3 or 4, indicating that they are somewhat spatially extended and thus are probably not appropriate for defining the celestial frame with the highest accuracy. Such sources, especially those with a structure index of 4, should be given specific attention in the ICRF maintenance process and be rejected in future realizations of the ICRF if they show unexpected behavior as we may anticipate from the value of their structure index.

An additional test consists in comparing structure index and ICRF source position accuracy on a statistical basis. For this comparison, we have plotted the distribution of uncertainties in right ascension and declination for each X band structure index class (Fig. 4). As shown in these plots, the histograms of source position uncertainties progressively deteriorate from an approximately Gaussian distribution for the structure index 1 class to an almost random distribution for the structure index 4 class. While the structure index 1 and 2 histograms look similar, the structure index 3 histogram has apparently an excess of sources near 0.3–0.4 mas position accuracy. This deterioration of the position accuracy is also confirmed when calculating the median and mean uncertainties in right ascension and declination for each X band structure index class. As shown in Table 1, such values are found to increase regularly as the structure index becomes larger. Note that only sources with more than 100 observations in the ICRF have been retained for this calculation. Position uncertainties for sources with a limited number of observations are dominated by the noise of the measurements rather than by systematic effects caused by extended structures. The results of Fig. 4 and Table 1 confirm the previous finding of Fey & Charlot (1997) which indicates that the more extended sources have larger position uncertainties. They also confirm that the structure index is an appropriate indicator for selecting the most suitable sources to observe in highly-precise astrometric and geodetic VLBI experiments.

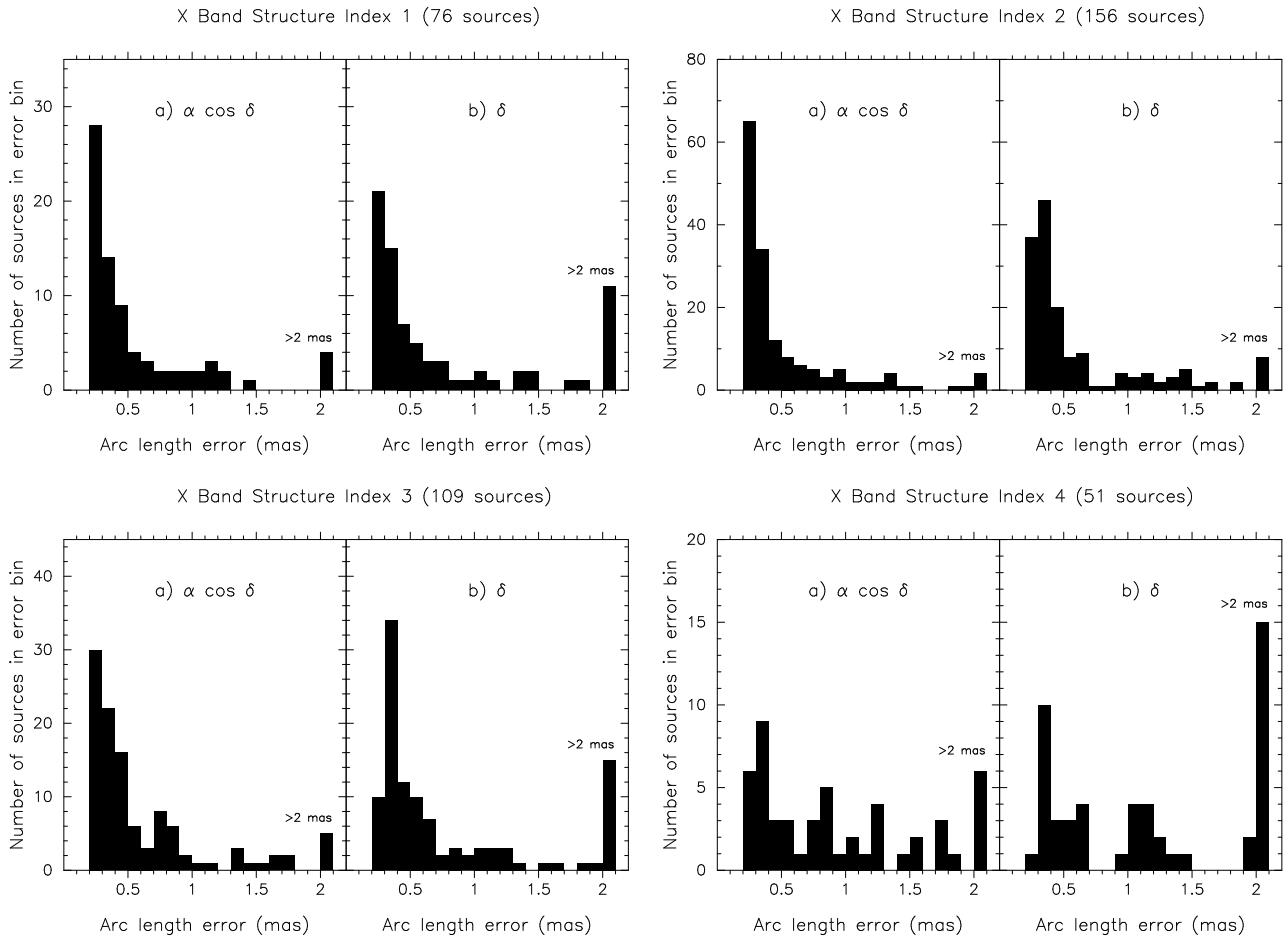


Fig. 4: Distribution of ICRF position uncertainties in a)  $\alpha \cos \delta$  and b)  $\delta$  for each X band structure index class.

Table 1: X band structure index versus ICRF mean and median position uncertainties in  $\alpha \cos \delta$  and  $\delta$ .

Structure index	Nb of sources	Mean uncertainty*		Median uncertainty	
		$\alpha \cos \delta$ (mas)	$\delta$ (mas)	$\alpha \cos \delta$ (mas)	$\delta$ (mas)
1	50	0.34	0.43	0.28	0.31
2	108	0.39	0.46	0.29	0.32
3	73	0.44	0.54	0.33	0.36
4	36	0.54	0.72	0.76	1.07

\*excludes sources with uncertainties in  $\alpha \cos \delta$  or  $\delta$  larger than 2 mas.

## 4 Conclusion

By using new VLBA images of ICRF sources, we have extended the initial work of Fey & Charlot (1997), completing the classification of 392 ICRF sources based on their observed structures. This sample covers approximately 90% of the ICRF catalog north of  $-20^\circ$  declination. Each source is assigned a structure index representing its compactness and astrometric suitability at the corresponding observed frequency band (X or S). This classification shows, as expected, that most of the ICRF defining sources have compact structures, whereas the majority of the ICRF “other” sources are spatially extended. A small percentage of the ICRF defining sources, however, is found to have extended radio emission unsuitable for high-precision VLBI astrometry and geodesy. These should be monitored

carefully in the future to further assess their quality.

A correlation between the structure index and the ICRF source position accuracy has been found, indicating that the more extended sources have larger position uncertainties. This confirms that the structure index is an appropriate indicator for selecting the most suitable reference frame sources. The structure index can also be used to estimate the additional noise introduced into the VLBI delay measurements by intrinsic source structure for application of source-dependent weighting scheme. In the future, we will continue to evaluate the astrometric suitability of the ICRF sources as new VLBI maps become available, and in particular report any structure index variation. We will also investigate the direct application of structure corrections to the VLBI delay observable to improve the position accuracy of the ICRF sources with excessive structure.

## References

Charlot, P.: 1990, *AJ*, 99, 1309.

Fey, A. L., Charlot, P.: 1997, *ApJS*, 111, 95.

Fey, A. L., Clegg, A. W., Fomalont, E. B.: 1996, *ApJS*, 105, 299.

Johnston, K. J., Fey, A. L., Zacharias, N., Russell, J. L., Ma, C., De Vegt, C., Reynolds, J. E., Jauncey, D. L., Archinal, B. A., Carter, M. S., Corbin, T. E., Eubanks, T. M., Florkowski, D. R., Hall, D. M., McCarthy, D. D., McCulloch, P. M., King, E. A., Nicolson, G., Shaffer, D. B.: 1995, *AJ*, 110, 880.

Ma, C., Arias, E. F., Eubanks, T. M., Fey, A. L., Gontier, A.-M., Jacobs, C. S., Sovers, O. J., Archinal, B. A., Charlot, P.: 1998, *AJ*, 116, 546.

## Extension and Maintenance of the ICRF

C. Ma  
Goddard Space Flight Center

T.M. Eubanks  
U.S. Naval Observatory

The ICRF (International Celestial Reference Frame) is the result of a long, carefully considered process, and the extension and maintenance of the ICRF are further steps to improve its usefulness. In the more distant future, based on the ever larger VLBI data set and continued research activities, a new realization of the ICRF will be made. For now the goals are more modest: determining positions of new sources consistent with the ICRF, improving the accuracy of some source positions, and monitoring the sources.

The fundamental concepts of the ICRF were developed and extensively discussed at the IAU Colloquium 127 on Reference Systems held in Virginia Beach in 1990. Under the leadership of J. Kovalevsky and J. Hughes, the General Theory of Relativity for space and time, the use of extragalactic radio objects, and the separation of the celestial reference frame from the equator and the ecliptic were summarized in nine recommendations adopted as a resolution by the XXIst IAU General Assembly in Buenos Aires in 1991. A working group under C. de Veigt was formed to select the list of radio sources to be used with emphasis on the need to connect the radio and optical frames. The XXIIInd IAU General Assembly in Den Haag in 1994 adopted the list and established a new working group under L. Morrison to define the positions of the radio sources in the list. This work was done by a subgroup of VLBI and celestial reference system specialists. The resulting ICRF catalog was adopted by the XXXIIIrd IAU General Assembly in Kyoto in 1997 and came into effect 1 January 1998, replacing the FK5. A new Working Group for the International Celestial Reference System (ICRS) under F. Mignard was formed to carry on the ICRF work, to extend the frame to other objects and frequencies, and to consider the consequences of the ICRF.

The data used to determine the ICRF radio source positions included 1.6 million pairs of dual-frequency delays and rates from 1979 through the middle of 1995. The data were contributed from several geodetic and astrometric observing programs, the vast majority of the observations coming from the former but most of the sources coming from the latter. The design of the analysis was intended to provide (1995) state of the art source positions, in particular to free the results from contamination from anomalous source behavior, geodetic noise, and systematic tropospheric effects. Positions of sources with excessive scatter or apparent motion (as determined from test solutions) were treated as arc parameters as were station positions. An elevation limit of 6 degrees was adopted to balance the need for observing geometry against the difficulty in correctly modeling the troposphere at low elevations. Both delays and rates were used to maximize the information available and to decrease correlations. Tropospheric gradients were estimated to remove a significant systematic effect. Because of the large number and high quality of observations, the formal errors for the positions were exceedingly small, but a detailed error analysis suggested that a floor of  $\sim 0.25$  mas was a better estimate of the accuracy of the catalog. The axes of the frame were aligned to the IERS realization of the ICRS with an error of  $\sim 0.020$  mas. The ICRF work was published in Ma and Feissel (eds.), IERS Technical Note 23, June 1997 and in Ma et al., *Astron. J.* 116:516-546, 1998 July. The IERS Technical Note has a large amount of supplementary material including source structure maps, source structure

correction plots, position time series, and source name aliases. Up to date maps and structure corrections are available from A. Fey, USNO and P. Charlot, Bordeaux Observatory, respectively.

The sources from the ICRF solution were divided after the fact into three categories: 212 defining sources that met a series of quality criteria; 294 candidate sources that failed one or more of the quality criteria, e.g., too few observations or observing interval too short; and 102 “other” sources (whose positions were arc parameters). While the distribution over the sky of the ICRF as a whole is quite uniform, the defining sources are sparser in the southern hemisphere because of a dearth of VLBI stations and limited observing. The “other” sources include a number with relatively bright optical counterparts that could be used to connect the radio and stellar frames.

Task Group T-1 of the IAU Working Group for the ICRS has the formal responsibility for maintaining and extending the ICRF. This includes both observing and analysis. However, the international VLBI community provides the observing and analysis resources for this work, so the IVS has an important role in carrying out this mandate. Since the ICRF was done in 1995, ~800 000 more observations including ~50 new sources have been acquired by geodetic and astrometric programs. These need to be integrated with the data and analysis used for the ICRF. The consensus of the Task Group is that the original ICRF solution need not be copied exactly to incorporate new data, but the new positions must be consistent with the ICRF at its stated level of accuracy, ~0.25 mas in overall source positions and ~0.020 mas in orientation. Positions will be determined for new sources, and updated positions and errors will be found for candidate sources with additional observations. The positions and uncertainties of the defining sources will not be changed since they are the actual realization of the ICRF. There will be some refinement in the analysis configuration, e.g., the use of the Niell mapping function, gradient parameters estimated more frequently than once per day, daily axis offset adjustments, etc. The data for new solutions made to update the ICRF will include the data used initially and whatever new data are relevant. The defining sources will be used in a no-net-rotation condition relative to the ICRF to assure that positions from new solutions are aligned with the ICRF.

Although an update to the ICRF will come from a single solution, it is hoped that several IVS analysis centers will provide source positions on a regular basis for use in the ICRF analysis. Comparison of results is an important part of checking for anomalies. The ICRS Section of the IERS Central Bureau has the responsibility for assuring that new information related to the ICRF is fully consistent with the ICRS. After the results from an update solution have been validated by the ICRS Section, the update will be available through the IERS and IVS web pages. It is anticipated that the time between ICRF updates will be about half a year, but preliminary positions of individual sources may be made available in less time for particular needs. In addition, it is planned to extend the position time series of all sources begun in IERS Technical Note 23 as part of monitoring source behavior.

While the updating process must adhere to the general pattern established for the ICRF in 1995, to advance VLBI astrometry requires new ideas and methods. These may include more sophisticated troposphere modeling, more systematic identification and treatment of anomalous source behavior, analysis of position time series, application of source structure corrections to delays and rates, and refining the distribution of added noise. Since the ICRF is now a unique contribution from VLBI, the IVS encourages such activities and will provide assistance in disseminating information about ICRF work.



# Relative astrometry and phase-reference mapping in the 1636+473 system using MERLIN and Global VLBI

M.J. Rioja <sup>a,b</sup> R.W. Porcas <sup>c</sup> S. Garrington <sup>d</sup> A. Alberdi <sup>e</sup>  
D.J. Saikia <sup>f</sup>

<sup>a</sup>*Observatorio Astronomico Nacional, Alcala de Henares, Spain*

<sup>b</sup>*Istituto di Radioastronomia, Via P. Gobetti 101, Bologna, Italy*

<sup>c</sup>*Max-Planck-Institut fur Radioastronomie, Auf dem Hugel 69, Bonn, Germany*

<sup>d</sup>*NRAL Jodrell Bank, Macclesfield, Cheshire, England*

<sup>e</sup>*Instituto de Astrofisica de Andalucia (CSIC), Granada, Spain*

<sup>f</sup>*National Centre for Radio Astrophysics, TIFR, Pune, India*

---

## Abstract

We present astrometric results and maps from simultaneous MERLIN and Global VLBI observations of the very weak core of the double-lobed radio source 1636+47B, using as reference the bright, compact, flat-spectrum quasar 1636+473 A, 20 arcsec away. The observations were made in May 1995 at 5 GHz. The phase-referenced VLBI map of the weak core, of resolution 1.5 mas, contains a high percentage of the core flux density seen in the MERLIN map. Further hybrid mapping iterations reveal a faint, one-sided core extension on the same side as the MERLIN jet. We investigate the effect of the structure in the strong quasar core on the astrometric separation measurement, and explore the effect of both temporal and other coherence losses on the phase-reference map. We relate our results to the structural asymmetry in weak AGN cores within the context of unification models.

---

## 1 Introduction

At arcsecond resolutions the radio source 1636+473 (4C47.44) consists of two components separated by 20 arcsec in PA 20°. The southern, compact, flat-spectrum component (A) coincides with a quasar of redshift 0.740 (Porcas et al, 1980; Kapahi, 1981); the northern, steep-spectrum component (B) has a flux density of  $\sim 150$  mJy at 5 GHz and is 10 arcsec in extent in PA 80°. There is no coincident optical emission visible on the Palomar Sky Survey.

The structure of 1636+473 was originally classified as of "D2" core-jet type (Browne et al, 1982; Saikia et al, 1984). However, recent higher-resolution radio observations (Saikia, priv. com.) reveal that B has a classical, double-lobe morphology, with a weak, central, compact core of  $\sim 7$  mJy within its structure. Thus 1636+473 consists of two (presumably independent) AGNs. We have made a VLBI and MERLIN phase-referencing study of this system, exploiting the close angular proximity of the strong (A) core to the weak (B) core to make an astrometric measurement of their separation, and to permit phase-reference imaging of the latter.

## 2 Observations

We made simultaneous MERLIN and Global VLBI observations of 1636+473 at 5 GHz on 12/13 May, 1995. We used the EVN antennas at Effelsberg, Westerbork, Medicina and Jodrell Bank (Mk2), and in the US the VLBA antennas at FD, HN, NL and OV, the Green Bank 140ft antenna, and the VLA in phased array mode. For the VLBI we used the MK3 recording system in mode B ("double speed") giving a total bandwidth of 56 MHz for the LHC polarisation channel. Both components of 1636+473 could be observed simultaneously at all antennas except the phased-VLA, where we switched the pointing between the A and B sources during the continuous VLBI scans (A-B-A cycles of 1.5/3.5/1.5 minutes and 1.0/2.5/1.0 minutes for 6.5 and 4.5 min scans, respectively). The VLBI correlation was made at the MPIfR, Bonn processor, using separate correlation passes at accurate A and B core positions, obtained from an analysis of our MERLIN image of the sources. Editing out of the VLA "off-source" correlations, calibration of the visibility amplitudes using antenna radiometry and gain data, and all subsequent analyses were performed using the NRAO AIPS package.

## 3 Analysis and Results

Our MERLIN image of 1636+473 showed A to be unresolved at 60 mas resolution, with a total flux density of 635 mJy. In contrast, most of the extended structure of 1636+473 B is resolved out; our map of the B subfield (figure 1) reveals a compact, unresolved core of 9.17 mJy, with faint traces of the extended emission, and a weak jet in PA  $80^\circ$ . (All maps are made with uniform weighting, and are plotted with contours at levels of -2, -1, 1, 2, 4, 8... etc, times the specified contour interval in the figure captions)

We made a VLBI hybrid map of 1636+473 A (figure 2), using standard fringe-fitting to determine antenna-based residual delays and rates, and many cycles

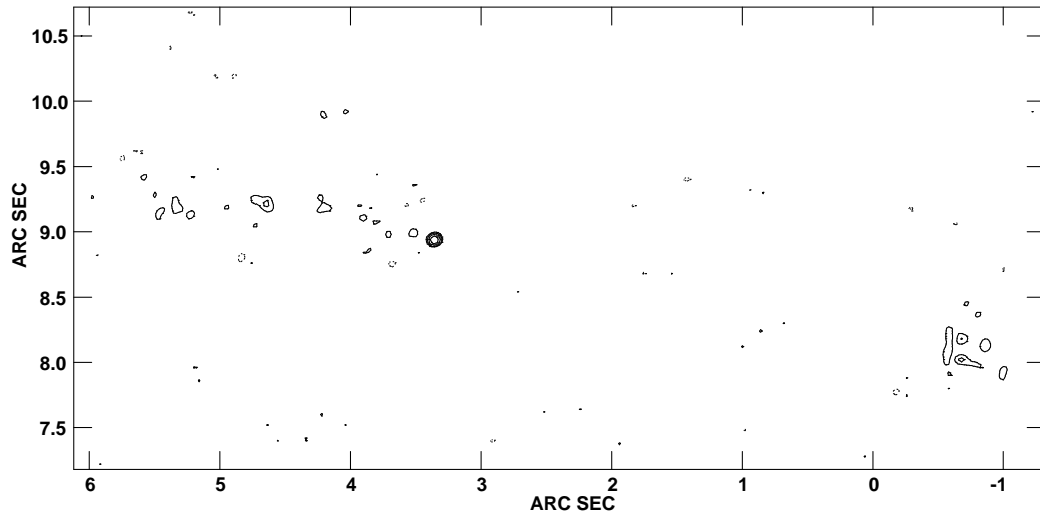


Fig. 1. MERLIN 5 GHz image of 1637+473 B; beam 60 x 60 mas; contour interval 0.6, peak 8.91, rms 0.20 (mJy/beam)

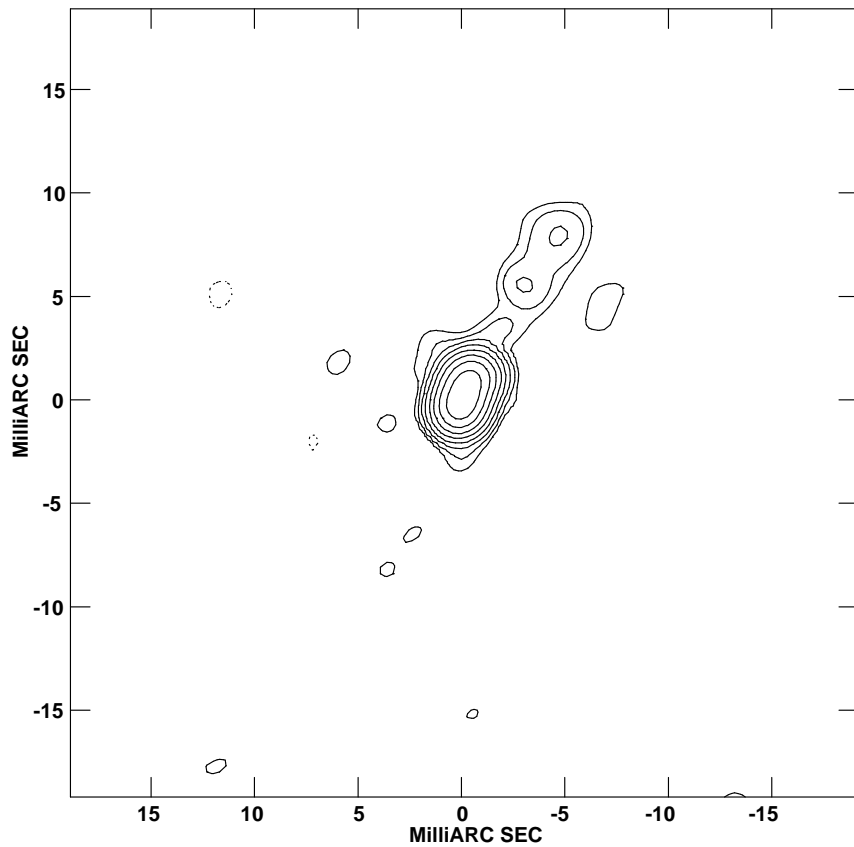


Fig. 2. VLBI 5 GHz hybrid map of 1636+473 A; beam 1.5 x 1.5 mas; contour interval 1.4, peak 331.3, rms 0.43 (mJy/beam)

of phase self-calibration, mapping and CLEAN deconvolution. Amplitude self-calibration was also applied in the last stages. At 1.5 mas resolution this quasar exhibits an extended core (1.9 x 0.3 mas in PA  $-22^\circ$ ) and a faint, one-sided

jet in PA  $-30^\circ$ , traceable out to  $\sim 10$  mas. The sum of the core and jet flux densities in the map is 603 mJy, some 94% of the MERLIN flux density. This may indicate missing, low-brightness emission, but is also the level of the relative calibration uncertainty between the MERLIN and VLBI data sets.

We made phase-reference maps of 1636+473 B (figure 3) after applying to

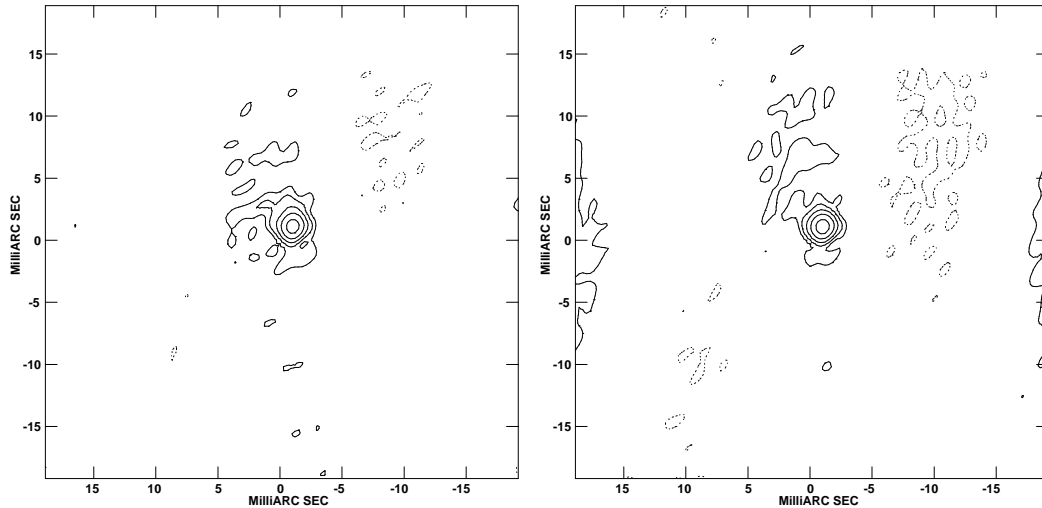


Fig. 3. VLBI 5 GHz phase-reference maps of 1636+473 B; beam 1.5 x 1.5 mas, contour interval 0.3 mJy/beam. Left: Using all data; peak 6.56, rms 0.13 mJy/beam. Right: Excluding baselines to VLA; peak 6.81, rms 0.12 mJy/beam

the B data the rate and delay corrections determined from fringe-fitting the A data, and the total phase and amplitude corrections from self-calibration. This procedure assumes an accurate separation of instrumental and structural phase contributions for A, a sufficiently precise geometrical model for correlation, atmospheric spatial coherence over 20 arcsec, and temporal coherence over the VLA source-switching interval for baselines to the VLA. The peak flux densities for maps made with and without VLA baselines are 6.56 and 6.81 mJy, respectively; this difference may be attributed to the coherence loss due to temporal phase fluctuations on baselines to the VLA.

The rms noise levels in these maps of B are 3 to 4 times lower than the noise level in the A map, but both are considerably above the "thermal noise" level expected. In the A map the residual noise level is probably dominated by data calibration errors and "mapping" noise. In the B maps there may be contributions from "coherence" errors in the transfer of instrumental phase between the two sources, and there may also be contributions from any unsuppressed response from the strong A source in the weak visibility data for B on short baselines.

We also made a hybrid map of 1636+473 B (figure 4), using the phase-reference map as an input for phase self-calibration and a longer solution interval (3 mins). As expected, in this map the peak flux density is higher, and the rms

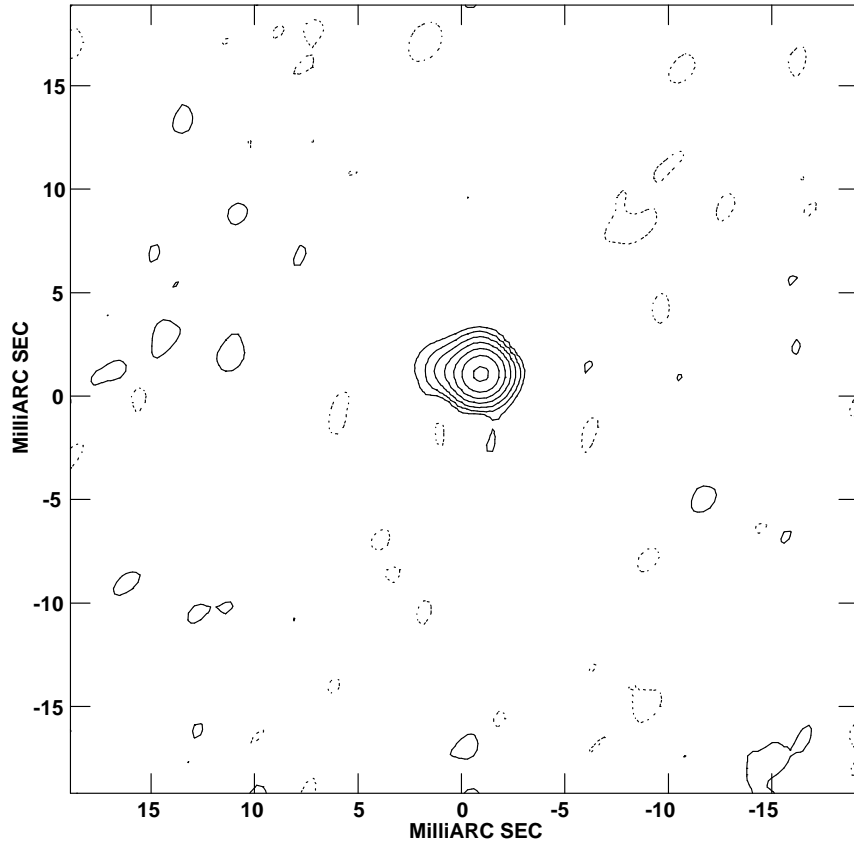


Fig. 4. VLBI 5 GHz hybrid map of 1636+473 B; beam 1.5 x 1.5 mas, contour interval 0.1, peak 7.38, rms 0.042 (mJy/beam)

noise lower, than in the phase-reference maps. The "coherence" losses of 8 to 12% in the phase-reference maps indicate that the requirements mentioned above for this procedure are not completely fulfilled. The hybrid map of B shows a faint  $\sim 2$  mas extension of the core in PA  $\sim 80^\circ$ , on the same side as, and pointing towards, the faint jet features seen in the MERLIN map. The total flux density of the core and extension is 8.75 mJy, i.e. 95% of the MERLIN core flux.

#### 4 Relative astrometry

The 1636+473 A hybrid map and B phase-reference maps were made after applying identical phase corrections to the raw visibility outputs from the A and B correlations. Differences between the position offsets of features of A and B from their respective map centres thus measure corrections to the difference between the A and B positions used for correlation. These positions, and measurements of the position offsets of the A and B cores from their map centres (made using the AIPS task MAXFIT) are presented in table 1. The

Table 1  
Positions used for correlation, and core position offsets in maps

Source	RA (J2000)	Dec (J2000)	map	RA offset	Dec offset
	hh:mm:ss.ssssss	dd:mm:ss.sssss	type	(mas)	(mas)
1636+473 A	16:37:45.136200	+47:17:33.80100	hybrid	-0.06	+0.09
			sup.res	+0.12	-0.43
1636+473 B	16:37:45.739200	+47:17:51.58100	ph.ref	-1.04	+1.17

very small correction of the B position (with respect to the A position) of  $\sim 1$  mas in each coordinate is remarkable, since the MERLIN positions were measured with a beam of 60 mas. A conservative estimate of the precision of the measured VLBI position offsets is 1/15 of the beam (i.e. 0.10 mas).

The extended and asymmetric nature of both cores limits the accuracy with which their peak positions can be specified, however, since these may be resolution-dependent. We made "super-resolved" maps of both A and B, using smaller map pixel sizes and CLEAN restoring beams (figure 5); cuts across the

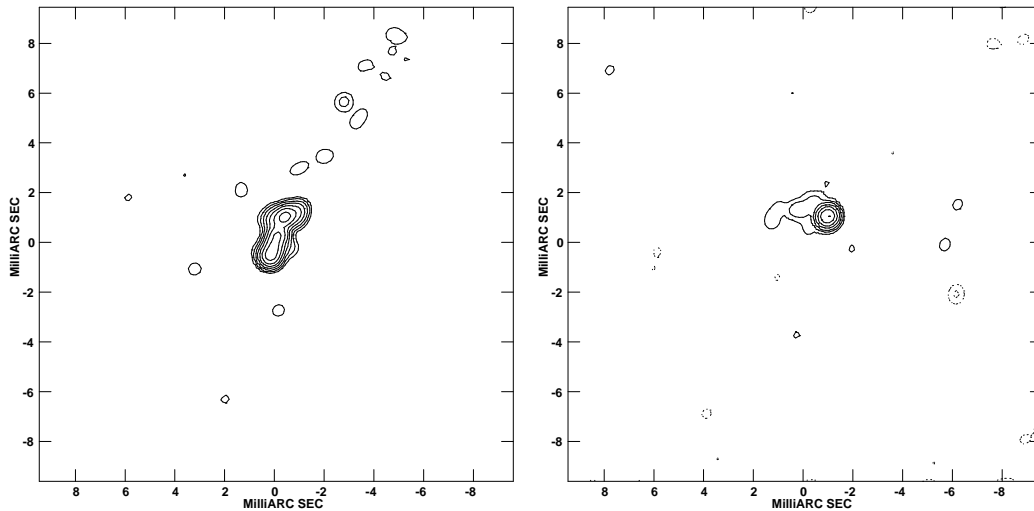


Fig. 5. VLBI 5 GHz "super-resolved" maps; beam 0.5 x 0.5 mas. Left: 1636+473 A, contour interval 1.4, peak 152.8, rms 0.39 (mJy/beam). Right: 1636+473 B, contour interval 0.1, peak 6.43, rms 0.030 (mJy/beam)

cores along the jet axes are given in figure 6. The extended core of A appears to consist of at least 2 or 3 sub-components. The position of the strongest of these is also given in table 1; it is offset from the lower-resolution "core" position by 0.55 mas in PA  $161^\circ$ . The extension of the B core appears to be caused by a weak, 0.4 mJy component, offset by  $\sim 1.3$  mas to the east. However, as the B hybrid map was produced with additional cycles of phase self-calibration, position offsets cannot be directly related to those in the A

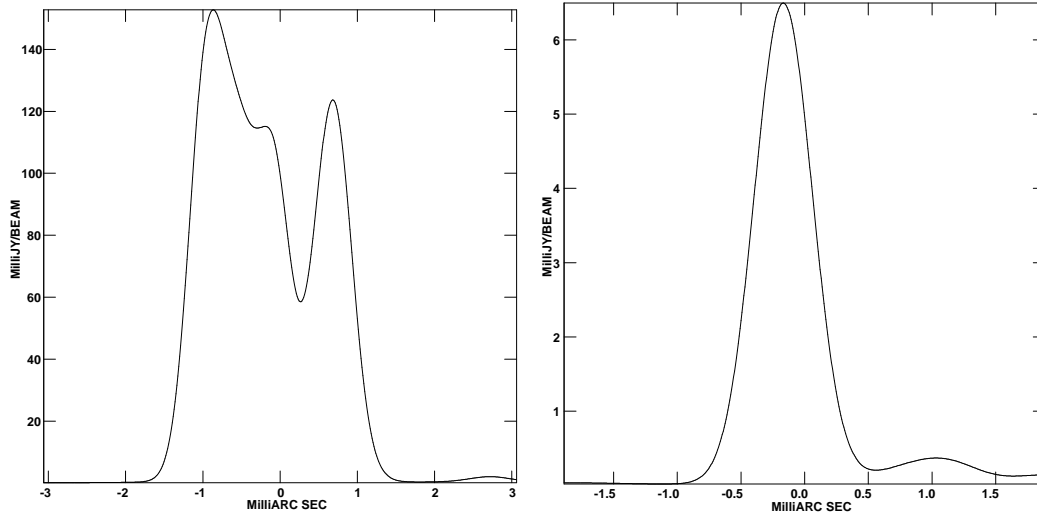


Fig. 6. Cuts across cores in super-resolved maps. Left: 1636+473 A in PA  $-17^\circ$ . Right: 1636+473 B in PA  $+83^\circ$

map. (In fact, the B core position offset moved  $+0.08$  and  $-0.11$  mas in RA and Dec, respectively, between phase-reference and hybrid maps)

## 5 Discussion

We have successfully mapped the 9 mJy core located within the extended emission of 1636+473 B. Errors in determining antenna phases on the reference source (A) and in transferring them over 20 arcsec cause "coherence" losses in the phase-reference maps and limit their dynamic range; temporal phase interpolation produces further degradation. We have measured astrometric corrections to the MERLIN relative positions of the A and B cores, with a precision of  $\sim 0.1$  mas; however, the "position" of at least the A core is resolution-dependent.

The compact nature of the 1636+473 B core, and its one-sided extension which is closely aligned with the direction of the MERLIN jet, confirm beyond any remaining doubt that it is an independent radio-emitting AGN, unrelated to the quasar 1636+473 A. Its mas-scale properties are similar to those of the weak quasar cores investigated by Porcas et al (1990) and Hough et al (1999). 1636+473 B has a value of 0.06 for R, the flux ratio between the core and extended lobe emission. In unified schemes (e.g. Orr & Browne, 1982; Barthel, 1989) this would suggest a relatively large angle to the line of sight, consistent with the obscuration of any non-thermal optical quasar nucleus by a torus. Asymmetries in the radio structure caused by Doppler boosting should be relatively mild in 1636+473 B; from the absence of detectable emission greater than 3 times the rms noise in the hybrid map, we can put a weak lower limit

to the jet/counter-jet brightness ratio of  $\sim 3$ .

## 6 Acknowledgements

We thank Michael Garrett and Bob Campbell for their comments on an earlier version of this paper.

## References

- Barthel, P.D., 1989, *ApJ*, 336, 606  
Browne, I.W.A., Orr, M.J.L., Davis, R.J., Foley, A., Muxlow, T.W.B., & Thomasson, P., 1982, *MNRAS*, 198, 673  
Hough, D.H., Zensus, J.A., Vermeulen, R.C., Readhead, A.C.S., Porcas, R.W., Rius, A., Rector, T.A., Lenz, G.C., Davis, M.A., & Snowdall, J.C., 1999, *ApJ*, 511, 84  
Kapahi, V.K., 1981, *A+A Supp*, 43, 381  
Orr, M.J.L., & Browne, I.W.A., 1982, *MNRAS*, 200, 1067  
Porcas, R.W., Urry, C.M., Browne, I.W.A., Cohen, A.M., Daintree, E.J., & Walsh, D., 1980, *MNRAS*, 191, 607  
Porcas, R.W., Flatters, C., & Owen, F.N., 1990, in: Zensus, J.A., Pearson, T.J. (eds), *Parsec-Scale Radio Jets*, Cambridge University Press, p.117  
Saikia, D.J., Shastri, P., Sinha, R.P., Kapahi, V.K., & Swarup, G., 1984, *J.A.A.*, 5, 429

# Phase-reference mapping of nearby stars: status report

W. Alef (MPIfR, Bonn)  
 A. Benz (ETH, Zürich)  
 J. Conway, M. Pestalozzi (Onsala)  
 T. Beasley (NRAO, Charlottesville)

## Abstract

We have observed radio emitting stars in phase-referenced mode with both the VLBA and the EVN in order to map their brightness distributions and to determine precise astrometric parameters. While the VLBA correlator uses the CALC 8 model, the older MK3 correlator model is not sufficient to make phase-referenced mapping possible using the visibility amplitude and residual phase. In the raw MK3 correlated data we have successfully replaced the correlator model with the CALC 8 model. We have shown that phase-reference mapping is possible with MK3 data for source separations of 2 to 3 degrees. At present we are exploring the possibility of removing ionospheric and atmospheric contributions, which are not modelled at all in CALC 8, and which decrease the SNR in phase-reference maps in general by a factor of 2 to 3.

## 1 Introduction

Standard VLBI observing techniques are sensitivity-limited to radio sources whose correlated flux can be detected by integration within the time interval for which the interferometer can be regarded as phase-stable. This time — the coherence time — ranges from a few seconds for the highest and lowest observing frequencies used in VLBI to 20 minutes and more for intermediate frequencies under favourable conditions. Another drawback of the standard methods is that the so-called phase self-calibration algorithms remove all astrometric information contained in the data.

The coherence of a VLBI interferometer can be extended by calibrating the phase instabilities. This is achieved by switching between the target and a nearby strong phase-calibrator on time scales shorter than the coherence time. At the same time absolute relative astrometric information can be retained (relative to the calibrator). This method is called phase-referencing. When used to map (weak) radio sources directly, we speak of phase-reference mapping, and the image of the observed object is recovered by Fourier-transforming<sup>1</sup> all the phase-calibrated data from the (u,v)- to the image-plane and subsequent de-convolution.

For astronomical VLBI observers it is very desirable if the production of phase-referenced images can be done within the framework of the most widely used astronomical data reduction and mapping software AIPS (Greisen, 1990) which is also used for reducing standard VLBI observations.

In AIPS nearly all programs that are needed for phase-reference mapping are already available. All of the data manipulation is done on the residual correlated data. The disadvantage of this approach is that bad correlator models like that used in MK3 correlators, or errors in the a priori interferometer geometry can lead to de-correlation in the phase-referenced image (see Fig. 1) such that the flux of the source to be mapped is spread around in the image so that the target cannot be detected anymore as it is swamped by the increased noise. In addition changes in the correlator model can make astrometric comparisons between different observing epochs difficult or even impossible.

To overcome the above mentioned problems one of us has written an AIPS task which allows to change the correlator model after the correlation (Beasley & Alef, 1998).

---

<sup>1</sup>The Fourier-transformation vector sums all the (u,v)-data, with a different phase gradient applied for each point in the image plane

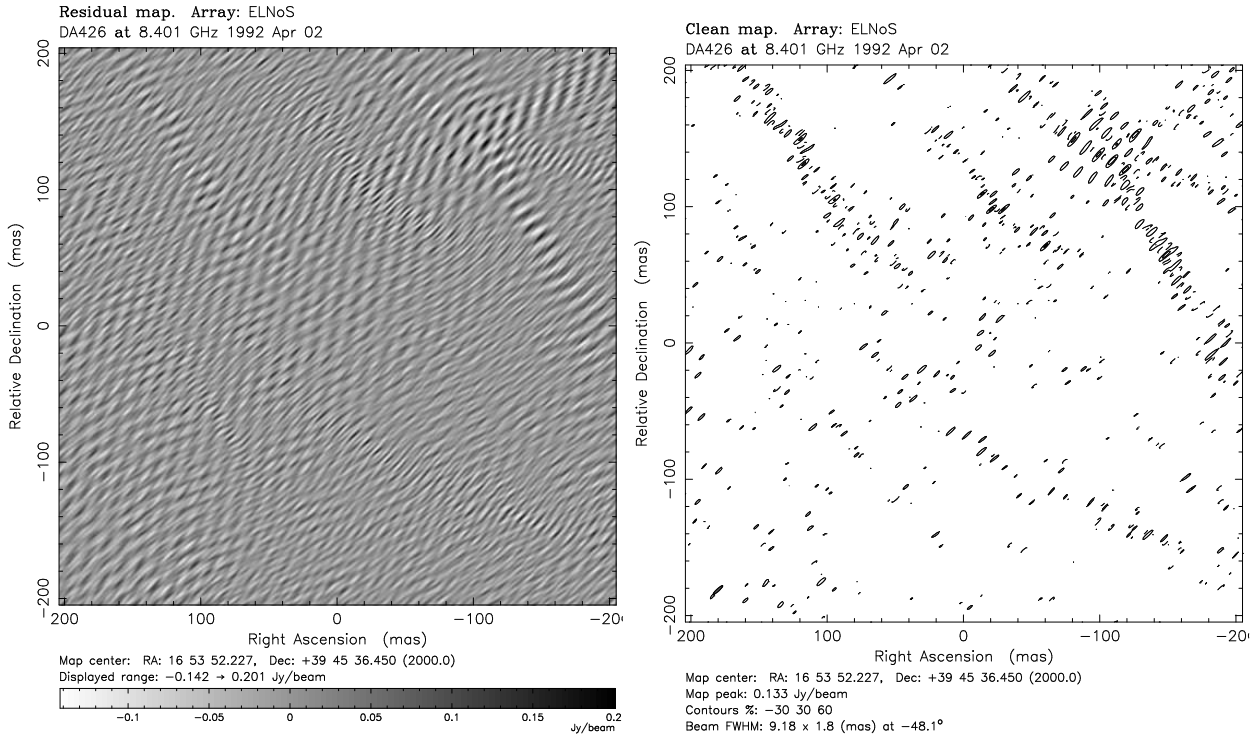


Fig. 1: The left picture shows the dirty (not de-convolved) image of the test target source. The right picture shows the same image, but de-convolved. The source flux appears spread in a wide area in the upper right corner of the images. This is due to errors in the interferometer geometry and a simplistic correlator model.

## 2 Observations

There is an increasing desire to extend the high-resolution studies of radio sources to objects with lower flux, which cannot be investigated anymore with the standard methods of VLBI interferometry. Our group is studying the radio emission from dwarf stars of spectral type M (dMe; Gary and Linsky, 1981), which produce emission from occasional flares as well as the persistent, low-level, slowly variable ‘quiescent’ component. Typical fluxes range from a few tens of mJy during flares down to about 1 mJy for the quiescent phases. Our main aim is to gain more understanding of the emission processes. Eventually we would like to make a radio image of suitable stars whose size matches the resolution properties of the available arrays. The most difficult and challenging project requires high precision astrometry: search for “small” planets orbiting at a few AU around nearby stars. With optimistic assumptions we should be able to detect a planet of 0.1 Jupiter mass circling a star with  $0.3 M_{\odot}$  at a distance of 5 pc.

So far our group has observed five different stars with typical fluxes around 1 mJy. We used both the VLBA supplemented by the high sensitivity of the tied VLA array, and the EVN (Effelsberg, Medicina, Noto, Onsala, Shanghai, Urumqi) together with telescopes of the geodetic network (Crimea, Madrid, Matera, South Africa, Wettzell). The observations were done at 8.4 GHz. The recording bit rates were 128 and 112 Mbit/s (Mode A) respectively. In all cases the telescopes switched back and forth between the star and a strong compact radio source — the phase calibrator — within 5 minutes in order to track the phase instabilities. The separation of target and reference was in all cases about  $2^{\circ}$  to  $3^{\circ}$ .

The theoretical  $1 \sigma$  image noise limit for both arrays for a full track and about five hours net data on the target is about  $50 \mu\text{Jy}$ . For a reliable detection of a point source we need about  $10 \sigma$ . Thus we should be able to detect point sources as weak as  $500 \mu\text{Jy}$ .

Not all of the EVN observations were successful, e.g. incompatibilities between geodetic and astronomical setups for the VC to IF patching (has to be done by hand) caused data loss. A hardware failure of the Effelsberg telescope made a complete observation worthless.

### 3 Software Development

All of the post-correlation data reduction was done in AIPS using the residuals to the correlator model. The data reduction path was as follows:

1. The raw correlated data was loaded from DATs. For VLBA data the AIPS task FITLD is used while MK3 data is read in with MK3IN. The VLBA correlator produces data in the cross-spectral domain with an antenna-based model stored with the data. MK3IN transforms the data from a baseline- and lag-based MK3 correlator to the cross-spectral domain and recovers an antenna-based correlator model from the baseline-based information in the data. After this initial step the data set is a file with all the raw correlation coefficients with weights (formal errors) and a set of tables with source, antenna, frequency, flag, and scan information, a calibration table which is filled and modified in the following steps, and maybe a table with the correlator model.
2. Phase-cal phases, parallactic angle corrections, and amplitude calibration were applied (stored in the calibration table). Data known to be bad were flagged.
3. The data of the phase-calibrator were fringe fitted with the antenna-based fitting task FRING. The structure phase of both sources is still contained in the data.
4. The resulting phase and delay measured on the calibrator were interpolated over the gaps in which the target source was observed. The phase ambiguities were resolved by using the fringe rates. Resulting values for the target source were stored in the calibration table
5. The data were split into a file per source and the calibration table is applied to the data of both the reference and the target, which scales the amplitudes and subtracts the (time-dependent) instrumental phase from the visibility measurements.
6. The phase-calibrator was mapped with standard phase self-calibration techniques. Positional information for this source is lost.
7. The structure phase derived from the image of the phase-calibrator is transferred to the target source file and subtracted. The phase-center of the image is now the reference point for the relative position of the target source.
8. The data of the target source were resampled onto a regular (u,v) grid, it was inverted and deconvolved in the image plane. The resulting phase-referenced image shows (assuming sufficient SNR) the true residual of the source positions used in the correlator model.

This worked well for VLBA data (with the above restrictions for inter-epoch comparisons). In order to make the above simple scheme feasible for MK3 data a new task PHREF was written which extracts the correlator model from the existing calibration table and replaces it with the CALC 8 model. This is reflected in a modified calibration table which has new calibration phases, rates and delays. After applying this table to the (u,v) data (step 5) the residual delays, rates and phases are equivalent to those that would have been produced using the VLBA correlator model. Station and source coordinates, clock parameters and time information are supplied via an external text file and can thus be different from the ones used at correlation time. This task has to be executed after step 1. The program was tested with short pieces of VLBA data with various errors in the interferometer geometry. The data corrected with PHREF was then compared to the same data correlated with the correct geometry. Some MK3 data correlated both at the Bonn MK3 correlator and at the VLBA correlator was used to test the MK3 mode of the program.

Known deficiencies are:

- The correction for the feed rotation of ALTAZ mounted antennas is not included in the CALC model and has to be applied with a different program.

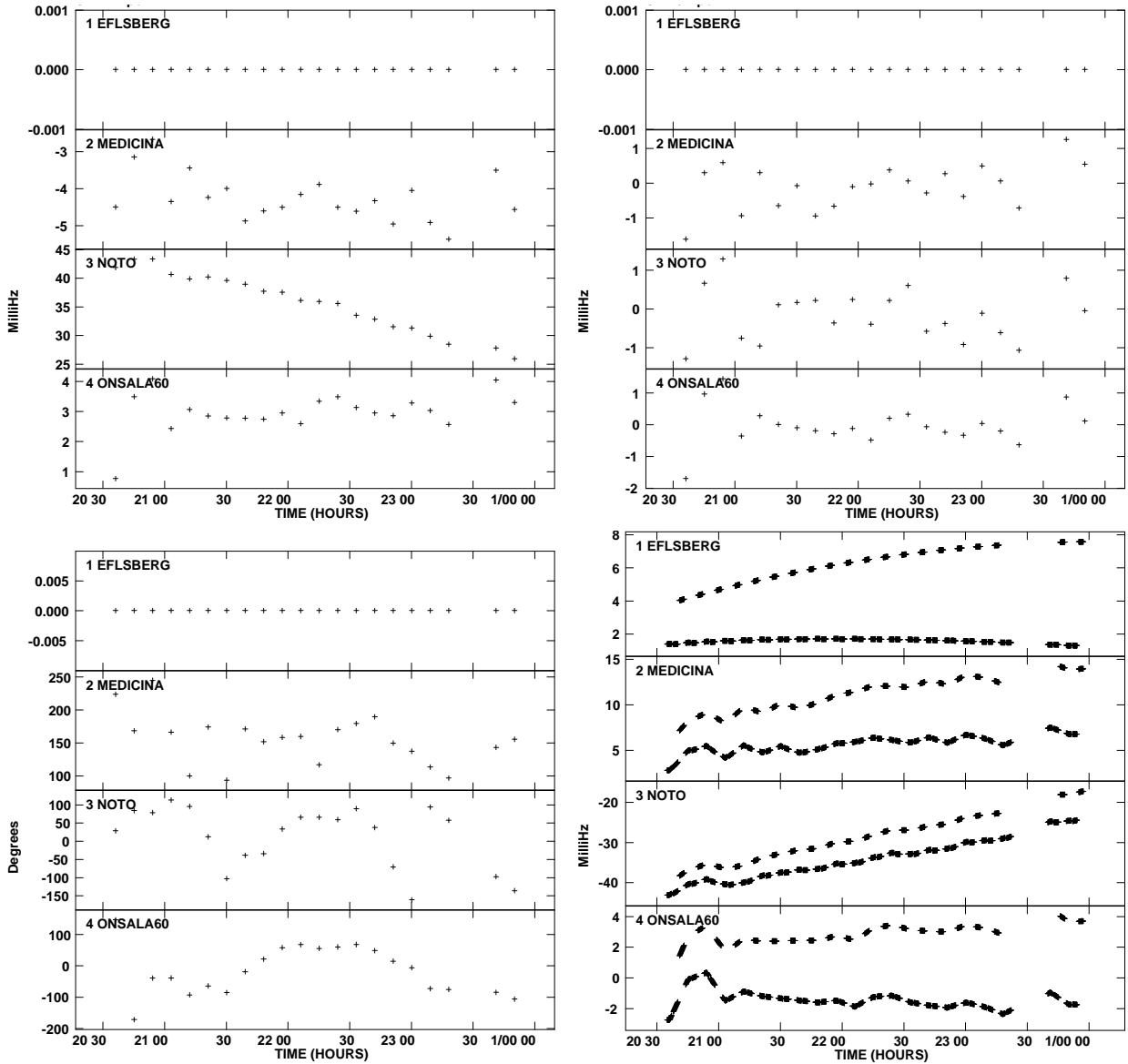


Fig. 2: The figures show residuals per station as calculated by AIPS task FRING. Effelsberg was used as the reference station. Its residuals were arbitrarily set to 0. From left to right are shown: a) residual rate in mHz for uncorrected MK3 data, b) residual rate in mHz for MK3 data corrected by PHREF, c) residual phase in degrees of the corrected data, d) the total correction in fringe rate as estimated by PHREF + FRING residuals

- No correction for ionospheric delay is possible at present, neither with measured values (e.g. GPS) nor with a model ionosphere.
- Only a station elevation dependant model of the dry atmosphere is used.
- Corrections for parallax are not implemented.
- Proper motion of stars cannot be taken into account. E.g. one star of our sample moves at 0.3 mas/h.

## 4 Results

We made further tests with MK3 data. A data set from a phase-referencing observation on two strong sources was analysed. As both a standard image and a phase-referenced image could be made, it was possible to verify how well the phase-reference mapping method works compared to the standard one.

A comparison of the fringe-fitting results of the calibrator (Fig. 2) shows that the original data has high residuals e.g. in fringe rate (Fig. 2a), while the corrected data gave residual fringe rates in a range of roughly  $\pm 1.5$  mHz per antenna (Fig. 2b). The residual phases are slowly varying and can even be connected by eye (Fig. 2c). The total correction e.g. in fringe rate can be seen in Fig. 2d. The two lines correspond to the two observed sources for which we used slightly wrong positions at correlation time.

The calibrator source was mapped using the standard phase self-calibration method. It is point like and has structure phases of less than  $\pm 5^\circ$ . Thus step 7 in the above recipe can be omitted. The data from the target source were calibrated with the interpolated rates, delays and phases. The corrected phase-referenced data was then interpolated onto a grid, Fourier-transformed and de-convolved.

The phase-referenced image with the corrected data (Fig. 3, left) is significantly better than the image made from the MK3 data without correcting the correlator model. By comparison with the standard image of the target source (Fig. 3, right) it becomes obvious though that the noise level is increased over the expected value; still a significant amount of flux is spread around in the image. The reason for this can be seen when the model phases are plotted against the phases which are corrected by the phase-referencing process (Fig. 4): on all baselines the measured and corrected phases scatter around the model by roughly  $\pm 40^\circ$ . This scatter is significantly larger than the formal error of the phases as derived from the SNR. This scatter is a result of the interpolation of the calibration phase between scans of the reference source and application to the target at a distance of  $2^\circ$  to  $3^\circ$ .

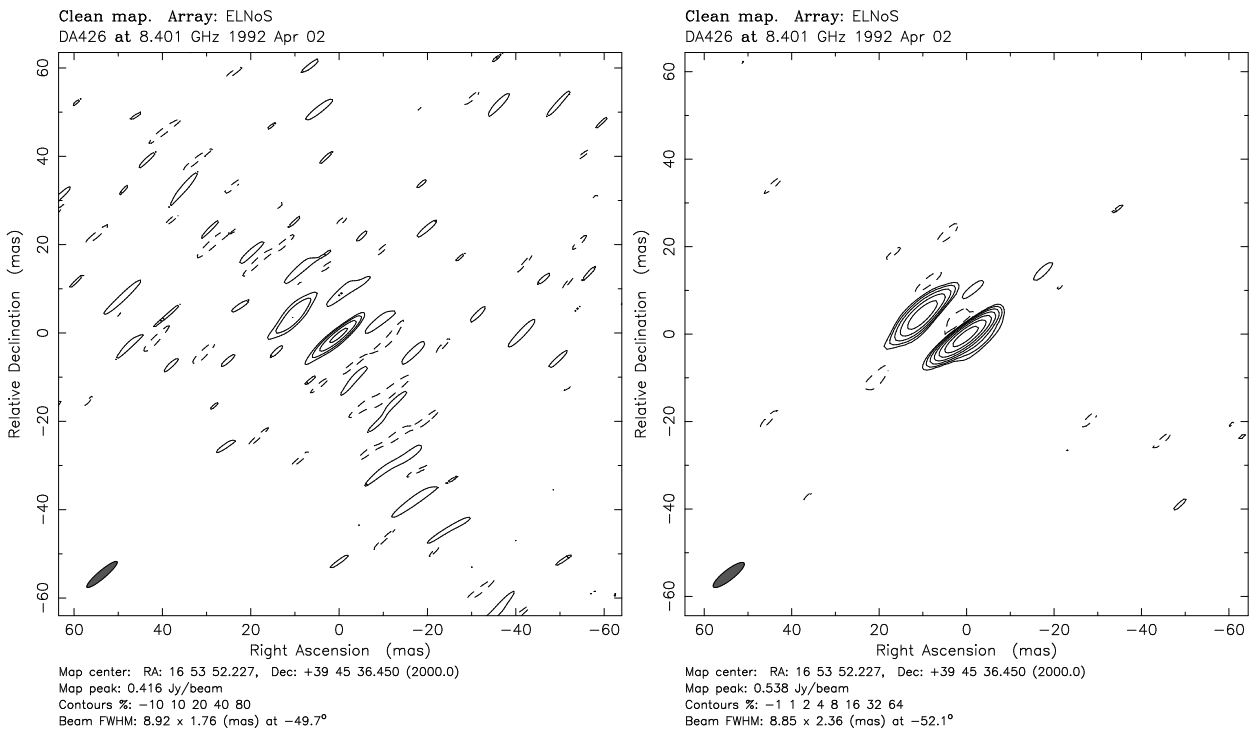


Fig. 3: The left figure shows a phase-referenced image of the target. It is significantly better than the image shown in figure 2. The flux is now close to the image center. A few sidelobes due to the phase interpolation are visible and lead to an increased noise level. The figure on the right shows the same source mapped with the conventional phase self-calibration method. The noise level is significantly lower than in the phase-referenced image.

It is a general finding that in phase-referenced images the recovered flux of the source is decreased while the noise in the image is increased. As a result the sensitivity is worse than the theoretical limit by roughly a factor of 2 to 3 as in this test case and other cases we (and other groups) investigated. Thus the theoretical limit for a detection of a point source is reduced from about 0.5 mJy to about 1.5 mJy.

While it is most likely that the loss of flux is due to temporal and spatial instabilities and effects not included in CALC 8 — mostly ionosphere and wet atmosphere — bugs in PHREF cannot be excluded

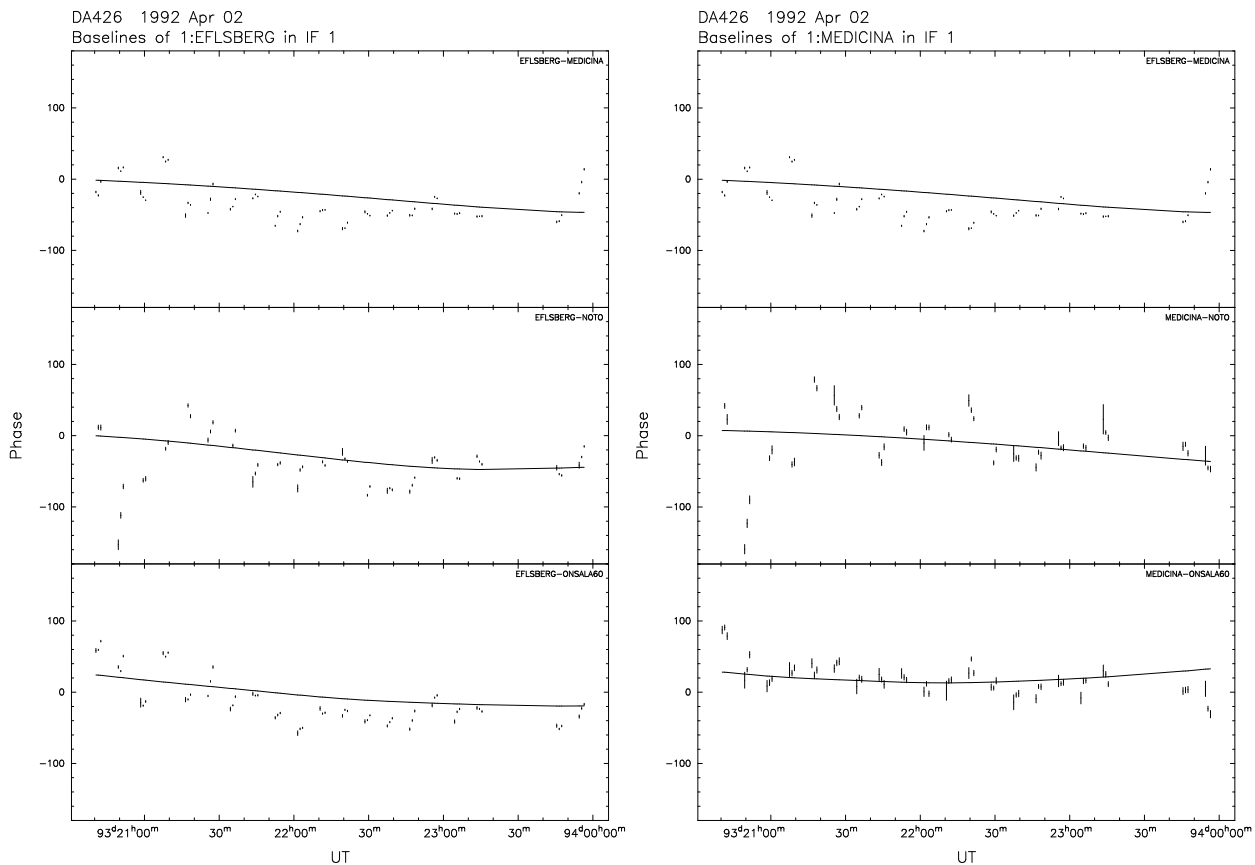


Fig. 4: The phases on the baselines to Effelsberg (left) and Medicina (right) are shown. The model phase is indicated by the lines. The phase-referenced phases scatter around the model phase. This scatter disappears completely and the phases match the model if they are self-calibrated.

completely (MK3 case). But any errors must be station and not baseline specific as self-calibrating the phase-connected data removes the phase scatter and recovers all of the flux. This means that if a source can be detected in a phase-referenced image, subsequent self-calibration will remove de-correlation in the image at the expense of astrometric precision. Similar results were found by other groups with VLBA data.

With our second test data set, L And was detected close to the fringe-fit signal-to-noise limit and thus could be mapped with both the traditional phase self-calibration and the phase-referencing methods, allowing us to compare the methods. We found significant de-correlation and in addition that structures seen in both images might not agree in the weak signal-to-noise domain (see Fig. 5). In the case of L And the image made directly with self-calibration is compatible with an unresolved point source, while the phase-reference image with subsequent self-calibration shows two roughly equal components. These two components are probably due to the side-lobe pattern in the phase-reference image which because of the low SNR could not be removed by the phase self-calibration.

## 5 Present and Future Work

A new AIPS task was written at NRAO to correct for the above mentioned effects of the path delay introduced by the ionosphere and its fluctuations. This task uses GPS measurements which are provided in IONEX format on various servers on the Internet. At present for the USA ionosphere images are available with a time spacing of 10 minutes, while for Europe the time intervals are still one hour. The new task undergoes extensive tests right now, but work by e.g. Ros, et al. (1999) has shown that GPS-based determinations of ionospheric delays can successfully be used for phase-referencing. Correcting the delay due to the wet component of earth's atmosphere is significantly more difficult.

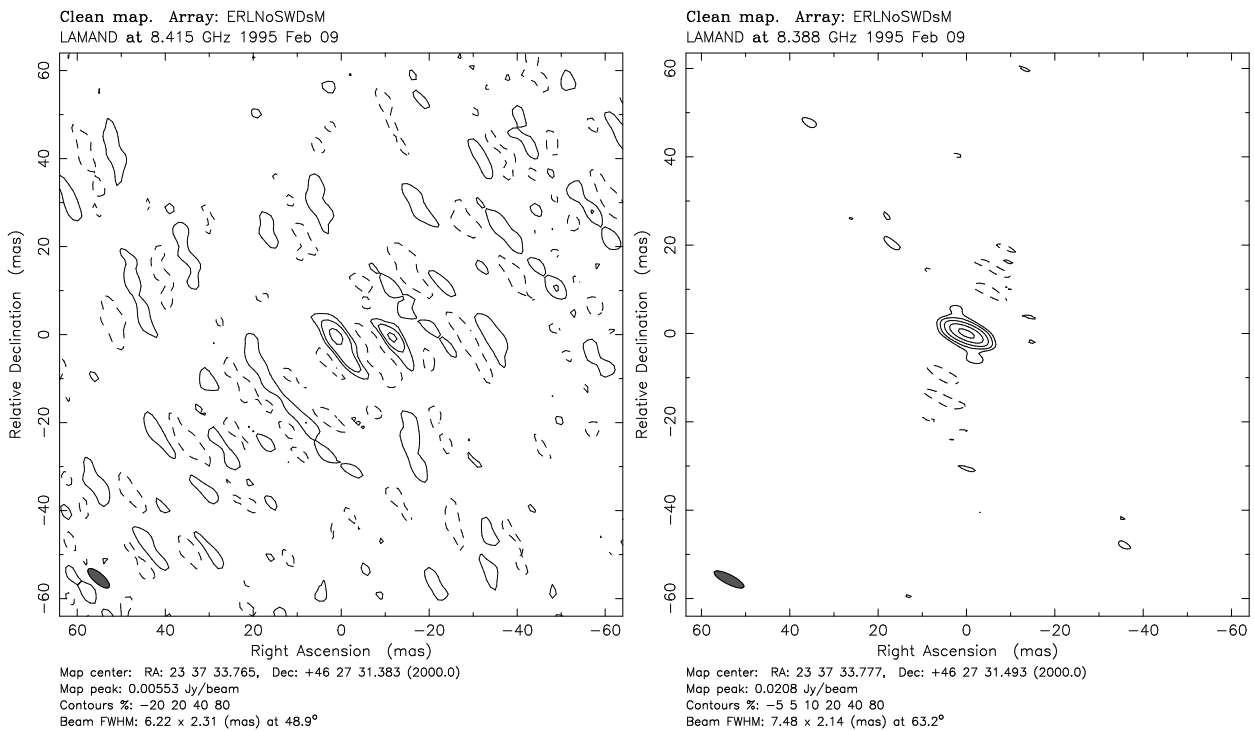


Fig. 5: The figure on the left is a phase-referenced image of the star L And. It shows two components above the noise. If the data is in addition self-calibrated with this image the sidelobes are removed, but two components remain. The image on the right is a image of the same source made with standard phase self-calibration starting from a point source. It has only one unresolved component. This comparison shows that structures so close to the noise level are fairly unreliable.

Tests with a task that uses ground-based measurements of pressure, humidity and temperature were only partly successful. This is due to the well-known fact that ground-based measurements may only describe the conditions in a thin layer over the telescope, while the wet delay is caused by a much thicker layer of the atmosphere. Possible improvements might be achieved by using water vapour radiometers or GPS measurements. A particularly interesting development is the new and very cheap (5000 \$) water vapour radiometer designed at Haystack observatory.

A further reduction of systematic errors is expected when we have CALC 9 available. We plan to upgrade the above described task PHREF to CALC 9 as soon as possible. In particular the new CALC features of proper motion and parallax will be very useful for the observations of stars.

Another scheme which might be used to solve for ionospheric and atmospheric delays is being investigated: two strong reference sources are observed together with the target source. The net observing time on the target is reduced, but the two strong sources can be analysed and the residual differenced phase can be used to determine and model all unknown quantities (Ros, 1997).

After all these problems have been solved the astrometric precision might be high enough to allow us to measure displacements of nearby dwarf stars by earth-like planets, provided the radio emission is not significantly more extended than the star's surface.

## 6 Conclusions

We and other groups have shown that VLBI observations of stars and other weak radio sources are possible with the phase-reference mapping technique. To exploit the full potential of the method more work has to be invested to reduce the effects that cause de-correlation in the phase-referenced images. Once all the disturbing influences are under control it might be possible to achieve routine astrometric precision of position measurements relative to the phase-calibrator of about 0.1 mas for sources fluxes of about 1 mJy and over source separations of 2° to 3°.

## 7 References

- Greisen E.W., 1990. "The Astronomical Image Processing System," in Acquisition, Processing and Archiving of Astronomical Images, eds. G. Longo and G. Sedmak, (Osservatorio Astronomico di Capodimonte and Centro di Formazione e studi per il Mezzogiorno), Naples, Italy.
- Beasley A.J.; Alef W., 1998. Radio Emission from Galactic and Extragalactic Compact Sources, ASP Conference Series, Volume 144, IAU Colloquium 164, eds. J.A. Zensus, G.B. Taylor, & J.M. Wrobel, p. 405.
- Gary D.E., Linsky J.L., 1981. ApJ 250,284
- Ros E., Marcaide J.M., Guirado J.C., Sardón E., Shapiro I.I., "A GPS-based method to model the plasma effects in VLBI observations", 1999, A&A, inpreparation
- Ros E., PhD Thesis, "Astrometria diferencial des precisi3n con VLBI en el Tri3nulo de Draco (y estudios de SN1993J)", Universitat de Val3ncia, Spain, 1997.

# **Advanced Technology Development in VLBI**

Alan R. Whitney  
MIT Haystack Observatory

1. Where is VLBI data-acquisition headed?
2. Mark IV correlator

## Where is VLBI Data-Acquisition Headed?

- Stay on tape?
- Disc?
- e-VLBI?
- VLBI is perhaps the world's single most voracious data-gathering activity in terms of collected **data-volume/day!**
- With the advent of Gb/sec recording systems, the near future foresees ~1000 Tb/day (that's a *Petabit/day*)
- In *most* cases, the single most significant driver is the **cost** of moving VLBI data from station to correlator.

### Comparison of available 1 Gbit/sec VLBI recording systems

	Mark IV	Toshiba D6
Recorder type	Multi-track linear	Multi-head helical scan
Data rate	1.024 Gbit/sec (expandable to 2 Gbit/sec)	1.024 Gbit/sec
Recording capacity per reel/cassette	$\sim 5 \times 10^3$ Gbits ( $\sim 1.1$ hours at 1 Gbit/sec)	$3.7 \times 10^3$ Gbits ( $\sim 1$ hour at 1 Gbit/sec)
Areal data density (not including overhead)	$\sim 23$ Mbits/in <sup>2</sup>	$\sim 95$ Mbits/in <sup>2</sup>
Error rate	$< 1 \times 10^{-4}$	$< 1 \times 10^{-11}$ (error corrected)
Read while write	No	Yes
Cost per reel/cassette	$\sim \$1000$	$\sim \$500$
Media cost per Gbyte	$\sim \$0.5$	$\sim \$0.12$
Estimated hardware cost (recording system only)	$\sim \$250,000$	$\sim \$500,000$
Typical headstack life	$\sim 3000$ hours	$\sim 1000$ hours
Approx. headstack replacement cost	$\sim \$20K$ (2 headstacks)	$\sim \$30K$ (entire head array)

# Disc vs. Tape? Magnetic vs. Optical?

Storage media cost only:

## Tape –

Mark IV:

Now: ~30 Mb/in<sup>2</sup> at ~\$0.50/GB

In 5 years: ~120 Mb/in<sup>2</sup> at ~\$0.12/GB

D-6:

Now: ~100 Mb/in<sup>2</sup> at ~\$0.12/GB

In 5 years: Unclear

## Magnetic Disc –

Now: ~3 Gb/in<sup>2</sup> at ~\$20/GB

In 5 years: ~15 Gb/in<sup>2</sup> at ~\$5/GB

In 10 years: ~100 Gb/in<sup>2</sup> at ~\$1/GB

## Optical Disc –

CD: 0.7 Gb/in<sup>2</sup>

DVD: 3.3 Gb/in<sup>2</sup>

Problems: Low data rate

Relatively high costs

## Optical Tape

- Terabit, Inc to announce 100 MB/sec at ~\$0.50/GB, **but** WORM! (WORM='write once, read many')
- Whole optical tape market is struggling with magnetic competition  
magnetic

## **e-VLBI: The Rationale**

- Improve overall system reliability by reducing dependence on tape recording systems in long term
- Automate stations; reduce operational station costs
- Monitor, test, debug stations in near real-time; improved data reliability
- Reduce processing turnaround time
- Will help to allow use of heterogeneous VLBI data-acquisition systems

## **Elements of Successful Wide-Area e-VLBI**

1. Easy connection to any available network of any speed
2. Cross-compatibility between all VLBI DAS's (i.e. Mark IV, VLBA, K4, S2); standardized data-transmission format preferred
3. For foreseeable future – asynchronous data transmission; implies significant local buffering at both DAS and correlator
  - Disc storage now ~\$20/GB and *dropping rapidly*
  - Mark IV tape is ~600 GB.
4. Affordable network price structures

Note: In this model, the network connection need not be directly at the station!

Expt type	#stations	Total data	Data-transmission time (total)			Comments
			1 Mbps	100 Mbps	1 Gbps	
Station Checkout	2	2 Gb	30 min	20 sec	2 sec	Observe strong source; 30 sec at 32 Mbps
'Small' 24-hr expt	5	55 Tb	1.7 yrs	6 days	15 hrs	128 Mb/sec/stn
'Large' 24-hr expt	15	1300 Tb	41 yrs	150 days	15 days	1 Gb/sec/stn

### Potential e-VLBI applications

## Sampling of Current Network Connection Costs

(based on telephone inquiries to several major communications companies in mid-1998)

### MCI

Green Bank – Washington – Wettzel

T1 \$12K/month (assumes availability in GB and Wettzel)

T3 ~\$150K/month (but no current guarantee of availability)

### Worldcom

Boston – London T1 \$28-30K/month

Boston – London T3 \$480K/month

Boston – Frankfurt T1 \$58K/month + \$1.5K/month Euro access charges

Boston – Washington T1 \$4K/month + \$1K/mo access charges

(~32% discount on 3-year contract)

Boston – Washington T3 \$33K/month + \$4.5K/mo/end site access charges

(~25% discount for 3-year contract)

### ATT

Wettzel – Westford T1.5 \$35K/month

T3 Not available

Westford – Wash T1.5 \$5.8K/month

T3 \$65K/month

Green Bank – Wash T1.5 \$6.3K/month

T3 \$46K/month

Notes:

T1 is ~1.4 Mbps

T3 is ~45 Mbps

## What is the future of e-VLBI?

- May be practical today for certain short, time-critical experiments, particularly over limited geographic range
- Practicality on global scale is primarily dependent on network costs
- Network backbone costs in U.S. are dropping faster than ‘Moore’s Law’ (12-month doubling time vs. 18-month doubling time)
- Installed capacity U.S. coast-to-coast recently expanded by x5 when Qwest ‘lit’ 100 fibers carrying 100 Tb/sec!
- Improvement in wavelength-division multiplexing on optical fiber promises ~4 Tb/sec/fiber
- Direct optical amplification used for long hauls, though expensive
- One of biggest hurdles is high-speed, economical *local* connections

### The Bottom Line!

- Despite amazing gains by the disc industry, tape is likely to be workhorse for most VLBI for at least 10 years, though disc may act as buffer storage for some e-VLBI data.
- VLBI can, and should(!), occasionally take advantage of the vast computer-industry R&D expenditures, most likely in a ‘snapshot’ mode, but may be expensive to adapt. VLBI will not be driver for industry.
- Global e-VLBI is not likely to be economical for some time, though e-VLBI will be practical in certain limited situations. Network prices are predicted to plummet in next few years as competition heats up, though local connections may remain a problem.
- Though e-VLBI is not practical now, the VLBI community would be well-advised to begin international collaboration to define standards. develop concensus, and lay the groundwork for e-VLBI .....’opportunity knocks for those who are prepared’.

# The Mark IV Correlator Project

## **VLBI Correlators (USNO;Haystack;JIVE;BKG/MPI):**

- 1 Gbit/sec/station (16 channels @ 32 Msamp/sec/channel max), expandable to 2 Gbit/sec/station
- Configurable to a variety of number of stations, up to 32 maximum
- Compatible with Mark IIIA, Mark IV and VLBA tape and channel formats

## **Westerbork CEI:**

- Up to 16 stations in a variety of configurations, operating at 40 Msamp/sec/channel max, up to 1 GHz total bandwidth.

## **SMA CEI:**

- Up to 10 stations in a variety of configurations, operating at 208 Msamp/sec/channel (multiplexed x4 and presented to correlator at 52 MHz), up to 4 GHz total bandwidth.

ALL USE SAME CORRELATOR BOARD AND CHIP!

## **Innovations**

- First large-scale VLBI international cooperative development effort
- First large-scale ‘station-based’ XL correlator
- First full-custom VLSI chip for VLBI correlation
- High-speed serial data links (~1 Gbps on small coax) for data distribution
- Station model intermixed with data from each SU
- Highly innovative way of managing ‘vernier-delay’ and phase-rotation/shifting in correlator chip

## **Mark IV VLBI Correlator Features**

- 1 Gbit/sec/station, expandable to 2 Gbits/sec/station
- Station-based architecture
- Scalable architecture allows up to 32 stations, 16 channels/station
- Full compatibility with Mark IIIA, Mark IV, VLBA
- 4X playback speedup compared to Mark IIIA correlator
- Efficient sub-netting
- Flexibility to exchange #baselines with spectral resolution
- Supports recirculation with 'Data Distributor' option
- Extensive use of VEX files for correlator operation/configuration
- HOPS post-correlation package

## **Division of Engineering Labor**

- Haystack
  - Correlator chip and board
  - VLBI correlator data-interface boards
  - SMA correlator data-interface boards
  - High-speed serial data links
- JIVE/EVN
  - Station unit
  - Data distributor
  - Control board
- Attempt to balance US/European contributions
- Software being independently developed

# VLSI Correlator Chip

- Developed as joint Haystack-UNM/NASA/SERC project
  - Functional specification, design, simulation at Haystack
  - Chip design at UMN/NASA/SERC under subcontract to Haystack
  - Fabrication at Hewlett-Packard foundry
- First packaged prototypes received Jan 95
- Commercial availability through UNM non-profit subsidiary  
~10,000 chips have been fabricated

## Correlator Board

### Features

- 32 VLSI correlator chips/board
- Access to 64 2-bit data streams, configurable through 64x64 custom ASIC cross-point switch; up to 64 Msamples/sec data rate
- 16,384 lags/board, flexibly configurable to real/complex
- Up to 128 baselines/board
- Cross-polarization and auto-correlation modes supported
- 16 modules required for 16-station, 1 Gbit/sec/station, 32 lags/baseline VLBI correlator (64 modules for 32 stations)
- 48 modules required for 6-station, 4 GHz BW SMA correlator; 96 modules required for expanded 8-station SMA correlator

### Status

- Has undergone exhaustive testing at Haystack, Dwingeloo
- Successfully tested to 70 MHz by CfA

## **1<sup>st</sup> static fringes - JIVE and Haystack - Aug 97**

Tested following correlator aspects --

- data flow through SU
- static delay correct within SU
- serial link performance
- input board/FIFO working
- correlator-chip arithmetic and counters

## **1st VLBI fringes - Haystack Oct 97**

Tested following correlator aspects --

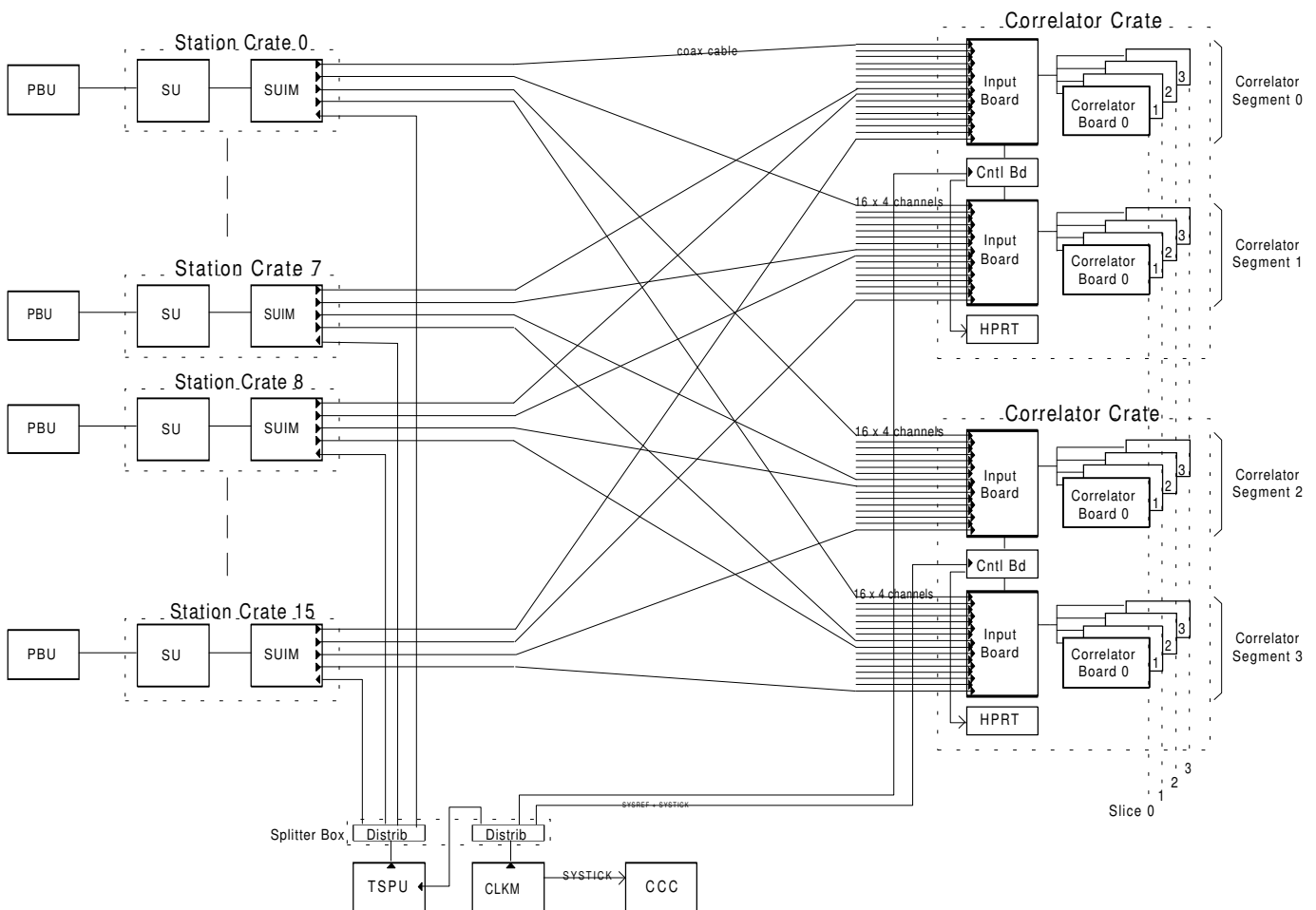
- CALC/genaroot spline model
- SU generation of correlator frame-header packets from splines
- correlator chip capture of header packets
- dynamic parameter calculations
- pipelining of parameters in SU and CU software
- correlator-chip delay trackers for both stations and baselines
- fringe rotation
- dynamic tap adjustment
- 90-deg phase shift on delay changes
- 2-tape-drive/2 SU fringes Feb 98 (JIVE) and April 98 (Haystack) after delivery of 2<sup>nd</sup> prototype Station Units

### **Software**

- Correlator control entirely based on 'VEX' files, including 'observe' files and VEX-like files for correlator configuration; this approach offers ease and flexibility to adapt to special requirements
- Message-based process interactions
- Relatively small amount of critical real-time control is needed due to model generation by SU's and embedded station-parameter-passing in data stream.
- Post correlation software is an extension to the HOPS package already in use with Mark 3/3A.
- Plan easy data-migration path to AIPS and FITS.

# Schedule

- Most hardware is ready except Station Units.
- Station Unit deliveries from Allied Signal expected March-April 99.
- Phase-cal modules in SU have lagged – problems are now believed to be corrected, but delivery of production units will not be until ~3Q99.
- Mark 4 correlator to be delivered to USNO in ~May 99 time frame with ‘Mark IIIA capabilities’, but without phase-cal capabilities.
- Mark 4 correlator to be delivered to BKG/MPI in ~July 99, without phase-cal capabilities.
- Software development is pacing initial deliveries.
- Additional software development will continue to support full capabilities, to be completed in 18-24 months following initial deliveries.



Mark IV Correlator Interconnection Block Diagram  
(16 stations, 1 Gbit/station))

# The Canadian S2-VLBI-System

WAYNE CANNON\*

## Abstract

The S2 VLBI System was developed in Canada as a low cost, high performance, 128 Mbit/sec VLBI system for use in geodesy and astrophysics. It consists of the S2 VLBI Data Acquisition System, the S2 VLBI Data Record System, the S2 VLBI Data Playback System, and the S2 VLBI Correlator. To date there are approximately 55 S2 VLBI Data Record and Playback systems in use for various astronomical purposes in more than a dozen countries. The S2 VLBI system features a frequency agile local oscillator for geodetic applications of group delay measurements by bandwidth synthesis (BWS) over 900 MHz as well as a frequency agile VLBI correlator for processing frequency switched VLBI observations. The S2 VLBI correlator also features multiple tone extractors and pulsar gating capabilities as well as high frequency lobe rotators capable of processing space VLBI observations with their attendant high Doppler rates. There are, in addition, three other "S2 Capable" VLBI correlators located in Sydney Australia, Mitaka Japan, and St. Petersburg Russia, with a fourth under development at the Astro Space Center in Moscow. These correlators are not designed to accommodate all the features of the S2 system, in particular frequency agile signal processing, but are nevertheless capable of processing S2 VLBI data tapes in a subset of S2 operational modes. The Mitaka correlator processes S2 data tapes by using S2 VLBI Data Playback Systems to copy them to VSOP data tapes before correlation. Other S2 correlators make use of S2 VLBI Data Playback Systems for direct input to the correlator. The Space Geodynamics Laboratory has begun development of the S3/S4 family of VLBI Data Record and Playback systems which will operate in the range from 1024 Mbit/sec to 4096 Mbit/sec and will feature a robotic tape changer for 24 hour unattended operation.

---

\*Space Geodynamics Laboratory, e-mail: wayne@sgl.crestech.ca

# Dual Channel Water Vapour Radiometer Development

**Borys Stoew and Carsten Rieck**

Onsala Space Observatory, Chalmers University of Technology, SE-43992 Onsala

A new instrument for measuring the atmospheric water vapour is being developed at the Onsala Space Observatory (OSO). It is a dual frequency microwave radiometer, measuring the sky brightness temperatures at the double-side bands centered at 21 GHz and 31.4 GHz respectively. Compared to the radiometer presently operating at the observatory, the new instrument is more compact and transportable. It will be used for comparisons at the Onsala site, especially studying the effect of narrower antenna beams. It will also be operated at other sites, e.g. in the Swedish GPS-network SWEPOS. Each channel uses two reference temperature black bodies (matched loads) for calibration: one "warm" - at regulated room temperature and one "hot" which is stabilized at 100 °C . The stability tests of the latter showed temperature bound within  $\pm 0.03^\circ$  around 100 °C . The recent work on the microwave part and the data acquisition (DAQ) system is presented together with the solution for the positioning of the radiometer.

## 1 INTRODUCTION

In space geodetic techniques like VLBI<sup>1</sup> and GPS<sup>2</sup>-based surveys of the motions of the Earth's crust a major error source is the wet delay. The wet delay is the equivalent excess propagation path of the radio wave caused by the water vapour in the atmosphere. Information about the integrated water vapour content in the atmosphere can be derived from measurements of the sky brightness temperatures on and off the water vapour absorption line at 22.235 GHz . The idea is not new and it has been implemented in the already operating water vapour radiometer (WVR) - ASTRID. The virtues of the new WVR are the narrow antenna beams, the enhanced precision of the positioning, the data acquisition / control system (DAQ), and the compactness of the instrument. We present a summary of the work carried out on a new water vapour radiometer being developed at OSO. Section 2 presents the microwave system and the overall construction of the instrument. Section 3 discusses the solution of the DAQ system.

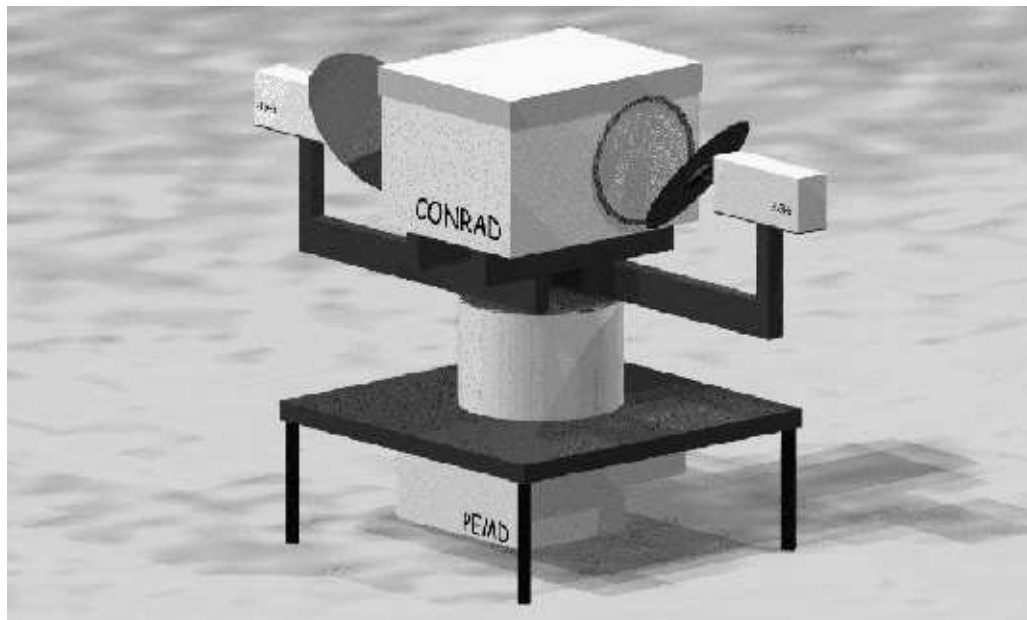


**Figure 1.** A view of the new WVR derived from the AutoCAD blueprints.

---

1. Very Long Baseline Interferometry.  
 2. Global Positioning System.

## 2 HARDWARE LAYOUT

The new WVR is equipped with two lens horn antennas - one for each of the two frequency bands. The two antennas are short but have rather large apertures. This suggested the usage of two pointing mirrors (one for each channel) for the different positions in the sky - a design which can be seen in Figure 1. The two mirrors (elevation) and the main axis (azimuth) are operated by stepping motors controlled by the positioning system run by sending commands from a personal computer (PC) to a microcontroller in the WVR.

The instrument is a dual frequency radiometer, with bands centered at 21 GHz and 31.4 GHz respectively. We will concentrate on the operation of only one channel, since the structure is identical for both channels (see Figure 2). The sky noise radiation enters the antenna towards the mixer through a mechanical and a ferrite switch. The voltage at the output of the detector is proportional to the total thermal noise power.

$$V_{sky} = G \cdot (T_{sky} + T_{sys}) \quad (1)$$

$$V_{warm} = G \cdot (T_{warm} + T_{sys}) \quad (2)$$

$$V_{hot} = G \cdot (T_{hot} + T_{sys}) \quad (3)$$

Ideally, the total system noise temperature should be split in two - the  $T_{sys}$  generated by all passive and active elements in the receiving system; and  $T_*$  which we assume to be the noise temperature of a black body - the sky, the “hot” or the “hot” load (depending on the configuration of the switches). In (1) the gain  $G$  and the temperature  $T_{sys}$  are not known, but can be calculated from the measured voltages  $V_{sky}$ ,  $V_{hot}$ ,  $V_{warm}$  and the controlled temperatures  $T_{hot}$ ,  $T_{warm}$ . Different algorithms for retrieving the wet delay from the observed sky brightness temperatures are described in [1].

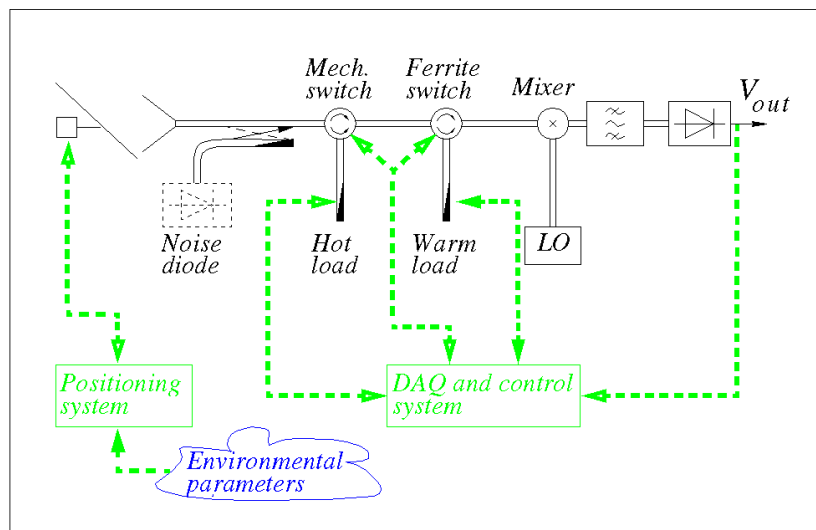


Figure 2. Structure of one microwave channel in the WVR.

The most important features of the microwave part and the data acquisition system are shown in Table 1.

**Table 1. Features of the microwave and the data acquisition system.**

Parameter	21 GHz channel	31.4 GHz channel
Lens horn antenna beam width	3°	2°
Physical temperature of the “hot” load (controlled)	100 °C	100 °C
Stability of the temperature of the “hot” load	±0.03°	±0.03°
Physical temperature of the “warm” load (measured)	~40 °C	~40 °C
Resolution of the ADC <sup>a</sup> measuring the output voltages, temperatures of the calibration loads.	16 bit	
Resolution of the DAC <sup>b</sup> controlling the temperature of the “hot” loads.	12 bit	
Communication with the PC	RS-232 (optical fibers) - up to 115200 bps	

- a. Analog to Digital Converter.  
 b. Digital to Analog Converter.

### 3 DATA ACQUISITION SYSTEM

The Data Acquisition (DAQ) and control system is based on the commercially available FieldPoint / LabVIEW 5 products. They provide high quality measurements (eight 16 bit ADCs) and current generators (eight 12 bit DACs), along with discrete input and output modules for the waveguide switches. The communication between the PC running LabVIEW and the FieldPoint DAQ and control units is carried out over RS-232 serial interface. The LabVIEW programming environment provides a good basis for fast and easy development of user friendly software of satisfactory computational speed.

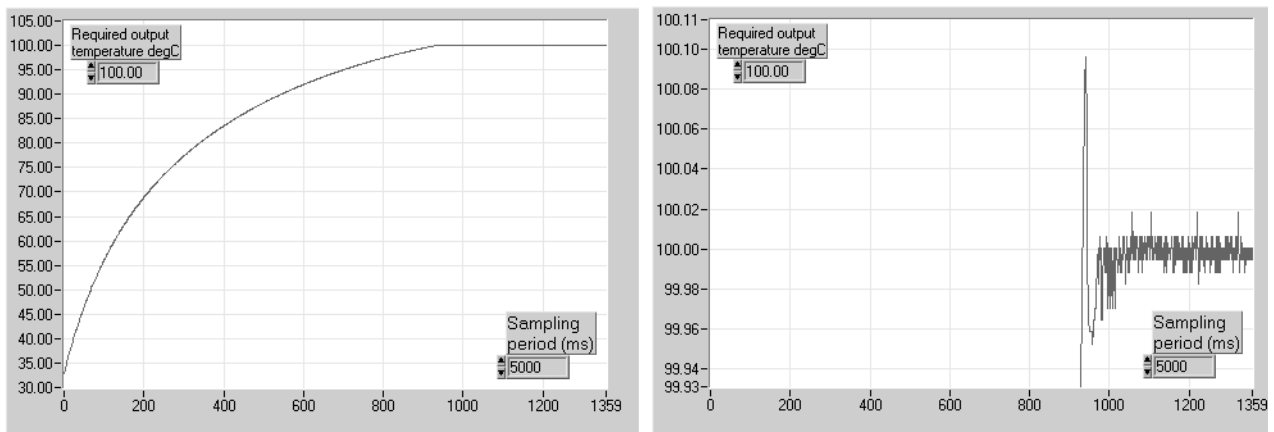


**Figure 3. Convergence and stability of the temperature of the calibration “hot” load.**

Software control is applied to the temperature of the calibration loads. Figure 3 shows the behaviour of the “hot” load for the 31.4 GHz band - the left figure presents the typical time needed for the “hot” load to heat up - approximately 5000 s or less than 1.5 hours<sup>1</sup>. The figure on the right is the same data zoomed

1. Since this is the slowest process taking place in the WVR, data acquired immediately after the start-up of the instrument should be discarded.

around 100°C. The temperature is confined within  $\pm 0.03^\circ$  which together with stable regime of the microwave hardware should ensure very slow changes in the gain from (1). A more detailed description of the choice of temperature control algorithm can be found in [2].

#### 4 POSITIONING SYSTEM

**Table 2. Features of the positioning system.**

Parameter	Azimuth value	Elevation value
Stepping motors	5 phase	5 phase
Gears with low dead motion (less than 2 arcmin)	1:100	1:50
Holding torque	37 Nm	5.5 Nm
Step resolution achieved after the gear boxes (full step mode)	0.0072°	0.0144°
Angular velocity for the different axes	10°/sec	> 10°/sec
Resolution of the ADCs measuring the output voltages from the environment sensors (eventually air pressure, temperature, humidity)	16 bit	
Communication with the PC	RS-232 (optical fibers)	

#### 5 PROSPECTIVES

The narrow beams of the lens horn antennas offer an instrumental basis for the evaluation and eventually improving the existing atmospheric delay models, especially for low elevations. The light weight and the size of the new WVR will allow studies to be carried out on various sites of interest.

#### REFERENCES

- [1] Elgered, G., “*Tropospheric Radio-path Delay from Ground-based Microwave Radiometry*”, repr. from chapter 5 in *Atmospheric Remote Sensing by Microwave Radiometry*”, edited by Janssen, M. A., John Wiley & Sons, 1993.
- [2] Stoew, B., “*Microwave Radiometry: Data Acquisition and Software Based Temperature Stabilization*”, M.Sc. thesis report, Chalmers University, Sweden, 1998.
- [3] Beillon, A. and M. Lager, “*Construction of a Dual Frequency Dicke Switched Water Vapour Radiometer*”, M.Sc. thesis report, Chalmers University, Sweden, 1992.

# On the Automation of the MarkIII Data Analysis System

W. Schwegmann and H. Schuh  
Deutsches Geodätisches Forschungsinstitut (DGFI)  
Marstallplatz 8  
D-80539 München  
Germany  
Tel.: +49/89-23031-202, Fax: +49/89-23031-240  
e-mail: schwegmann@dgfi.badw.de

**Abstract:** A faster and semiautomatic data analysis is an important contribution to the acceleration of the VLBI procedure. A concept for the automation of one of the most widely used VLBI software packages the MarkIII Data Analysis System was developed. Then, the program PWXCB, which extracts weather and cable calibration data from the station log-files, was automated supplementing the existing Fortran77 program-code. The new program XLOG and its results will be presented. Most of the tasks in the VLBI data analysis are very complex and their automation requires typical knowledge-based techniques. Thus, a knowledge-based system (KBS) for support and guidance of the analyst is being developed using the AI-workbench BABYLON, which is based on methods of artificial intelligence (AI). The advantages of a KBS for the MarkIII Data Analysis System and the required steps to build a KBS will be demonstrated. Examples about the current status of the project will be given, too.

## 1 Introduction

Based on the inertial reference system of extragalactic radiosources VLBI is an extremely precise geodetic technique for monitoring the Earth rotation and for the realization of the global reference system. However, the costs are relatively high and there is still a delay of five days minimum between the time of observation and the availability of the results. If this gap could be shortened considerably this would allow to monitor the Earth rotation parameters (ERPs) and the relative station motions in near real-time. This could be extremely useful for high precision positioning and navigation. Results in near real-time could also be used as references for other 'on-line' observing methods, e.g. laser gyros or supra-fluid helium gyros, as well as for observing transient astronomical phenomena.

The paper presents a concept for the automation of the MarkIII Data Analysis System, a widely used VLBI software system (Ryan et al., 1980). This concept has been developed at DGFI, Munich, within a research project called 'Applications of Methods of AI for the VLBI Data Analysis'. The goal of the project is to accelerate and automate the VLBI data analysis. It belongs to a general proposal for VLBI in near real-time that was presented by Schuh (1995), where the means for automation and acceleration of the VLBI procedure are described for all steps of the VLBI procedure, i.e. scheduling, observation, correlation and data analysis. When looking at the work done by the analyst during the course of VLBI data analysis, it can be seen that almost all tasks can be supported by typical AI methods, as proposed by Schuh (1991, 1993). Some tasks can be realized by additional algorithms or crosschecks conventionally programmed within the existing software. This paper gives examples for both, the automation with conventional methods and with methods of AI, and shows the advantages of knowledge-based techniques.

A first successful realization of an on-line VLBI-System is the Japanese Keystone project. In this project four radiotelescopes in the Tokyo area produce geodetic results in near real-time. It is part of the Japanese Earthquake Prediction Programme (Yoshino, 1994, Koyama et al., 1998).

## 2 Reasons for the development of a Knowledge-Based System

In the next few years the number of geodetic VLBI observing sessions will increase considerably. The degree of automation within the present MarkIII Data Analysis System is very low. Most steps during the data analysis have to be carried out manually and the data analysis is very complex and often requires the analyst's (expert's) decisions. Already today there is a shortage of qualified experts and the analyst's training takes a long time. Moreover, even experienced analysts make time-consuming errors. Wrong results could lead to misinterpretations and to incorrect conclusions. This leads to the necessity of a faster and even semiautomated data flow during the data analysis, what can only marginally be achieved by faster computers. Thus, the goal should be to make the VLBI data analysis faster and safer by ensuring that less failures and less errors are made even by less experienced analysts. According to the description of a knowledge-based system (KBS) (Sundermeyer, 1991) a KBS can be used to model the knowledge needed for the VLBI data analysis and to use this knowledge for solving the complex problems within the data analysis automatically. A KBS is less susceptible to errors, allows to conserve the analyst's knowledge and to check his decisions. More information about KBS can be found in Schnupp et al. (1989).

## 3 Automation of VLBI data analysis

To examine the possibilities for the automation of the different steps within the data analysis, the data flow inside the MarkIII Data Analysis System was analysed. Especially the applicability of knowledge-based techniques was investigated but it was also considered, to automate some steps with conventional programming techniques by supplementing the existing program-code. Therefore the data flow inside the MarkIII Data Analysis System was subdivided into five parts each related to a superior task: correlator output, a-priori information, generation and modification of databases, log-file processing and data analysis (see Fig. 1).

The demands on a software which should automate the data analysis differ for each of the parts. Table 1 shows to which degree a KBS would be useful in the different parts of the data analysis. A KBS can be used as a teaching system and for special aspects of the data processing. The main application, however, will be for decision-support, diagnosis and analysis of results in *Part V*.

KBS for	data control and verification	education	diagnosis	decision support	analysis of results
Part I	■	■	■	■	■
Part II	■	■	■	■	■
Part III	■	■	■	■	■
Part IV	■	■	■	■	■
Part V	■	■	■	■	■

Tab. 1: Possibilities for the application of a KBS in the VLBI data analysis.

After having thoroughly analysed the data flow inside the MarkIII Data Analysis System the program PWXCB in *Part IV* was automated. This could be done so far with conventional programming techniques that is by supplementing the existing program-code written in Fortran77, because the knowledge needed for these tasks is relatively simple. The new program is called XLOG and is described in the next section.

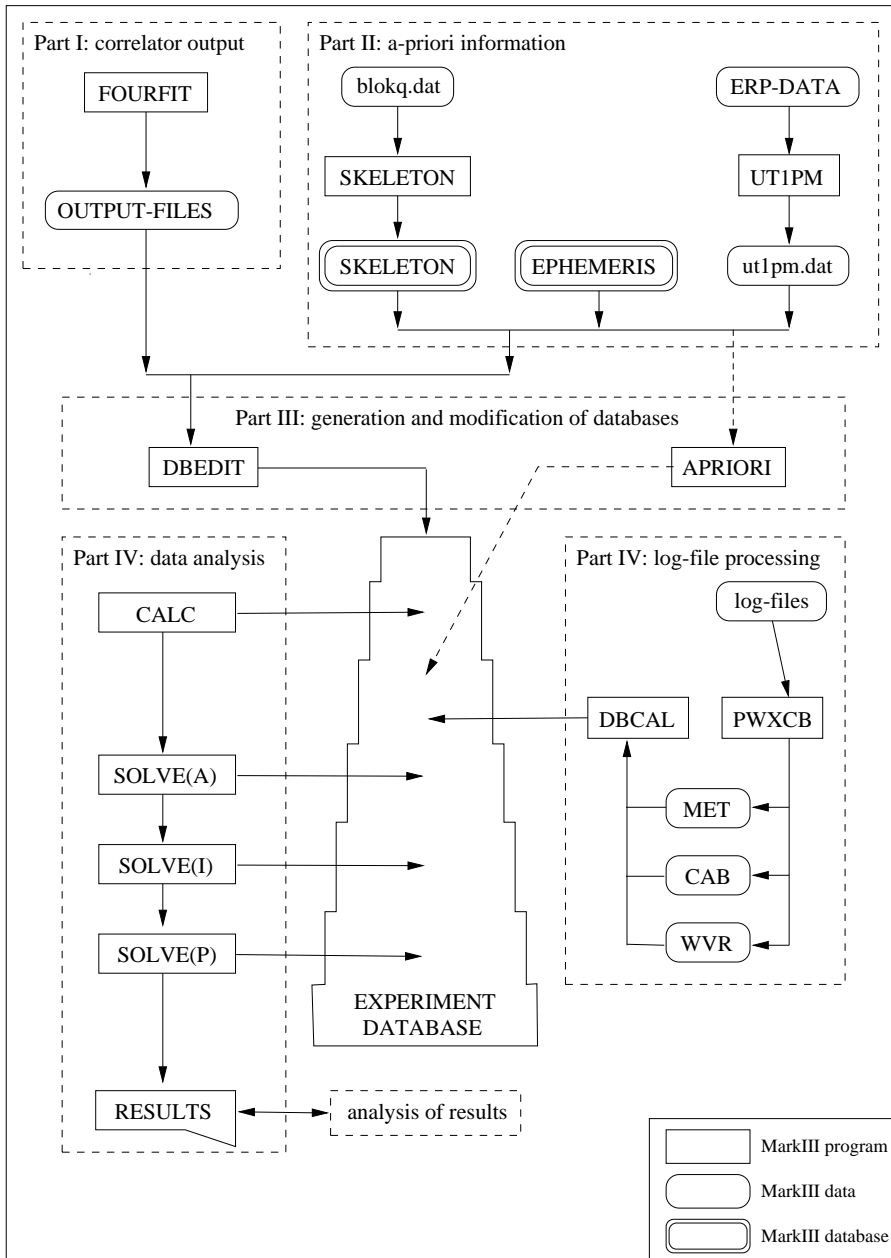


Fig. 1: Flow chart of the standard MkIII Data Analysis System.

### 3.1 Automatic processing of station log-files

During the analysis of VLBI experiments the meteorological data and the cable calibration data have to be read from the station log-files and are entered into the experiment database. For that purpose the program PWXCB extracts the meteorological and cable calibration measurements from the station log-files and stores the data in separated files, the so called ‘calibration files’ (see Fig. 1, *Part IV*). The data from these files are entered into the database by the program DBCAL. Creating the calibration files can be very time-consuming because of wrong entries in the log-files which have to be corrected manually. In addition, the extracted data have to be checked with respect to their plausibility. These tasks shall be performed now by an automated version of PWXCB called XLOG. All possible errors had to be considered when developing the software, even if they appear quite implausible, to obtain a high reliability of the automation. XLOG considers offsets, gaps and single outliers in the data, too few data, wrong entries in the log-files (e.g. missing keywords, mixing up temperature and pressure, etc.) and obvious met sensor problems (e.g. constant temperatures entered in a log-file which is an indication for a sensor failure).

The program can be started by several user-modes: In the semi-automatic mode the analyst has to confirm all actions done by the program, i.e. original and edited data are plotted by XLOG and the analyst is asked to decide which data should be used or if he wants to edit the data manually with PWXCB. In the fully automatic mode the analyst is asked for a confirmation only if there are problems with the automatic processing of the data, e.g. if suspicious data were detected but not deleted, if more than 10 % of all data points were deleted, etc. In a third user-mode the program runs without user interaction and no messages are printed on the screen. In this case the analyst is able to check the results by looking at the output files of XLOG which contain information about the automatic proces-

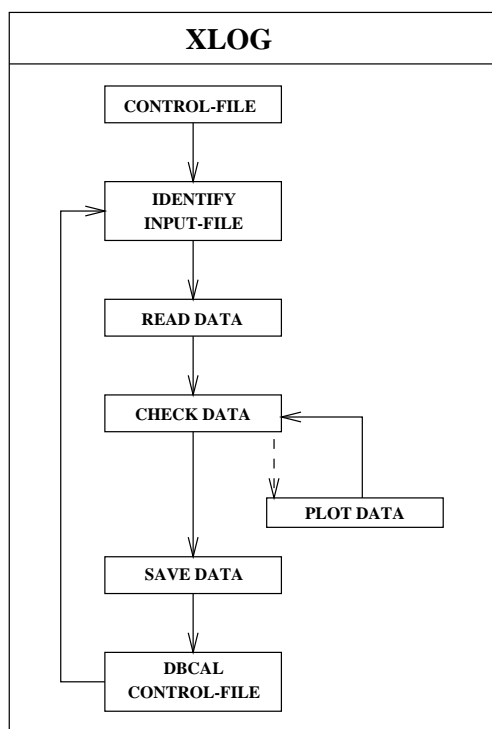


Fig. 2: Data flow of the program XLOG.

ing of the log-files. More details about the user-modes can be found in the users-guide of XLOG. The data flow inside XLOG is shown in Fig. 2. The program starts reading the control-file which contains all necessary information to process the log-files automatically, e.g. user-mode, input-filelist, experiment descriptor, etc. Then the program runs through the following steps for every input-file. First the program identifies the type of the input file (MarkIII-, MarkIV-log-file or an existing calibration file). The data extracted from the input-file will be checked with respect to their plausibility and will be saved if they are o.k. and the next file from the input-filelist is going to be processed. If there are problems during the automatic processing or if XLOG runs in semi-automatic mode, warning messages are sent to the analyst and the original and edited data are plotted. Then the analyst is able to check the plausibility with stronger or weaker conditions to find wrong data. If the results are still not o.k., the analysts is able to decide that the original data should be used and be processed with PWXCB. Finally XLOG creates the control-file for the program DBCAL.

The automatic processing of the log-files was checked on real data. Thereto about 200 station log-files which had been already processed manually were reprocessed with XLOG. Almost 25 percent of the 200 log-files have had wrong entries and had to be edited manually. The comparison of the results showed a success rate of better than 96 percent of the automated version compared to manual editing which means that basically the same results were achieved. For four percent of all cases the log-files were not processed correctly by XLOG, but in all cases the program wrote warning messages into the output files and on the screen. An example for successful automatic editing of cable calibration data is shown in Fig. 3. The cable sign was detected by XLOG and written into the cable calibration file. The offset within the data (see left part of Fig. 3) was deleted, too. To demonstrate which errors could be detected by XLOG Fig. 4 shows the automatic editing of intentionally falsified meteorological data (see left part of Fig. 4) by the present version of the program. All obvious errors were detected by XLOG. Merely at the end of the experiment there is a problem when no data are available for three hours which reveals some weaknesses of the conventionally programmed version of XLOG. Hence there is a difference of almost eight degrees centigrade between the last data point before the gap and the first point after. At present XLOG cannot decide if this is a measurement error or if the data after the gap are correct because this requires the knowledge and the experience of the analyst about the usual weather conditions at the station. In such case, the analyst will be warned by XLOG and he will edit the data manually. Anyway, using the current version of XLOG a considerable amount of time and effort can be gained. At present, a beta-version of XLOG is being tested for routine application. It is planned to release version 1.0 in Spring 1999.

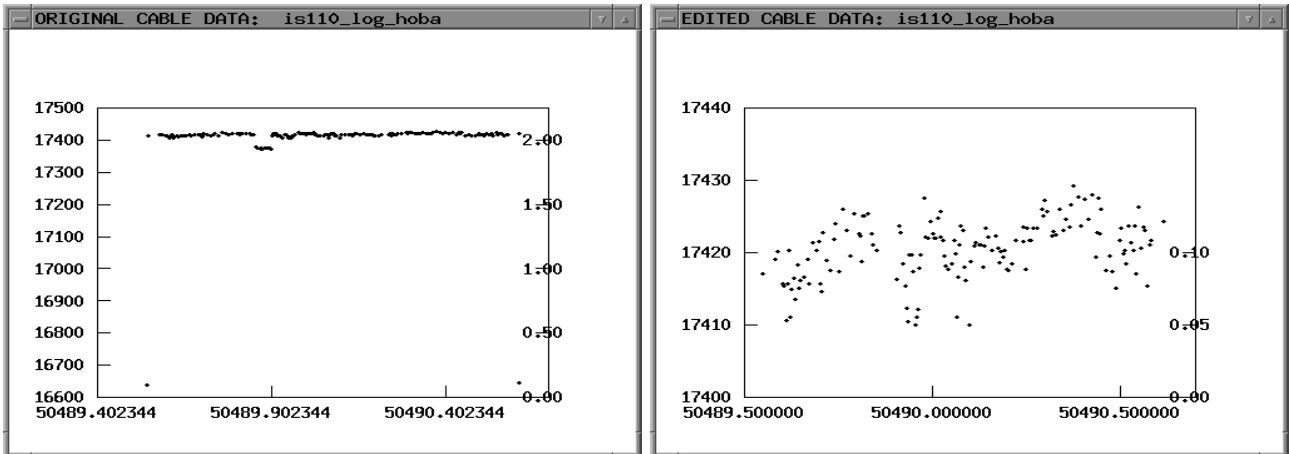


Fig. 3: Comparison of original cable measurements at a VLBI station from the log-file (left) and the data after automatic processing with XLOG (right).

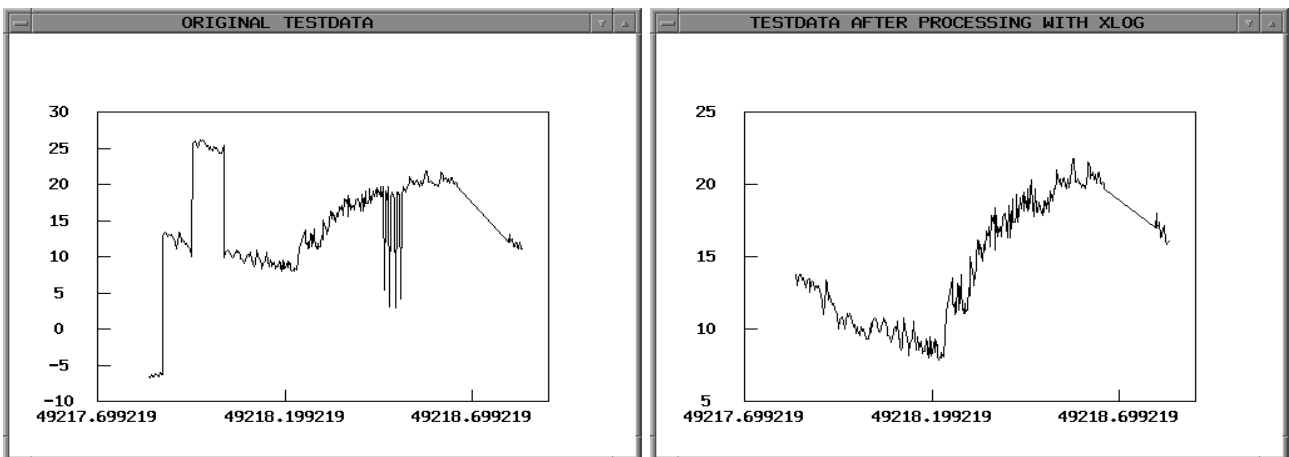


Fig. 4: Comparison of intentionally falsified temperature measurements at a VLBI station (degrees centigrade) from the log-file (left) and the data after automatic processing with XLOG (right).

## 3.2 A knowledge-based system for the VLBI data analysis

### 3.2.1 General remarks

The KBS for the automation of VLBI data analysis with the MarkIII Data Analysis System will be developed to support the analyst in an implicit and explicit manner. Implicit means that all steps done by the analyst are checked by the system in the background. The analyst only notes these checks, if the system sends a warning message. Explicit means that the analyst is able to consult the system anytime to solve a problem.

The development of a KBS can be supported efficiently by AI software tools. Thus the AI-workbench BABYLON (Christaller et al., 1992) is going to be used for our purpose. BABYLON contains formalisms for knowledge representation, a problem solving component to process the knowledge and an explanation component to tell the user how the system arrived at a solution. BABYLON is implemented in LISP, the most common AI programming language. It was developed by the 'Gesellschaft für Mathematik und Datenverarbeitung (GMD)' in Sankt Augustin, Germany. To construct a KBS using BABYLON, the knowledge needed for the problem must first be collected, structured and organized (knowledge acquisition). This knowledge has to be formally represented and stored in the knowledge base (knowledge representation). The efficiency of a KBS depends on the quality of the knowledge within the knowledge base, which should be modular, flexible and extensible. Because the general procedure of VLBI data analysis is very similar in all VLBI analysis programmes, the system is being designed to

be transferable to other VLBI software packages like Occam (developed at the Universities of Bonn, Madrid and Saint Petersburg) or MASTERFIT/MODEST (developed at Jet Propulsion Laboratory, Pasadena, CA). Therefore the knowledge base will be built to a high degree independently from the MarkIII Data Analysis System. A system interface will be needed to acquire data from the MarkIII Data Analysis System and to control the data analysis with the KBS.

### 3.2.2 Automation of the standard VLBI data analysis

At present the KBS is going to be developed for the automation of a single VLBI experiment according to the standard procedure applied for analysing geodetic VLBI data (Nothnagel, 1995). The system should automate the steps of *Part V* (see Fig. 1) of the VLBI data analysis:

1. Group delay ambiguity shifting
2. Ionosphere calibration
3. Update of the data base
4. Final parameterization

Every step contains several subsequent tasks, which are sometimes trivial from the point of view of an expert but have to be considered by the KBS. The main problem when automating these tasks is the representation of the knowledge, because the methods used by the problem solving component are in principle the same for both, trivial and complex tasks. A trivial task is for example the correct parameter setting of the clock parameters during the group delay ambiguity shifting. The following examples are given to show how the different knowledge representation formalisms of BABYLON can be used to represent the knowledge about this task. The knowledge needed for this task according to Nothnagel (1995) can be summarized by the following rules:

- One station of a VLBI experiment has to be used as reference station for which no clock parameters will be estimated.
- The reference station should be in the central area of the network.
- The reference station should not be known for strong clock variations.
- For ambiguity shifting only the first two clock parameters (clock offset and rate) are estimated at each station except the reference station.

To represent this knowledge and to define the steps to control the correct setting of the clock parameters the following formalisms are used:

- Frames to represent the stations and their attributes (e.g. name of a station, characterization of the clock (*bad* if it is known for strong clock variations otherwise it is *good*), etc.).
- Behaviours to change the attributes of a station, for example to set the clock parameters to [0 0], which means that the station is going to be used as reference station:

```
(defbehaviour (vlbi-station :set-clock-reference) ()
  ← :put 'clock-para [0 0])
```

- Prolog to analyse the situation, for example to check if by mistake a station is set as reference station. The result of the 'Prolog clause' *is-wrong-reference-clock* is *TRUE* if the clock is described as *bad* and if the clock parameters at the station are set to [0 0]:

```
((is-wrong-reference-clock _station)
  ←
  (is [0 0] (← _station :get 'clock-para))
  (is bad (← _station :get 'clock)))
```

- Rule-sets to check the clock parameter settings and to control the analysis, for example to check if by mistake more than one station was set as reference station:

```
(defrule-set :test-multiple-reference-clock
  (rule-1 ($and (is-reference-clock _station1)
                (is-reference-clock _station2))
    ($execute
      (SAY ''There are multiple defined clock references'')
      (← _station1 :set-clock-2p)
      (← _station2 :set-clock-2p)
      (find-implications :define-clock-reference :do-all))))
```

The rule `test-multiple-reference-clock` uses the behaviour `is-reference-clock` to check if a specific station is set as reference. If more than one station is set as reference a message is plotted to the screen, the behaviour `set-clock-2p` is used to set the clock parameters of all stations to [1 1] and the rule-set `define-clock-reference` is started to define a reference station.

The knowledge is stored in two knowledge bases. One contains all knowledge with respect to the stations and the other contains the knowledge for the clock parameter settings. This is necessary because the informations about the stations are going to be used in other steps of the data analysis, too. Thus the modularity of the knowledge bases is guaranteed.

To check the clock parameter settings the system performs the following steps:

1. check if more than one station is defined as reference, if yes:
  - (a) set the clock parameters of all stations to [1 1]
  - (b) define one reference station
2. check if the reference station can be used as clock reference, if not:
  - (a) set the clock parameters to [1 1]
  - (b) find a correct reference station

To automate the tasks of the VLBI data analysis described above for each step several knowledge bases have to be created. These knowledge bases contain the knowledge which is necessary to solve the specific problem and can be merged to automate the data analysis of single VLBI experiments.

## 4 Conclusions

To automate the VLBI data analysis either conventional programming techniques or methods of artificial intelligence can be used. The automation of *Part IV* of the MarkIII Data Analysis System by supplementing the existing Fortran77 program-code was successful but has also shown the weaknesses of conventional methods. Knowledge-based techniques are much more practical for the automation of the VLBI data analysis, because they allow an explicit modelling of the multifaceted knowledge needed for these tasks. At present the KBS is going to be built for the most complex and time consuming step in the VLBI data analysis: the selection of parameters inside *Part V* in Fig. 1.

## 5 Acknowledgements

The research project 'Applications of Methods of AI for the VLBI Data Analysis' is supported by the Deutsche Forschungsgemeinschaft (DFG), project Schu 1103/2-1.

## References

- Christaller, T., di Primio, F., Schnepf, U. and Voss, A., eds., *The AI Workbench Babylon, Knowledge-Based System Book Series*, Academic Press, London/New York, 1992.
- Koyama, Y., Kurihara, N., Kondo, T., Sekido, M., Takahashi, Y., Kiuchi, H. and Heki, K., *Automated Geodetic Very Long Baseline Interferometry Observation and Data Analysis System*, Submitted to *Earth, Planet and Space*, 1998.
- Nothnagel, A., *VLBI Data Analysis User's Guide*, Geodetic Institute of the University of Bonn (GIUB), Internal Report, 1995.
- Ryan, J. W., Ma, C. and Vandenberg, N. R., *The Mark III VLBI Data Analysis System*, NASA Goddard Space Flight Center, publication X-945-80-25, 1980.
- Schnupp, P., Huu, C. T. N. and Bernhard, L. W., *Expert Systems Lab Course*, Springer-Verlag, Berlin/Heidelberg, 1989.
- Schuh, H., *Design of an Expert System for VLBI Data Analysis, Proceedings of the 8th Working Meeting on European VLBI for Geodesy and Astrometry, Dwingeloo, June 1991*, Report MDTNO-R-9243, Survey Department of Rijkswaterstaat, Delft, The Netherlands, pp. IV53–IV58, 1991.
- Schuh, H., *An Expert System for the Selection of Parameters in Solve, Proceedings of the 9th Working Meeting on European VLBI for Geodesy and Astrometry, Sept. 1993*, Mitteil. a. d. Geodätischen Instituten der Rhein. Friedr. Wilh. Univ. Bonn, No. 81, pp. 79–86, 1993.
- Schuh, H., *A concept for real-time VLBI, Proceedings of the 10th Working Meeting on European VLBI for Geodesy and Astrometry, May 1995*, edited by R. Lanotte and G. Bianco, agenzia speciale italiano, pp. 51–56, 1995.
- Sundermeyer, K., *Knowledge-Based Systems: terminology and references*, BI-Wissenschaftsverlag, Mannheim/Wien/Zürich, 1991.
- Yoshino, T., *Crustal Deformation Monitoring in Tokyo Metropolitan Area by Space Geodetic Observation, Journal of the Communication Research Laboratory, 41(3)*, pp. 1–9, 1994.

# Phase Centre Determinations at GPS-Satellites with VLBI

HAYO HASE\*

## Abstract

The collocation of various geodetic space techniques provides the tie of satellite reference systems into the quasi-inertial reference system of radio sources. The concept of a fundamental station is the ideal realization for collocating instruments on Earth's surface. A challenge is to tie satellite transmitters of navigation systems directly into the International Celestial Reference Frame, the most accurate realization of a quasi-inertial reference system with VLBI measurements. An orbit determination of the phase centre of the satellite transmitters complement existing orbit determinations. For VLBI-type determinations some research and development work needs to be done. For this purpose a new type of dual beam radio telescopes will be of advantage. If the method will be successful an *inertial frame service* is possible in the future.

## 1 Global Reference Systems

In (space) geodesy two kinds of reference systems play an important role:

- celestial reference frame (CRF),
- terrestrial reference frame (TRF).

Reference systems are necessary to describe measurements for the determinations of position and velocity in space. In principle the determined position and velocity can be expressed only relative to the measuring platforms, which are moving themselves. Therefore a strong interest exists in the definition and availability of a globally available inertial reference systems.

Within the solar system the catalogue of fix stars was used for more than a century as an inertial reference system. However with the increase of accuracy and the long time span of observations of the measurements, the proper motion of galactic stars is in contradiction to the realization of an inertial system. The development of radio astronomy and of the Very Long Baseline Interferometry observation method allows the observation of the most remote objects in the universe. Today the very distant extragalactic quasars are providing the most accurate realization of a global inertial system. The proper motion of the very distant quasars is often negligible, but variations of the source structure require continuous monitoring programmes. The small changes of the radio objects themselves request the expression *quasi-inertial system*.

The optical reference frame became obsolete when VLBI demonstrated a higher astrometric accuracy of about two magnitudes in the reference frame of quasars. This was acknowledged by the IAU recommendation [1]:

*The ICRF will be based on radio sources observed by VLBI and will therefore replace the optical objects of the FK5, beginning from January 1st, 1998.*

---

\*Bundesamt für Kartographie und Geodäsie, Fundamentalstation Wettzell, e-mail: hase@wettzell.ifag.de

This recommendation is meaningful, since VLBI is now responsible for the primary quasi-inertial reference frame. Any kind of results from non-VLBI space geodetic measurements are comparable only, if they can be expressed relative to the inertial frame ICRF based on radio sources.

The only measurement technique which gives access to the inertial frame of distant radio sources with the best current level of accuracy is the Very Long Baseline Interferometry (VLBI).

## 2 Tie of Reference Frames

It is possible to generate (periodically) global solutions for each individual geodetic space technique including all the participating measuring platforms. The result are terrestrial reference frames for each single technique. One of the geodetic tasks is to compare these independent results of baselines or station coordinates. The comparison is possible:

- if the individual techniques are collocated at one site and the of the reference points can be provided by a local survey. This is best realized by operating fundamental stations for geodesy.
- if the individual techniques can be collocated in space; e.g. retroreflector for satellite laser ranging (SLR) at GPS satellites.

There exists another option since GPS-satellites and VLBI-techniques are using from the electromagnetic spectrum similar wavelengths: microwaves. The question arises:

**Why don't we use astrometric VLBI methods to tie the GPS satellite orbits directly into the ICRF?**

## 3 Astrometry

In astrometry the phase-referencing method is applied to measure weak sources relative to known quasars. If the angular separation between both objects should not exceed about  $5^\circ$  in order to assume the same atmospheric effects on the propagation of the signals. If both sources are observed alternating then the most accurate method of phase-differencing is applicable.

The ICRF is based on about 608 radio sources which are distributed over the entire sky. The statistical distribution on a sphere results in an averaged angular separation of each ICRF reference source of about  $9^\circ$ .

## 4 GPS

Currently are 27 GPS satellites on an orbit, of which 24 are operating. At one ground location at middle latitudes 7 to 8 GPS satellites are above the horizon for about 4.5 hours each. In this article GPS serves as an example. The idea of monitoring phase centres of GPS-transmitters applies to any other navigation system, like e.g. GLONASS or newer developments.

The orbits of GPS satellites are represented usually by the movements of the centres of mass. But the measurements with GPS refer to the centre of phase at the transmitting and receiving antennae. Since GPS uses two different carrier frequencies there are two different phase centres at the transmitter, which can be assumed to be offset to each other. (For simplicity in following the singular form is used in this article.) The centre of phase and the centre of mass of the extended GPS satellites are minimisation offset by more than one meter. Due to the perturbations of the orbits due to solar wind,

Earth shadow and gravitation the orientation of the offset between centre of mass and centre of phase are subject of temporal changes. As result the orientation of the eccentricity vector between the centre of phase as the geodetic reference point and the centre of mass as the dynamical reference point is not fixed in space and requires continuous monitoring and orbit determinations. The International GPS Service computes daily precise orbits of the GPS satellites based on ground stationed GPS permanent receivers. The residuals range typically from 2–20 cm.

VLBI has the potential to verify these GPS orbit determinations.

## 5 Phase Centre Determination of GPS-Transmitter with VLBI

The VLBI-method of phase-referencing would allow to observe GPS-transmitters during apparent approaches to radio sources. GPS-transmitters are very strong sources compared with quasars, but phase-referencing method will enable high accuracy for the orbit determination due to the of atmospheric effects (fig. 1).

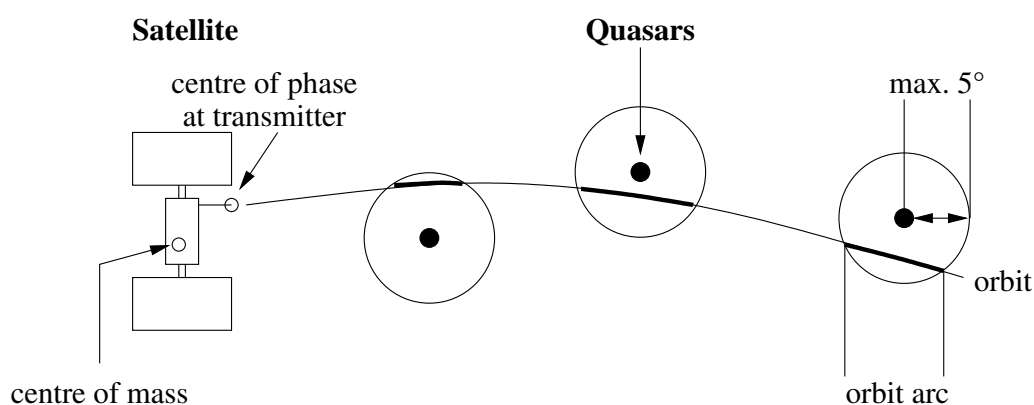


Fig. 1: Apparent approaches of satellite to ICRF radio sources. Phase-referencing astrometry can be carried out within a range of about 5 degree of angular separation.

Assuming that 608 sources and 24 GPS transmitters are observable, there should be statistically always globally six apparent approaches and at each site one apparent approach with less than  $5^\circ$  angular separation observable. The orbit of the phase centre would be determined in arcs which need to be interpolated when no radio source is available.

For those kind of observations some *research and development* problems have to be solved:

- Phase referencing on quasar pairs is static, while phase referencing on quasar and GPS-transmitter is kinematic. Interferometry models will need to include velocities of transmitters relative to Earth rotation.
- Phase referencing with quasar pairs is done in same spectrum for each source, while GPS frequencies are in L-band and the ICRF is based mainly on S/X-band observations. Astrometric determined positions of quasars show sometimes dependency on the observed frequencies. Is it possible to translate the phases between different spectra? If this is not possible, then the quasars must be observed in L-band or future navigation satellite projects should be equipped with S- and X-band transmitters.
- Method of the interpolation of orbit arcs achieved from phase-referencing method must be investigated.

- Introduction of satellite tracking routines to the antenna control units and PC Field System for alternating observations between quasar and transmitter.
- Method of simultaneous observation of two objects requires a new observing instrument: Dual beam radio telescope with movable eccentric second feed. The advantage is the continuous simultaneous observation of both objects relating to the same reference point at the antenna. The large reflector would observe the weak quasar, while the eccentric feed would observe strong satellite transmitter. The main reflector tracks by compensating the Earth rotation, while the ex-centric feed compensates for the satellite orbit in the inertial frame (fig. 2).
- GPS-transmitters seen in an altitude of 20000 km with a VLBI baseline of about 6000 km would allow to make a three-dimensional orbit determination (near-field). The 3-D position needs to be transformed in to the unit-sphere ICRF (far-field).

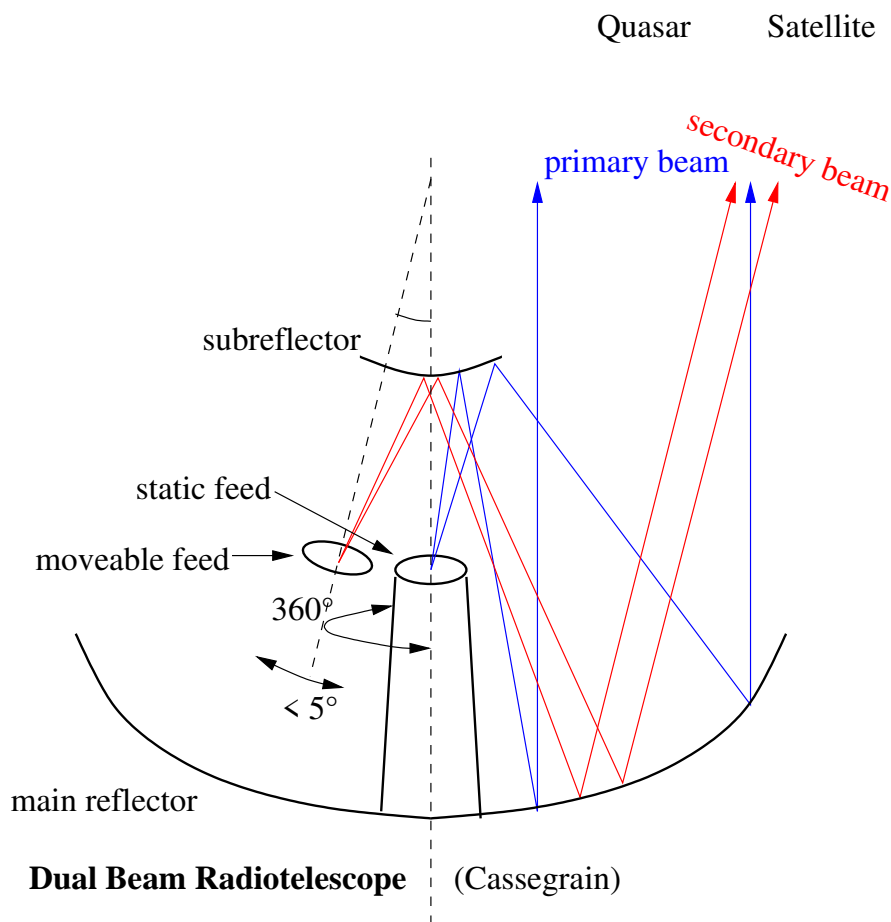


Fig. 2: Dual beam radio telescope for simultaneous phase-referencing VLBI observations. The primary beam tracks the quasar by compensating Earth rotation while the secondary beam tracks the satellite by compensating in a given range of maximum  $5^\circ$  angular separation the satellite movement. The result is a very precise orbit arc of the transmitter relative to the position of a quasar.

The advantages of *simultaneous* observations of quasar and transmitter with the dual beam radio telescope are:

- Direct continuous phase comparisons.
- Intersection of radio telescope axes is the ground based geodetic reference point for quasar and transmitter observations without eccentricity. This is of importance for the tie of ground based geodetic networks.

The observation schedule will contain pointings to GPS-transmitter whenever an apparent approach is observable and to quasars in between. The quasars will be selected due to the apparent approaches and due to the optimisation for the determination of Earth orientation parameters. The benefits of such observation schedules are:

- It will be possible to **decorrelate the orbital errors from earth orientation variations.**
- Orbits of the phase centre of the GPS-transmitter should be derived with about **3-6 cm accuracy in an inertial frame.**
- If orbits of transmitters are determined in the ICRF in return the observation of nutation and earth rotation can be performed with the much denser global GPS permanent network.

## 6 Outlook

Let us assume, that a new instrumental generation consisting of dual beam radio telescopes with real-time-VLBI infrastructure will be available in a global network. Applying dual beam VLBI techniques with simultaneous observations to the existing (or a new generation of) navigation satellites would allow the orbit determination on the level of a few centimetres directly tied in the ICRF. New navigation satellite programmes could be designed VLBI friendly by choosing frequencies which are also in the S/X-band regime and by higher altitudes for the transmitters for new space navigation purposes. The centimetre-level in accuracy of orbits obtained by VLBI-methods should reflect higher accuracy by positioning on the ground as well, since less hypothesis about the orbits themselves and the signal propagation through atmosphere are involved.

If the navigation satellites can be directly measured in the quasi-inertial frame of the ICRF, the deep space navigation can use the strong signals of the navigation satellites. Tied into the ICRF they provide stable reference points for high precision space navigation manoeuvres. While the remote space vehicle could navigate with the relatively strong signals from the navigation satellites rather than those weak signals from quasars, it will be also possible to include the remote space vehicle in the VLBI observation programme. VLBI phase referencing method will allow precise orbit determination also at larger distances of any transmitter.

The extension of the quasi-inertial reference frame of quasars with directly tied navigation satellites could be used as a backbone for an *inertial frame service*.

## References

- [1] Ma, C., Arias, E.F., Eubanks, T.M., Fey, A.L., Gontier, A.-M., Jacobs, C.S., Sovers, O.J., Archinal, B.A., Charlot, P.: The International Celestial Reference Frame as Realized by Very Long Baseline Interferometry, *The Astronomical Journal*, 116, S. 516-546, July 1998

# Characteristics of a Ring Laser for Geodesy

**Ulrich Schreiber, Manfred Schneider**  
Forschungseinrichtung Satellitengeodäsie  
Fundamentalstation Wettzell  
D- 93444 Kötzing, Germany

**Geoffery E. Stedman**  
Department of Physics and Astronomy  
University of Canterbury  
Private Bag 4800  
Christchurch, New Zealand

**Wolfgang Schlüter**  
Bundesamt für Kartographie und Geodäsie  
Aussenstelle Wettzell  
D- 93444 Kötzing, Germany

## Abstract

Large Ring lasers are not yet used for geophysical applications. C-II is a prototype for such a device and has a square optical path with side 1 m. One difference with the earlier C-I laser testbed - and similarity to an aircraft gyro - is its monolithic construction. It is housed 30 m underground in a New Zealand military bunker. The measured ringdown time of 0.20 ms corresponds to a quality factor  $6 \times 10^{11}$  and a finesse  $9.4 \times 10^4$ . for the observed exit beam power of 10 pW, this gives an angular rotation sensitivity  $4 \times 10^{-9}$  rad/s/sqrt(Hz). C-II performance limits therefore rival those of Sagnac matter- wave gyroscopes ( $2 \times 10^{-8}$  rad/s/sqrt(Hz), Gustavson et. al., Phys. Rev. Lett. 78, 2046-9 (1997)). This also corresponds to a quantum noise line width of 220 microhertz, consistent with that observed (172 microhertz) in the direct spectrum and with the coefficient of inverse time in the Allan variance plot.

**Keywords:** Ring laser gyroscope, Sagnac effect, earth rotation

## 1. INTRODUCTION

Ring lasers are known mostly from their application in inertial aircraft navigation, where they are used due to their many advantages over mechanical gyroscopes employing spinning masses. The relationship between the imposed rate of rotation and a splitting of the frequency of two counter-rotating laser beams enclosing a given area **A** is given by the Sagnac equation (1) for active cavities:

$$\delta f = \frac{4\mathbf{A} \cdot \boldsymbol{\Omega}_e}{\lambda L} \quad (1)$$

where  $L$  is the perimeter of the ring and  $\lambda = 633$  nm the wavelength of the HeNe laser, while  $\boldsymbol{\Omega}_e$  is the rate of earth rotation. Under ideal conditions this defines the unbiased operation of ring laser gyroscopes.

The C-II ring laser project involves a multinational and multi-institutional collaboration (as detailed in the acknowledgements). Its planning was reported at the Stuttgart Symposium Gyro Technology 1996 [1]. C-II was installed in January 1997 and we report here some of the results obtained so far.

## 2. THE C-II EXPERIMENT

Details of the rationale and design of C-II and the mathematical formulae needed to analyse these results in the manner done below have been published elsewhere [1, 2] and we summarise here only a few key points. C-II has a square beam path, with side 1.000 m, mirror mountings machined and polished to an accuracy of 10 arc sec, and two flat mirrors diagonally opposed, with two curved mirrors of radius 6.0 m on the other diagonal (figure 1). The supermirrors have total losses including transmission of each mirror of 1.2 ppm when new. The path is bored out of a solid piece of Zerodur,  $1.2 \times 1.2 \times 0.18$  m, except that in two cut-out sections the path and laser gas are bounded by tubes, one of which functions as a gain tube (under r.f. excitation) and the other of which is available to access beams for research purposes.

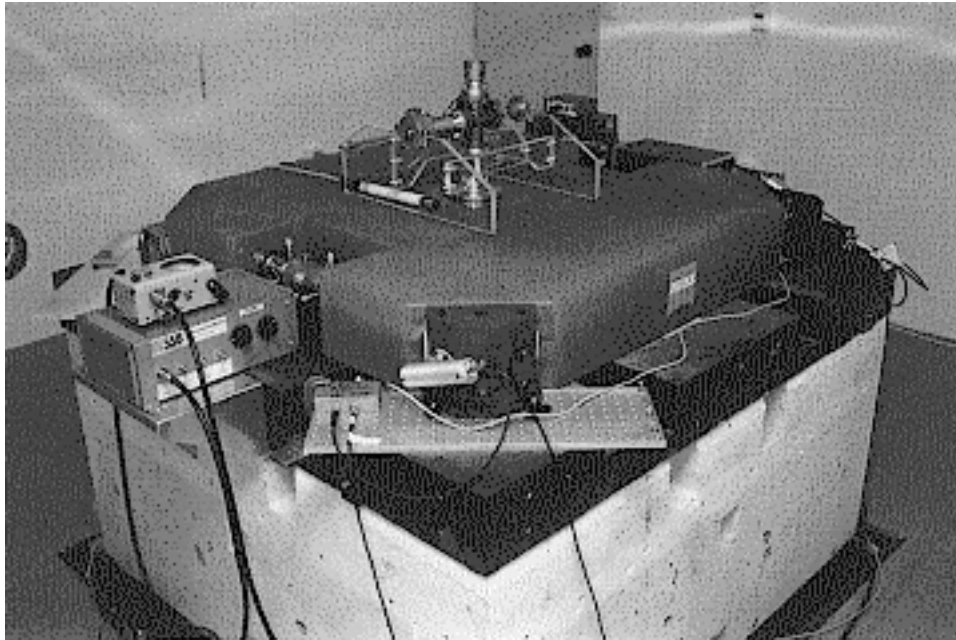


Figure 1: *Photograph of the C-II ring laser at its site in the cashmere cavern in Christchurch, New Zealand*

The d.c. component from a single beam is used to monitor the emergent optical beam power, and to servo the radio frequency amplitude for driving the plasma in order to keep the beam amplitude at a predetermined level. For monomode operation with this servoing system the required plasma power is typically 0.8 W, the plasma length 10 mm, and the exit beam power (measured for the quantum noise calculation to follow) 10 pW. Any higher power level leads to appreciable excitation of adjacent longitudinal modes. The Earth Sagnac rate nominally 79.4 Hz, was obtained with a measure of pushing and pulling associated with ambient pressure and believed to result from mirror backscatter, details have been published elsewhere [3]. The Sagnac frequency was stable, showing no variation to a precision of 1 mHz when the gain tube was used to vignette the beam, driving the servoed r.f. power to 1.2 W. With a 4 mm gain tube, the laser operated consistently in TEM(0,0). Transverse modes were absent under virtually all conditions.

The ringdown time was determined to be 0.20 ms as shown in figure 2. This translates into a quality factor of  $6.0 \times 10^{11}$ , and a cavity finesse of  $9.4 \times 10^4$ . We believe this to be a record for the passive quality factor of an optical resonator.

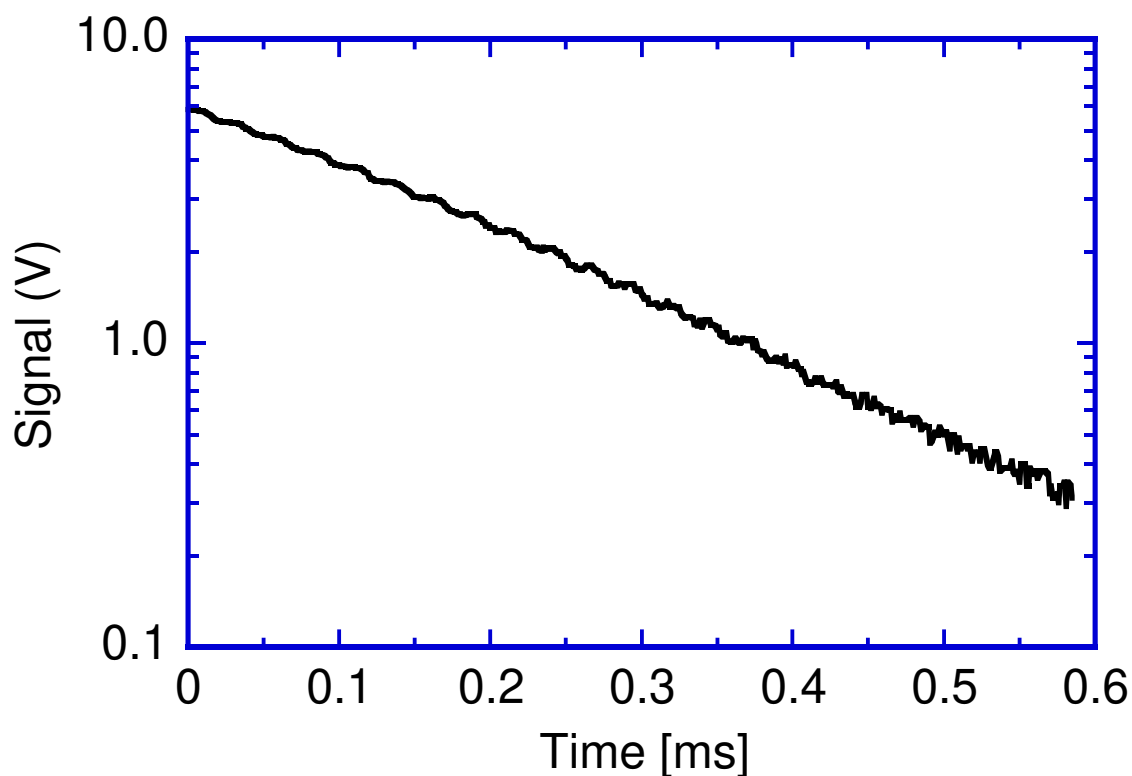


Figure 2: Ringdown time measurement on the C-II ring laser. The  $1/e$ - value is reached 0.2 ms after the driving power was cut off.

One of the major requirements for a longterm stable ring laser operation is a constant ambient temperature. Therefore the ring has been located in an underground cavern at Cashmere, New Zealand, which was originally built in World War II for defence purposes

and has no use otherwise. The mechanical and temperature stability are greatly superior to those of alternative sites, for example, the typical temperature excursion of the C-II pier is less than 10 mK over a few hours, and microseismic background effects may be monitored. This project therefore serves as another illustration of the increasing use of gyros for peaceful and purely scientific purposes [2].

This cavern environment has unusually good thermal and mechanical stability, and its availability has helped to meet the ultimate performance limits of such a device. When combined with the observed output power (10 pW) and mirror transmission of 0.24 ppm, this implies a circulating energy of 1.1 pJ and, with the observed ringdown time, a total power loss (mainly from scatter and transmission) of 5.6 nW. Together, these results imply a quantum noise induced full width half maximum of 220 microhertz. This is in good agreement with the observed value of 172 microhertz of the measurement shown in figure 3. It also agrees well (to within a factor of 2) with an Allan variance study of the output frequency in such runs (figure 4). At the right side of the Allan variance plot of two sample runs the instrumental drifts from scaling factor variations caused by atmospheric pressure changes are the dominating error sources.

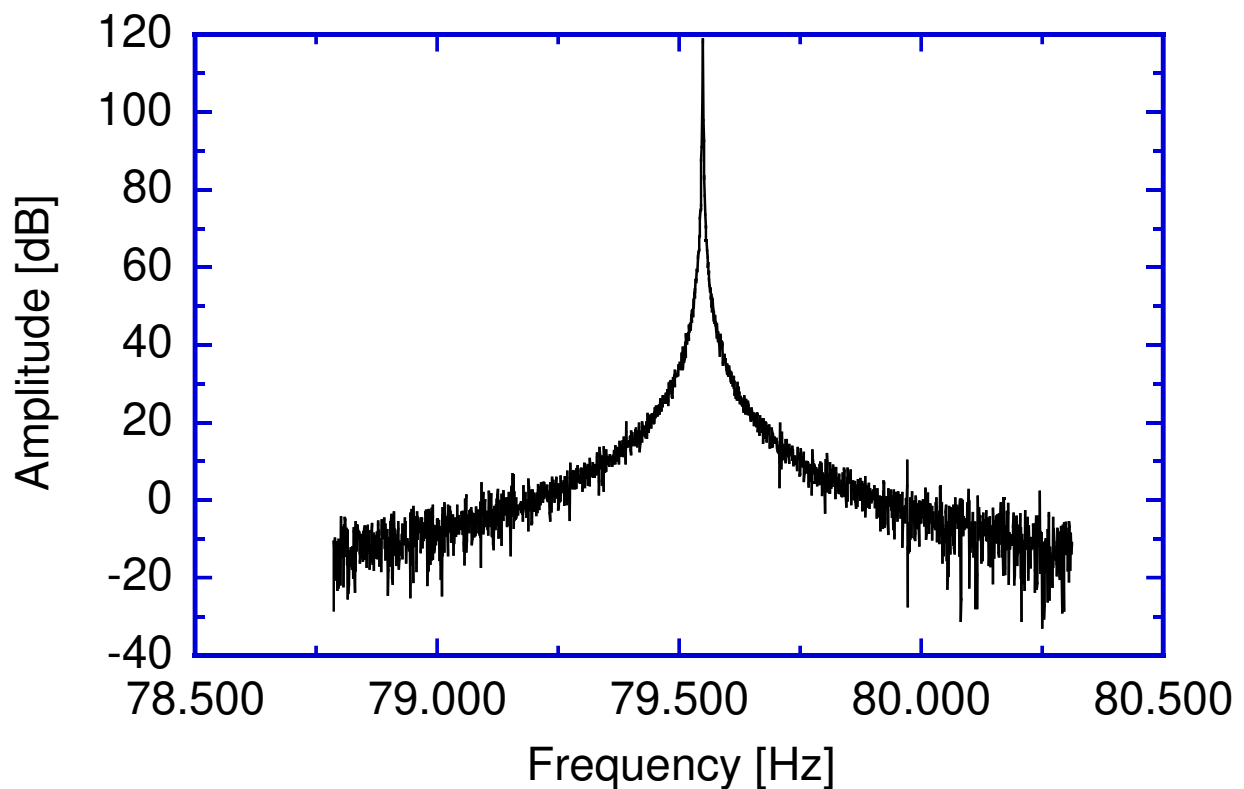


Figure 3: A sample spectrum from the C-II ring laser. The full width at half maximum was determined to be 172 microhertz.

The defining relationship [4] is that the Allan variance times sample time is half the one-sided power spectral density, itself (within a quantum noise picture) the above-mentioned

full width at half maximum power divided by pi. This argument renders C-II of sensitivity  $4 \times 10^{-9} \text{rad/s}/\sqrt{\text{Hz}}$ , somewhat greater than that of atomic gyros (Gustavson et al. (1997) who obtained  $2 \times 10^{-8} \text{rad/s}/\sqrt{\text{Hz}}$ , Lenef et al. (1997) who obtained  $3 \times 10^{-7} \text{rad/s}/\sqrt{\text{Hz}}$ ).

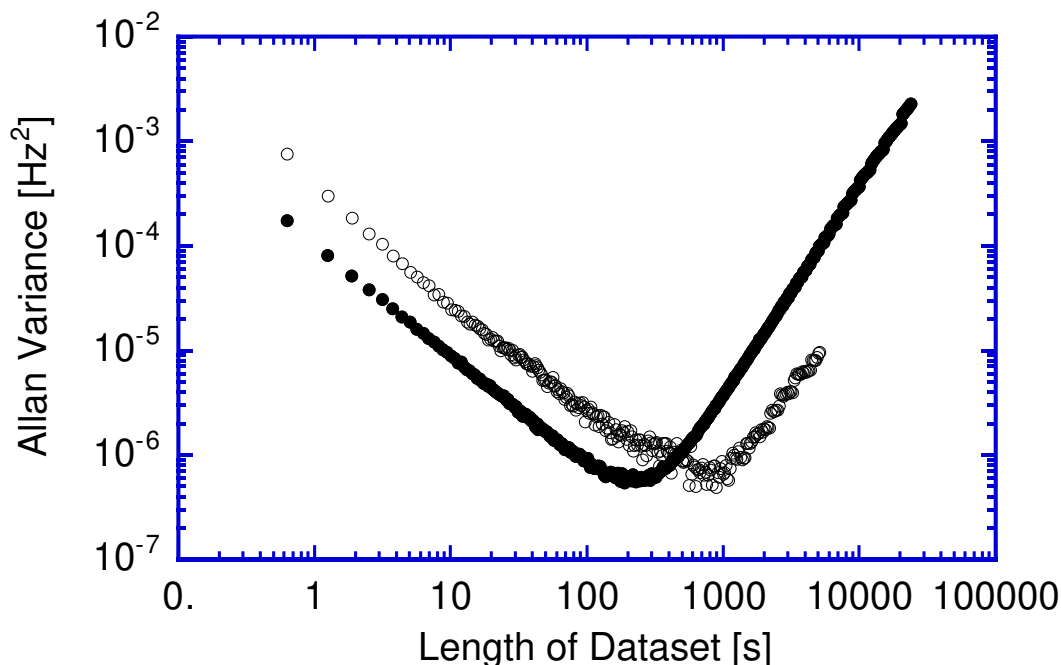


Figure 4: *Allan variance plots for two sample runs. C-II currently produces the lowest scatter for a dataset length of 300 to 1000 s. For runs longer than that scaling factor variations introduced by changes in the atmospheric pressure are the dominant error source.*

A scanning Fabry-Perot, a Newport SR-130 supercavity, is used for monitoring the absolute frequency of the C-II beam relative to that of an external Winters iodine- stabilised HeNe reference laser. The resultant frequency information is used to servo a piezo on one supermirror, stabilising the perimeter, and this has significantly reduced the drift in the Sagnac frequency. The residual drift now has an rms variation typically of a few millihertz as shown in figure 5.

An online display is available at:

[http://www.phys.canterbury.ac.nz/research/ring\\_laser/latest.html](http://www.phys.canterbury.ac.nz/research/ring_laser/latest.html)

This drift itself is significantly reduced by continuing development, including the implementation of pressure compensation and numerical correction methods, which is now well in progress. Figure 5 shows the difference between the raw data and the current simple correction model.

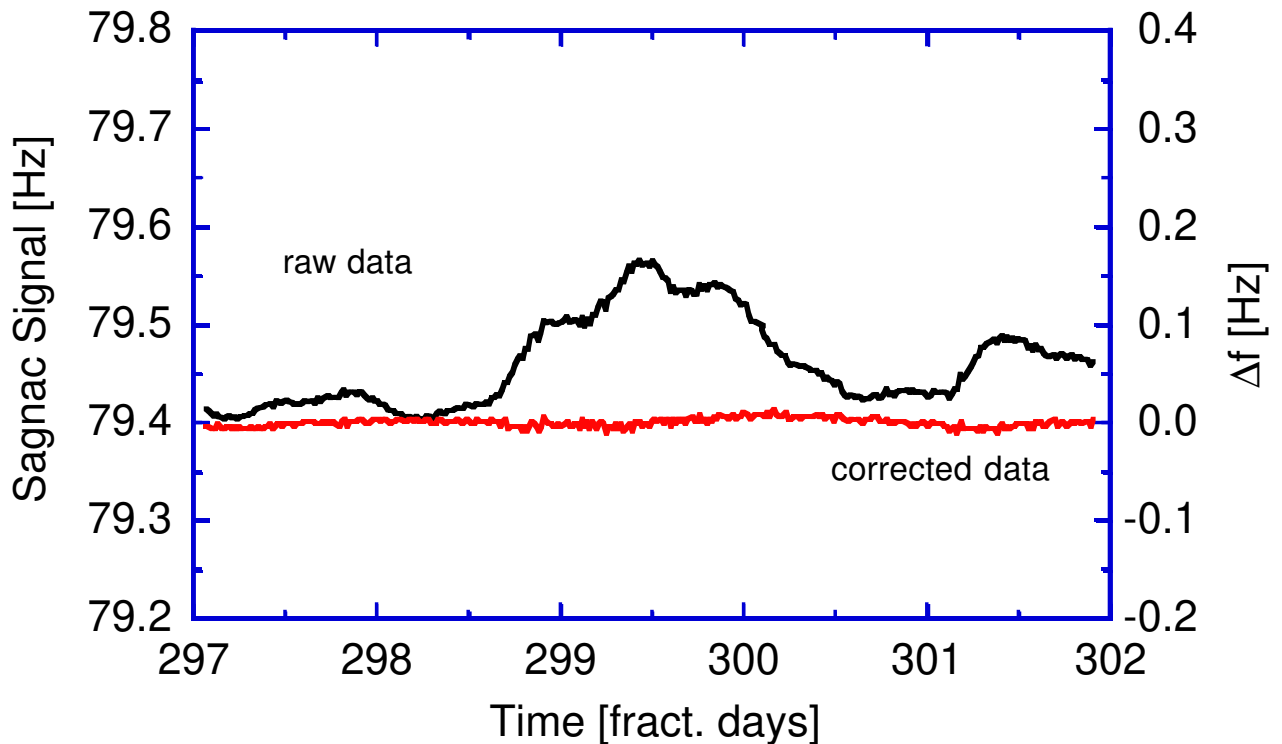


Figure 5: *A sample plot of the Sagnac frequency over time. The raw data shows excursions which are caused by the atmospheric pressure variations. A correction model which takes fluctuations of the scaling factor into account smoothes the timeseries of the Sagnac frequency substantially.*

### 3. SUMMARY

These results, and in particular the reduction of drift to a few millihertz, are reassuringly close to the original projections, and augur well for the eventual performance of C-II reaching the parts-per-million level (of the Sagnac frequency) precision as proposed in its original conception. This indicates that the C-II laser system is fulfilling its intended purpose of acting as a prototype and testbed for the much larger ( $4m \times 4m$ ) laser G, itself under construction for the detection of short-term fluctuations in Earth rotation [1, 2].

### 4. ACKNOWLEDGEMENTS

We acknowledge Prof. H. R. Bilger's initial design of C-II. The project was funded by "Bundesamt für Kartographie und Geodäsie, Frankfurt and Forschungseinrichtung Satellitengeodäsie der Technischen Universität München, also University of Canterbury, Christchurch, New Zealand together with the Marsden Fund of the Royal Society of New Zealand under contract UOC 513. The collaboration worked on detailed design together with the manufacturers Schott (Mainz) and Carl Zeiss (Oberkochen) in Germany.

## References

- [1] H. R. Bilger, U. Schreiber, and G. E. Stedman; “Design and application of large perimeter ring lasers”, *Symposium Gyro Technology (Stuttgart, September 1996)*, 8.0 - 8.24.
- [2] G. E. Stedman; “Ring- laser tests of fundamental physics and geophysics”, *Reports Progr. Phys.* 60, 615 - 683 (1997).
- [3] U. K. Schreiber, C.H. Rowe, D.N. Wright, S.J. Cooper, G.E. Stedman; “Precision stabilization of the optical frequency in a large ring laser gyroscope”, *Applied Optics*, Vol. 37, No. 36, 8371 - 8381, (20.12.1998).
- [4] H. R. Bilger; “Low frequency noise in ring laser gyros”, *SPIE 487 (Physics of Optical Ring Gyros)*, 42 - 48 (1984).